

**Tuneable collagen I and poly(N-isopropylacrylamide)
based hydrogels for tissue engineering applications of
mesenchymal stem cells**

Amanda Louise Barnes

Doctor of Philosophy

University of York

Biology

May 2014

Abstract

Due to their multipotency, mesenchymal stem cells (MSCs) are used to model and regenerate many connective tissues. Their behaviour varies with the environment they are maintained within, therefore different tissue scaffolds are required for each application to suitably mimic the tissue being engineered. Although hydrogels used as cell scaffolds are able to mimic certain tissue properties, this is often at the expense of others. Collagen for example is cell adhesive, but lacks the mechanical properties of native tissues. One method to address this challenge is to create hybrid scaffolds, combining materials that separately mimic one, or more of the desired tissue properties, resulting in an optimal scaffold. Furthermore by adjusting the composition of the components within such a gel, a panel of scaffolds can be designed with variable properties for multiple MSC applications. Both collagen and poly(NIPAM-*co*-styrene-*graft*-NVP) (NSN) hydrogels undergo gelation at physiological temperatures, enabling cell encapsulation, but individually are less than ideal as cell scaffolds. In this thesis it was demonstrated that combining these two materials produced hydrogels with the biocompatibility and cell adhesiveness of collagen and the mechanical strength of NSN. Through varying the composition of these bio-synthetic hydrogels, a repertoire of materials was produced with a range of mechanical properties and porosities. Hydrogels with low concentrations of NSN, contained fibrillar collagen networks, with no evidence of syneresis whilst gels with higher concentrations of NSN had superior mechanical properties, but were prone to syneresis. Two applications of MSCs were examined using the collagen-NSN gels, the development of an artificial lymph node model and injectable scaffolds for cartilage repair. The backbone of the lymph node consists of a heterogeneous network of stromal cells, which are mesenchymal. Through treating MSCs with the factors involved in lymph node organogenesis, they were induced into a lymphoid mesenchyme phenotype. These were seeded hybrid gels with low concentrations of NSN to develop 3D networks. Increasing the NSN concentration perturbed the morphology and migration of the MSCs within the hydrogels, and produced a scaffold with mechanical properties that mimic those of the lymph node. The tougher hydrogels were also able to support MSCs in 3D. Although the mechanical properties of these gels approached native cartilage, the chondrogenic capacity of the encapsulated cells was reduced compared with MSCs cultured in cell-only 3D pellets. The gels require further optimising for use as scaffolds for cartilage repair. The novel collagen-NSN hydrogels presented in this thesis, have potential as scaffolds for numerous applications as the exact composition of the gels can be tuned to alter their physical properties and therefore direct cell fate.

Table of Contents

Abstract	1
List of Tables.....	7
List of Figures	8
Acknowledgements	11
Author's Declaration.....	12
<u>Chapter 1 Introduction</u>	<u>13</u>
1.1 Background to the project	13
1.2 Tissue Engineering and Regenerative Medicine.....	13
1.2.1 Historical perspective	15
1.3 Mesenchymal stromal cells	17
1.3.1 Sources of MSCs	19
1.3.2 Cell surface markers of MSCs.....	19
1.3.3 Differential capacity of MSCs.....	20
1.4 The in-vivo cell microenvironment	23
1.4.1 The extracellular matrix	24
1.4.2 Cell-ECM Adhesions.....	27
1.5 2D versus 3D cell culture	30
1.6 Using matrix properties to direct cell fate.....	32
1.6.1 Matrix elasticity	32
1.6.2 Matrix porosity and pore size	34
1.6.3 Cell shape	36
1.7 Cell scaffold	38
1.8 Hydrogels as cell scaffolds	39
1.8.1 Biological hydrogels.....	40
1.8.2 Synthetic Hydrogels	43
1.8.3 Temperature responsive polymers.....	44
1.9 Poly(N-isopropylacrylamide) hydrogels.....	45
1.9.1 Temperature dependent behaviour of PNIPAM.....	46
1.9.2 Factors effecting the LCST	49

1.9.3	Biological applications of PNIPAM.....	51
1.9.4	PNIPAM hydrogels for regenerative medicine	53
1.9.5	Overall Research Aims.....	56

Chapter 2 Development of collagen I and poly(NIPAM-co-styrene-graft-NVP) hybrid gels 59

2.1	Introduction	59
2.1.1	Bio-synthetic hydrogel systems.....	59
2.1.2	PEG based biosynthetic gels	59
2.1.3	Interpenetrating polymer networks.....	60
2.1.4	Hyaluronan-NIPAM hydrogels	60
2.1.5	Gelatine NIPAM hydrogels.....	62
2.1.6	Chitosan-NIPAM hydrogels.....	62
2.1.7	Alginate-NIPAM hydrogels	63
2.1.8	Collagen PNIPAM scaffolds	63
2.1.9	Conclusions on bio-synthetic PNIPAM hydrogels.....	63
2.2	Aims and synopsis.....	64
2.3	Methods	66
2.3.1	Polymer Synthesis	66
2.3.2	Synthesis of semitelechelic oligo(NVP).....	66
2.3.3	Functionalisation of oligo(NVP)	66
2.3.4	Synthesis of poly(NIPAM-co-styrene-graft-NVP)	67
2.3.5	NMR analysis of oligomers and graft polymers.....	67
2.3.6	GPC analysis of oligomers and graft polymers.....	68
2.3.7	MALDI-TOF mass spectroscopy	68
2.3.8	Turbidity Measurements.....	68
2.3.9	Rheological Measurements	69
2.3.10	Collagen I extraction from rat tail tendon	69
2.3.11	Collagen I gel formation.....	70
2.3.12	Formation of hydrogels	70
2.3.13	Syneresis Measurements	71
2.3.14	SEM imaging.....	71

2.4 Results	71
2.4.1 Synthesis of oligo(N-vinylpyrrolidone) macromonomers.....	71
2.4.2 Synthesis of Poly(NIPAM- <i>co</i> -styrene- <i>graft</i> -NVP)	81
2.4.3 Poly(NIPAM- <i>co</i> -styrene- <i>graft</i> -NVP) is thermoresponsive at physiological temperatures	82
2.4.4 Fabrication of NSN and collagen I hybrid gels.....	89
2.4.5 Collagen I reduces syneresis in Poly(NIPAM- <i>co</i> -styrene- <i>graft</i> -NVP) gels.....	91
2.4.6 Mechanical strength of hybrid gels vary with NSN content	91
2.4.7 Internal structure of hybrid gels varies with NSN concentration	95
2.5 Discussion	98
2.5.1 Synthesis of poly(NIPAM- <i>co</i> -styrene- <i>graft</i> -NVP)	98
2.5.2 Thermoresponsive behaviour of NSN	99
2.5.3 Conclusions on the LCST of NSN	102
2.5.4 NSN-collagen hybrid gel properties with blend.....	103
2.6 Conclusion	109
Chapter 3 <u>Tissue Engineering Applications of collagen I – NSN gels</u>	110
3.1 Introduction	110
3.1.1 Lymph node function and structure.....	111
3.1.2 Development of lymphoid organs	113
3.1.3 Maturation of FDC and FRC stromal networks	114
3.1.4 Current developments in modelling LN.....	115
3.1.5 Articular Cartilage	116
3.1.6 Structure and composition of articular cartilage	116
3.1.7 Cartilage repair strategies	120
3.1.8 Tissue engineering cartilage	121
3.2 Aims and synopsis	123
3.3 Methods	125
3.3.1 Cell Culture	125
3.3.2 Mycoplasma testing.....	126
3.3.3 Induction of lymphoid mesenchyme phenotype in ADSCs	126
3.3.4 Flow cytometry.....	126

3.3.5	Adipogenic differentiation.....	128
3.3.6	Osteogenic differentiation	128
3.3.7	Chondrogenic differentiation.....	128
3.3.8	Oil Red O staining.....	129
3.3.9	Alizarin Red staining.....	129
3.3.10	Alkaline Phosphatase staining.....	129
3.3.11	pNPP and pico green assays.....	130
3.3.12	Culturing MSCs within hybrid gels.....	130
3.3.13	ADSC Spheroids	131
3.3.14	ADSC viability in low NIPAM content gels.....	131
3.3.15	Imaging.....	132
3.3.16	cDNA synthesis and qPCR.....	133
3.3.17	MTT viability assay.....	136
3.3.18	Alcian blue staining.....	136
3.3.19	Statistics.....	136
3.4	Results: In-vitro modelling of lymphoid mesenchyme.....	137
3.4.1	Cytokine treatment induces a lymphoid mesenchyme phenotype in 2D ADSCs.....	137
3.4.2	Lymphoid mesenchyme induction reduces the differential capacity of 2D ADSCs.....	137
3.4.3	The lymphoid mesenchyme phenotype is reversible.....	145
3.4.4	Development of 3D models of lymphoid stroma	150
3.4.5	Effect of 3D environment upon lymphoid mesenchyme phenotype	159
3.5	Results: Cartilage engineering using high NSN content gels.....	164
3.5.1	Isolation and characterisation of BM-MSCs for cartilage therapies	164
3.5.2	NSN-collagen hybrid gels for cartilage repair.....	165
3.6	Discussion	173
3.6.1	Adipose derived stem cells for modelling lymphoid mesenchyme.....	173
3.6.2	Induction of a reversible lymphoid mesenchyme phenotype in 2D ADSCs 174	
3.6.3	3D stromal networks can be formed within hybrid gels.....	178

3.6.4	Lymphoid mesenchyme induction in 3D	180
3.6.5	Isolation of bone marrow derived MSCs for cartilage repair	183
3.6.6	Potential of High NSN content hydrogels for cartilage repair	184
3.7	Conclusion	187
Chapter 4	<u>General Discussion</u>	188
1.10	Synthesis and properties of collagen-NSN hydrogels.....	189
1.11	Development of an aLN using ADSCs and collagen-NSN hydrogels.....	191
1.12	Potential of collagen-NSN hydrogels for injectable cartilage regeneration	193
1.13	Effect of hydrogel composition on gelation mechanism and resulting	193
	properties.....	
1.14	Future Work	194
1.15	Conclusion	195
	Abbreviations	197
	References	201

List of Tables

Table 1-2: Structures and composition of collagen proteins.....	25
Table 1-3 Elastic moduli of several tissues and organs.....	33
Table 2-1 Molecular weight averages of NVP oligomers and NSN.....	72
Table 2-2 Expected products of macromonomer synthesis and functionalisation.....	81
Table 2-3 Phase transition temperatures as determined by turbidity(cloud point) and rheology (gel point).....	86
Table 2-4 Shear mechanical properties of NSN and Col –NSN gels.....	94
Table 3-1 Primary Antibodies.....	127
Table 3-2 Secondary Antibodies.....	127
Table 3-3 Primer sequences.....	135
Table 3-4: Summary of cytokine induced lymphoid mesenchyme experiments.....	162

List of Figures

Figure 1-1: Differential capacity of mesenchymal stromal cells.....	18
Figure 1-2: Structure of the collagen molecule.....	26
Figure 1-3: Cell-ECM adhesions.....	28
Figure 1-4: Differences in 2D cell culture compared with <i>in-vivo</i> and 3D culture conditions	29
Figure 1-5 Chemical structures of polysaccharide based gels.....	42
Figure 1-6: Thermoresponsive polymers that exhibit a LCST	45
Figure 1-7 The conformational change of PNIPAM upon increase in temperature is dictated by polymer structure.	46
Figure 1-8 Coil- globule collapse of PNIPAM in aqueous solution at the LCST.....	47
Figure 1-9: Representative phase diagram showing the concentration dependence of the phase transition temperatures of a polymer in aqueous solution.....	48
Figure 2-1 Synthetic route to poly(NIPAM- <i>co</i> -styrene- <i>graft</i> -NVP).....	73
Figure 2-2 Molecular weight distributions of NVP oligomers and NSN.....	74
Figure 2-3 ¹ H-NMR spectra of NVP oligomers.....	75
Figure 2-4 MALDI-ToF spectra of NVP oligomers.....	78
Figure 2-5 Possible initiation mechanisms during ONVP-OH.....	79
Figure 2-6: Gelation of NSN at physiological temperature.....	83
Figure 2-7 ¹ H-NMR spectrum of NSN in MeOH	84
Figure 2-8 Effect of temperature on turbidity of NSN solutions.....	85
Figure 2-9 Determination of accurate rheology % strain rates and frequency NSN ₅ at 0 and 37 °C.	88
Figure 2-10 Determination of NSN ₁₀ gel point by rheology.....	90
Figure 2-11 Syneresis index of NSN, collagen and hybrid gels.....	92
Figure 2-12 Behaviour of hybrid gels under shear forces	93
Figure 2-13 SEM micrographs of collagen and hybrid gels.....	96
Figure 2-14 Fibre diameters measurements of collagen and NSN fibres in hybrid gels	97
Figure 2-15 Mechanisms of gel formation in different hydrogel blends.....	108
Figure 3-1 Schematic of lymph node structure.	112
Figure 3-2 Distribution of chondrocytes and collagen within articular cartilage.....	118

Figure 3-3 Extracellular matrix of articular cartilage.....	119
Figure 3-4: 2D ADSCs can be induced into a lymphoid mesenchyme phenotype upon	138
Figure 3-5 Lymphoid mesenchyme induction inhibits 2D ADSC adiogenesis.	140
Figure 3-6: Lymphoid mesenchyme induction inhibits 2D ADSC osteogenesis.....	141
Figure 3-7: IL-4 lymphoid mesenchyme induction of 2D ADSCs does not affect adipogenesis	142
Figure 3-8: IL-4 lymphoid mesenchyme induction of 2D ADSCs does not affect mineralisation	143
Figure 3-9: IL-4 lymphoid mesenchyme induction of 2D ADSCs affects ALP activity but not cell proliferation	144
Figure 3-10: Priming of 2D ADSCs with lymphoid mesenchyme inducing cytokines does not affect adipogenesis	146
Figure 3-11 Priming of 2D ADSCs with lymphoid mesenchyme inducing cytokines does not affect osteogenesis.	148
Figure 3-12 Expression of lymphoid mesenchyme markers ICAM-1 and VCAM-1 decreases in adipogenic 2D ADSCs	149
Figure 3-13 Development of 3D ADSC stromal networks in collagen gels.	151
Figure 3-14 ADSCs encapsulated within col-NSN hydrogels are viable.....	153
Figure 3-15: ADSCs cultured within the hybrid gels can be released and re-plated as 2D monolayers.	154
Figure 3-16: Hybrid gels do not release cytotoxic products into cell culture media....	155
Figure 3-17 ADSC networks and cell morphologies in hybrid gels are affected by gel composition.	157
Figure 3-18 HT1080s invasion into collagen and hybrid gels is affected by hydrogel composition.	158
Figure 3-19 Analysis of spheroids as 3D models of lymphoid stroma.	160
Figure 3-20 Lymphoid mesenchyme induction in 3D is lower than 2D	161
Figure 3-21 Characterisation of cell surface markers and differential capacity of BM- MSCs.	166

Figure 3-22 GAG expression in BM-MSCs cell pellets following chondrogenic differentiation .	167
Figure 3-23: Collagen II expression in BM-MSCs cell pellets following chondrogenic differentiation.	168
Figure 3-24 Viability of BM-MSCs with col-NSN ₅ hydrogels.	170
Figure 3-25 GAG expression in BM-MSCs containing col-NSN ₅ hydrogels following chondrogenic differentiation .	171
Figure 3-26: Collagen II expression in BM-MSCs containing col-NSN ₅ hydrogels following chondrogenic differentiation.	172
Figure 4-1 Proposed mechanism of col-NSN gelation and cellular adhesion.	196

Acknowledgements

Without the support of a great number of people this PhD could not have been possible. I would like to thank my supervisors Dr. Mark Coles, Prof. Stephen Rimmer and Dr. Paul Genever for giving me the opportunity to work on this project and for providing assistance and support over the past four years.

My colleagues within the Centre for Immunology and Infection, the Biomedical Tissue Research Group in York and the Polymer and Biomaterials Laboratory in Sheffield have provided a wealth of support and advice. I would like to particularly thank Katherine Brown for her help in polymer synthesis and analysis, Matt Lakins and Roger Leigh for assistance in producing collagen gels and imaging and Bridget Glaysher for help with cell culture and assistance in developing the lymph node models. The technical staff at Sheffield and York have also provided invaluable support and training during my research, particularly Melanie Hannah, Meg Stark, Graeme Park and Karen Hodgkinson. I would also like to thank my thesis advisory panel, Jenny Southgate and Dani Ungar for providing suggestions and advice throughout my PhD.

Special thanks to my close friends within the biology department: Amy Sawtell, Dan Peters, Poppy Marriott and David Wortley for providing some well needed light relief during the daily challenges a PhD has thrown at me. Lastly I would like to thank my family, and most importantly Ed for putting things into perspective when things went wrong, and helping to calm and comfort me. Without them I would not have been able to accomplish this thesis.

Author's Declaration

The research within this thesis has not been previously submitted for any other degree, at any other institution and was written and performed by the author unless otherwise stated. Initial collagen extraction from rat tails was performed by Roger Leigh, and samples for SEM imaging were prepared with assistance from and imaged by Meg Stark. Additional images for figures were provided by Julia Marshall, Amy Sawtell and Anne Thuery and are acknowledged within figure legends as appropriate.

Chapter 1 Introduction

1.1 Background to the project

Tissue engineering and regenerative medicine aims to replace or repair tissues *that* have become damaged or worn out. The term tissue engineering was coined by the pioneers in the field, Robert Langer and Joseph Vacanti in their 1993 Science Paper¹. They defined ‘Tissue engineering is an interdisciplinary field that applies the principles of engineering and the life sciences toward the development of biological substitutes that restore, maintain or improve tissue function’¹. Where the biological substitutes were either a) the use of isolated cells or a cell substitute, b) tissue inducing substances, such as growth factors in combination with methods for delivery; or c) cells placed within or on matrices¹. The research in this thesis concerns the latter method, using a combination of cells seeded within a three dimensional (3D) scaffold and delivery of the appropriate soluble cues and growth factors to stimulate growth into the tissue of interest. The terms tissue engineering and regenerative medicine are often used interchangeably, generally tissue engineering defines the creation of a tissue *in-vitro*, whilst regenerative medicine encompasses the whole field, including tissue engineering as well as the use of cells, scaffolds and bioactive molecules *in-vivo* to generate tissues using the body’s own ability to repair.

1.2 Tissue Engineering and Regenerative Medicine

Due to improvements in health care and lifestyle, the population is living longer, and with an increasing ageing population. The worldwide population of older persons (aged 60 plus) was 841 million people in 2013, and this is expected to rise to over 2 billion by 2050². It was also predicted that for the first time in 2047, the older population will exceed the number of children². Associated with this increase in the older population, will be the increase in age-related disorders and degenerative disease, and therefore high demand to replace damaged and failing tissues and organs. Current treatments include organ donation, implantation of artificial prosthetics and drug therapies however these treatments are not always ideal. There are limited sources of donor organs³, and where

they are available they can be rejected by the immune system of the patient⁴. Artificial prosthetics such as hip and knee replacements have a limited life span⁵, and they can release metal and polymer wear particles which stimulate immune responses and are prone to loosening^{6,7}. Whilst drug therapies may only have short term results or simply help to alleviate pain and inflammation⁸. Ultimately the best way to repair a tissue is with an exact functional replica, using patient's own cells, which is the goal of regenerative medicine.

Tissue engineering also has *in-vitro* applications in research and therapeutics. Through creation of models of tissues and organs we can further our understanding of human body physiology. Tissues within the body are complex, made up of multiple cell types, including parenchyma, supporting stromal cells and vasculature all contained within a complex mix of extracellular matrix (ECM) proteins. Models enable a reductionist bottom -up approach to research. Basic models using a single cell type and simplified ECM can be probed to study the effect of a single stimulus on a system, to build a bigger picture of *in-vivo* behaviour. *In-vitro* models could also reduce the need for animal models in research. Animal research is now banned for the testing of cosmetics, and tissue engineering approaches have been used to develop skin models as alternatives. Such skin models are also used for wound healing when there is no source of allogeneic or autogenic donor tissue.

The research within this thesis describes the development of a novel thermoresponsive hydrogel composed of collagen I and poly(N-isopropylacrylamide) (PNIPAM), for use as a cell scaffold to support mesenchymal stromal cells (MSCs). The blend of collagen and PNIPAM in the hydrogel can be easily tailored, which results in variation of the physical properties, therefore the hydrogel has potential for use in multiple applications. Within this introduction the phenotype and differential capacity of MSCs will be discussed, followed by an introduction into how cells respond to their 3D environment. An introduction will then be given to PNIPAM with examples of PNIPAM based materials currently used in tissue engineering.

1.2.1 Historical perspective

Research into the field began with the approaches clinicians were taking to replace and reconstruct tissues, using donor tissue from another site of the body or the implantation of prostheses. Early methods involved tissue replacements that were more structural, rather than functional. For example repair of the bladder was initially performed using synthetic, non-biodegradable materials, including rubber and silicone. These generally failed due to infection and host-foreign body reactions⁹. Grafts of peritoneum, placenta, pericardium were used as alternatives, however removal of tissue from another site of the body can often lead to donor site morbidity. The next logical step, was to evaluate whether tissue could instead be engineered.

One of the earliest examples of tissue replacement was the development of skin substitutes to provide barrier function and reduce infection following wounding. Autologous grafts have been used since the 19th century¹⁰, and more recently cadaveric grafts¹¹. In many patients autologous grafting is not an option, due to the extent of damage and shortage of donor skin, this is particularly the case for patients with burns, therefore replacement approaches moved towards the use of cultured epithelial cells to reconstitute the epidermis. Billingham and Green demonstrated this in animal models¹², and this was followed by Rheinwald and Green, who developed improved techniques to culture human epidermal keratinocytes in multilayer sheets using lethally irradiated fibroblasts as a feeder layer^{13,14}, these could then be transferred as intact sheets as grafts onto the wound¹⁵. These multilayer cell sheets were however very fragile and integration and healing was poor where the underlying dermis was also damaged and not well vascularised¹⁶.

Therefore biological and synthetic biomaterials were developed as dermal substitutes to cover the wound bed and promote revascularisation prior to epidermal repair¹⁶. One of the leading products is Integra, an off-the-shelf product, composed of bovine collagen and shark chondroitin sulphate on a silicone membrane, which acts as a temporary wound dressing¹⁷. Allogenic donor skin is also used in a similar manner¹⁸. More recently bilayered products have been developed, which provide a barrier function like

the dermal substitutes and an epidermal layer composed of differentiated keratinocytes¹⁶. Apligraf® a ‘living’ skin construct, is composed of a differentiated layer of keratinocytes in the epidermal layer, and a dermal layer of fibroblasts within a bovine collagen scaffold^{19,20}. It has been shown to be efficacious in the treatment of chronic ulcers compared with control treatments²⁰.

Methodologies for culturing and expansion of other primary cells were also developed, and contributed to the development of the growing field. For example, corneal epithelial cells that can be grown in sheets or on matrices for corneal repair²¹, schwann cells to be used alongside tubular grafts for peripheral nerve repair²², chondrocytes for cartilage repair²³, urothelial cells for bladder regeneration²⁴, hepatocytes to restore liver function²⁵ and mesenchymal cells²⁶ that can be differentiated into bone and cartilage. The latter will be discussed in more detail in the following sections.

In addition to developing methods to culture and expand primary cells and fabricate scaffolds, inductive growth factors and proteins have potential in tissue engineering. Prior to the identification of bone morphogenetic proteins (BMPs), it had been suggested in articles by Lacroix, as early as 1945²⁷ and later by Urist²⁸, that bone contained a protein that could promote new growth. Urist showed transplantation of demineralised bone could induce the growth of new bone in rats and rabbits²⁸. These proteins were later identified as the growth factors, bone morphogenetic proteins (BMP's)²⁹.

In 1993 Joseph Vacanti and Robert Langer pulled together the research that had been developing in the field and defined tissue engineering in their seminal science paper¹. Research groups across the world were developing methodologies to engineer tissues derived from all three germ layers. Prior to this Langer had successes, publishing seminal papers which paved the way for the field. He developed new polymeric materials for sustained drug release over 100 days³⁰. Previous materials that had been developed elicited inflammatory responses *in-vivo*. In collaboration with Vacanti, Langer also published the first example of primary cell culture within 3D matrices *in-vitro*. They demonstrated primary hepatocytes and intestinal cells could be cultured

within synthetic polymers and subsequently engrafted *in-vivo*³¹. The ‘Vacanti Mouse’ also raised interest in the field, particularly media hype, where a polyglycolic acid-poly(lactic acid) (PGA/PLA) scaffold seeded with bovine chondrocytes was grafted on to the back of a athymic mouse³². Although the ear was purely cosmetic the study demonstrated how synthetic scaffolds could be fabricated into precise geometries.

In 2006, Antony Atala et al, demonstrated autologous bladder repair could be performed using a biopsy of healthy bladder from each patient and expanding the urothelial and muscle cells in culture. These were then seeded on a shaped scaffold of collagen or a composite of collagen and PGA. When implanted the composite scaffold led to normal bowel function, and improved bladder function²⁴. Another major success of the field followed in 2008, when a tissue engineered trachea was used to replace a narrowing bronchus of a 30-year old women with end-stage airway disease³³. A donor trachea was decellularised and seeded with culture expanded epithelial cells and chondrocytes derived from the patient, within a specialised bioreactor. When implanted *in-vivo* to replace the damaged left bronchus, functionality was immediately restored. Five years later the patient has had no complications³⁴, providing very promising results to the field.

The above examples demonstrate research in the field is very multidisciplinary combining polymer chemistry, molecular biology, anatomy, cell biology, cell signalling and engineering disciplines. These collaborations have enhanced understanding and will continue to further the successes in the field.

1.3 Mesenchymal stromal cells

In response to injury and during homeostasis, adult stem cells proliferate and differentiate to remodel and repair damaged tissues. Due to their ability to differentiate into many cell types, they are a popular cell source in regenerative medicine. They are defined by their ability to self renewal and asymmetrically divide producing identical daughter cells. They exist as small populations within specialised “stem cell” niches found in many tissues, and self renew in the absence of differentiation cues. Currently

several types of adult stem cells have been identified, including haematopoietic and mesenchymal, which both have niches in the bone marrow. Several niches of stem cells are present in the skin, which have been demonstrated to maintain the epidermis, hair follicle and sebaceous glands³⁵⁻³⁷. Within the crypts of the intestine there are a population of stem cells which differentiate into the epithelial cells of the intestine³⁸, and neural stem cells have been identified within niches in the brain and spinal cord³⁹⁻⁴¹. The ability to stimulate stem cell differentiation to repair tissues offers great promise in the field of medicine.

MSCs can be easily isolated and expanded *in-vitro* from a range of tissues. Typically tissue explants are digested enzymatically and/or mechanically to release a single cell suspension. The mononuclear cell fraction is then isolated by centrifugation into mononucleated cells, and contaminating red blood cells are removed by cell lysis. MSCs are then enriched by their plastic adherence, where lymphocytes are lost in cell passaging.

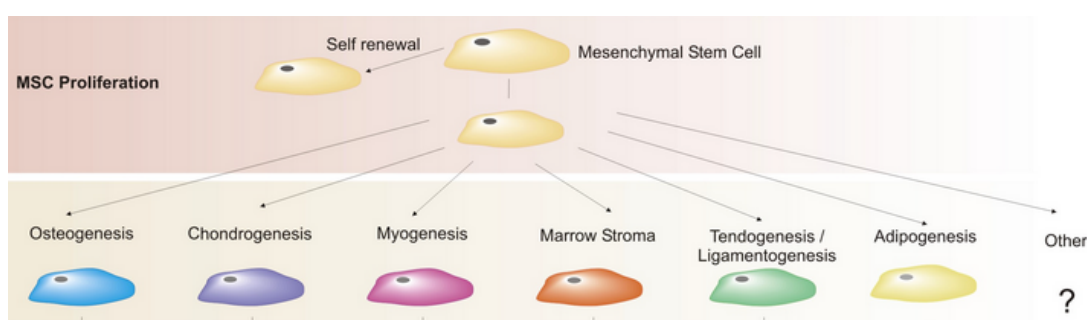


Figure 1-1: Differential capacity of mesenchymal stromal cells. Within the niche MSCs remain multipotent and self renew. Given the right stimuli they can differentiate towards multiple lineages⁴².

Although MSCs are considered stem cells, the isolated cell populations are more appropriately referred to as mesenchymal stromal cells, as the cell population is heterogeneous, and only a fraction of the cells are multipotent. MSCs have the capacity to differentiate into various mesenchymal and connective tissues including and probably not limited to bone⁴³⁻⁴⁵, cartilage⁴⁶⁻⁴⁸, fat^{49,50}, muscle^{51,52}, ligament and tendon⁵³. Furthermore undifferentiated and differentiated MSCs are non-immunogenic, and may

have immunosuppressive properties and can therefore be used therapeutically from allogeneic sources^{54,55}.

1.3.1 Sources of MSCs

MSCs can also be isolated from other sources as well as bone marrow, including adipose tissue derived (ADSC)⁵⁶⁻⁵⁸, umbilical cord blood^{59,60,61} (UC-MSC), periosteum⁶², dermis and skeletal muscle⁶³. The use of ADSCs as a source of autologous or allogeneic cells for regenerative medicine is increasing in popularity as the cells can be harvested far easier than bone marrow, and generally in larger quantities when isolated from adipose tissue lipoaspirates. Isolation of UC-MSCs is not as reproducible as ADSCs and BM-MSCs therefore these cells are less well characterised^{64,65}, furthermore some groups have shown UC-MSCs may not be able to undergo adipogenic differentiation^{61,65}.

ADSCs share many similarities with BM-MSCs, cells from both sources can differentiate into bone, fat and cartilage and express the frequently used MSC markers CD73, CD90 and CD105^{56-59,66}. However comparison of differentiation specific genes have shown ADSCs may have a greater adipogenic potential than BM-MSCs, whilst BM-MSCs are more osteo- and chondrogenic^{67,68}, indicating that while some of the MSCs found within each tissue are multipotent, there may be a larger proportion of tissue specific progenitors.

1.3.2 Cell surface markers of MSCs

The international society for cellular therapies classifies a MSC as a cell which is plastic adherent in culture, able to differentiate into adipocytes, osteoblasts and chondrocytes *in-vitro* and expresses the cell surface markers CD73, CD90 and CD105 but not CD45, CD34, CD14 or CD11b, CD79 or CD19 and HLA-DR in order to exclude haematopoietic cells⁶⁹. This combination of cell surface markers is crucial for defining MSCs, as no one cell surface marker is specific for only MSCs. CD73 and CD105 are

expressed by endothelial lineage cells found in the bone marrow, and CD90 is also a marker of T-lymphocytes, neuronal and innate lymphoid cells⁷⁰.

MSCs maintained in culture are likely to become senescent and lose their multipotency, thus hindering their therapeutic use. The common MSC markers CD73, CD90 and CD105 are unaffected by passage number⁷¹ and differentiation⁷² and although they can be used to define MSCs, they may not be a useful indication of their differential capacity. Stro-1 and CD106 are both expressed by mesenchymal progenitors, and decrease with time in culture and induction of differentiation^{72,73}. Selection of double positive Stro-1⁺ CD106⁺ cells enriched the isolated mono-nuclear cells from bone marrow for colony forming unit – fibroblasts (CFU-Fs), another characteristic of MSCs, indicating these markers may be the more useful for identifying the most multipotent MSCs⁷⁴.

There is also some variation seen in cell surface markers between BM-MSCs and ADSC's. Zuk et al. isolated CD34⁻, CD106 (VCAM-1)⁻, Stro-1⁺ expressing ADSCs^{56,57}, whilst Gronthos et al observed the opposite⁶⁶. Comparative studies of BM-MSCs and ADSCs, have also yielded conflicting results, both Kern and Noel et al. found only BM-MSCs to express CD106, and only ADSCs expressing CD34^{65,68}. Whilst Wagner et al. isolated CD34⁻ CD49d⁻ CD106⁺ BM-MSCs and CD34⁻ CD49d⁺ CD106⁻ ADSCs. These differences may be explained by variations in the experimental techniques used for isolation and passage number at analysis⁵⁸.

1.3.3 Differential capacity of MSCs

Multipotent cells within bone marrow were first identified by Friedenstein^{75,76} and Owen^{43,77,78}, who showed whole bone marrow aspirates or *in-vitro* expanded bone marrow fibroblastic cells implanted *in-vivo* within diffusion chambers or beneath the renal capsule, could differentiate into bone, marrow and cartilage. Initially all cells in the chambers differentiated toward a chondrogenic lineage, and regions of bone tissue were formed later, similarly to endochondral ossification during embryonic development^{46,77-80}. Cell seeding density and proximity to vasculature and nutrients also

effected cell commitment, chondrogenesis favoured high cell density and hypoxic conditions whilst the opposite was found for bone formation^{81,82}. Friedenstein also demonstrated that isolated bone marrow cells seeded at low density *in-vitro* were able to form colonies from single cells, now named CFU-Fs⁸³. The colonies were able to undergo at least 30 population doublings in culture and still differentiate *in-vivo* towards cartilage and bone⁸⁴. Differential capacity was found to vary between clones, indicating the bone marrow stromal cell (BMSC) population is a heterogeneous containing a mix of progenitors²⁶.

Following on from research on *in-vitro* haematopoietic stem cell (HSC) colony differentiation assays, Owen et al. explored *in-vitro* differentiation of BMSC. BMSC colonies maintained in culture displayed alkaline phosphatase activity, a marker of osteogenesis, where the expression varied between colonies and was enhanced when the cells were treated with hydrocortisone⁴⁵. BMSCs were also shown to differentiate into adipocytes when they were used to support haematopoietic stem cells *in-vitro*. The presence of horse serum and hydrocortisone induced the differentiation, characterised by the accumulation of lipids within the cells^{49,50,85}. Many *in-vitro* and *in-vivo* studies on BMSC followed, with varying conditions used to induce differentiation^{86,87}. *In-vitro* culturing of MSCs in the presence of dexamethasone stimulated both adipogenesis and osteogenesis⁸⁸, where the osteogenesis could also be enhanced with bone morphogenetic protein 2 (BMP-2)⁸⁹. Human BMSCs expressed alkaline phosphatase *in-vitro* but repeating diffusion chamber studies with the human BMSCs failed to stimulate osteogenesis⁹⁰. Nevertheless when the cells were implanted *in-vivo* on calcium phosphate scaffolds bone formation occurred⁹¹. Bennett et al. performed *in-vivo* diffusion chamber studies on fibroblastic and adipogenic induced colonies derived from the same rabbit bone marrow. Both cell types were able to form bone *in-vivo* indicating that fat and bone cells have a common pre-cursor⁹². Successful *in-vitro* chondrogenic differentiation was performed using low oxygen concentrations⁹³, transforming growth factor- β 3 (TGF- β 3) treatment and densely packing cells into pellets to maintain the cells in a spherical morphology⁴⁷. Due to the ability of the BMSC to differentiate towards mesenchymal tissues, they were later named mesenchymal stem cells⁴⁴.

Although MSCs were first reported by Friedenstein, the first study which proved the existence of a multipotent population of cells in the human bone marrow with capacity to differentiate into fat, bone and cartilage was by Pittenger et al. nearly 40 years later²⁶. Similarly to the observed differentiation of BMSCs to osteoblasts and adipocytes when treated with hydrocortisone, Pittenger also used glucocorticoids to stimulate *in-vitro* differentiation. MSCs were induced towards fat with 1-methyl-3-isobutylxanthine (IMBX), dexamethasone (DEX), insulin, and indomethacin, characterised by the presence of oil red O (ORO) staining lipids within the cells. Osteogenic differentiation, demonstrated by alkaline phosphate activity, occurred when MSCs were treated with DEX, β -glycerol phosphate, and ascorbate, whilst chondrogenesis was induced by culturing MSCs in dense cell pellets, in serum free media supplemented with TGF- β 3, where the pellets contained a matrix rich in type II collagen and proteoglycans. These differentiation conditions are now widely accepted and used for MSC differentiation.

Pittenger examined the tri-lineage potential of six MSC colonies derived from single cell clones²⁶. Each clone had the same cell surface marker expression. Every colony could differentiate into bone, five were fat forming and only two could form cartilage. This again demonstrated the MSC population contained within bone marrow is heterogeneous, although some cells have a tri-lineage potency, others are limited and may be progenitors for a specific mesenchymal tissue.

Additionally MSCs may have a trans-differentiation potential, where under specialised culture conditions or in co-culture with other cell types, can differentiate into somatic cells of differing germ layers. MSCs injected into central nervous system of neonatal mice engrafted within the brain and expressed markers of mature astrocytes and neurons⁹⁴. *In-vitro* this result was repeated by exposing MSCs to beta-mercaptoethanol or dimethylsulfoxide and butylated hydroxyanisole⁹⁵. Treated cells displayed a neuronal phenotype, expressing neuron-specific enolase, NeuN, neurofilament-M, and tau. Morphologically the cells resembled neurons with long processes and filopodia at their extremities⁹⁵. However the extent of the differentiation process was questionable. The transition to a neuronal phenotype was rapid and reversible. When the differentiation conditions were applied to other cells types, cytoplasmic retraction and actin

reorganisation was also observed in fibroblasts, HEK293 cells, rat PC-12 cells, as well as MSCs^{96,97}. Characterisation of untreated MSCs also demonstrated cells subjected to *in-vitro* ageing express neuronal markers⁹⁸, suggesting that the morphological and phenotypic changes observed in the MSCs were likely to be artefacts of the culture system.

In-vivo MSCs may potentially differentiate into cardiomyocytes. Although MSCs injected into the heart of CB17 SCID/beige mice had low engraftment (0.44 % after 4 days), immunohistochemistry revealed the engrafted cells expressed markers β -myosin heavy chain, α -actinin, cardiac troponin T, and phospholamban and levels similar to the host cardiomyocytes⁹⁹. In co-culture with neonatal rat cardiomyocytes in aligned conformations, a proportion of the MSCs differentiate into cardiomyocytes *in-vitro*¹⁰⁰. Dependant upon the alignment the MSCs were conductive and expressed cardiac markers, sarcomeric α -actinin, cardiac troponin I and connexin¹⁰⁰. As with the neuronal differentiation these results have also been questionable¹⁰¹. Although other reports demonstrate the expression of cardiac markers on MSCs, the action potentials are less repeatable^{102,103}, potentially due to the age of cell donor or contaminating CD45 cells.

1.4 The in-vivo cell microenvironment

In-vivo MSCs are situated within specialised niches, a complex environment of ECM, stromal cells, vascular networks and soluble molecules, which maintain their self-renewal capacity and potency. In this environment the MSCs make a plethora of cell-cell and cell-ECM adhesions, whilst *in-vitro* they are cultured in a two dimensional (2D) sheet, on a flat and rigid polystyrene surface that does little to recapitulate the *in-vivo* stem cell micro-environment. Therefore to appropriately engineer and model tissues and organs, it is important to consider the composition and architecture of their *in-vivo* microenvironment and how these affect the cellular behaviour and the properties of the tissue.

1.4.1 The extracellular matrix

The ECM is compiled from a mix of proteoglycans and fibrous proteins, and has broad variation between tissues. Collagen is the most abundant protein within the ECM, providing the general structure of tissues, in the form of fibrils and networks. Collagen types I, II, III, V and XI are fibril forming, creating structures that resist shear, compressive and tensile strains and therefore are found in tendons, cartilage and skin. Collagen I is the most abundant and found in most tissues. Networks of collagen types IV, VIII and X are found in basement membranes providing surfaces for cell attachment and organising other ECM components into barriers between tissues^{104,105}.

The basic unit of all collagens is the collagen molecule, a triple helix of polypeptide alpha chains, where each polypeptide chain contains approximately 100 amino acids (Figure 1-2). The collagen I triple helix contains two α_1 chains and a α_2 single chain, it is 300 nm in length and 1.5 nm wide. For every type of collagen the basic molecule contains three alpha chains, where these may or may not be identical (Figure 1-2,

Table 1-1). The amino acid sequence of each chain contains repeats of glycine-X-Y, where the glycine residue lies in the centre of the helix allowing the chains to tightly pack together, and X and Y are generally proline or hydroxyproline. The fibril forming collagens contain uninterrupted Gly-X-Y triplets, resulting in banded fibrils¹⁰⁶. When secreted from the cell the individual collagen molecules laterally assemble into collagen fibrils, crosslinked together through aldol bonds. Collagens IX and XII contain interruptions in the alpha chains, where non collagenous sequences are present. These collagens associate with the fibril forming collagens.

Alongside collagen, elastin fibres are present in the skin and blood vessel to provide further resilience and as their name suggests, elasticity¹⁰⁷. Linking the various ECM components together is a series of adhesive proteins, including laminin, fibronectin and tenascin^{108,109}. These proteins are essentially the glue of the ECM, binding collagen and cells and playing roles in cell adhesion, migration and differentiation. Deficiencies in these proteins can result in the weakening of tissues and muscular dystrophies¹¹⁰.

Type	Chain	Molecular structure	Supermolecular structure	Localisation
I	$\alpha 1(I)_2, \alpha 2(I)$	300 nm	67 nm banded fibrils	Soft tissues, bone
II	$\alpha 1(II)_3$	300 nm	Small 67 nm banded fibrils	Cartilage, vitreous humor
III	$\alpha 1(III)_3$	300 nm	Small 67 nm banded fibrils	All soft tissues
IV	$\alpha 1(IV)_2, \alpha 2(IV)$	390 nm C globular domain	Non-fibrillar networks	All basement membranes
V	$\alpha 1(V), \alpha 2(V), \alpha 3(V)$	300 nm N globular domain	Small fibres	Most intestinal tissues
VI	$\alpha 1(VI), \alpha 2(VI), \alpha 3(VI)$	150 nm N and C globular domains	Microfibrils, 100 nm banded fibrils	Most intestinal tissues
VII	$\alpha 1(VII)_3$	450 nm	dimer	Anchoring fibrils
VIII	$\alpha 1(VIII)_3$?	networks	Some endothelial cells
IX	$\alpha 1(IX), \alpha 2(IX), \alpha 3(IX)$	200 nm N globular domain	Associated with fibril forming collagens	cartilage
X	$\alpha 1(X)_3$	150 nm C globular domain	Small fibres, networks	Hypertrophic cartilage
XI	$\alpha 1(XI), \alpha 2(XI), \alpha 3(XI)$	300 nm	Fibril forming	cartilage

Table 1-1: Structures and composition of collagen proteins.
Adapted from¹⁰⁶.

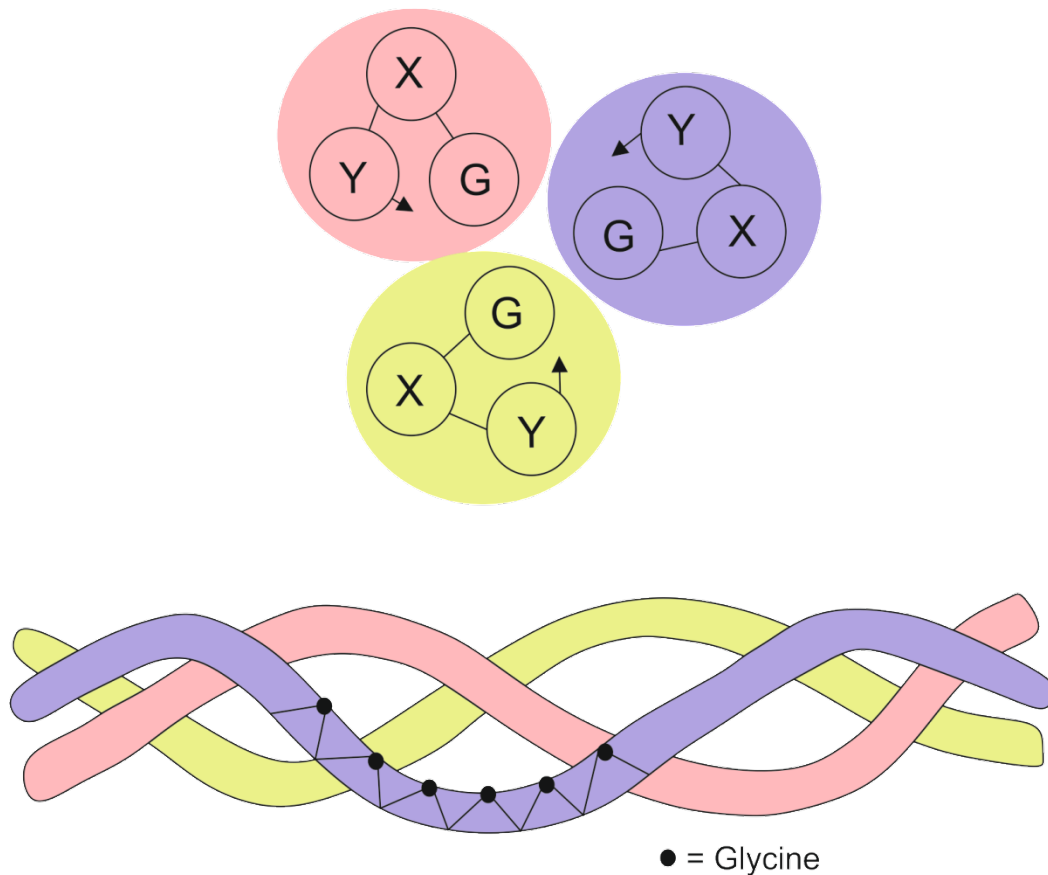


Figure 1-2: Structure of the collagen molecule.

Cross-section through and side view of a collagen triple helix. In each type of collagen the basic molecule is a triple helix of polypeptide alpha chains. The amino acid sequence is generally repeats of Gly-X-Y, where the small glycine residue is situated in the center of the helix.

Most of the extracellular space within tissues is occupied by large aggregates of proteoglycans, which consist of a core protein, with glycosaminoglycan (GAGs) side chains, which vary from one side chain in decorin, to over 100 in the larger cartilage proteoglycan, Aggrecan. GAGs are formed of repeating disaccharides, containing an amino sugar and numerous sulphated and carboxylate sugars, which give proteoglycans their high negative charge. As a result of the high charge density and structure, proteoglycans remain unfolded as large extended structures, providing additional compressive strength within tissues and maintaining large volumes of water. This high negative charge also causes an osmotic pressure and proteoglycans can guide the

migration of small molecules within the ECM. Within the ECM the small leucine-rich proteoglycans also organise and stabilise the collagen network.

1.4.2 Cell-ECM Adhesions

Many cell types are dependent upon attachment and cell-cell and cell- ECM adhesions to provide signals to instruct cell fate. In the absence of a surface to adhere too, cells undergo controlled cell death by anoikis¹¹¹. Cells adhere to the ECM through transmembrane receptors of the integrin family, which become activated and linked to the actin cytoskeleton of the cell through the anchoring protein talin (Figure 1-3). Integrins are composed of an α and β subunit, currently 18 α and 8 β subunits have been identified that assemble into 24 different integrins¹¹². Integrins are not specific for one particular ECM component, the ligands expressed on the ECM can be bound by more than one integrin, and most ECM proteins can bind to several integrins, therefore identifying their specificity is complex. The amino acid sequence, arginine-glycine-aspartic acid (RGD) is a common ligand found on fibronectin, laminin, vitronectin and tenascin¹¹³. As it can be recognised by many integrins and cell types, and is only 3 amino acids long, enabling easy synthesis, the RGD sequence is frequently used in cell adhesion studies and often introduced into polymeric biomaterials to improve cell adhesion¹¹⁴. Similarly collagen I has a short recognition sequence for integrins $\alpha_1\beta_1$ and $\alpha_2\beta_1$ ¹¹⁵.

Where there are integrin ligands at high density, they cluster together to form tight focal adhesions, enhanced by the binding of vinculin to the integrin/talin complex^{116,117}. Using the RGD sequence, 440 nm, the 'Hubbell limit', was found to be optimal for integrin binding, and a ligand spacing of 140 nm was shown to be optimal for the development of focal adhesions¹¹⁷⁻¹¹⁹. Associated with focal adhesions is a large complex of molecules forming the adhesome, which transmits the action of cell adhesion into re-organisation of the actin cytoskeleton and multiple signalling pathways (Figure 1-3)¹¹⁹. Activation of the focal adhesion kinase by integrin binding regulates GTPases of the Rho and Arf families, which can subsequently modulate cell adhesion and migration through actin polymerisation¹²⁰.

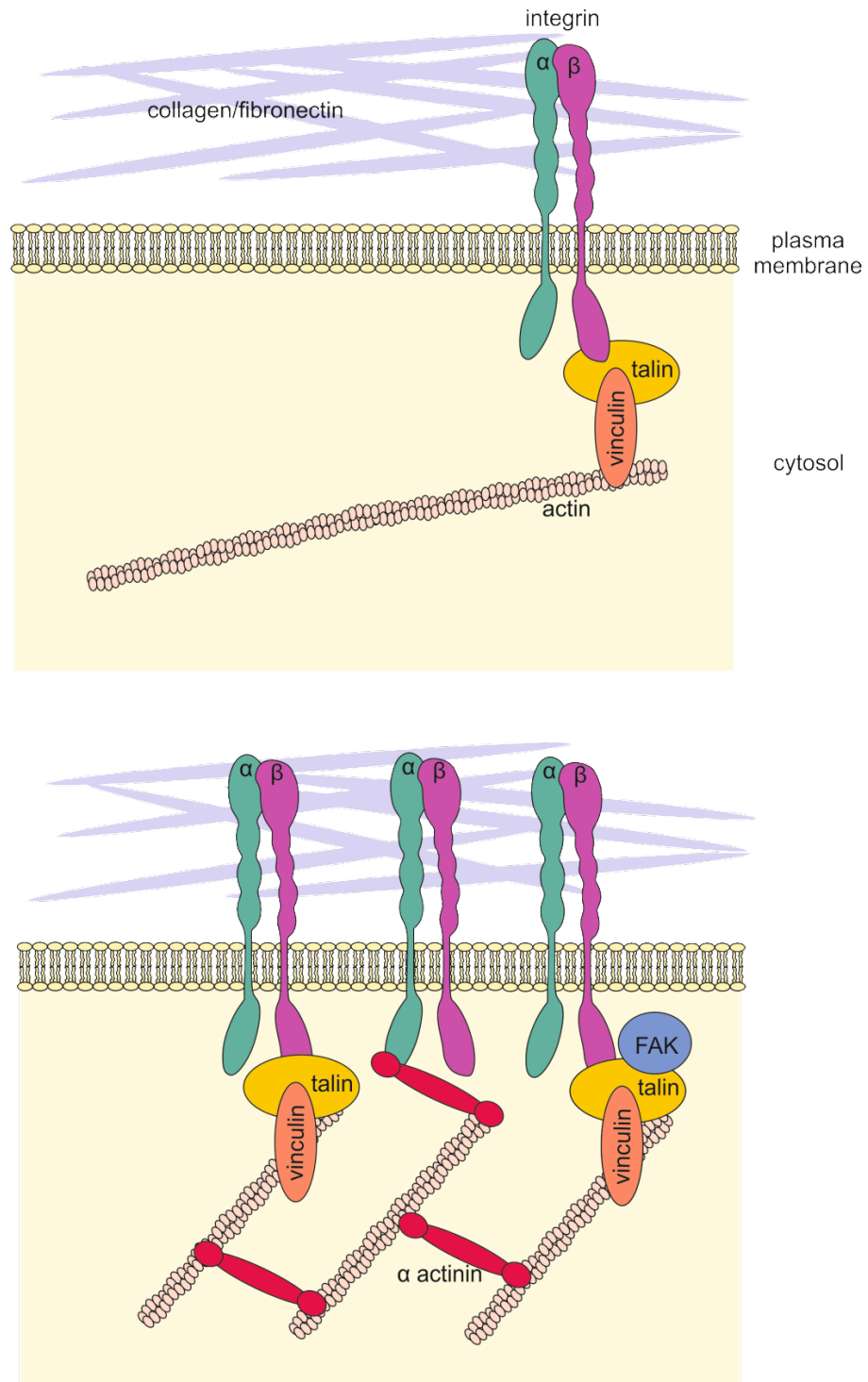
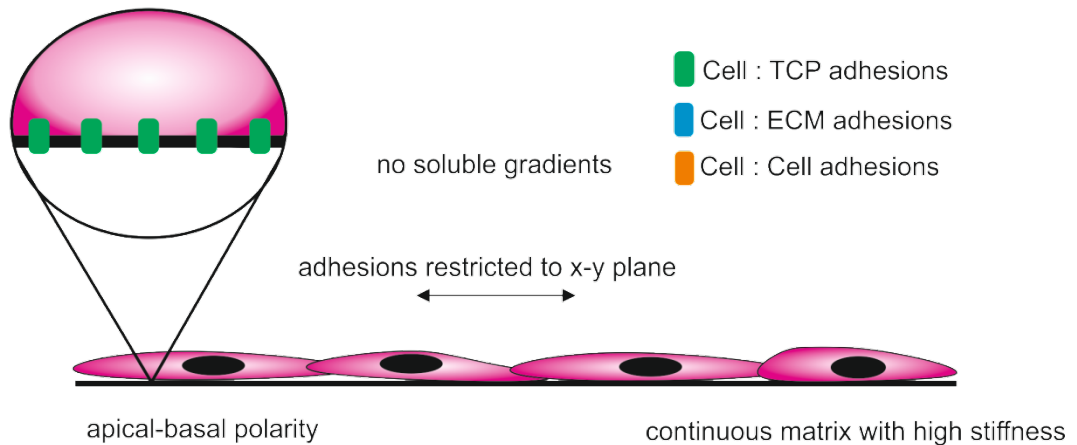


Figure 1-3: Cell-ECM adhesions.

Cells bind to the ECM via integrins, which recognise ECM ligands (amino acid sequences, for example RDG) in collagen and fibronectin within the ECM. Within the cell the cytoplasmic domain of the integrins is activated by talin and vinculin, linking the ECM to the cell actin cytoskeleton. Where a high density of ECM ligands is present, integrin clustering occurs leading to the formation of a focal adhesion. Within the cell the integrins are associated with the focal adhesion kinase(FAK), and the actin cytoskeleton re-organises into aligned stress fibres.

2D



3D

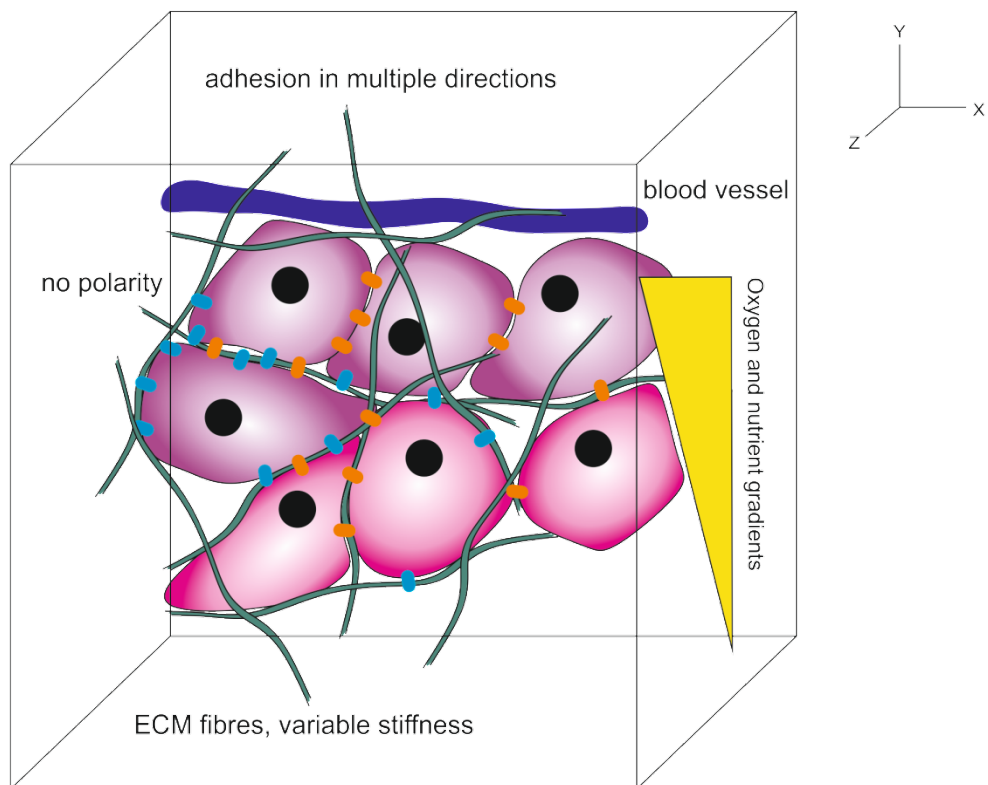


Figure 1-4: Differences in 2D cell culture compared with *in-vivo* and 3D culture conditions
 In 2D culture cells are grown as a flat monolayer on rigid TCP. The cells make adhesions with the TCP and minimal cell-cell adhesions only in one plane. *In-vivo*, or 3D culture cells make multiple cell:ECM and cell:cell adhesions, in multiple directions. The cells are cuboid in morphology and oxygen/nutrient/metabolite gradients also exist the further the cells are from the blood supply/air interface.

1.5 2D versus 3D cell culture

Cell adhesion differs with regards to cells interacting with synthetic surfaces, as these do not contain the ligands found in natural ECM. Polystyrene tissue culture plastic (TCP) is probably the most frequently used synthetic surface for cell attachment. Polystyrene is a hydrophobic surface, and is therefore plasma treated to give the surface a negative charge and stimulate protein absorption. When cultured in serum containing media, fibronectin, vitronectin and other adhesive proteins found on the cell surface can adhere to the charged TCP, and subsequently cells can indirectly adhere via integrin binding to the proteins. In the absence of serum, the attraction of cell surface proteins to the charged surface can also promote cell adherence. Alternatively TCP can be coated with collagen or fibronectin prior to cell culture to provide a cell adhesive surface. Furthermore during culture cells synthesise ECM components, which can also bind the TCP and permit cell adhesion of proliferating and migratory cells. Cell culture on TCP also differs from the *in-vivo* microenvironment, as the cells are cultured in 2D flat monolayers. The cell-cell and cell-TCP interactions are limited to one side of the cell, and the cells become spread and flattened, exhibiting morphologies that differ from the *in-vivo* microenvironment (Figure 1-4).

When grown within a 3D scaffold cells are in a more natural environment, with similarities to their *in-vivo* microenvironment. Rather than the apical-basal polarisation cells experience when cultured on TCP, scaffolds promote multi-directional cell-ECM adhesions and cell-cell interactions in multiple directions to neighbouring cells. Although some cells types, for example epithelial cells, where the polarisation is relevant, for most cell types, including MSCs, it is unnatural. Therefore cells also exhibit a different morphology than in 2D, depending on the cell type and availability of ligands for cell attachment (discussed in more detail later) cells are more cuboidal and rounded in morphology¹²¹. This change in morphology can result in a change in cell phenotype, where the most significant example of this is chondrocyte cell culture. When grown on 2D surfaces, chondrocytes dedifferentiate, when re grown back in 3D culture within gels their physiological phenotype is then restored¹²².

Accompanying the change in adhesions and cell shape, are changes in the cytoskeleton of the cell¹²³. As previously discussed, integrin binding and the formation of focal adhesions are linked directly to the actin cytoskeleton of the cell¹¹⁶. Clusters of focal adhesions induce the formation of aligned stress fibres within the cell cytoskeleton. Through these adhesions any movement within the ECM is directly transduced into the cell, via mechanotransduction¹²⁴. In response to forces, cell-cell, and cell-ECM adhesions the cytoskeleton of the cell is a dynamic structure which constantly adapts to its environment. Within the cell the Rho G-proteins (Rho, Rac) have been shown to be involved in changes in gene expression with changes in the cell shape. They play roles in actin polymerisation, focal adhesion formation and cytokinesis¹²⁵. Rho and Rac activate the serum response factor (SRF) and the transcription factor NF- κ B¹²⁵, and it has been shown endogenous expression of RhoA increases in differentiating MSCs in response to cell shape¹²³. Therefore in 2D, where the substrate is flat and static and cells are flattened and these influences on cell behaviour are likely to be minimal or absent.

Furthermore the 3D environment provides stimuli to cells that may not occur in 2D. Induction of chondrogenesis in MSCs and chondrocytes requires a 3D pellet of cells to promote cell condensation and differentiation²⁶. The sprouting of new blood vessels in angiogenesis is promoted by hypoxia and gradients of pro-angiogenic factors such as vascular endothelial cell growth factor and angiopoietin-1, which are also absent in 2D^{126,127}. In 2D culture, generally speaking, every cell is exposed to the same concentrations of nutrients and oxygen, as every cell has a similar surface area interacting with the surrounding environment, i.e. the cell culture media. In 3D scaffolds and in-vivo gradients of oxygen and nutrients are present¹²⁸. The further a cell is located from a blood supply or the deeper it is within the scaffold, the less oxygen and nutrients will be available as they are unable to diffuse into the tissue. Therefore a cell located closer to a blood supply may be phenotypically different than another at a greater distance under hypoxic conditions^{129,130}.

1.6 Using matrix properties to direct cell fate

In standard *in-vitro* assays of MSCs the growth media is supplemented with soluble molecules to promote differentiation, however cell behaviour and differentiation can also be controlled by physical factors. The microenvironment in which a cell is found influences its behaviour, where cell shape, adhesions, substrate mechanical properties, substrate topography and applied forces all act together to determine cell fate. Therefore it is important to understand these physical mechanisms when designing biomaterials, to provide the appropriate physical cues and improve the biomimicry of engineered tissues.

1.6.1 Matrix elasticity

Most tissues within the body are soft and viscoelastic, having mechanical properties similar to both a viscous liquid that can flow when deformed, and an elastic solid that is able to deform and return to its original structure when the stress is removed. Adipose and brain tissue are examples of the softest materials in the body, and muscle, cartilage and tendon are at the other end of the spectrum (Table 1-2). The mechanical properties of each tissue are essential for function; tendon and ligament require high elasticity and strength to withstand the tensile forces exerted upon them during movement.

Variation in the elasticity of substrates that cells are adhered to, affects their differentiation. When a cell makes adhesions onto a soft hydrogel, the gel has low resistance to the forces exerted onto it, and can be easily deformed and give way, resulting in a rounded cell with few adhesions and an absence of focal adhesions. On stiffer materials cells are less able to contract the matrix and spread out, making multiple focal adhesions with the gel¹³¹. With an increase in focal adhesions the actin cytoskeleton within the cell is under greater tensile forces, and becomes aligned and contains pronounced stress fibres. Substrates with variable mechanical stiffness have been fabricated from acrylamide gels coated with collagen or fibronectin, to allow for cell attachment. When fibroblasts, epithelial and endothelial cells were seeded at low density onto these surfaces, the degree of cell spreading, focal adhesions and actin stress fibres increased with surface stiffness^{131,132}. A similar effect is observed in 3D collagen

systems. Fibroblasts within stiff gels anchored to TCP, contained pronounced stress fibres. In free floating gels where the fibres were unconstrained, the cells were rounded and no actin bundles were observed¹³³.

Tissue	Tissue source	Elastic Modulus
Achilles tendon	Rat	310 MPa (T)
Articular cartilage	Bovine	950 KPa (C)
Skeletal muscle	Rat	100 KPa (T)
Carotid artery	Mouse	90 KPa (P)
Cardiac muscle	Mouse	20 - 150 KPa (T)
Skeletal muscle	Mouse	12 KPa (A)
Lung	Guinea pig	5-6 KPa (T)
Breast tumour	Human	4 KPa (C)
Kidney	Swine	2.5 KPa (R)
Breast	Human	2.2 KPa (I)
Liver	Human	640 Pa (C)
Brain	Swine	260 - 490 Pa (I)
Lymph node	Human	120 Pa (V)
Fat	Human	17 Pa (I)

Table 1-2 Elastic moduli of several tissues and organs.

As determined by compression (C), tension (T), perfusion (P), indentation (I), rheology (R), AFM (A), indentation (I) and vibrational resistance (V)¹³⁴.

Culturing of MSCs on acrylamide gels of increasing elasticity, directed their differentiation towards either neurons, myoblasts and osteoblasts¹³⁵. MSCs varied in morphology on the different substrates, on the gels approximating brain tissue (E = 0.0-1 KPa) MSCs were highly branched. As the elasticity increased to mimic muscle tissue (E = 8-17 KPa), MSCs were spindle shaped and on the stiffest matrices (E = 25-40 KPa), comparable to osteoid, MSCs displayed an osteoblastic cuboidal morphology. Accompanying the morphological changes were the expression of early stage lineage specific RNA transcripts¹³⁵. Addition of blebbistatin or myosin light chain kinase inhibitor, ML7, at the time of cell plating, prevented the matrix specific cell spreading, indicating non muscle myosin II is involved in matrix directed differentiation. Therefore suggesting MSCs can be directed towards a specific lineage by matching the mechanical properties of the substrate to the native tissue.

Matrix elasticity is also able to influence cell migration, akin to chemotaxis. 3T3 cells cultured on collagen/acrylamide matrices which has a gradient of elasticity, preferentially migrated from the soft to stiff regions and in doing so increased in speed and spreading¹³⁶. Cells on the stiffer gel retracted at the soft gel boundary, and changed orientation. There are exceptions however to this behaviour, activated neutrophils grown on acrylamide gels of variable stiffness are able to spread out and adhere to even the softest gels (2 Pa) as well as on glass surfaces, suggesting some cell types are able to spread on matrices without exerting high traction forces¹³². Likewise malignant cells are able to grow in a substrate independent manner. H-ras-transformed NIH 3T3 cells could spread and were more metabolically active on soft substrates compared with untransformed cells¹³⁷.

1.6.2 Matrix porosity and pore size

To remain viable cells require a supply of oxygen and nutrients and removal of metabolic waste products. *In-vivo* localised vasculature performs this role. Cell scaffolds need to contain a level porosity to allow mass transfer to occur, as cells situated 100 – 200 μm from a capillary or oxygen supply will not survive¹³⁸. Porosity and pore size also effects the ability of cells to migrate into matrices¹³⁹. Where the pore size is too small, cells are unable to migrate into the centre of the matrix and preferentially adhere to the periphery of the scaffold. Conversely when the pore size is too large the density of ligands for cell attachment may not be high enough to allow cells to properly adhere^{140,141}. Furthermore cells require pores large enough to permit cell-cell interactions and voids to produce ECM¹⁴².

The effect of pore size on attachment can be cell type dependent¹⁴³. Fibroblasts, smooth muscle cells (SMC) and micro-vascular endothelial cells (MVEC) cultured on collagen – GAG matrices with varying pore sizes (106-150, 63-106, 38-63 and $>38 \mu\text{m}$) and porosity (99% and 75%) had differing behaviour. Every cell type was unable to migrate into the centre of the 75% porosity matrices. On the 99% porosity matrices fibroblasts were adherent on all pore sizes and displayed no variation in metabolic activity. SMCs favoured matrices with larger pore size, whilst MVECs showed little difference in

metabolic activity between matrices but could assemble into multicellular networks as the pore size decreased. Every cell type was unable to migrate into the centre of the 99% porosity matrices where the pore size was less than 38 μm ¹⁴³.

MC3T3-E1 osteogenic cells were also cultured on collagen-GAG matrices with variable pore sizes (mean pore size 85 - 325 μm)^{144,145}. Cell attachment and proliferation showed a non-linear dependence with pore size. Initially cell numbers were high on matrices with 120 μm pores, low on matrices with intermediate pore sizes and were at their maximum in matrices with 325 μm pores. After 7 days the number of cells in each matrix increased linearly with pore size. These results suggest osteoblasts initially adhere strongly to small pores, however they are unable to migrate within the matrix and therefore the cell number remains low, while in matrices with larger pores, cells can migrate through the matrix and proliferate resulting in higher cell number¹³⁹. The effect of the pore size on osteogenesis was not examined in this study. Chondrocytes seeded *in-vitro* on collagen I sponges of variable pore size de-differentiated with time in culture. However in sponges with smaller pores (20 μm), a larger number of chondrocytes maintained the chondrogenic phenotype displaying a rounded morphology, and expressing higher level of GAGs¹⁴⁶.

MSCs seeded onto silk scaffolds with varying porosity with depth and cultured in osteogenic media, initially formed a greater number and thinner trabecular like structures in the small pores (112-224 μm) however with 5 weeks in culture there was no significant difference between the small and large pores (400 - 500 μm)¹⁴⁷. *In-vivo*, pore size had a more pronounced effect on osteogenesis. Osteocalcin content and alkaline phosphatase activity, markers of osteogenesis, peaked in hydroxyapatite scaffolds loaded with BMP-2 scaffolds with pore sizes of 300 – 400 μm ¹⁴⁸. Capillaries were also present in some of the larger pores. Differentiation of MSCs in honeycomb BMP-2 hydroxyapatite scaffolds, containing a series of tunnels of differing width also showed how the size of voids influenced osteogenesis. In small tunnels (90 -120 μm) cartilage tissue was found throughout, bone formation only occurred on the periphery or within wider tunnels (300 – 400 μm) where vasculature was also present¹⁴⁹. Taken together these results demonstrate pore size not only effects cell attachment but also the

availability of nutrients through diffusion and capillary infiltration in larger pores *in-vivo*, with chondrogenesis occurring in the hypoxic areas of scaffolds.

It is important to consider cell seeding of scaffolds with regards to pore size and porosity. Cell encapsulation during *in-situ* matrix formation, which is common among stimuli responsive hydrogels should lead to a uniform distribution of cells. Therefore the range of pore sizes required for the matrix would be smaller, as larger pores would not be required to permit cell migration throughout the matrix. However *in-situ* encapsulation of cells may force cells into smaller pores than they would migrate into and exert mechanical forces onto the cells also directing their behaviour. Also highly porous scaffolds implanted *in-vivo* may have poor mechanical properties.

1.6.3 Cell shape

As matrix stiffness and pore size, influences cell spreading and morphology, they are closely linked to the impact of cell shape on cellular behaviour. Although *in-vivo* adipose tissue and cartilage have completely different mechanical properties, MSC differentiation towards adipocytes and chondrocytes both favour rounded cell morphologies, which have been achieved through culturing on soft acrylamide gels¹⁵⁰. Therefore simply mimicking the ECM stiffness may be less important compared with how the matrix stiffness, porosity and topography contribute together to effect cell shape. Changes to cell shape and adhesions directly correlate with changes inside the cell and re-organisation of the cytoskeleton, which in turns regulates gene expression through Rho proteins¹²⁵.

Using micro-patterned substrates with adhesive fibronectin regions, the effect of cell shape and size on cell behaviour has been examined. Endothelial cells seeded onto such surfaces spread to the size of fibronectin regions, where apoptosis decreased with increasing the size of the adhesive area¹¹⁸. The cell shape, and metabolic activity also increased when the endothelial cells were cultured on arrays of regularly spaced fibronectin islands, allowing cell spreading over a wide area. Focal adhesions were concentrated on the fibronectin islands. MSC differentiation is also affected when

adhered to similar surfaces. MSCs cultured on large islands, were able to spread and make multiple substrate adhesions, differentiating towards osteoblasts, whilst MSCs cultured on small regions, were unable to spread and displayed adipogenic commitment¹²³. As cell density can also effect cell spreading, shape and size it is not surprising that it also affects MSC differentiation. Cultured in a combined adipogenic and osteogenic media, cells at high density which are less able to spread, differentiate towards adipocytes, while cells at low density can spread and differentiate towards osteoblasts^{151,152}. Chondrogenesis is also affected by cell shape. In classical *in-vitro* assays of MSC differentiation, adipogenesis and osteogenesis can be induced from 2D monolayers of MSCs using a cocktail of soluble factors, whilst chondrogenic differentiation requires the cells to be maintained in a rounded state, using high density cell pellets⁴⁸. Similarly chondrocytes will lose their *in-vivo* phenotype when removed from cartilage and cultured in 2D monolayers¹⁵³. Culturing of embryonic stem cells (ESCs) at a high density, preventing cell spreading, also promotes chondrogenesis. Under these conditions, the cells have rounder nuclei and express cellular condensation and chondrogenic markers, type II collagen and SOX9¹⁵¹.

The nano-scale topography of cell culture surfaces has also been shown to affect cell shape. Micro-patterned acrylamide hydrogels with alternating 100 μm regions of variable stiffness, to mimic neurogenic and myogenic ECM's were fabricated to assess the impact of both topography and stiffness on ADSC behaviour. ADSCs preferentially adhered, aligned and elongated on the stiffer myogenic gel sections, expressing myogenic marker β -tubulin¹⁵⁴. Surfaces patterned with pits and pores have been shown to stimulate osteogenesis of MSCs in the absence of soluble factors. On the patterned surfaces MSCs have a less fibroblastic morphology, and show greater spreading, adhering to the surface features^{155,156}. In a similar manner to MSCs on the large fibronectin adhesive regions, nickel patterned surfaces are also osteogenic. MSCs spread out along the surface features and have a high number of focal adhesions and actin stress fibres¹⁵⁷. Surprisingly chondrocytes cultured on the same patterned surfaces, exhibited a rounded morphology, maintaining their *in-vivo* phenotype, possibly due to the limited areas for adhesion, in contrast to the MSCs, which spread across the pores¹⁵⁸.

However the caveat with most of these studies is they are performed in 2D environments. In 3D, the cell surface for attachment is unlikely to be flat and additional cell-cell and cell-ECM contacts would occur in all directions. They are however good examples of probing *in-vivo* cellular behaviour with respect to one feature. In summary, the elasticity, surface patterning, and porosity of materials can all contribute to cell attachment, the shape and size a cell adapts. This provides outside-in-signalling to direct cellular behaviour.

1.7 Cell scaffold

The cell scaffold is a template for new tissue growth and repair, providing support to the residing cells. From the above discussion it is clear that scaffolds need to be designed carefully for tissue engineering application. Additionally to directing cell fate, when designing the scaffolds the following must also be considered. Biodegradability: does the scaffold need to remain permanently or be replaced by newly regenerated tissues? and how fast should be scaffold degrade to promote optimal tissue repair? Scaffold mechanical properties: again in addition to directing cell fate the scaffold needs to be mechanically compatible with the environment it is to be implanted within. A scaffold with a low tensile modulus would not be compliant for tendon repair. The main classes of scaffolds are polymers, encompassing natural and synthetic materials, ceramics and glasses. Decellularised tissues are also commonly used, falling into the natural polymer category. These 3D materials are typically fibrous networks or porous structures.

Ceramics and bioactive glasses and glass ceramics are popular candidates for bone tissue engineering scaffolds. These are crystalline scaffolds made from inorganic compositions, and range from non-porous, inert materials such as aluminium oxide, to non-porous surface active ceramics that attach to the bone surface¹⁵⁹. The original bioglass was developed by Larry Hench and is composed of silicon dioxide, sodium oxide, calcium oxide and phosphorous pentoxide in varying proportions¹⁶⁰. The silicon dioxide content influences the formation of the glass and its bioactivity. Naturally occurring hydroxyapatite present in teeth and bones, has an osteoinductive effect, and therefore it is produced synthetically for use as a bone scaffold, or as coating for bone

scaffolds implants¹⁶¹. Cells are seeded onto the glasses after fabrication and allowed to infiltrate into the scaffold.

Polymeric materials are popular scaffold choices as they can be designed and tailored to control the chemical and structural properties of the resulting materials. Biodegradable PGA/PLA systems have tuneable degradation rates based on the composition of PGA versus PLA¹⁶². For cell attachment, RGD sequences can incorporate into synthetic polymers during synthesis¹⁶³. Tuneability in the structural and physical properties of the polymers is also beneficial for the development of methods for fabrication. 3D printing for example requires polymers with optimal viscosity for droplet formation and subsequent gelation/setting. Polymer scaffolds can be fabricated as fibrous networks by electro-spinning or cross-linked into hydrogels by chemical cross-links or physical cross-linking¹⁶².

1.8 Hydrogels as cell scaffolds

Hydrogels are an attractive choice for use as cell scaffolds. These are highly hydrophilic 3D polymer networks, which can maintain large volumes of water and have visco-elastic mechanical properties similar to soft tissues. IUPAC defines a hydrogel, as a ‘gel in which the swelling agent is water’¹⁶⁴. They can be made from natural or synthetic polymers or a combination of both. Hydrogels are formed from polymer chains joined together into a network through crosslinking by chemical covalent bonds or through physical interaction between chains, such as entanglements, electrostatic attractions, van der Waals and the hydrophobic effect. They can be as simple as a mix of single linear polymers that are chemically crosslinked, and may contain copolymers to add additional functionality. They may also be made from polymers with branching and grafts to modify the size and shape of the networks formed, or exist as interpenetrating polymer networks, where two distinct polymer networks are formed around each other. Further information about the different hydrogels used in tissue engineering and regenerative medicine can be found in the comprehensive reviews by Mooney^{165,166} and Hubbell¹⁶⁷.

1.8.1 Biological hydrogels

One obvious method to mimic the environment of cells *in-vivo* is to use a natural ECM or components from it. Hydrogels can be formed from collagen, fibrinogen and GAGs as well as gels made from components of algae and seaweed. ECM based hydrogels offer advantages over synthetic materials as they are biocompatible and already contain ligands for cell attachment and migration.

Collagen and gelatine

Collagen I is the most common biological based hydrogel used as a cell scaffold. It is the most abundant protein in the ECM and can easily be extracted from rat-tail tendon^{168,169} and bovine dermis¹⁷⁰. Dissolving rat tail tendons in acetic acid breaks down the collagen fibrils into the collagen molecules. These can self-assemble *in-vitro* in a temperature dependent manner when neutralised. As the gel formation is temperature dependent cells can be encapsulated within a collagen matrix during the gelation.

To permit cell migration and mass transfer, collagen gels containing a low mass fraction are required for cell culture (0.2 -0.4 wt%). At these concentrations the gels are mechanically weak and prone to cell contraction, and therefore unsuitable for some applications which require slower degradation and remodelling, or for fabrication of micro- and nano-structured scaffolds. Increasing the mass fraction of collagen is one method to improve the mechanical strength of the resulting gel. Equilibrium moduli of collagen gels prepared at 37 °C, increased from 30 Pa for a 3 wt% gel to 1800 Pa for a 20 wt% gel¹⁷¹. This increase in mechanical strength was attributed to an increase in fibre numbers, as there was no change in fibril diameter when the concentration was increased. The high mass fraction gels displayed some biocompatibility, due to the increase in fibre density and therefore a probable decrease in pore size and mass transfer, the remodelling and cellular invasion in the gels was significantly decreased¹⁷¹.

Changing the gelation temperature of the collagen gels may also increase their mechanical strength. Initially small numbers of collagen molecules laterally nucleate

together followed by growth into fibrils. At lower temperatures the lag phase during nucleation is extended as the hydrophobic effect is weakened and lateral growth dominates, leading to larger collagen fibrils. There are conflicting results over the effect of larger fibrils on mechanical strength, where Yang et al. have shown low temperature gelation and larger fibrils increases mechanical strength¹⁷², whilst Raub et al. found the opposite¹⁷³.

Collagen can be denatured by hydrolysis, which disrupts the triple helix of the collagen molecules to produce gelatine an alternative collagen based hydrogel¹⁷⁴. The denaturing process is irreversible; therefore gelation is not possible without the use of glutaldehyde to crosslinks the molecules to form hydrogels. As no fibrillar assembly occurs either in gelatine hydrogels they are mechanically weak compared with collagen.

Polysaccharide gels

As another major component of the ECM, and their ability to maintain large volumes of water, hyaluronan (HA) and GAGs are common choices for hydrogels. HA is a non-sulphated linear polysaccharide containing repeats of β -1,4-D-glucuronic acid and β -1,3-N-acetyl-D-glucosamine, and is involved in wound healing and regeneration *in-vivo*, as well as promoting angiogenesis (Figure 1-5)^{175,176}. As HA is water soluble it requires cross-linking to form gels. The hydrogels can degraded and remodelled *in-vivo* by hyaluronidase¹⁷⁷.

Hydrogels can also be made from naturally occurring polysaccharides, chitosan and alginate from the exoskeletons of crustaceans and brown algae respectively (Figure 1-5). In contrast

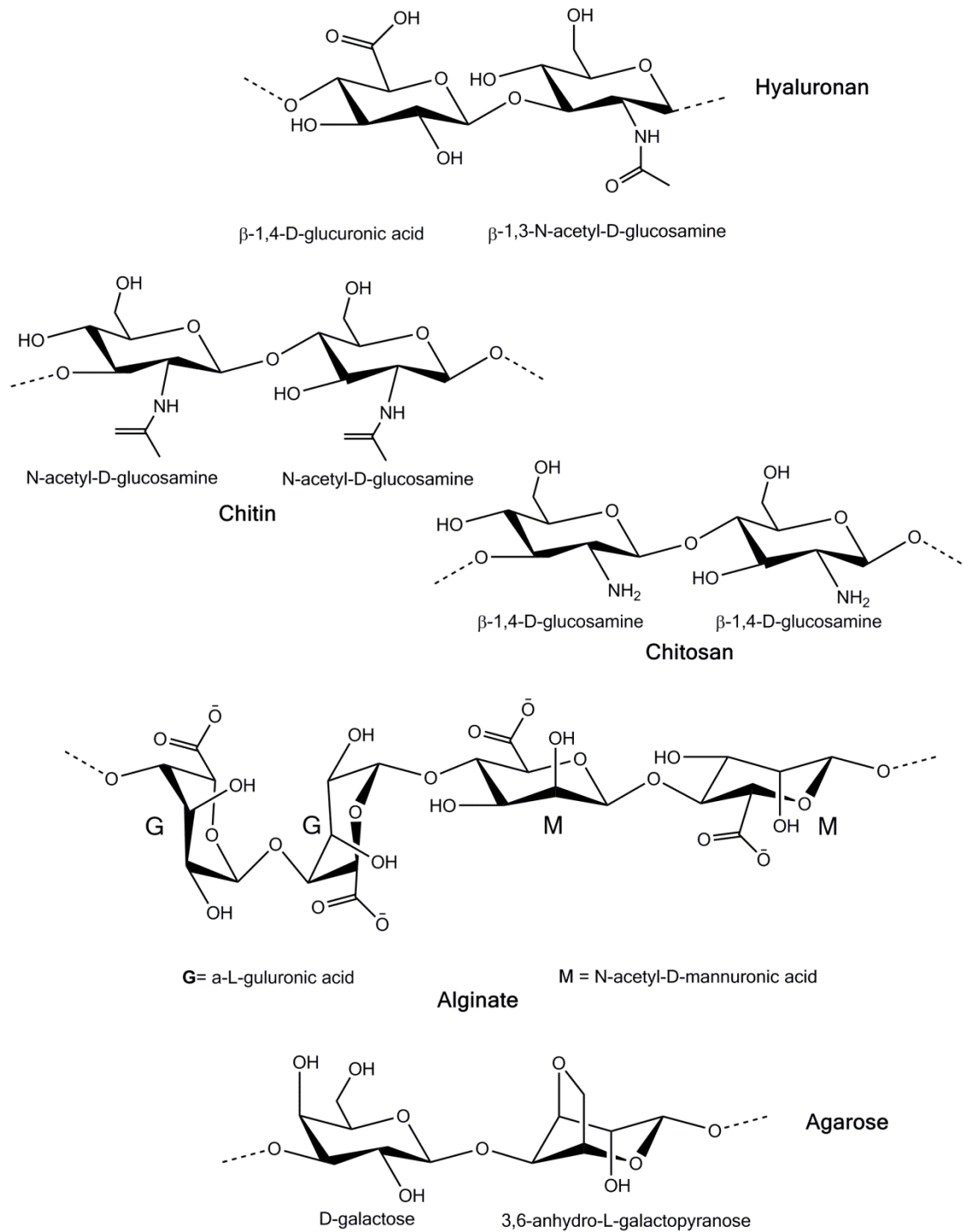


Figure 1-5 Chemical structures of polysaccharide based gels. Hyaluronan contains repeats of β -1,4-D-glucuronic acid and β -1,3-N-acetyl-D-glucosamine. Chitin contains a mixture of chitin (N-acetyl-D-glucosamine) and deacetylated chitosan (β -1,4-glucosamine), dependant on the the degree of deacetylation. In alginate sugars exist in homopolymeric blocks of α -L-guluronic acid and β -1,4-D-mannuronic. Agarose is composed of D-galactose and 3,6-anhydro-L-galactopyranose.

to HA chitosan contains a random distribution of saccharides, β -1,4-glucosamine and N-acetyl-D-glucosamine, dependant on the degree of deacetylation. Alginate contains homopolymeric blocks of α -L-galuronic acid and β -1,4-D-mannuronic. Both require addition of ionic species in order to form gels, chitosan through complexes with polyelectrolytes¹⁷⁸, and alginate with divalent cations such as calcium¹⁷⁹. The properties of the resulting hydrogels are determined by the ratio of each saccharide unit, which varies between sources, and their molecular weight¹⁸⁰. Chitosan gels can be degraded *in-vivo* by lysozyme. Although alginate gels are not degradable, loss of calcium ions results in collapse of the gel, therefore many alginate gels are also chemically crosslinked. Without modification alginate gels are not cell adhesive, and are commonly functionalised with adhesive ligands such as RGD sequences¹⁷⁹, while the positive charge of chitosan at physiological pH promotes cell adhesion.

Agarose is another naturally derived polysaccharide extracted from seaweed and composed of D-galactose and 3,6-anhydro-L-galactopyranose (Figure 1-5). It is commonly used for electrophoresis and non-cell adhesive coatings for TCP as it not cell adhesive. Agarose was one of the first hydrogels used to maintain chondrocytes *in-vitro* as the cells were unable to adhere and spread, and maintained their *in-vivo* phenotype¹²².

1.8.2 Synthetic Hydrogels

However the use of naturally occurring materials as scaffolds does have its limitations. Natural hydrogels can be quickly remodelled and degraded by cell secreted proteases and are generally mechanically weak, unless used at high concentrations which do not permit mass transfer. They also have the risk of disease transmission from animal derived materials. Synthetic polymers are an alternative, their chemistry and architecture can be tailor made and tuned to vary water content, mechanical properties and degradation rates to create hydrogels fit for purpose. This includes the addition of biological molecules and peptide sequences to improve cell adhesion and behaviour. Synthetic hydrogels have been used in contact with body for many years, poly(2-hydroxyethyl methacrylate) (PHEMA) has FDA approval and is used by large numbers of the population in the form of contact lenses¹⁸¹.

Furthermore many hydrogels are stimuli-responsive and undergo conformation or chemical changes in response to an external stimulus. This is very advantageous for use in regenerative medicine, as hydrogels networks can be formed in response to temperature change and pH, stimuli that exist within the body, rather than by use of crosslinking that often requires harsh chemical conditions in which cells and biological materials may not survive. Therefore stimuli-responsive polymers have many opportunities in biological systems. The most researched examples to date include 1) cell encapsulation in polymer solutions prior gelation to obtain uniform distributions of cells, 2) subsequent cell release for hydrogels analysis by reversing the stimuli, 3) drug molecule release from hydrogels upon changes of temperature and pH and 4) non-invasive delivery of hydrogels by injection, allowing hydrogels to form *in-situ*. Polymers can respond to a whole range of stimuli additionally to temperature and pH including biological agents such as antigens/enzymes, exposure to mechanical forces application of an electrical and magnetic field, changes in ionic strength and light, and in some cases the polymers can multiple responses to different stimuli.

1.8.3 Temperature responsive polymers

Temperature-responsive polymers undergo a conformation change when heated or cooled, for the biological polymers previously mentioned: gelatine and agarose this occurs with a decrease in temperature, at their upper critical solution temperature. More surprising a class of thermoresponsive synthetic polymers display the reverse behaviour, becoming insoluble with increases in temperature in a reversible manner. Polymers of N-isopropylacrylamide (NIPAM) are the best characterised examples used for biological applications, as their lower critical solution temperature (LCST), the temperature where they become insoluble is close to body temperature. Other acrylamide based polymers also possess LCSTs which vary with the hydrophobicity of amide substituent¹⁸² (Figure 1-6). Poly(N-vinylcaprolactam) (PVCAP)¹⁸³, poly(methyl vinyl ether) (PMVE)¹⁸⁴, poly(vinylpyrrolidone) (PNVP)¹⁸³, poly(ethylene glycol) (PEG)¹⁸⁵ also exhibit insolubility with increases in temperature, but have LCSTs close to room temperature, or significantly higher than 37 °C and therefore are less suitable for biological applications.

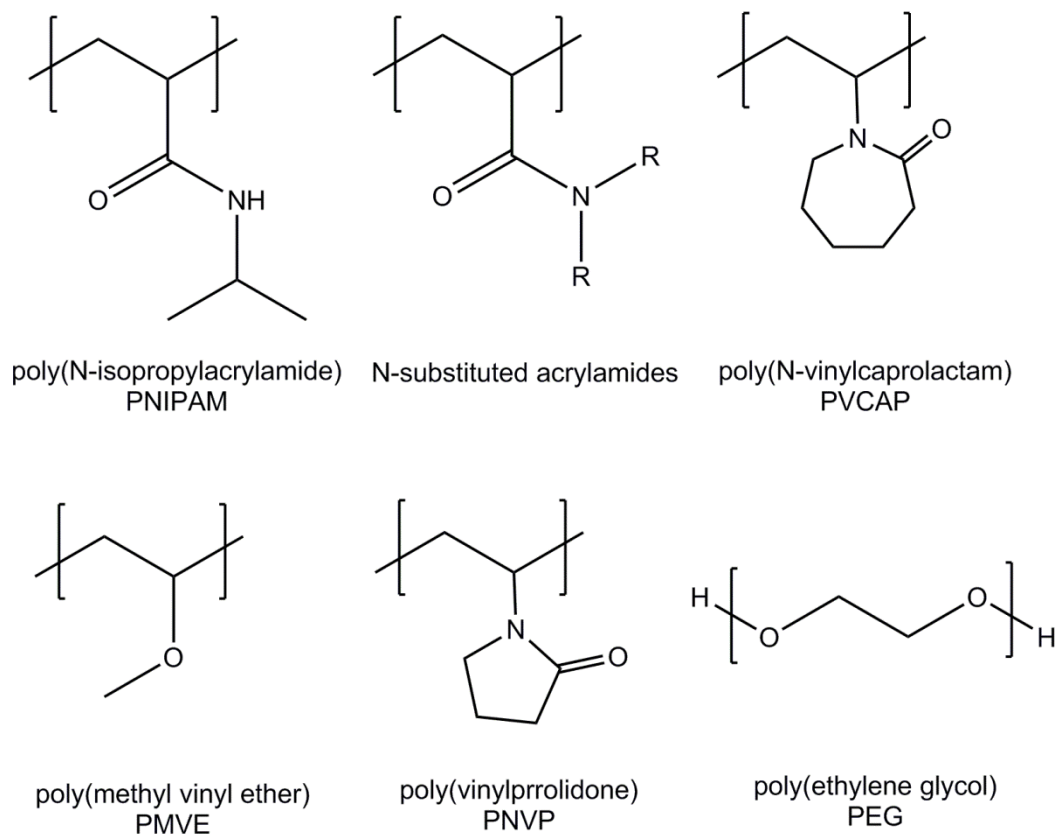


Figure 1-6: Thermoresponsive polymers that exhibit a LCST

1.9 Poly(*N*-isopropylacrylamide) hydrogels

Upon an increase in temperature, when dissolved in aqueous solution, chains of PNIPAM undergo a phase transition and collapse from an elongated random coil conformation into a smaller globule. The physical change is based upon the structure and immobilisation of the polymer. PNIPAM chains immobilised on a surface, will collapse when heated changing the surface properties from hydrophilic to hydrophobic. Free chains in solution collapse into globules and aggregate together, while crosslinked networks exhibit deswelling and swelling as a function of temperature (Figure 1-7).

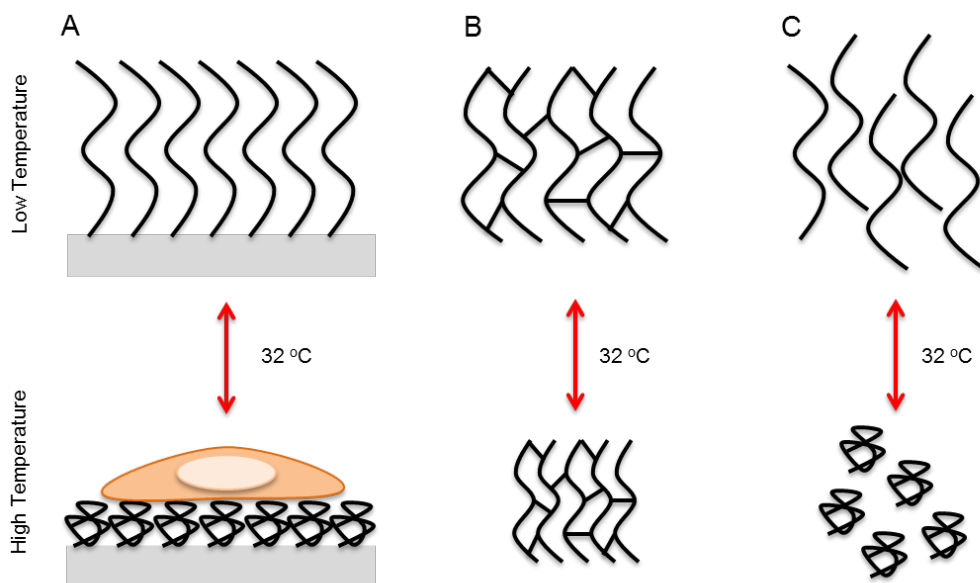


Figure 1-7 The conformational change of PNIPAM upon increase in temperature is dictated by polymer structure.

With an increase in temperature above the LCST, PNIPAM grafted onto surfaces collapses into globules, changing the surface wettability from hydrophilic to hydrophobic, rendering the surface cell adhesive (A). PNIPAM crosslinked networks deswell with an increase in temperature (B) and free PNIPAM chains in solution, collapse into globules and precipitate, creating physically cross-linked hydrogels (C).

1.9.1 Temperature dependent behaviour of PNIPAM

PNIPAM monomers contain a hydrophilic amide group and hydrophobic isopropyl group (Figure 1-6). When polymers of PNIPAM are dissolved in water, below the LCST, the amide group is able to hydrogen bond with water, whilst the isopropyl groups cannot and water molecules surrounding the hydrophobic groups become ordered into ice-like cages. It is the balance between the hydrophilic and hydrophobic groups in PNIPAM that govern the phase transition (Figure 1-8).

The mixing of a polymer in a solvent at a given temperature is a spontaneous process and the Gibbs free energy of mixing, ΔG_{mix} , is negative.

$$\Delta G_{mix} = \Delta H_{mix} - T\Delta S_{mix} \quad \text{where } \Delta G_{mix} = \text{change in Gibbs free energy of mixing}$$

$$\Delta H_{mix} = \text{change in enthalpy of mixing}$$

$$T = \text{temperature}$$

$$\Delta S_{mix} = \text{change in entropy of mixing}$$

PNIPAM is able to dissolve in water below the LCST as the exothermic formation of hydrogen bonds between the amide and water outweighs the negative entropy change of water ordering around the isopropyl groups. As the temperature is increased, hydrogen bonds between the amides and water begin to break, and in order for ΔG_{mix} to remain negative, the entropy of the system has to increase. The PNIPAM chains collapse into globules, reducing the hydrophobic groups exposed, and the water molecules can be released from the ordered cages. This is analogous to the hydrophobic effect seen when proteins fold in aqueous solutions.

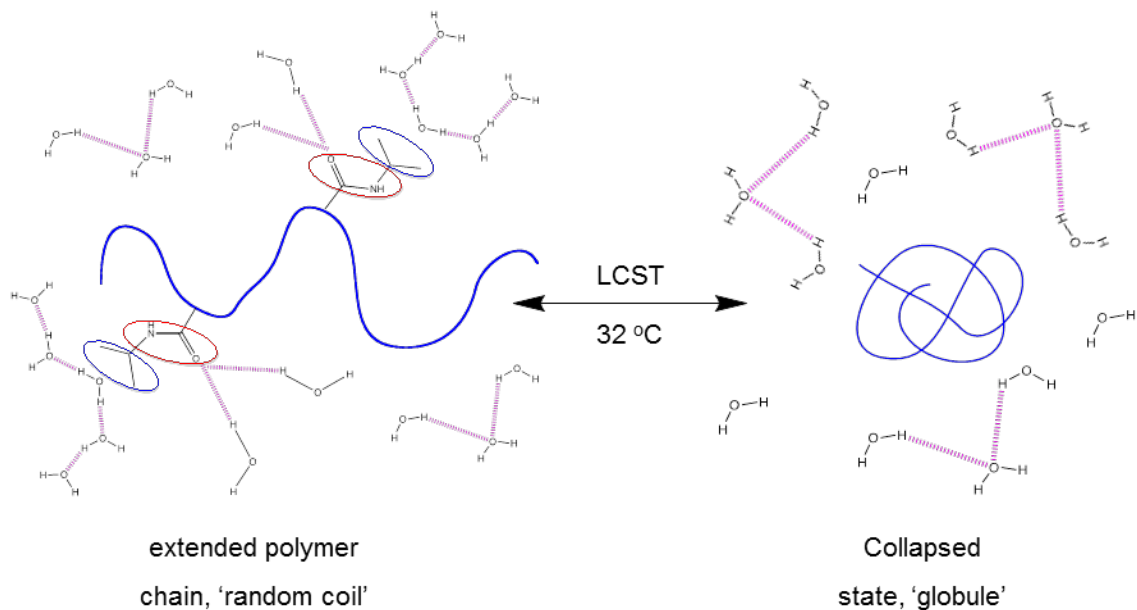


Figure 1-8 Coil- globule collapse of PNIPAM in aqueous solution at the LCST. Below the LCST, PNIPAM exists as extended coils (blue line), the amide groups (circled in red) hydrogen bond with water, whilst water orders in cages around isopropyl groups (circled in blue). Above the LCST, PNIPAM collapses into globules releasing ordered water molecules.

The LCST for a given polymer in solution is determined experimentally from the phase diagram of the polymer/ water mixture. The LCST is the minimum point in the phase separation curve, that is plotted from polymer concentration versus temperature. A representative phase diagram of a polymer with a LCST is shown in Figure 1-9. Where a phase diagram has not been drawn, but instead the temperature is determined for only one concentration this is referred to as the cloud point, when it has been determined by turbidity, or phase transition temperature rather than the LCST. Throughout this thesis the temperature measurements performed refer to cloud points/phase transition temperatures rather than the LCST.

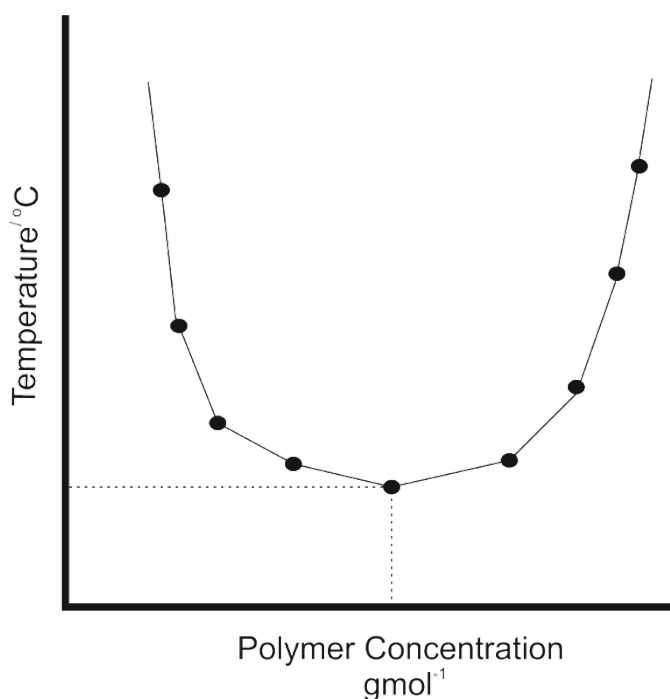


Figure 1-9: Representative phase diagram showing the concentration dependence of the phase transition temperatures of a polymer in aqueous solution. The LCST is the minimum point of the curve.

When the phase transition occurs, the change in PNIPAM chain conformation is not a simple coil – globule switch, as there are several intermediate states involved in the collapse. The change in polymer chain conformation has been explored experimentally by using extremely dilute solutions (0.001 – 0.0005 wt%) to enable the study of

individual PNIPAM chains when the phase transition occurs. The transition precedes by at least a two-step mechanism, initially single chains collapse into crumpled coils, which then later aggregate together.^{186–190}

Winnik et al. used double labelled PNIPAM chains with donor and acceptor chromophores to investigate this coil-globule collapse^{187,191}. Non-radiative energy transfer occurred between the chromophores when they were in close proximity, where the efficiency of the energy transfer increased with the polymer collapse. In the absence of interactions between neighbouring chains, an increase in the efficiency of the transfer occurred just before the phase transition temperature, indicating intra-chain collapsing occurs. This initial intra-chain collapses was also shown using Time-Resolved Anisotropy Measurements (TRAMS). Where the segmental mobility of individual polymer chains sharply decreased below the phase transition temperature.^{186,188}

Static (SLS) and dynamic light scattering (DLS) measurements have also demonstrated the presence of a crumpled coil prior to globule formation. By measuring the radius of gyration, R_g , the hydrodynamic radius, R_h , and the ratio of R_g and R_h , one can calculate the size and conformation of the polymer chains at a given temperature^{190,192,193}. As the temperature of the PNIPAM solutions is increased from the theta temperature (the temperature where a polymer in solution behaves ideally, any interactions between monomers are neglected and the polymer is in a coil confirmation) to 30.6 °C, $\langle R_g \rangle = \langle R_h \rangle$, whilst R_g and R_h decrease in value, indicating the conformation of the polymer is not changing, whilst the size is. In this initial stage of the phase transition the polymer coils collapse into crumpled coils, but the overall volume the polymer occupies does not change. Above 30.6 °C, $\langle R_g \rangle / \langle R_h \rangle$ rapidly decreases and the coils collapse into tight globules which aggregate together.¹⁹⁴ Fluorescence techniques to analyse the coil-globule transitions also demonstrate the presence of a crumpled state.¹⁹¹

1.9.2 Factors effecting the LCST

Linear polymers of PNIPAM typically have an LCST of 32 °C¹⁹⁵, which varies with the molecular weight of the polymer. The balance of hydrophobic and hydrophilic groups in

a thermoresponsive polymer, controls the temperature of the phase transition and therefore any changes to the structure and composition of polymer and the solvent, which affect this balance will also affect the temperature of the LCST.

Copolymerisation

To adapt PNIPAM for various applications it is commonly copolymerised to add functionality. Copolymerisation of NIPAM with hydrophobic or hydrophilic monomers can decrease or increase the LCST, as the balance between groups able to hydrogen bond with water and the hydrophobic effects are shifted¹⁹⁶. Linear copolymers of PNIPAM containing 8.9 mol% or 16.9 mol% styrene, had a decreased cloud point from 32 °C to 20 and 9 °C respectively.¹⁹⁷ Below the cloud point the NIPAM-styrene polymer chains have decreased segmental mobility compared with PNIPAM only, indicating the hydrophobic styrene within the polymer may be forming intra-molecular aggregates prior to the chain collapse. Copolymers of NIPAM and modified NIPAM, where the isopropyl group is replaced with a larger, more hydrophobic alkyl substituent, also have a decreased cloud point¹⁹⁸. As the size of alkyl substituent and proportion in the copolymer increases a decrease occurs in the cloud point. Similarly copolymerisation of NIPAM with PHEMA also decreases the cloud point¹⁹⁹.

Hydrophilic monomers N-vinylpyrrolidone (NVP)²⁰⁰ and N,N-dimethylacrylamide (DMAA)¹⁹⁹ copolymerised with NIPAM, increase the cloud point of the resulting polymer. Free radical polymerisation of NIPAM and NVP was carried out at temperatures below and above the LCST. Synthesis at 30 °C resulted in a random distribution of NVP within the PNIPAM chains whilst synthesis at 60 °C afforded polymers with NVP distributed on the end of the chains as the PNIPAM collapsed into globules during the synthesis allowing copolymerisation with NVP occur only at the exposed chain ends. The cloud points of the two polymers was higher in randomly distributed NIPAM-*co*-NVP polymer, as the hydrophilic groups with the NIPAM chain disrupts the hydrophobic-hydrophilic balance and push the chain collapse to higher temperatures. These results demonstrate that the effect of copolymerisation on the phase

separation temperature is dependent upon both the quantity and size of the co-monomer, and its location relative to PNIPAM.

Polymer Architecture

From the examples above, it is evident that the distribution of monomers in the polymer affects the temperature of the phase transition. In graft and block copolymers the segments of each monomer can behave almost independently of one another. Block copolymers of NIPAM with poly(lactic acid) (PLA)²⁰¹ and PEG²⁰² maintain a cloud point of 32 °C, whilst random polymers of the same composition are not thermoresponsive. Similarly the cloud point of copolymers with a styrene^{203,204} or acrylic acid²⁰⁵ backbone grafted with PNIPAM macromonomers were similar to PNIPAM, whilst random polymers were not. PNIPAM grafts have also been used to induce the collapse of non-thermoresponsive poly(dimethylacetamide) (PDMAC) when the density and molecular weight of the grafts is high enough²⁰³.

Presence of Salt

PNIPAM based polymers used for biological studies tend to be maintained in cell culture media or solutions designed to mimic the *in-vivo* physiological salt concentrations. The presence of kosmotropic anions such as MgSO₄ and CO₃, reduce the LCST of thermoresponsive polymers, and the effect of different anions follows the Hofmeister series. This is due to the competitive hydrogen bonding between anions and the amide of PNIPAM for water molecules, thus weakening the hydrogen bonding between water and the NIPAM amide and shifting the LCST to lower temperatures^{206,207}.

1.9.3 Biological applications of PNIPAM

PNIPAM based polymers have been used for drug delivery, releasing encapsulated molecules at the LCST. Block copolymers of PNIPAM, with a hydrophobic monomer, such as butyl methacrylate²⁰⁸ and methyl methacrylate²⁰⁹ can form micelles with a hydrophobic core and PNIPAM exterior. During the formation of the micelles drug

molecules can be trapped within the hydrophobic core. Upon increase in temperature the PNIPAM chains on the outside of the micelle, collapse and release the enclosed drug. However further modifications are often required to control the mechanism of drug release, as the temperature responsive behaviour of PNIPAM often leads to a quick burst, rather than prolonged release.

Traditionally adherent cells grown on TCP are harvested using enzymes such as trypsin. However these methods of cell detachment, which non-specifically cleave cell- ECM adhesions can affect the cell phenotype. Trypsin is also animal derived and could lead to disease transmission, which is not ideal for cellular therapies. Coating TCP with PNIPAM chains can be used as an alternative method to detach cells. Furthermore as the detachment does not involve the use of any enzymes, cell-cell adhesions are not disrupted either, and intact cell sheets can be obtained. Below the phase transition temperature, PNIPAM chains grafted to surfaces are extended and hydrated, upon heating the chains collapse into globules close to the TCP surface, generating a hydrophobic surface (Figure 1-7). Cells can then attach to the PNIPAM chains through soluble proteins in the media. When confluent, the cell sheets can be detached by increasing the temperature causing the PNIPAM to once again extend and hydrate, releasing the cells²¹⁰⁻²¹². This technique can be further modified to create patterned cell sheets. Through copolymerising PNIPAM with a hydrophobic monomer and lowering the phase transition temperature, TCP surfaces can be modified to contain PNIPAM coated regions that can switch between cell adhesive and non-cell adhesive at different temperatures. Initially the temperature can be increased to the phase transition of the hydrophobically modified PNIPAM, and cells can be attached to these regions, while the more hydrophilic PNIPAM chains are still extended and non-cell adhesive. Subsequently the temperature can be raised such that the remaining polymer collapses and a second cell type can attach to these now cell adhesive regions. Patterned sheets of hepatocytes and endothelial cells have been fabricated in this manner, to mimic their paracrine cellular interactions within the pancreas and liver^{213,214}. Basic 3D tissues can also be made by layering the cell sheets obtained from PNIPAM surfaces. Alternating sheets of fibroblasts, and endothelial cells patterned in channels, have been layered to create primitive vascular networks²¹⁵. ADSC sheets have also been prepared on

PNIPAM surfaces, for repairing scarred myocardium. Delivery of the cells within an intact sheet, maintained them at the site of injury. Over 4 weeks the sheet thickened and became populated with new blood vessels, reducing the scarring in the damaged tissue²¹⁶.

1.9.4 PNIPAM hydrogels for regenerative medicine

The thermoresponsive nature of PNIPAM also lends itself to use as an injectable scaffold, as cells may be suspended in the aqueous polymer solution below the phase transition temperature and then injected *in-vivo* or transferred to moulds and allowed to gel encapsulating cells uniformly within the resulting gel²¹⁷. When linear polymers of PNIPAM undergo the solution-gel transition they initially form hydrogels the shape and volume of the mould and initial polymer solution. However as gelation is mediated by the aggregation of polymer globules into a continuous phase, some of the water is expelled from the polymer networks, in a process known as syneresis, and the hydrogel shrinks^{218,219}. To reduce this syneresis and therefore maintain water content and volume, PNIPAM is commonly crosslinked or copolymerised. Mikos et al. synthesised syneresis free acrylate functionalised PNIPAM hydrogels. These undergo tandem gelation, initially through the phase transition and then by chemical cross-linking, preventing syneresis from occurring^{217,218}.

PNIPAM hydrogels have been researched for a vast number of applications, using multiple cell types and in many combinations with copolymers, therefore this review will focus on applications of PNIPAM hydrogels in tissue engineering of connective tissues and MSCs.

Copolymers of PNIPAM and N-acryloxysuccinimide (NASI) have been engineered to control the release of growth factors to stimulate osteogenesis. The NASI groups on the polymer are able to couple with exposed amine groups on lysine and arginine within protein growth factors such as BMP-2. Coupled with the thermoresponsive behaviour of PNIPAM, the aim of this copolymer was the delivery of BMP-2 to the site of bone repair, by injection, and then retain the BMP-2 within the scaffold at the site of injury

for a slow and continued release²²⁰. Compared with PNIPAM – BMP-2 mixtures without the functionality, PNIPAM-NASI provided prolonged release of BMP-2 *in-vivo* over 14 days.

The use of PNIPAM-NASI-BMP-2 also had a greater osteoinductive potential compared with injections of BMP-2 only²²¹ indicating that thermoresponsive polymers can bind and sustain a release of growth factors *in-vivo*. Further functionality was added to the polymer, with the addition of RGD sequences, which promoted adhesion of C2C12 cells onto the PNIPAM-NASI-RGD hydrogel. However with improved cell adhesion, NIPAM-NASI- BMP-2 stimulated osteogenesis of C2C12s *in-vitro* was comparable to polymers without RGD, and interestingly in the absence of BMP-2 the PNIPAM scaffolds were more osteogenic than 2D TCP controls²²². These results suggest PNIPAM based hydrogels can induce cell differentiation without necessarily providing a substrate for cell adhesion, and have osteoinductive properties in the absence of soluble factors. PNIPAM hydrogels containing pentaerythritol diacrylate monostearate, acrylamide and hydroxyethyl acrylate have been shown to be calcified in serum containing media in the absence of cells²¹⁸. This intrinsic ability of the hydrogels to develop bone like matrix could explain the osteoinductive properties of the previous polymer in the absence of BMP-2.

To produce PNIPAM hydrogels that would not exhibit significant syneresis, Healy et al. synthesised copolymers and semi-interpenetrating (sIPN) networks of PNIPAM with hydrophilic acrylic acid (AAc), which maintained over 90% water from the parent solution, upon gelation. These hydrogels also contained peptide crosslinks containing matrix metalloprotease -13 (MMP-13) degradable sequences to facilitate remodelling of the matrix²²³. IPNs are a class of polymer containing two or more networks that are partially intertwined among each other, but not covalently crosslinked. They are synthesised by crosslinking one of the networks in the presence of the other, and therefore cannot be separated from each other without breaking chemical bonds²²⁴. A sIPN differs from an IPN because the polymers can be separated from each other and only penetrate each other on a molecular scale, due to the entanglements of the polymers²²⁵.

Below the phase transition temperature, these gels were mechanically weak with complex moduli of 1-2 Pa, therefore injectable. This increased to 100- 300 Pa at the phase transition, dependent on the crosslinking density, but these are still weak gels^{226,227}. Osteoblasts were able to migrate within the sIPN's, degrading the gel through the peptide sequences. Later addition of RGD sequences improved osteoblast adhesion, but without RGD it appears the degradable peptides still permitted cell adhesion and migration as the cells can create voids in the matrix and produce their own ECM²²⁶. In a rat femur ablation assay, the degradable sIPNs were implanted within the bone and remodelled trabecular like tissue was visible after a 4-week period, no significant differences were observed in the remodelling of the sIPNs without RGD. Where sIPNs were implanted without degradable sequences the extent of remodelling was reduced²²⁷. Soft sIPNs (70 Pa) were also suitable substrates for maintaining the pluripotency of ESCs. Compared with TCP, the sIPNs allowed ESCs to adhere and retain their undifferentiated phenotype, expressing OCT4 and SSEA-4.²²⁸

More recently the sIPNs have been used to deliver BM-MSCs into the heart for the repair of heart tissue following myocardial infarction. *In-vivo* the BM-MSCs were proliferative and their adhesion and spreading improved with increasing mechanical strength of the hydrogel. Over 6 weeks the heart tissue thickened and the presence of the bulk gel was undetected²²⁹. Left ventricle function, which gave an indication of the success of the therapy, showed no difference between cell laden sIPN and sIPN only injections, suggesting that the hydrogel has good cellular infiltration from the surrounding tissue as a result of the degradable crosslinks.

Poly(NIPAM-co-AAc) hydrogels synthesised by another group, have been used to maintain the phenotype of chondrocytes *in-vitro*. Within the hydrogels chondrocytes maintained their rounded morphology and synthesised collagen II and aggrecan^{230,231}. These results are in contrast to Healy's hydrogels, however they used a 10 wt% gel, rather than 4-5 wt%, resulting in much tougher gels (900 Pa) and these do not contain the degradable links Healy et al used. This highlights how variations in crosslinking, concentration and polymer architecture but the same chemical composition can generate a wide range of hydrogels that are injectable from PNIPAM. PNIPAM hydrogels have

also been used to induce chondrogenesis. Several groups have created hydrogels able to encapsulate chondrogenic growth factors. From poly(NIPAM-co-AAc) hydrogels containing DEX, ascorbate, TGF- β 3 and chondrocytes implanted into nude mice, a collagen II and GAG rich tissue formed, where the chondrocytes had spherical morphologies and appeared within lacunae like structures similar to native cartilage²³².

Tougher hydrogels has been made from combinations of PNIPAM and PEG. PNIPAM with PEG grafts of varying length and density, also have reduced syneresis. Equilibrium water content increased with the length of the PEG grafts, while the stiffness of the hydrogels fell. Variations in PEG resulted in hydrogels with 35 – 71% water content, and complex moduli of 205 KPa – 52 KPa²³³. Therefore these hydrogels were proposed as injectable treatments for repairing the nucleus pulposus, a tissue exposed to high compressive strains. PNIPAM-PEG copolymers at the other end of the spectrum that had high water content, but low mechanical properties, could encapsulate the neurotrophic factors, brain-derived neurotrophic factor (BDNF) and neurotrophin-3 (NT-3) for injectable repair of spinal cord neural tissue. *In-vitro* the factors were released biologically active over 4 weeks. BM-MSCs were also viable within the gels, spreading and proliferating over a 21 day culture period²³⁴.

These examples demonstrate the wide variety of applications of PNIPAM based hydrogels for regenerative medicine. Using their thermoresponsive nature, the gels can be delivered by injection and they are able to release small molecules for regenerative medicine therapies to repair defects in bone, cartilage, the heart and the spinal cord. Furthermore they can be used as *in-vitro* systems to maintain the *in-vivo* phenotype of MSCs.

1.9.5 Overall Research Aims

As discussed there is huge potential for hydrogels for regenerative medicine, however they are not without their limitations. Synthetic polymers are largely non-cell adhesive and non-degradable. Where natural materials are highly biocompatible but do not possess the mechanical strength or long term survival synthetic materials have.

Furthermore each hydrogel is generally only fit for one purpose due to the large variation in ECM between different tissue types. Water content, cellularity, elasticity and mechanical strength all vary between tissues and organs. Therefore there is a gap in the development of hydrogels for a material that can be used for a variety of applications, where the properties can be easily varied. Furthermore one of the requirements for a material to be commercially viable in the field and to be used therapeutically is affordability. This is alongside the ability to reproduce the fabrication process, ease of mass production and methods for sterilisation, transport and storage. The potential of a single hydrogel for multiple applications, helps to alleviate problems with commercial viability. Furthermore if the hydrogels encourage and permit cell infiltration it could be used as an off the shelf therapy for multiple patients and would require less regulatory hurdles in commercialisation. In the absence of cells the product would be considered a medical device rather than a device and cellular therapy combination.

Therefore this thesis explores the development of a bio-synthetic hydrogel composite of PNIPAM and collagen I, to exploit the biocompatibility of collagen and the mechanical strength and thermoresponsive properties of PNIPAM. Varying the proportions of collagen and PNIPAM in the hydrogel will be performed to examine the effect of the composition on the material properties of the hydrogel. This thesis describes the synthesis and characterisation of the bio-synthetic hydrogel followed by examples of its application for two different stem cell applications. Hydrogels with low mechanical properties are used for creating an *in-vitro* model of the lymph node, showing the utility of the composite for research applications, while hydrogels with a higher mechanical strength are then investigated as potential injectable treatments for cartilage repair.

Initially the synthesis and characterisation of poly(NIPAM-*co*-styrene-*graft*-NVP), and the properties of the resulting hydrogel when it is combined with collagen I will be presented in Chapter 2. Then two potential applications of the bio-synthetic scaffolds are explored in Chapter 3.

Specifically the aims of this thesis are to;

1. Synthesise and characterise Poly(NIPAM-*co*-styrene-*graft*-NVP)
2. Determine the material properties of hybrid gels of collagen I and Poly(NIPAM-*co*-styrene-*graft*-NVP)
3. Identify how different blends of the hybrid gels may be used for two different MSC based tissue engineering application

Chapter 2 Development of collagen I and poly(NIPAM-co-styrene-graft-NVP) hybrid gels

2.1 Introduction

2.1.1 Bio-synthetic hydrogel systems

To improve the biomimicry of PNIPAM based hydrogels, bio-synthetic hydrogels containing a combination of PNIPAM and natural ECM components have been fabricated. Although cell adhesion ligands and protease specific sequences can be synthetically incorporated into PNIPAM to improve adhesion, they do not always have a significant effect on the bulk hydrogel properties, and the properties they confer are not easily tuned without re-synthesising the polymer. Bio-synthetic hydrogels with varying combinations of two (or more) synthetic and natural polymer networks, have been produced by several research groups to examine their potential as cell scaffolds.

2.1.2 PEG based biosynthetic gels

Seliktar et al. have developed composite gels of linear PEG cross linked with fibrinogen to improve the tissue remodelling of PEG based gels, as the protease substrate sites within fibrinogen permit gel degradation^{235,236}. Fragments of fibrinogen were PEGylated by reaction of acrylate functionality at the PEG chain ends with the free thiols of fibrinogen. Further PEG-diacrylate (PEG-DA) addition in the presence of UV initiation crosslinked the gel together. Several hydrogels were made with varying molecular weights of PEG-DA. Interestingly the elasticity of the hydrogels and the *in-vitro* degradation rate decreased with increasing PEG molecular weight, potentially due to larger pore size. The elastic modulus did however increase with polymer concentration. The addition of fibrinogen significantly decreased the mechanical properties compared with PEG only gels, due to a reduction in crosslinking between adjacent PEG chains²³⁵. However fibrinogen improved cell adhesion of endothelial cells on the hydrogel surface and the spreading of SMCs within gels compared with PEG only gels. When the degree of crosslinking was increased through addition of more

PEG, the porosity of the gels reduced, which in turn decreased cell attachment and migratory ability of SMCs²³⁶.

2.1.3 Interpenetrating polymer networks

Biosynthetic hydrogels have been made in the form of interpenetrating networks (IPN). Where the monomers within the IPNs are hydrophilic, hydrogel IPNs can be produced. Blends of PVP and gelatine in a 1:1 ratio produced hydrogels with good swelling, compressive strength and cell attachment, while PVP only gels were elastic, but not cell adhesive²³⁷. Similarly with the PEG-fibrinogen gels, inclusion of gelatine decreased the compressive strength of the hydrogel whilst improving cell adhesion. Bio-synthetic semi-IPNs (sIPN) have also been synthesised from gelatine and acrylamide. The greatest tensile strength for the series was observed in sIPNs where only one of the polymer networks was crosslinked²³⁸. In these gels the crosslinked gels are able to maintain structure, whilst the second component could temporarily deform under the applied strain. This demonstrates how two polymer networks combined can work together to resist strains. The sIPNs were most elastic when the polyacrylamide was crosslinked, and gelatine was mobile. A similar behaviour is seen in the ECM matrix of cartilage, where aligned collagen fibrils are maintained in a weaker GAG gel. In the reverse gel where gelatine was crosslinked, the gel was weaker than crosslinked acrylamide only gels, highlighting how effective bio-synthetic hydrogels can be, where a synthetic polymer can provide additional strength to a biological hydrogel. PHEMA is commonly used as a biomaterial, even though it is non-cell adhesive. Again by crosslinking PHEMA into IPNs with gelatine, cell adhesion of fibroblasts was improved²³⁹. *In-vivo* the IPNs integrated into the surrounding tissue and were remodelled, furthermore the elastic moduli of the IPN, 80 KPa was greater than either PHEMA, 56 KPa, or gelatine, 36 KPa, films alone.

2.1.4 Hyaluronan-NIPAM hydrogels

To take advantage of the thermoresponsive nature of PNIPAM, several hydrogels have been made from natural ECM components grafted with PNIPAM chains. Unmodified HA is water-soluble and usually functionalised or crosslinked in order to form gels.

Matsuda et al. used grafting of PNIPAM chains to HA to produce water insoluble gels, and drive the gel formation with temperature²⁴⁰. The phase transition of the gels occurred around 34 °C, and decreased slightly with increasing PNIPAM graft length and densities. As the gels were not cell-adhesive they were explored as non-tissue adhesive coverings for surgical repair. In a rat cecum abrasion model, HA-g-PNIPAM prevented adhesion of surrounding tissues to the damaged area²⁴¹. HA-g-PNIPAM gels have also been used for ADSC culture²⁴². Hydrogels were synthesised with 28 and 53 wt% PNIPAM, again with increasing PNIPAM concentration, the elasticity increased and pore size decreased. The ADSCs were unable to spread and attach to the gel and remained in a rounded state. Although the 53 wt% PNIPAM contained more viable ADSCs after 28 days cell culture and were less prone to enzymatic degradation, the lower PNIPAM may be more biocompatible as ADSCs were able to degrade and migrate out from the gel. Peroglio et al. also produced HA grafted with PNIPAM. As the molecular weight of the grafts increased, the hydrogels became more prone to syneresis, but increased in mechanical strength up to 16 KPa²⁴³, demonstrating how the composition needs to be carefully tailored to produce the best performing hydrogel. The weaker gels were used for *ex-vivo* implantation of BM-MSCs into a bovine dissected spine, as a possible therapy for nuclear pulpous repair. After 1 weeks culture in chondrogenic media the implanted cells were producing a collagenous matrix, more efficiently than *in-vitro* pre-differentiation BM-MSCs²⁴⁴.

Another approach to combine PNIPAM with HA, was through direct mixing of a PNIPAM and acrylic acid (AAc) copolymer, PNIPAM-*co*-AAc, with HA prior to gelation. As the gels are not adhesive, they were used for chondrocyte differentiation, supplemented with combinations of TGF- β 1 and dex and implanted into nude mice. Over 8 weeks the factors were slowly released from the gels. Chondrogenesis was improved by incorporating HA into the hydrogels compared with just PNIPAM-*co*-AAc²⁴⁵, and the most significant differentiation was observed using the combination of all factors and HA, due to the prolonged release of TGF- β 1 and dex and the biomimetic scaffold^{246,247}.

2.1.5 Gelatine NIPAM hydrogels

In contrast to the HA-g-PNIPAM hydrogels, gelatine-g-PNIPAM hydrogels are more cell adhesive^{241,248–251}. Hydrogels were formed from solutions of gelatine-g-PNIPAM at concentrations over 5 wt %, and as the ratio of PNIPAM to gelatine (P/G) increased the minimum gelation concentration fell. The phase transition temperature varied between 33 – 34 °C, decreasing as the P/G increased. The compressive strength and elastic moduli of the gels also followed a similar trend, reaching 222 and 8.7 KPa respectively for the 20 wt% gels with the highest PNIPAM content^{249,250}. Cell viability, spreading and proliferation of fibroblasts and human umbilical vein endothelial cells (HUVEC) increased with P/G as these gels contained a more open network as a result of the large hydrophobic aggregates that are formed within the gel²⁴⁹.

Gelatine-g-PNIPAM showed potential for tissue engineering of cartilage²⁵². Chondrocytes behaved similarly to fibroblasts within the gels, they were rounded with minimal spreading, but this is typical of the cell type. They also had the best viability in the gels with a high P/G ratio. Over 12 weeks in culture the cells arrested in the G₀/G₁ stage and synthesised a cartilaginous matrix of proteoglycans and type II collagen. The response of mechanical loading on the gels approached that of native collagen with time in culture. Although the gels can form *in-situ* within native cartilage, the authors pre-cultured chondrocytes within the gels prior to implantation, as the phase transition temperature of the gels was close to 37 °C and there were concerns over gel leakage with minimal changes in temperature. The pre-cultured tissue was secured in full thickness defects with fibrin glue and sealed with a periosteal flap. Examination of the tissue after 5 weeks showed a GAG and collagen II rich matrix, which had the histological appearance of native cartilage when pre-cultured *in-vitro* prior to implantation²⁵². Although this use of PNIPAM-HA hybrids was able to regenerate high quality cartilage, the technique still required invasive surgery.

2.1.6 Chitosan-NIPAM hydrogels

Chitosan grafted with PNIPAM has also been designed for cartilage repair²⁵³. Compared with hydrogels of PNIPAM, chitosan-g-PNIPAM had larger shear moduli

and water content. Chitosan-g-PNIPAM was subsequently grafted onto HA, producing gels with similar water content, but they were generally weaker. *In-vitro* chondrogenic differentiation was most successful in HA-g-(chitosan-g-PNIPAM), potentially due to the presence of HA in native cartilage, and with 6 weeks differentiation the shear moduli of the chondrogenic gels approached 70 KPa.

2.1.7 Alginate-NIPAM hydrogels

PNIPAM has been grafted to the surface of porous alginate gels to add a level of temperature control to the swelling and deswelling of the gel²⁵⁴. Thermoresponsive swelling improves the functionality of alginate gels for stimuli responsive drug release. The porosity of the alginate gels, results in fast swelling of only one minute. When functionalised with PNIPAM, the gels also quickly de-swell at the phase transition temperature. The effect is increased when the PNIPAM is grafted onto the surface of the alginate pores, as these are within the gels that are in contact with fluid.

2.1.8 Collagen PNIPAM scaffolds

Currently the only scaffolds produced that combine collagen with PNIPAM, are fabricated from copolymerisation of PNIPAM and a diethylene glycol diacrylate (DEGDA) crosslinker around a pre-formed collagen sponges²⁵⁵. PNIPAM was incorporated into the sponges to improve the mechanical properties of collagen for tissue engineering applications. Addition of PNIPAM increased the shear moduli of the collagen sponge and introduced temperature dependent swelling and deswelling into the scaffolds. To date they have not been used in combination with cells.

2.1.9 Conclusions on bio-synthetic PNIPAM hydrogels

Although there are numerous examples of bio-synthetic hydrogels based on PNIPAM, there are limitations in their applications. Some of the hydrogels discussed above require crosslinking with UV or through synthetic routes to form gels. Upon crosslinking they form hydrogels with high mechanical strength, however the gelation is accompanied with an increase in viscosity and the materials cannot be implanted *in-*

vivo. Although gels made from HA-g-PNIPAM gelled with an increase in temperature their application in cartilage repair was only shown to be successful when the gels were pre-cultured and then implanted. However their thermoresponsive behaviour was amenable to cell encapsulation. Many of the gels were non-cell adhesive and therefore used as scaffolds for cartilage repair as MSCs and chondrocytes require a rounded morphology to commit to a chondrogenic lineage. The mechanical properties of the different gels could be varied through changing the composition of the synthetic to natural component. Generally, addition of a natural polymer to synthetic, decreased the mechanical properties compared with the synthetic polymer alone, however the materials were stronger than the natural materials and now contained biological functionality. There is however a lack of materials that can be tuned without further chemical synthesis, and as many natural gels can gel with increases in temperature, there is potential for hydrogels where both the synthetic and natural polymers gel *in-situ* forming physical networks among each other. Lastly the majority of gels are only used for engineering of highly mechanically compliant tissues, such as cartilage. The addition of a thermoresponsive element to a natural ECM based hydrogel could also have many applications in the engineering of softer tissues such as the kidney, liver or lymph node. These hydrogels do however show the potential of bio-synthetic PNIPAM based hydrogels as they can support cells viability and differentiation *in-vitro* and *in-vivo* and their composition can lead to very varied mechanical properties.

2.2 Aims and synopsis

There is currently a range of bio-synthetic hydrogels for tissue engineering, yet there are no tuneable materials, as the composition of the hydrogel is pre-determined from the synthesis. A technology gap exists for a material that can be tailored for multiple applications at the time of use, therefore reducing the need for multiple tissue engineering products. At present, there are no other hybrid gel systems composed of PNIPAM and collagen, which are not chemically crosslinked together, and gel simultaneously among each other. A hybrid gel created by simply mixing a synthetic and biological polymer in the desired proportions, has potential as an off the shelf scaffold for multiple applications. Presented within this chapter is the synthesis and

characterisation of poly(NIPAM-*co*-styrene-*graft*-NVP), (which will be referred to as NSN for simplicity) and the development of a hybrid gel system which combines NSN with collagen I. The effect of the blend of collagen to NSN in the gels, on the resulting gel properties will be assessed by mechanical testing, syneresis experiments and SEM imaging.

The aims of this chapter are:

1. Synthesis of poly(NIPAM-*co*-styrene-*graft*-NVP)
2. Determine the structure, size and thermoresponsive behaviour of poly(NIPAM-*co*-styrene-*graft*-NVP)
3. Identify the physical properties of hybrid gels of collagen I and poly(NIPAM-*co*-styrene-*graft*-NVP)

2.3 Methods

2.3.1 Polymer Synthesis

All glassware was dried in a 60 °C oven prior to use to remove residue water and solvents.

2.3.2 Synthesis of semitelechelic oligo(NVP)

Oligomers of NVP (ONVP) were prepared as described below. N-vinyl-2-pyrrolidone (NVP, Sigma Aldrich) was distilled under reduced pressure and the first fraction kept for synthesis. Distilled NVP was stored at – 20 °C prior to use. 2-isopropoxyethanol (IPE, Sigma Aldrich) (4.6 eq) was charged to a 3-necked flask equipped with a reflux condenser and gas bubbler that was subsequently sealed using a rubber septum. IPE was used as both a solvent and chain transfer agent in the polymerization. Prior to the addition of further reagents, nitrogen was bubbled into the solution for 15 minutes. Azobisisobutyronitrile (AIBN, BDH) (3.5×10^{-3} eq) was dissolved in a minimum quantity of IPE and added via syringe into the flask. Nitrogen was bubbled into the reaction for another 15 minutes. NVP (1 eq) was then added via syringe and the reaction mixture stirred at 60 °C, under nitrogen for 3 hours. The remaining solvent in the reaction mixture was removed *in vacuo* yielding a clear viscous liquid. The polymer was then purified by adding the concentrated reaction solution slowly to a rapidly stirring excess (20x product volume) of diethyl ether, and the precipitate dried overnight *in vacuo*. The glassy white solid (ONVP) was precipitated again from dichloromethane (DCM) into diethyl ether and dried for 24 hours *in vacuo*.

2.3.3 Functionalisation of oligo(NVP)

The hydroxyl end groups of ONVP were functionalised with 4-vinylbenzyl chloride (VBC) to give vinylbenzyl functionalized NVP oligomers (ONVP-VB). Sodium hydride (17.6 eq, Sigma Aldrich) was washed 3 times in anhydrous diethyl ether under nitrogen in a sealed flask and subsequently dissolved in anhydrous dimethylformamide (DMF) (10 ml). 4-Vinylbenzyl chloride (VBC, Sigma Aldrich) (40 eq) and nitrobenzene (50 μ m, Sigma Aldrich) were diluted in anhydrous DMF (5ml) and added via syringe

to the flask. ONVP (1 eq) was dissolved in a minimum of anhydrous DMF and added to the flask. The reaction mixture was stirred at room temp for 24 hours in the dark. Remaining solvent was removed *in vacuo* and the resulting viscous liquid added slowly to a rapidly stirring excess (20x product volume) of diethyl ether. The precipitate was dried overnight *in vacuo*. The glassy white solid (ONVP-VB) was precipitated again from a minimum quantity of methanol/DCM (1:9) into diethyl ether and dried for 24 hours *in vacuo*.

2.3.4 Synthesis of poly(NIPAM-co-styrene-graft-NVP)

Prior to use NIPAM (Sigma Aldrich) was recrystallised. Briefly, NIPAM was dissolved in a minimum quantity of hexane:toluene (40:60) with gentle heating. The solution was cooled at -20 °C for 30 minutes and the recrystallised NIPAM dried *in vacuo*. NIPAM was recrystallised two further times and dried *in vacuo* for at least 24 hours to remove residue solvent. NIPAM (31.45 mmol) and AIBN (0.335 mmol) were dissolved in 1,4-dioxane (10ml), once dissolved styrene (Sigma Aldrich) was added (3.495 mmol) and the solution transferred to a glass ampule. The functionalised NVP oligomer (ONVP-VB) (0.035mol) was dissolved in a minimum quantity of 1,4-dioxane and added to the ampule. The ampule was subjected to 3 freeze- thaw cycles and sealed under vacuum. The reaction mixture was heated at 60 °C overnight and the resulting liquid added slowly to a rapidly stirring excess (20x product volume) of diethyl ether. The glassywhite solid was precipitated again from DCM into diethyl ether and dried for 24 hours *in vacuo*. The resulting solid was dissolved in a mixture of ethanol:acetone (3:7) and ultra filtered using a ultrafiltration cell (Millipore) and 10,000 Mw cut off cellulose filter. The filtrate was precipitated again in diethyl ether. The solid was then dissolved in ultra pure water and freeze dried to give a fluffy white solid. The polymer was stored under nitrogen at -20 °C due to its hygroscopicity.

2.3.5 NMR analysis of oligomers and graft polymers

Hydrogen nuclear magnetic resonance (¹H-NMR) spectra were obtained using Bruker Avance 400 spectrometre using a 12 ppm sweep width. 25 mg of the sample of interest

was dissolved in deuterated solvent and filtered through glass wool to remove any insoluble material.

2.3.6 GPC analysis of oligomers and graft polymers

Gel permeation chromatography (GPC) was performed using 5 mg of the sample of interest dissolved in 2ml of degassed DMF. Each sample was run on PL gel mixed B columns (10 mm particle size, 100-10 Å pore size, Polymer Laboratories) equipped with an refractive index detector. A flow rate of 1ml/min was used and the samples run for 40 minutes in a mobile phase of degassed DMF supplemented with 0.01% MgCl. Columns were calibrated using poly(methylmethacrylate) (PMMA) standards. Three colour-coded standards were run on the columns, each containing a mixture of five monodisperse PMMA polymers. Red vial: 2,000/30,000/300,000/1,500,000 g mol⁻¹, yellow vial: 1,000/13,000/130,000/1,000,000 g mol⁻¹ and green vial: 500/7,000/70,000/500,000 g mol⁻¹. Average molecular weights of samples were obtained using Agilent Cirrus GPC software. Mean values of 3 replicates were calculated for the number average molecular weight, weight average molecular weight and dispersity index.

2.3.7 MALDI-TOF mass spectroscopy

Matrix assisted laser desorption time-of-flight spectroscopy (MALDI-ToF) spectra were obtained for the ONVP oligomers using a Bruker Reflex III spectrometer operating in positive ion reflectron mode. The instrument was calibrated with Angiotensin II and Insulin standards. Each sample was dissolved in chloroform (8mg/ml) and combined with dithranol matrix (10 mg/ml in chloroform) and sodium iodide (2mg/ml in methanol) at a ratio of 2:2:1.

2.3.8 Turbidity Measurements

Dilute solutions of NSN were dissolved in either milli Q water or basal cell culture media and heated from 0 – 60 °C and then cooled straight away back to 0 °C. The absorbance at 500 nm was measured during the heating and cooling runs using a Jasco

ETC-505T peltier temperature controlled Jasco V-560 UV-Vis spectrometer. The cloud point was determined from the heating run as the point of inflection from the baseline.

2.3.9 Rheological Measurements

Rheological measurements were obtained using a TA Instruments Rheology Advantage AR-G2 cone and plate rheometre fitted with a 40mm cone. The plate was fitted with a peltier control and julabo F24 water bath. 800 μ l of each sample was pipetted onto the plate, which was held at 0 °C and the cone lowered to zero gap ensuring the sample was not overfilled. Any excess sample was removed by pipetting or using a paper towel. Samples were held at the starting temperature for 1 minute prior to any experimental runs.

2.3.10 Collagen I extraction from rat tail tendon

Prior to extraction rat tails were rinsed and thawed in 95% ethanol. The epidermis was removed from each tail by making a cut down the length of the tail using a scalpel, taking care to not cut into the underlying tendon bundles. Using a haemostat the top of the tail was clamped, whilst a second haemostat was used to pull the epidermis away from the tail. To remove the tendons, the tail was clamped at the proximal end using a haemostat and the tendon bundles immediately proximal to the haemostat were severed using a scalpel. Tendons were removed from the tail joint by joint, a second haemostat was used to clamp and break the joint at the distal end of the tail. The joint and associated tendons were then pulled away from the tail and the tendons cut from the joint and stored in sterile water. The process was repeated for each joint in the tail to isolate as much of the tendons as possible.

The isolated tendons were washed three times in dH₂O and once in 95% ethanol and then dissolved in 0.5 M acetic acid (50ml / 1g of tendon, Sigma Aldrich) for 30 hours with gentle stirring at 4 °C. The dissolved tendon solution was then centrifuged for 1 hour at 20,000g at 4 °C and the supernatant maintained to remove any un-dissolved proteins. The supernatant was freeze dried in aliquots to obtain solid collagen I. As the tendons contain other ECM proteins these may also be solubilised during the extraction.

In order to maintain reproducibility in extractions, dissolution time in acetic acid was kept constant in each extraction as well as the volume of acetic acid the tendons were dissolved in.

2.3.11 Collagen I gel formation

All collagen solution preparation was performed on ice. Freeze dried collagen I was dissolved in 0.02M acetic acid at concentrations between 3.33 – 6.66 mg/ml. To produce a working solution the collagen I stock was diluted with 10X DMEM (1 part DMEM to 9 parts collagen) and gently mixed to prevent the formation of air bubbles. The working stock was neutralised with 1M NaOH until the pH reached 7.5 (verified using pH testing strips and phenol red indicator). To create moulds for the gels, a metal ring was adhered to a glass coated Petri dish (MatTek) using vacuum grease for imaging applications, or within a 24 well plate for other applications. Prior to gel formation the metal rings and Petri dishes were washed in 95% ethanol and coated with 1wt % polyethyleneimine for 10 minutes (PEI, Sigma Aldrich). The PEI was washed away with 95 % ethanol and the ring and dishes left to air dry. 1 wt% glutaraldehyde (Sigma Aldrich) was coated onto the PEI surface and left for 30 minutes, and washed well with dH₂O. 30ul of the neutralised collagen was pipetted into the ring taking care not to introduce air bubbles into the solution, and the gel was allowed to set at 15 °C for 30 minutes. The gels were then covered in basal cell culture media and transferred to a tissue culture incubator.

2.3.12 Formation of hydrogels

NSN was dissolved in basal cell culture media at concentrations between 0.25 – 10 wt % to create a working stock. To improve dissolution the solutions were kept at 4 °C on a rocker for up to 48 hours, until all the solid had dissolved. 30ul of the hydrogel stock was transferred into metal ring moulds (6mm diameter, 1mm depth) and the gels allowed to set for 30 minutes at 37 °C in a tissue culture incubator. After 30 minutes the gels were coated in cell culture media, taking care not to damage the gel during pipetting. Hybrid gels of NSN and collagen I were created by mixing the two solutions together at the appropriate concentration on ice prior to setting the gels in the metal ring

moulds. The hybrid gels are set at 37 °C for 30 minutes and then coated in cell culture media. The gels are denoted NSNx for NSN only gels or Col-NSNx, where x is the final concentration of the NSN gel by %weight/volume. For all gels the final collagen concentration is 0.3 wt%.

2.3.13 Syneresis Measurements

A series of hybrid gels were mixed and gelled within metal ring moulds in replicates of 3 and incubated at 37 °C. The gels were photographed using an upright Zeiss stereomicroscope equipped with a Zeiss Axiocam MRc5 camera, over 51 hours. Syneresis was calculated by measuring the surface area of each gel using Fuji (Image J) software. The syneresis index was calculated as $Area_t / Area_i$, where $Area_t$ is the area of the gel at a given time point and $Area_i$ is the initial volume.

2.3.14 SEM imaging

Preformed hybrid gels were removed carefully from molds using fine tipped forceps and quickly flash frozen in liquid nitrogen on copper grids. The bulk of the gel was broken off of the grid to expose the internal structure of the gel. Each gel was freeze-dried and sputter coated in gold. SEM images were obtained on a JOEL JSM -7600 F field emission scanning electron microscope, operating at 3 kV. Fiber diameters were calculated by measuring random selection of each image. Each micrograph was divided into a numbered 6x7 grid and 10 boxes chosen at random. At least 10 fiber diameter measurements were taken from each box using Image J. The average fiber diameter and SEM was calculated for each sample.

2.4 Results

2.4.1 Synthesis of oligo(N-vinylpyrrolidone) macromonomers

The graft copolymer, poly(NIPAM-*co*-styrene-*graft*-NVP) (NSN) was prepared via a 3-step synthesis as described in section 2.3.1 (Figure 2-1). Graft copolymers, or brush/comb polymers have a linear backbone, from which pendant chains, grafts or brushes are attached. The synthesis of a graft copolymer is typically performed by the

addition of a reactive monomer within the polymer backbone where grafts can later be attached. Subsequently a second polymerisation can be initiated from the reactive monomer or an already synthesised polymer chain can be bonded to the reactive position. NSN was prepared using a third approach, where macromonomers of NVP were synthesised with a polymerisable end group in the α – position. The macromonomers were subsequently grafted to the polymer backbone in a second polymerisation step as the backbone of the polymer formed. Initially the pendant NVP grafts were synthesised via chain transfer to solvent, which produced oligomers containing the repeating NVP unit, functionalised at the α - position with 2-isopropoxyethanol (ONVP-OH) (**1**). To enable addition of the NVP grafts to the NIPAM and styrene backbone the α chain end of ONVP-OH was functionalised with 2-vinylbenzyl chloride to give ONVP-VB (**2**). Lastly monomers of NIPAM, styrene and the ONVP-VB underwent free radical polymerisation to afford a graft copolymer with a NIPAM and styrene backbone and pendant NVP chains (**3**).

¹H-NMR, GPC and MALDI-ToF were used to confirm the expected products of each reaction step. ONVP-OH elutes from the GPC column as one broad peak, which has a number average molecular weight (M_n) of 13500 g mol⁻¹, with an elution time of 19– 26 minutes (Table 2-1). The polydispersity index (PDI), the ratio of M_n to the weight average molecular weight (M_w) indicates how broad the molecular weight distribution of a polymer is. ONVP-OH has a PDI of 2.56, typical of a polymer synthesised by free radical polymerisation. The molecular weight distribution is bell shaped, with a slight skew of higher weight fractions at higher molecular (Figure 2-2).

	Molecular weight (g mol ⁻¹)		PDI
	M_n	M_w	
ONVP-OH	13500	34300	2.56
ONVP-VB	14500	29000	2.01
NSN	30400	91500	3.01

Table 2-1 Molecular weight averages of NVP oligomers and NSN. As determined by GPC.

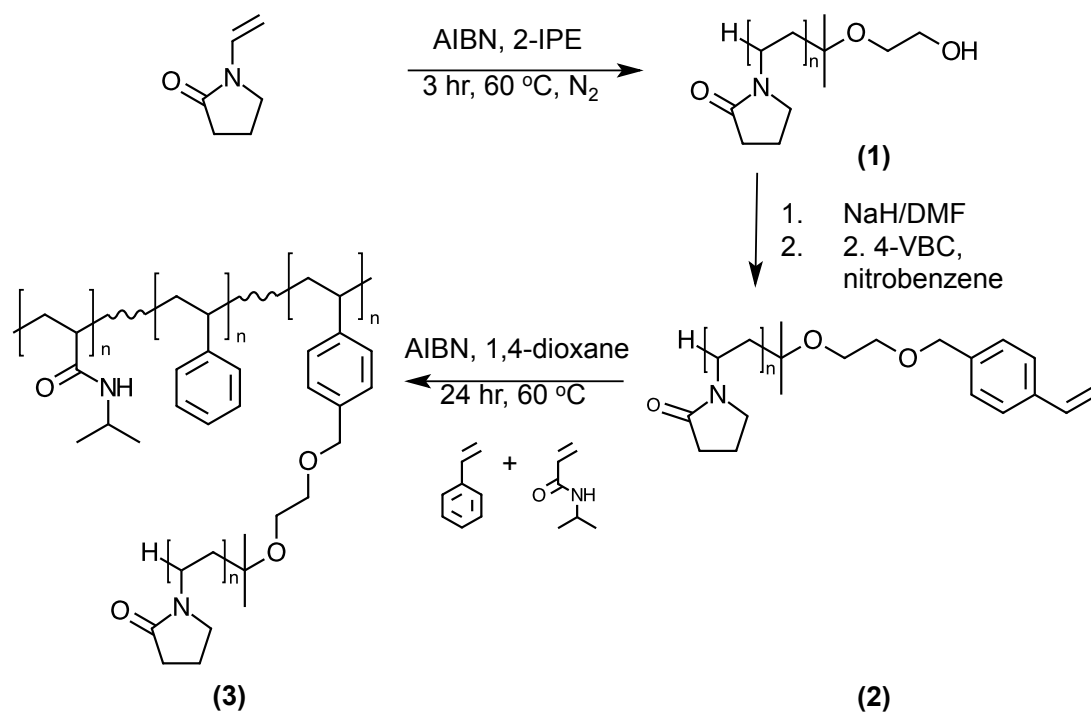


Figure 2-1 Synthetic route to poly(NIPAM-co-styrene-graft-NVP)

Initially NVP oligomers are synthesised by chain transfer to solvent (ONVP-OH), and subsequently functionalised with vinylbenzyl chloride to give polymerisable ONVP-VB. Finally the grafts and backbone of the polymer are formed *in-situ*.

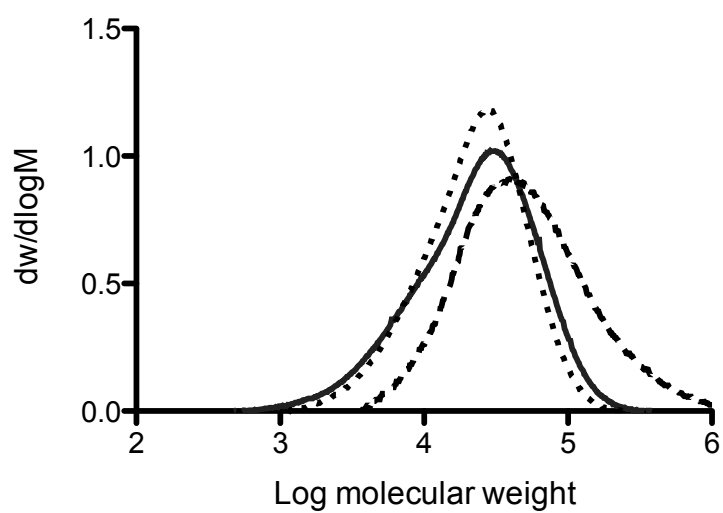


Figure 2-2 Molecular weight distributions of NVP oligomers and NSN. ONVP-OH (solid line), ONVP-VB (dotted line) and NSN (dashed line)

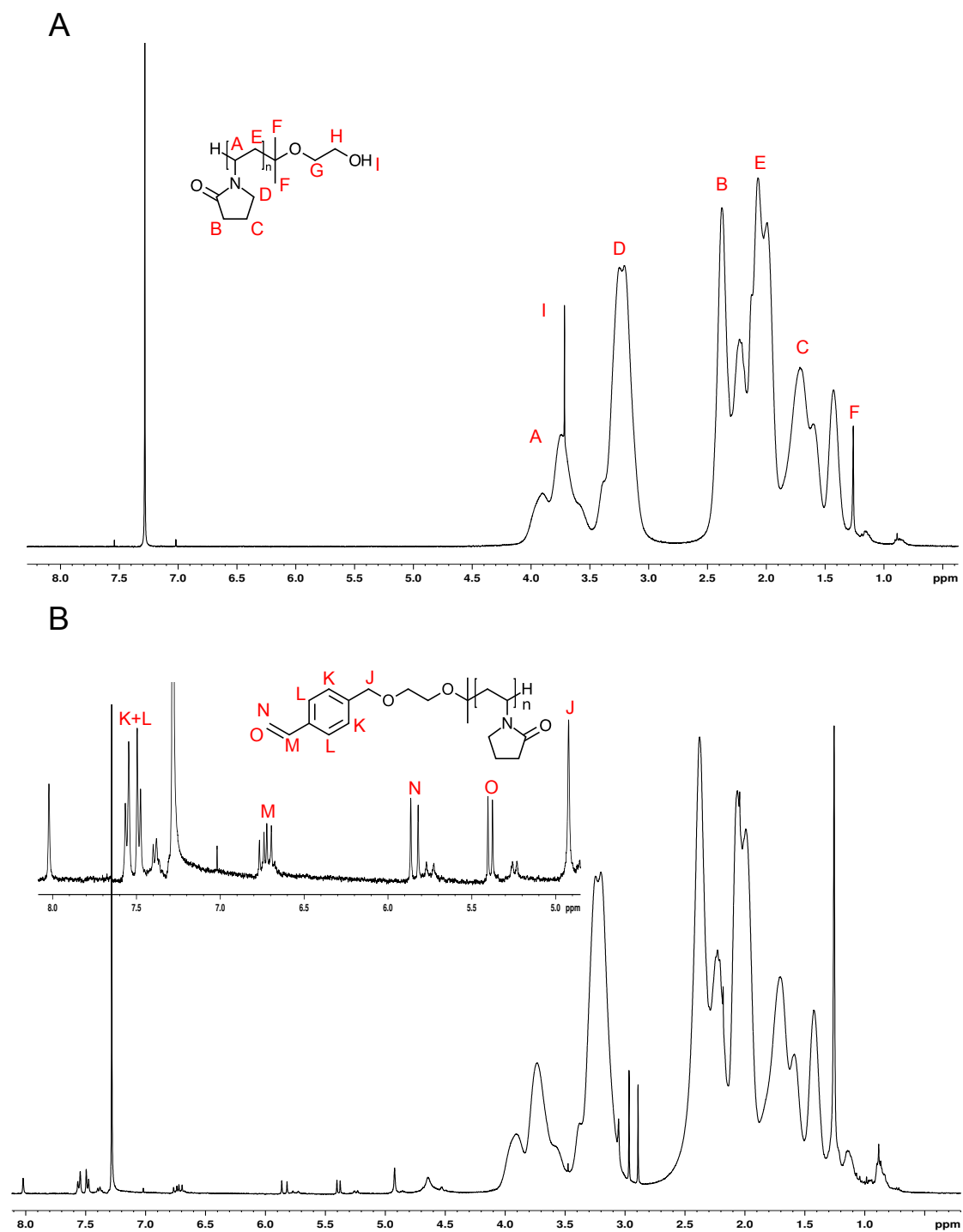


Figure 2-3 $^1\text{H-NMR}$ spectra of NVP oligomers.
ONVP-OH(A) and ONVP-VB (B) in CDCl_3

The chemical shifts of the $^1\text{H-NMR}$ of ONVP-OH are detailed below. $^1\text{H-NMR}$ spectrum for ONVP-OH confirms polymerisation has occurred, as the chemical shifts are broad rather than narrow, which would be seen if the monomer was present. The presence of the isopropoxy end group cannot be confirmed by the NMR as the chemical shifts of the repeating NVP unit overlap with their expected shifts (Figure 2-3A). The end group peaks will also be significantly smaller by NMR, as each polymer has an average number of 121 NVP monomers ($M_n / 111.14$) per each isopropoxy ethanol end group. The presence of the end group can however be confirmed through MALDI-ToF analysis as discussed later. The $^1\text{H-NMR}$ spectrum is consistent with results published by Liu et al²⁵⁶ and Lapworth et al²⁵⁷.

ONVP-OH (3) $^1\text{H-NMR}$ (400 MHz, CDCl_3) δ/ppm : 4.1 -3.5 (t/m, br, $\text{CH}_2\text{-(N)CH-CH}_2\text{-}$, backbone), 3.69 (s, possible -OH) 3.5 – 3.0 (m, br, -N- $\text{CH}_2\text{-CH}_2\text{-}$, pyrrolidoneM), 2.5 – 1.9 (m, br, C(O)- $\text{CH}_2\text{-CH}_2\text{-}$, pyrrolidone and (N)CH- $\text{CH}_2\text{-}$, backbone), 1.9 -1.3 (m, br, - $\text{CH}_2\text{-CH}_2\text{-CH}_2\text{-}$, pyrrolidone) 1.24 (s, - $\text{CH}_3\text{-C-CH}_3\text{-}$, end group)

The functionalised ONVP-OH, ONVP-VB was characterised in the same manner. $^1\text{H-NMR}$ shows functionalisation of ONVP-OH by the appearance of well resolved peaks in the downfield region of the spectrum (6-8 ppm) corresponding to the aromatic ring and alkene end groups introduced by vinyl benzyl functionalization (Figure 2-3B). These peaks do not appear broad as each polymer chain only contains one functional unit, and the chemical shifts do not overlap. The M_n of the ONVP-VB is similar to ONVP-OH, as only the end group has been altered, the overall size in the polymer chains is not effected (Figure 2-2, Table 2-1). However slight changes should be expected due to changes in average polymer size following purification when smaller chains may be removed.

ONVP-VB (2) $^1\text{H-NMR}$ (400 MHz, CDCl_3) δ/ppm : 7.59- 7.44 (dd, aryl protons), 6.77- 6.68 (m, $\text{CH}_2\text{=CH-}$), 5.88- 5.71 (d, $\text{CH}_2\text{-CH-}$), 5.42-5.45 (d, $\text{CH}_2\text{-CH-}$), 4.95 (s, - $\text{CH}_2\text{(O)-CH}_2\text{-}$, backbone), 4.1 -3.5 (t/m, br, $\text{CH}_2\text{-(N)CH-CH}_2\text{-}$, backbone), 3.69 (s, -OH) 3.5 – 3.0 (m, br, -N- $\text{CH}_2\text{-CH}_2\text{-}$, pyrrolidone), 2.5 – 1.9 (m, br, C(O)- $\text{CH}_2\text{-CH}_2\text{-}$,

pyrrolidone), 1.9 -1.3 (m, br, overlapping peaks of $-\text{CH}_2-\text{CH}_2-\text{CH}_2-$, pyrrolidone and (N)CH- CH_2- , backbone) 1.24 (s, $-\text{CH}_3-\text{C}-\text{CH}_3-$, end group)

To demonstrate that the synthesis of ONVP-OH proceeded by chain transfer to solvent and to deduce what proportion of ONVP-OH was successfully functionalised to ONVP-VB, MALDI-ToF mass spectroscopy analysis was employed. As MALDI-ToF uses a matrix-assisted approach in ionization, large molecules can be analysed without fragmentation. The MALDI-ToF mass spectrum of ONVP-OH shows a series of repeating mass peaks, where the signals in each series of repeats corresponds to an oligomer with the same number of repeating monomer units and a differing end group. Each series is separated by the mass of the NVP monomer, $111.14 \text{ g mol}^{-1}$ (Figure 2-4A).

For each NVP oligomer to contain the functional 2-isopropoxyethanol end group, the polymerisation must have proceeded by transfer to solvent (Figure 2-5 scheme 3), rather than direct initiation by AIBN (Figure 2-5 scheme 4). The degree of initiation by chain transfer to solvent can hence be determined by comparison of the peak heights of 2-isopropoxyethanol and AIBN functionalised oligomers. Although initiation by chain transfer is the dominant initiation in the initial synthesis of the oligomer, direct initiation does occur. The expected mass of each end group was calculated using chemdraw, and these were correlated with the appropriate MALDI-ToF peak (Figure 2-4A, Table 2-2). There are two prominent peaks in the ONVP-OH MALDI-ToF spectrum, where the larger of the two, peak A, corresponds to an oligomer with α -isopropoxyethanol, ω -H end functionality (Figure 2-4C). This is the result of chain transfer initiation and hydrogen abstraction termination to give a mass/charge ration (m/z) of $(104.08 + 1 + 23) + n(111.14)$. Where the mass of a proton is included for the termination end group and the mass of a sodium cation from the MALDI ionization. The smaller series of peaks, peak B, corresponds to an oligomer with a cyano end group from initiation by AIBN, and termination by hydrogen abstraction, $m/z = (69.06 + 1 + 23) + n(111.14)$.

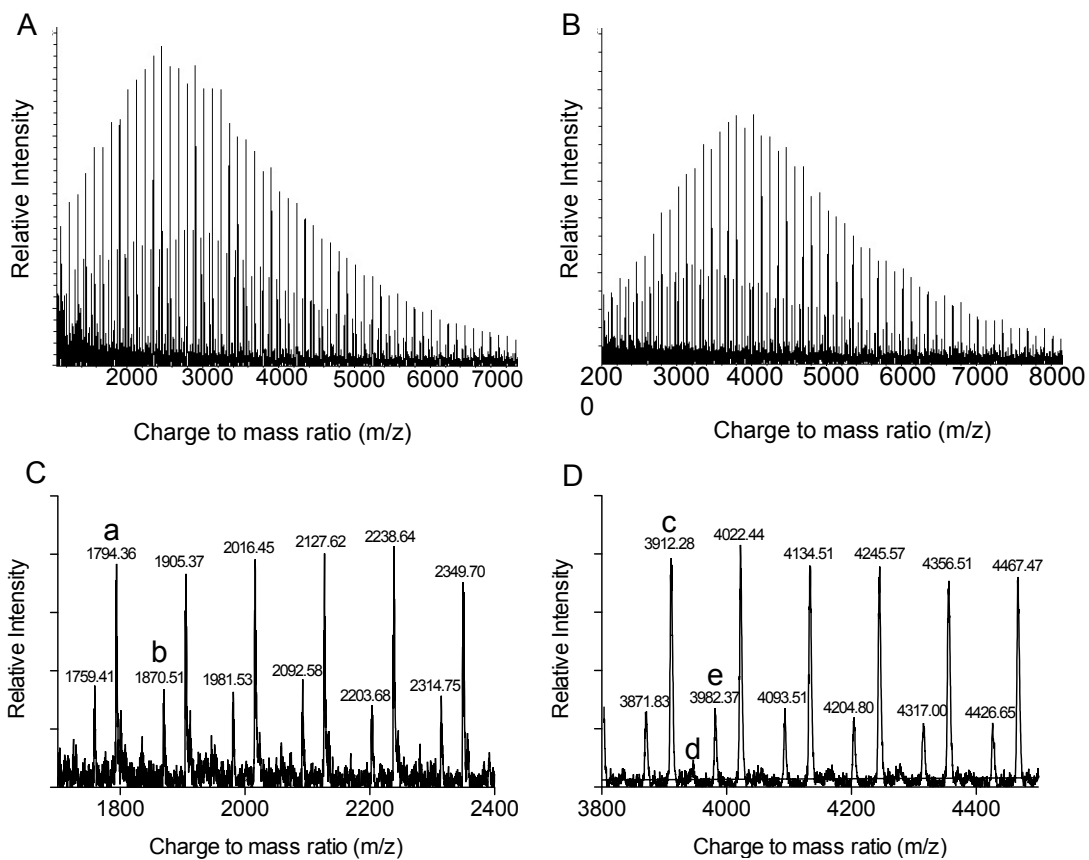


Figure 2-4 MALDI-ToF spectra of NVP oligomers. ONVP-OH (A) and ONVP-VB (B), and expanded regions of spectra A (C) and B (D).

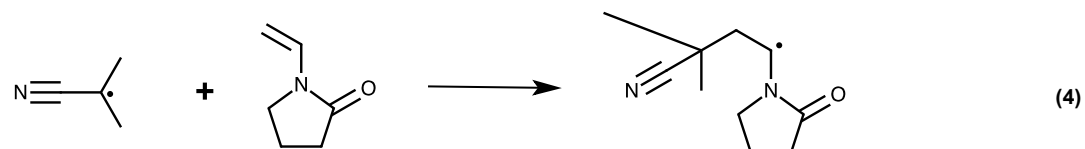
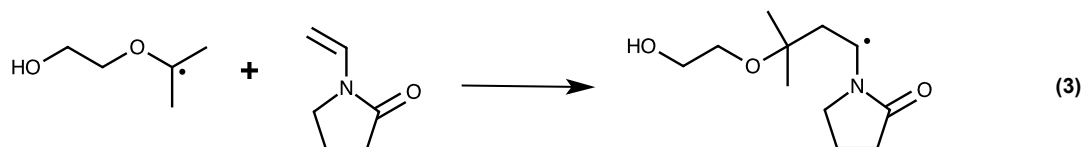
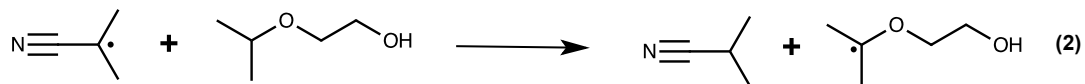
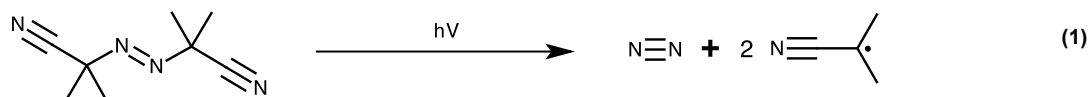


Figure 2-5 Possible initiation mechanisms during ONVP-OH.

Heat treatment causes AIBN to decompose into 2-cyanoprop-2-yl radicals (1). 2-cyanoprop-2-yl radicals initiate 2-isopropoxyethanol radicals (2) or directly initiate NVP polymerisation (4). Radicals derived from 2-isopropoxyethanol initiate NVP polymerisation (3).

The proportion of each end group was calculated as shown below (Equation 2.1) and the equation modified as required for OH and AIBN end groups (Table 2-2). Peaks with low resolution at low and high molecular weights, were excluded from calculations, as well as those that could not be distinguished above baseline noise. Where an isotope pattern has been resolved the most abundant isotope peak was used for the calculation. Chain transfer was the dominant initiation resulting in 61.08% of the product, whilst 38.92% of the resulting product was initiated by AIBN.

$$\%EG = \frac{h_{VB}}{h_{VB} + h_{OH} + h_{AIBN}} \times 100$$

Equation 2.1

where, h_{VB} : height of ONVP-VB end group peak

h_{OH} : height of ONVP-OH end group peak

h_{AIBN} : height of ONVP-AIBN end group peak

The functionalised oligomer, ONVP-VB, should show a repeating series of three peaks, however only two of the peaks are clearly resolved (Figure 2-4D). The larger of the two peaks is functionalised ONVP-OH, giving rise to an m/z of $220.15 + 1 + 23 + n(111.14)$ (peak C) and has α -vinyl benzyl and ω -H end functionality. The smaller series of peaks correspond to the remaining AIBN initiated oligomer (peak E). The third peak that should be apparent would be from any remaining ONVP-OH that has not been functionalised (peak D). However this is not clearly resolved, is of low intensity and hidden beneath the non-isotopically resolved ONVP-VB peak C. Where an ONVP-OH end group could be resolved this was included in calculation for proportion of functionalised end groups. This low abundance indicates most of the ONVP-OH starting material has been functionalised with vinylbenzyl chloride. As expected the highest proportion of oligomers are the vinyl benzyl functionalised product, at 81.67%. Which shows a 20% increase in proportion compared with the 61.08% of ONVP-OH

starting material that was present. Which indicates that the samples were not uniform in composition or that some ONVP-OH was lost in precipitation steps.

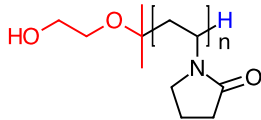
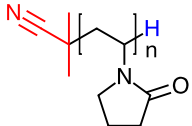
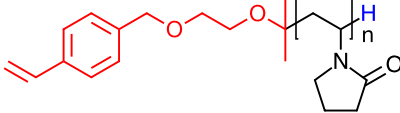
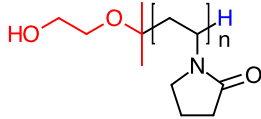
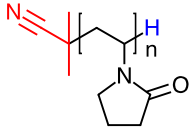
	Peak	Adduct	End group mass (g mol ⁻¹)	% End group
ONVP-OH	A		104.08	61.1
	B		69.06	38.9
ONVP-VB	C		220.15	81.6
	D		104.08	6.0
	E		69.06	16.9

Table 2-2 Expected products of macromonomer synthesis and functionalisation

2.4.2 Synthesis of Poly(NIPAM-co-styrene-graft-NVP)

As the ONVP graft content within NSN will affect the properties of the resulting hydrogel, including the phase transition temperature and the water content, the proportion of reagents in the NSN polymerisation was calculated to produce a polymer with 10 mol% NVP. As only 81.67 % of the ONVP-VB product was functionalised as shown by MALDI-ToF, this was accounted for in reaction quantities. As with the

oligomers the polymerisation of the NSN polymer was confirmed by $^1\text{H-NMR}$ (Figure 2-7). A large peak is visible at 1 ppm arising from the NIPAM isopropyl group, and the aromatic region is now broad rather than well defined as it contains peaks corresponding to the styrene aromatic ring as well as the benzyl groups in each ONVP oligomer. The $^1\text{H-NMR}$ profile of ONVP is still visible, however the peaks are smaller as only 10 mol% of the total NSN polymer is ONVP. By GPC analysis NIPAM-S-NVP has an M_n of 30400 g mol^{-1} (Figure 2-2).

NSN (3) $^1\text{H-NMR}$ (400 MHz, CDCl_3) δ/ppm : 7.51-6.51 (m, br, aryl protons overlapping with $-\text{NH-CH}-(\text{CH}_3)_2$), 4.00 -3.52 (br, s, $-\text{CH}-(\text{CH}_3)_2$), 4.00-1.20 (br, m, overlapping signals of PVP), 1.20-0.80 ($-\text{CH}-(\text{CH}_3)_2$)

2.4.3 Poly(NIPAM-co-styrene-graft-NVP) is thermoresponsive at physiological temperatures

Poly(NIPAM-co-styrene-graft-NVP) dissolved in cell culture media and heated to 37°C resulted in a self-supporting gel. When cooled at 4°C the hydrogel liquefied and was a viscous flowing liquid (). To assess the thermoresponsive properties of poly(NIPAM-co-styrene-graft-NVP) in more detail cloud point/turbidity and rheological methods were performed. The two techniques complement each other as they determine the phase transition temperature based on different properties. By using UV-Vis spectroscopy the phase transition temperature is determined from the cloud point. During the sol-gel phase transition of PNIPAM, the polymer chains collapse from an extended coil to a globule and precipitate out of solution, causing the solution to become cloudy and turbid. The onset of the precipitation is measured by a change in absorbance and the temperature where this occurs is defined as the cloud point. Dilute solutions of polymer are used for turbidity measurements to prevent complete aggregation of the polymer and gelation, and in order for the absorbance to remain low (<1-2). The phase transition temperature as determined by the cloud point /turbidity method for NSN in pure water occurred at $26\text{--}28^\circ\text{C}$ (Table 2-3). Varying the heating rate from $1^\circ\text{C}/\text{min}$ to $0.3^\circ\text{C}/\text{min}$ had a small effect on the cloud point increasing it by a degree for a 0.1 wt% solution in water (Figure 2-8). Varying the concentration of the

polymer in water to 0.05 wt% but maintaining the heating rate of 0.3 °C/min had no effect on the cloud point.

The behaviour of NSN in water upon cooling was also examined. The cooling curves of all solutions regardless of the rate of temperature change did not mirror the heating curves, as the gel-sol transition occurred at lower temperatures than the sol-gel transition. However the slopes of the cooling and heating curves are similar, suggesting that once the transition begins the rate of the transition is the same in both directions.

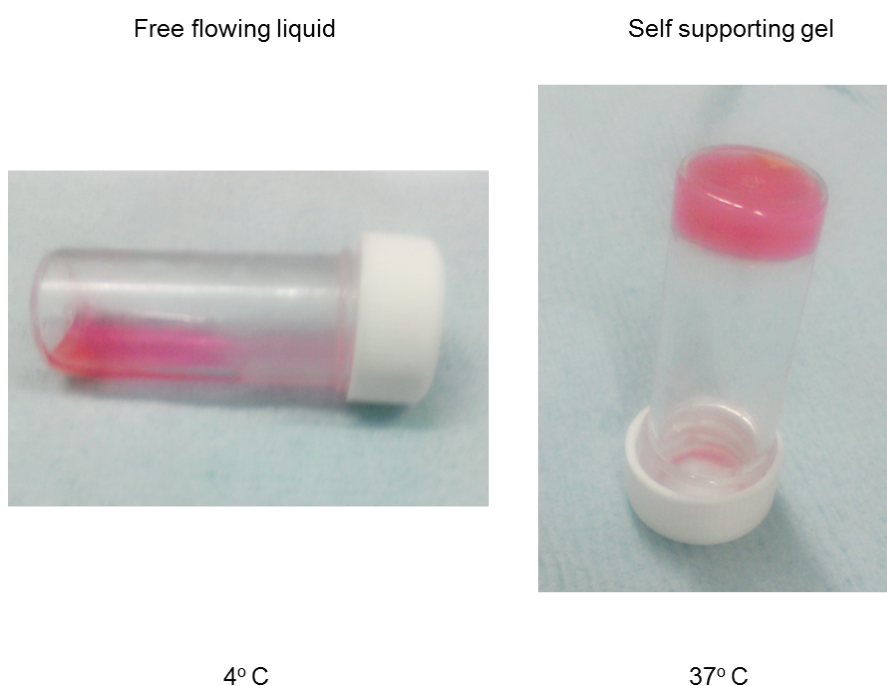


Figure 2-6: Gelation of NSN at physiological temperature.
At 37 °C, 5 wt% NSN forms a self-supporting gel. When cooled to 4 °C the gel liquefies.

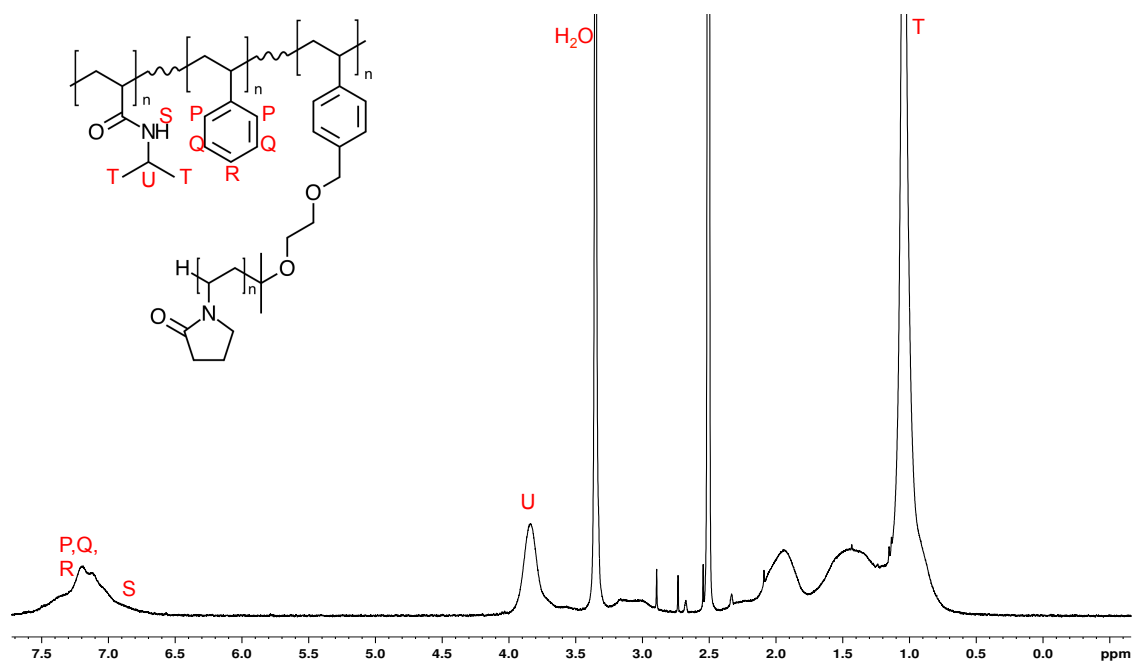


Figure 2-7 $^1\text{H-NMR}$ spectrum of NSN in MeOH

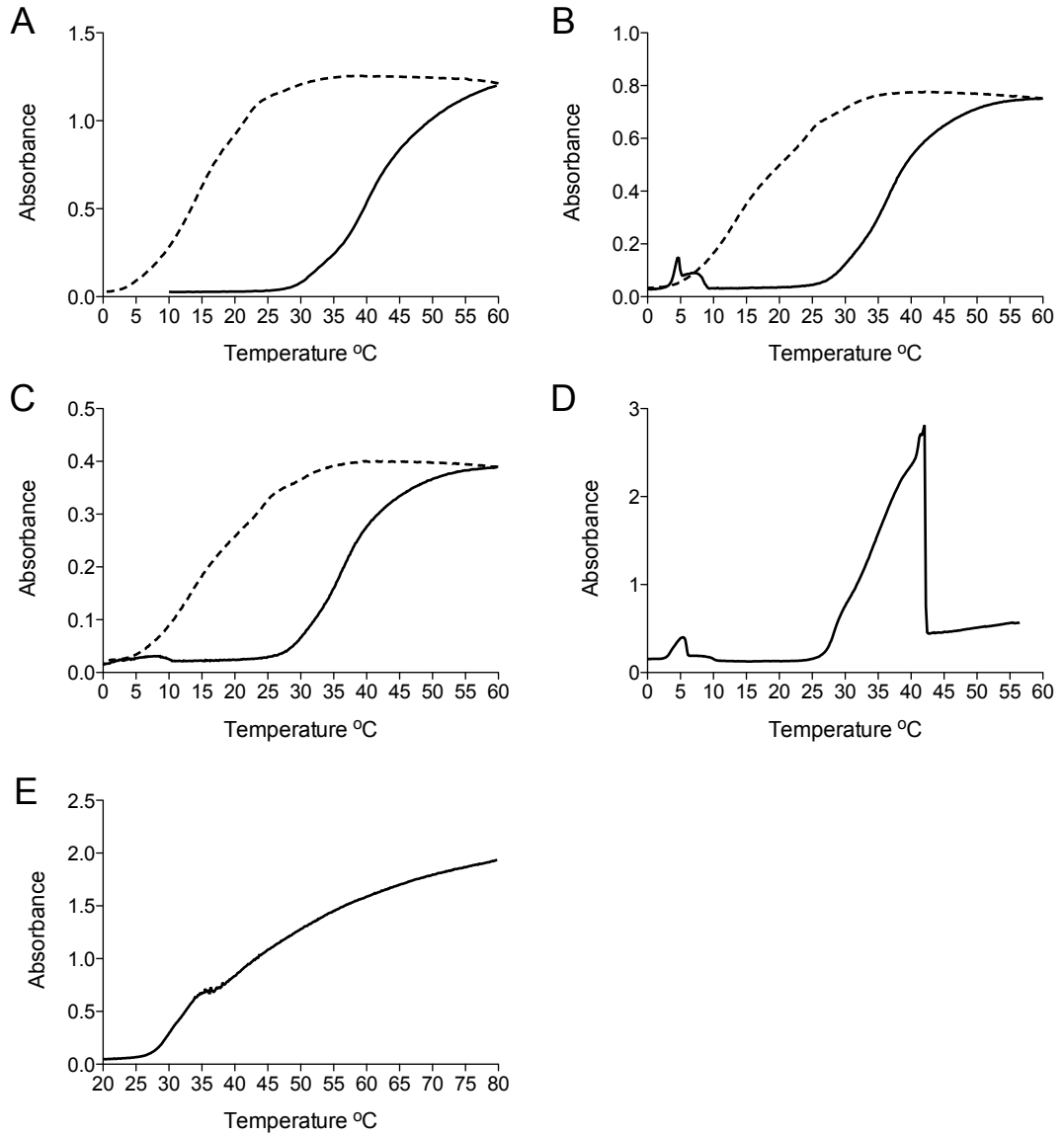


Figure 2-8 Effect of temperature on turbidity of NSN solutions. 0.1 wt% in water, heated/cooled 1 °C/min (A) and 0.3 °C/min (B). 0.05 wt% NSN, heated/cooled 0.3 °C/min (C). 0.1 wt% (D) and 0.05 wt% NSN (E) in DMEM heated/cooled 0.3 °C/min. Solid lines represent heating of solutions and dashed lines represent cooling.

Turbidity			Rheology			
Sample	Heating rate	Cloud Point(°C)	Sample	Crossover (°C)	2 nd transistion (°C)	3 rd transistion (°C)
NSN _{0.1} H ₂ O	1 °C/min	28.5	NSN ₁₀ DMEM	8.1	23.5	33.5
NSN _{0.1} H ₂ O	0.3 °C/min	26.9	NSN ₅ DMEM	9.3	24.0	34.3
NSN _{0.05} H ₂ O	0.3 °C/min	27.0				
NSN _{0.1} DMEM	0.3 °C/min	26.7				
NSN _{0.05} DMEM	0.3 °C/min	26.9				

**Table 2-3 Phase transition temperatures as determined by turbidity(cloud point) and rheology (gel point)
Subscript numbers represent NSN concentrations.**

Turbidity was not ideal for determining the phase transition temperature of NSN dissolved in cell culture media (DMEM). During the sol-gel transition of 0.1 wt% solutions in DMEM, the polymer aggregated together, the solution was no longer homeogenous and the absorbance could not be measured (Figure 2-8D). The cloud point could still be determined from the heating curve, as the aggregation occurred after the onset of turbidity. The cloud point was similar to 0.1 wt% NSN in water, 27 °C. To avoid or reduce the aggregation of the polymer, 0.05 wt% solutions of NSN in DMEM were also tested. Although less aggregation occurred, solutions of 0.05 wt% NSN in DMEM did not plateau during the heating runs (Figure 2-8E). These solutions also had cloud points of 27 °C. The cooling runs of NSN in DMEM also behaved differently compared with the same heating rate and concentrations as the water solutions. The turbidity continued to increase during the cooling run therefore these results has not been included.

The phase transition temperature was also determined from dynamic mechanical analysis (DMA), specifically rheology. Rheology is the study of how a material flows.

The technique can be used to look at the deformation of a material under an applied shear force. As hydrogels are viscoelastic materials and can behave like an elastic solid and a viscous liquid I looked at the rheological response in terms of the storage (G') and loss modulus (G''), which characterise the contribution of the solid and liquid components of the material respectively. When $G' > G''$ the material is in a solid state, and when $G' < G''$ the material is liquid.²⁵⁸ We define the temperature when G' exceeds the value of G'' and gelation occurs as the gel point, as an alternative measurement of the phase transition temperature. As the technique determines the phase transition temperature based on gelation, NSN solutions were used where the concentration was greater than the minimum gelation concentration. The ratio of G' to G'' otherwise known as the loss tangent, $\tan \delta$, can also be used to assess the state of the polymer. When $\tan \delta = 1$, the viscous and elastic properties of a polymer are equal, when $\tan \delta$ is below 1 the polymer is more elastic and solid like.

In order to make accurate measurements, appropriate testing parameters were chosen where the gels behave in a viscoelastic region. A suitable percentage strain was determined by varying the % strain applied on the gel between 0 – 100 % and maintaining the oscillating frequency constant at 0.5 Hz. At a given % strain a viscoelastic gel will stop deforming elastically and become permanently deformed, therefore a % strain for future measurements is chosen where deformation will not be permanent. Likewise an appropriate oscillating frequency was chosen for further rheological testing by performing a frequency sweep between 0.01 – 10 Hz. Subsequent experiments to determine the gel point involved temperature ramps, therefore the viscoelastic region was identified for NSN₅ gel in DMEM at 0 °C and 37 °C (Figure 2-9).

At 0 °C, below 1% strain, the moduli of the NSN solution was noisy due to the low mechanical strength of the dissolved polymer and low applied strain (Figure 2-9A). Above 1% strain a viscoelastic response was observed, even at high % strains. Whilst in a liquid state the NSN solution is able to flow and resist deformation. At 37 °C the opposite effect is seen. At low % strains the gel can resist deformation, but above 3%

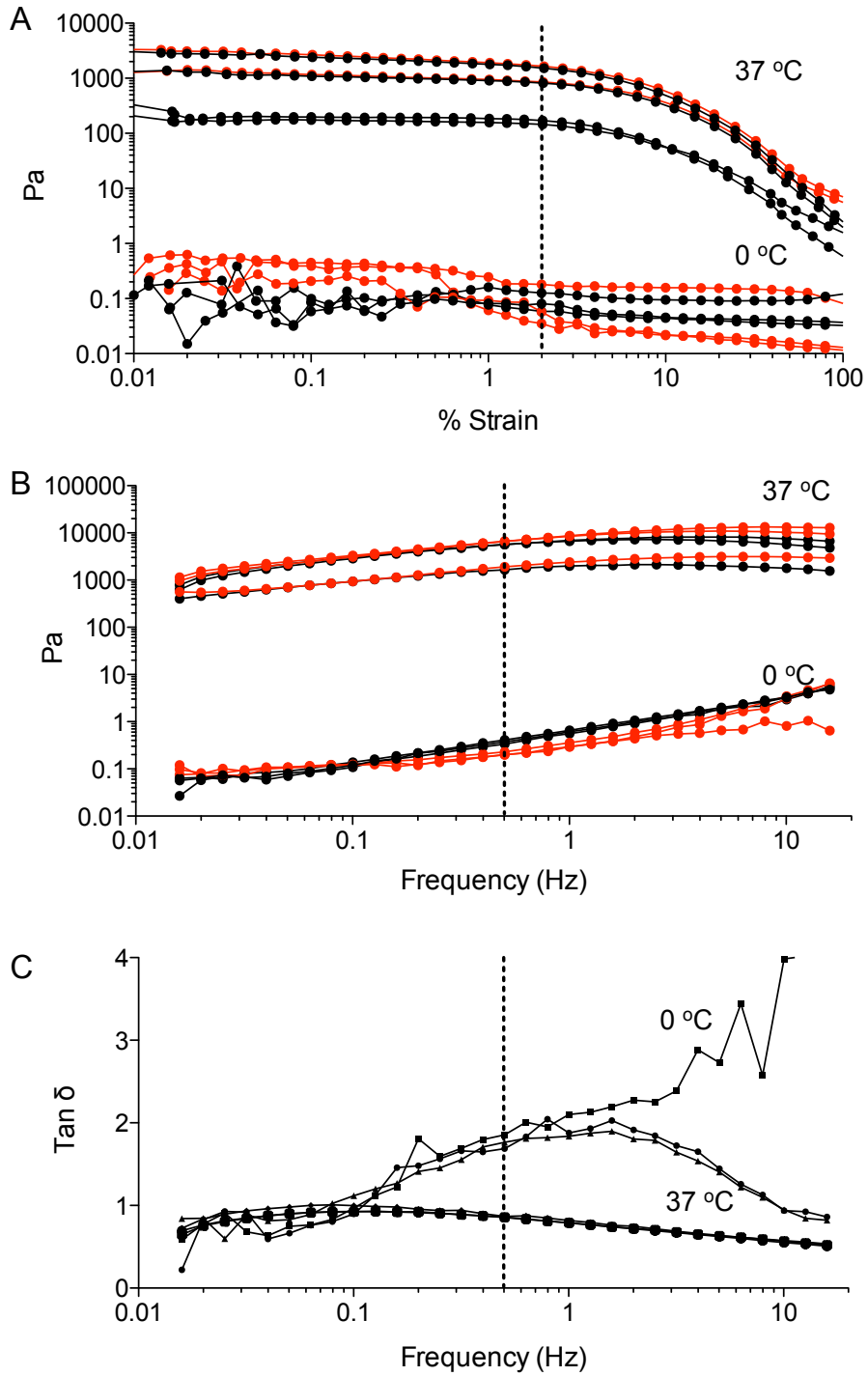


Figure 2-9 Determination of accurate rheology % strain rates and frequency NSN₅ at 0 and 37 °C. % Strain sweeps performed between 0.01 and 100 % strain (A) and frequency sweeps of 0.01 to 10 Hz (B). Red and black lines represent G' and G'' respectively. The effect of frequency on Tan δ (C).

strain the complex modulus decreases and the material begins to deform plastically. Therefore a 2% strain was used for all subsequent experiments. At 0 °C when the polymer remains in a dissolved state, the moduli are dependent on frequency, slowly increasing as the polymer has newtonian like behaviour (Figure 2-9B). The same is observed for $\tan \delta$, which increases with frequency up until 2 Hz. At 37 °C the moduli steadily increase with frequency, however between 0.5 – 1 Hz they appear dependent of frequency. $\tan \delta$ decreases slightly during the frequency sweep at 37 °C, but compared to the 0 °C sweep it is relatively independent of frequency, indicative NSN was in a gel state (Figure 2-9C). Therefore 0.5 Hz was chosen for further rheology experiments.

Temperature sweeps between 0 – 40 °C, at a heating rate of 1 °C/min, were carried out using NSN₁₀. The G' - G'' crossover gel point occurred at temperatures lower than expected compared to the turbidity results (Figure 2-10) this was also observed for NSN₅. From the curves of the storage and loss moduli, NSN appears to go through three transitions upon an increase in temperature, which can be more clearly seen within $\tan \delta$ values. Below 5 °C both the storage and loss moduli are low where G' is greater in value, both values begin to increase above 5 °C and crossover around 10 °C. Above the gelation temperature both moduli continue to increase and linearly with changes in gradient around 23-24 °C and again at 35 °C. Although the G' - G'' crossover occurs lower than expected the moduli undergo a sharp increase at 23-24 °C, close to the temperature suggested for the phase transition temperature by turbidity. At 23-24 °C the value of $\tan \delta$ also begins to increase suggesting the gel is becoming less elastic and more viscous. This could be an effect of water expulsion from the gels as the polymer chains form globules, in agreement with the turbidity results, which suggest the coil-gobule transition occurs around this temperature.

2.4.4 Fabrication of NSN and collagen I hybrid gels

Hybrid gels were created by gently mixing NSN with solubilised collagen I on ice and allowing the solutions to gel in the presence of each other. The collagen concentration was 0.3 wt% in all gels, and NSN concentrations were 2.5, 1.25, 0.5 and 0.25 wt%. 5 wt% NSN gels and 0.3 wt% collagen gels were used as controls in each experiment.

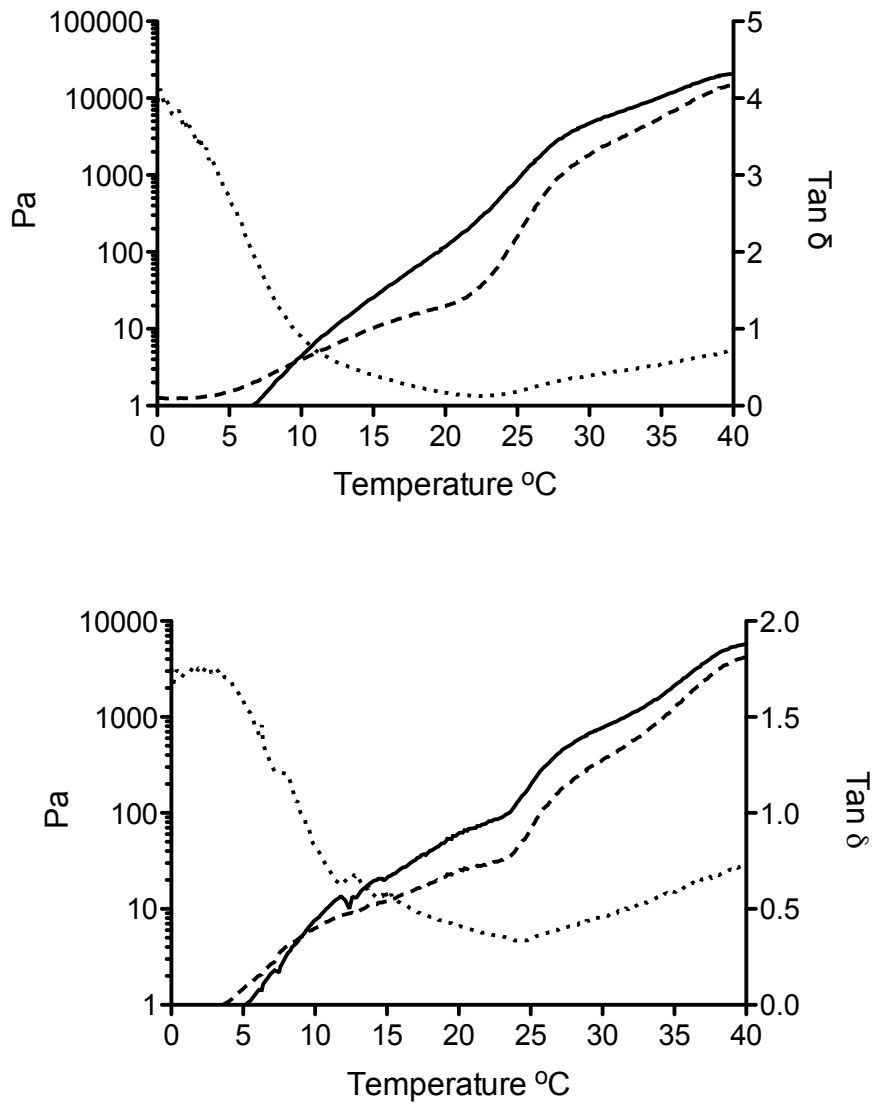


Figure 2-10 Determination of NSN₁₀ gel point by rheology. Effect of temperature on G' (solid line) G'' (dashed line) and Tan δ (dotted line) of NSN10 (A) and NSN5 (B). Asterisks on the curves represent a sudden change in gel properties.

Solutions below 2.5 wt% NSN were unable to gel into self-supporting gels, whilst gels did form from NSN concentrations lower than 2.5 wt%, when blended with collagen.

In order to create reproducibly sized gels with a flat upper surface, metal washer moulds were used. The rings produced gels 6mm in diameter with a 1 mm depth. Gels that had been cast within 96 well plates, were not uniform the dimensions, as the gels formed a meniscus with the sides of the well.

2.4.5 Collagen I reduces syneresis in Poly(NIPAM-co-styrene-graft-NVP) gels

The syneresis was most significant in the hydrogel only gel, NSN₅, whilst no shrinking was observed in acellular collagen only gels (Figure 2-11). The syneresis in the NSN only gel continued for at least 36 hours after the initial gelation had occurred. However within the hybrid gels where the concentration of collagen was similar to the concentration of NSN very little syneresis occurred. The syneresis of the gels was quantified by a syneresis index equal to the surface area of the gel at a given timepoint ($Area_t$) divided by the initial gel surface area ($Area_i$). The least syneresis was observed for Col-NSN_{0.25}, with an index of 0.953. The indices for Col-NSN_{0.5} and Col-NSN_{1.25} were similar to Col-NSN_{0.25}, 0.92 and 0.93 respectively. As the NSN concentration increased the index decreased, where the index for Col-NSN_{2.5} is 0.56 approaching the index for a pure NSN₅ gel of 0.31.

2.4.6 Mechanical strength of hybrid gels vary with NSN content

The shear mechanical properties of the hybrid gels were investigated using rheology, using the % strain and frequency previously determined in section 2.4.3. This analysis was carried out at 37 °C only, as the hybrid gels may ultimately be used as an injectable and therefore would gel at body temperature, unless the gelation temperature was otherwise controlled *in-vivo*. Constant % strain and frequency was applied to each gel for 30 minutes. Time sweeps of collagen were only performed for 20 minutes as G' and G'' had plateaued within this period. Solubilised collagen gelled within the initial 1 minute temperature equilibration of the rheometre heat plate prior to the run, with G' remaining higher G'' for the entire 20 minute run (Figure 2-12A). Within the first 10

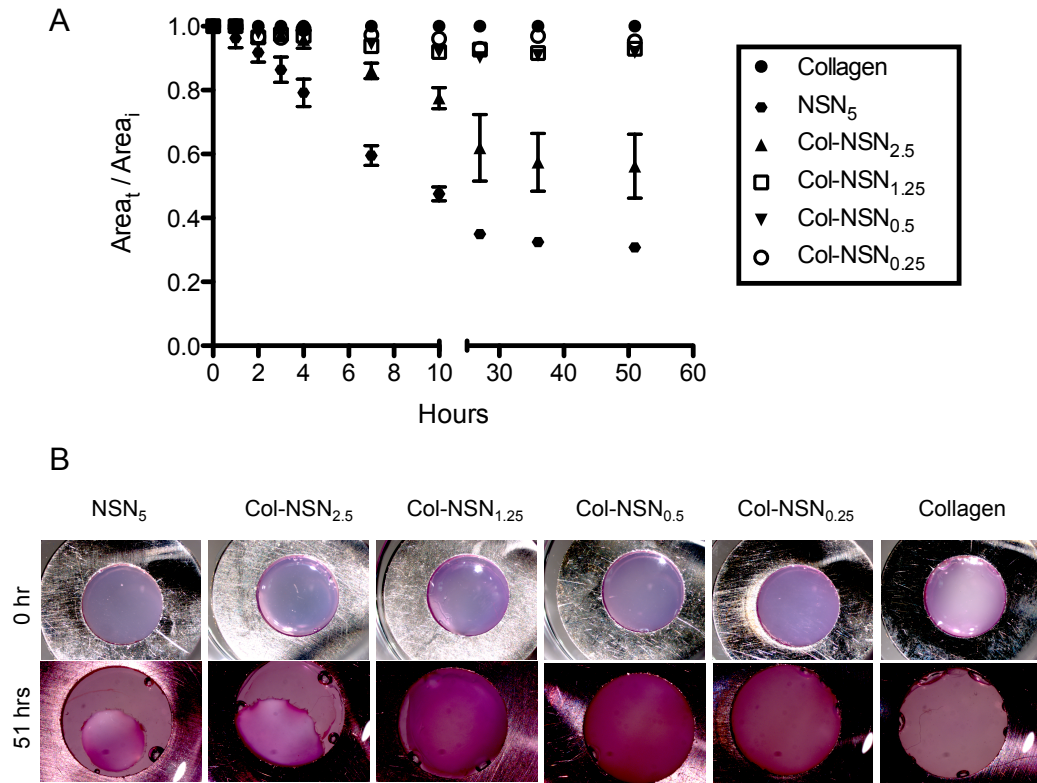


Figure 2-11 Syneresis index of NSN, collagen and hybrid gels.
 Gels maintained at 37 °C for 51 hours (A) and representative images of gels used for measurements (B) Results are mean ±SEM (n=3).

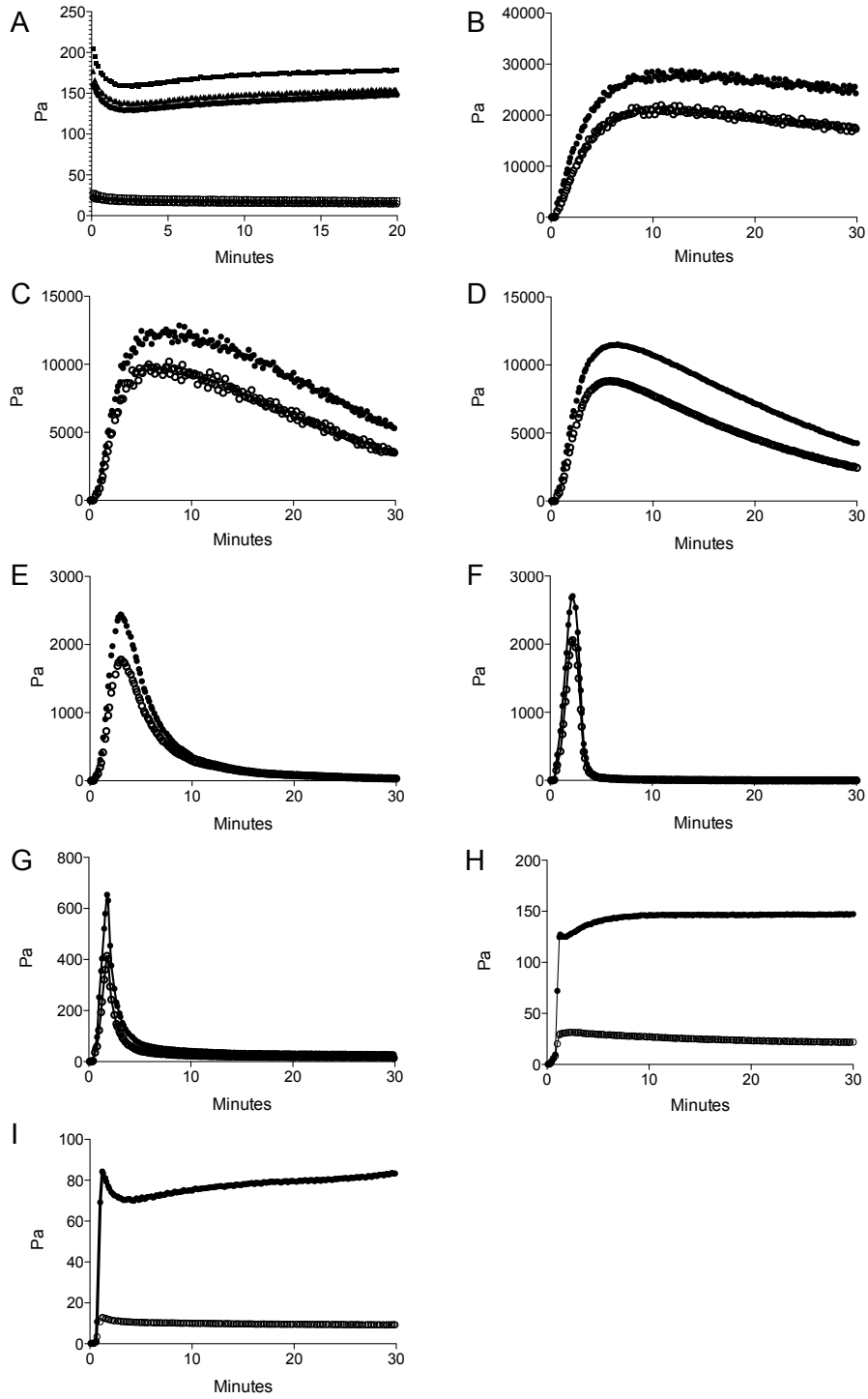


Figure 2-12 Behaviour of hybrid gels under shear forces
 Evolution of G' (solid circles) and G'' (open circles) during 30 minute dynamic time sweeps at 37 °C. Collagen (A), NSN₁₀ (B), NSN₅ (C), Col-NSN₅ (D), NSN_{2.5} (E), Col-NSN_{2.5} (F), Col-NSN_{1.25} (G), Col-NSN_{0.5} (H) and Col-NSN_{0.25} (I). %strain and frequency were maintained at 2% and 0.5 Hz throughout.

minutes both G' and G'' increased sharply and then began to plateau. During the second half of the run the moduli continued to increase slowly to a maximum of 160 Pa.

Sample	G'_{peak} (Pa)	G''_{peak} (Pa)	G'_{final} (Pa)	G''_{final} (Pa)
NSN₁₀	30817	23326	29253	21054
NSN₅	10652	8457	2401	1569
NSN_{2.5}	2692	2006	33	30
Col-NSN₅	11282	8641	3965	2311
Col-NSN_{2.5}	1410	1044	2	1
Col-NSN_{1.25}	426	270	13	8
Col-NSN_{0.5}	124	15	124	15
Col-NSN_{0.25}	79	9	79	9
Collagen	160	40	160	40

Table 2-4 Shear mechanical properties of NSN and Col-NSN gels

Compared with the collagen results, the runs for NSN₅ and the hybrids display a different trend (Figure 2-12B-G). Gelation occurred during the initial rise in temperature of the plate to 37 °C and G' remained larger than G'' through out the runs, similarly to collagen. However in contrast to the collagen gels which reach a peak in the storage and loss moduli and plateau or slowly continue to increase displaying strain-stiffening, the hybrid gels reach a peak in their storage and loss moduli and then rapidly fall and begin the plateau. The rate at which the moduli fall is roughly proportional to

the concentration of NSN within the gel where the lower concentration of NSN within the gel, the faster the rate of decrease in the moduli. When the NSN concentration is similar to collagen (Col-NSN_{0.5} and Col-NSN_{0.25}), the gels are able to maintain their mechanical strength. There is also evidence of strain stiffening in these gels.

To assess the shear moduli of the hybrid gels, an average value for both the storage and loss moduli was calculated for the peak moduli (G'_{peak} and G''_{peak}) and final moduli (G'_{final} and G''_{final}) after a 30 minutes time sweep at constant temperature, % strain and frequency (Table 2-4). The values were averages of 10 measurements of the moduli at the peak and the end of the run (n=3). In the case of some hybrids where the NSN concentration was similar to the collagen concentration the final moduli values were also the peak values, as the collagen was undergoing strain-stiffening and responsible for the bulk mechanical properties of the hybrid gel. Although there was an initial very sharp peak this was excluded from calculations.

The initial stiffness of Col-NSN gels during the runs, defined by G'_{peak} and G''_{peak} , increased with the NSN concentration, where the effect of NSN on the moduli of the hybrid gel's was most substantial in the Col-NSN₅, Col-NSN_{2.5} and Col-NSN_{1.25} (Table 2-4). NSN concentrations lower than 1.25 wt% had little effect on increasing the mechanical strength of the gel compared to collagen alone. The stiffness of NSN gels was also determined in the same way. Again increasing the concentration of NSN increased the mechanical strength, but the relationship was not directly proportional. The stiffness of the Col-NSN₅ hybrid gel was roughly equal to the sum of the individual NSN₅ and collagen gels, however this was not a trend for all blends, the peak moduli of Col-NSN_{2.5} was half the value of NSN_{2.5} alone.

2.4.7 Internal structure of hybrid gels varies with NSN concentration

To assess the structure of the hybrid gels, how it varies between the blends, and to infer how the structure of the hybrids may affect the mechanical properties, SEM microscopy

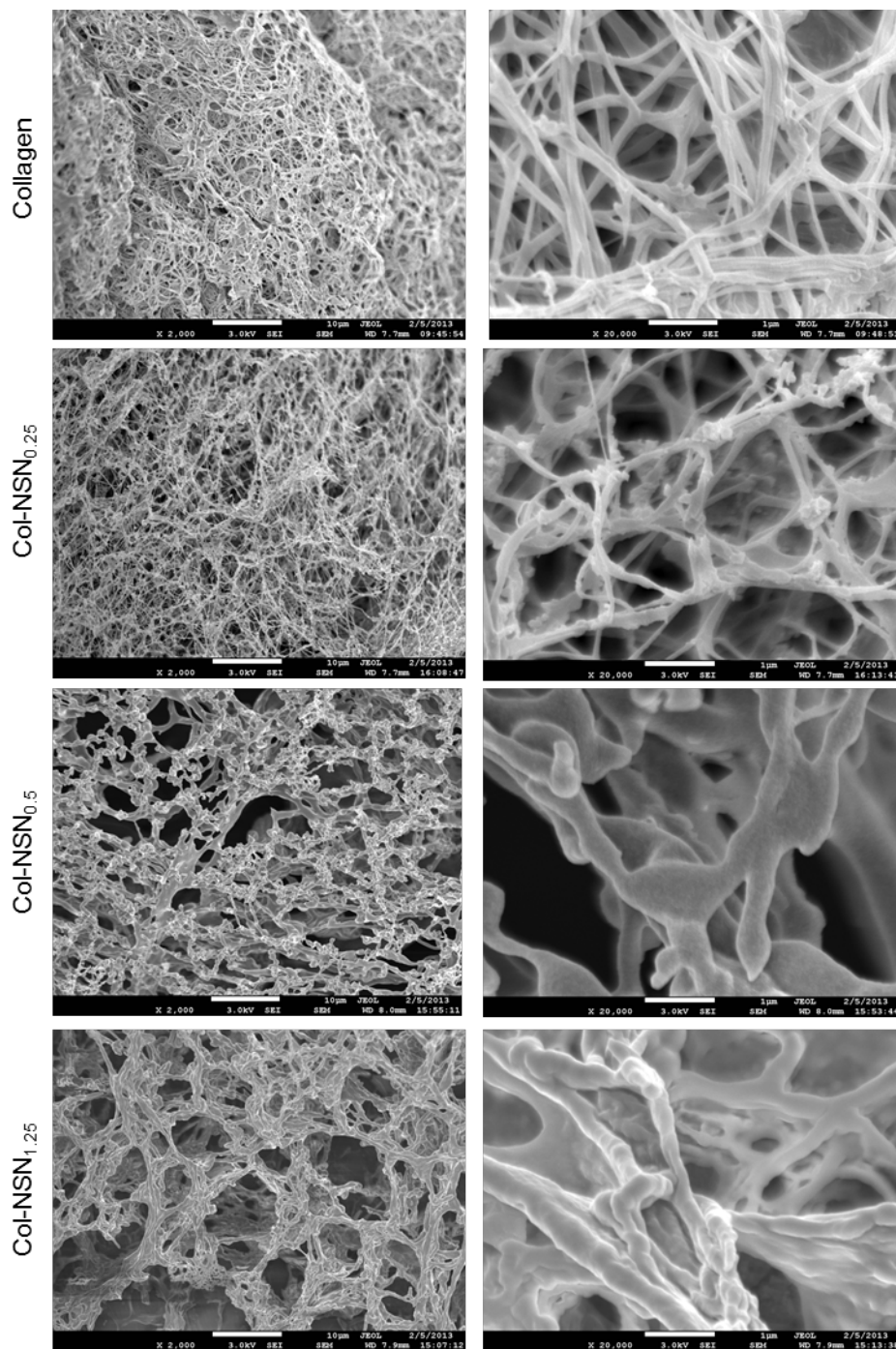


Figure 2-13 SEM micrographs of collagen and hybrid gels. Scale bars are 10 μm in the upper row and 1 μm in the bottom.

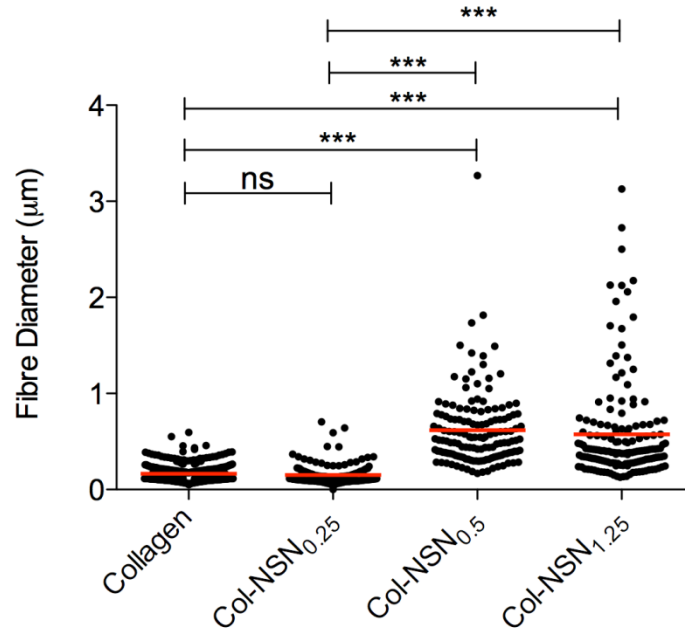


Figure 2-14 Fibre diameters measurements of collagen and NSN fibres in hybrid gels

was performed. Collagen gels contain a network of thin, delicate fibrils, uniform in diameter along their length (Figure 2-13) In some areas aligned, parallel fibrils can be observed forming into thicker fibres. To assess changes in the collagen network upon inclusion of NSN fibril diameter measurements were carried out using Image J analysis software. At least 10 fibril diameter measurements were taken from 20 random areas of each micrograph. The collagen fibrils ranged between 100 – 300 nm in diameter (Figure 2-14).

Inclusion of NSN within the gels altered the gel microstructure. Col-NSN_{0.25} has a similar fibrillar network to collagen gels, the variation in the fibril diameter within the network was not significantly different from collagen gels, but the gel also contained rounded aggregates randomly attached to the fibrils. At the higher NSN concentrations, the fine collagen network is less obvious in the SEM images. The collagen network is less dense and there are larger voids within fibrils, as the entire network appears to be coated with the globular NSN particles. The fibril diameters within the hybrid varied from 100 nm, where collagen fibrils were exposed up to 3 µm, in regions where NSN

appeared to be aggregated on to the collagen. The number of the thicker collagen-NSN fibril aggregated increased with NSN concentration. Inclusion of NSN within the hydrogels resulted in more diffuse and porous structures compared with collagen alone.

2.5 Discussion

2.5.1 Synthesis of poly(NIPAM-co-styrene-graft-NVP)

Synthesis of ONVP-OH, ONVP-VB and poly(NIPAM-co-styrene-graft-NVP) gave the same results as previously published²⁵⁷. There are similarities in molecular weight distributions of ONVP-OH, ONVP-VB and NSN within this thesis and the ¹H-NMR spectra of each product also matches the results of the previously published values.

As the ONVP-VB synthesis proceeds via chain transfer to solvent, the initiation of the polymerisation can proceed by direct initiation from the AIBN derived primary radical (Figure 2-5 scheme 4) or chain transfer from the solvent (Figure 2-5 scheme 1-3). This method of oligomer synthesis, yielding functionalised chain ends has been previously shown to occur through several initiation reactions, including direct initiation from the primary radical, 2-cyanoprop-2-yl radical, however chain transfer to solvent was the dominant reaction²⁵⁹. When 3-methylbutan-2-one and AIBN were used to generate NVP oligomers with methyl ketone end groups, chain transfer to solvent was also the dominant initiation, and in comparison with the above, results in a small proportion of NVP oligomers that had been initiated by the 2-cyanoprop-2-yl radical²⁵⁶. Various solvents have also been used as chain transfer agents in order to generate NVP oligomers including ethyl L-lactate²⁶⁰ methyl isobutyrate, methyl propionate, diethyl malonate and diethyl-2-methylmalonate²⁶¹. This route of synthesis results in low molecular weight polymers, suitable for peptide functionalization and graft synthesis. MALDI-ToF was employed to determine the proportion of NVP oligomers, which had the iso-propoxy end group. 81% of ONVP-OH was functionalised from a hydroxyl end group to 4-vinyl benzyl, in agreement with the previous study.²⁵⁷

At high molecular weights and high polydispersity the sensitivity of MALDI-ToF decreases, therefore only well resolved peaks were included in analysis. To obtain

'cleaner' MALDI-TOF spectra and reduce the PDI of the ONVP-OH oligomers, fractionation techniques could be adopted during the precipitation stages and confirmed by GPC.

2.5.2 Thermoresponsive behaviour of NSN

Determination of the phase transition temperature of NSN by turbidity and rheology, gave different values, 26-28 °C and 8-9 °C respectively. The variation seen in these values could be attributed to the technique used for the analysis, as each method measure the transition through different properties. Rheological methods define the phase transition temperature at the gel point, when the storage modulus, G' is equal to the loss modulus, G'' , and the elastic properties of the polymer exceed the viscosity. Whilst turbidity measurements determine the cloud point of PNIPAM, the temperature when PNIPAM becomes insoluble, forms aggregates and precipitates, causing clouding of the solution. This is measured by changes in absorbance. A third technique that is commonly used to determine the phase transition temperature thermodynamically is differential scanning calorimetry (DSC) which measures the endotherm produces as the hydrogen bonding network between the polymer and water is disrupted when PNIPAM phase separates.

One possible explanation for the discrepancies in the techniques could be the effect of polymer concentration on cloud point measurements. A true LCST value can only be determined from a phase diagram examining polymers at a range of concentrations, as the phase transition temperature will vary. Boutris et al. saw a 10 °C decrease in cloud point measurements whilst varying the concentration from 0.5 – 22 wt% for low molecular weight PNIPAM ($M_n = 9000 \text{ g mol}^{-1}$)²⁶². They also observed the values calculated for the phase transition temperature for 1 wt% PNIPAM were 5 °C lower when determined by DSC compared with turbidity measurements, indicating cloud points from turbidity are higher in temperature than the phase transition temperature. Lower concentrations were not analysed in their study, and the effect on the cloud point could be more extreme at even lower concentrations. However both Winnik¹⁸⁷ and Fulshige²⁶³ have shown at higher molecular weights, $< 1700000 \text{ g mol}^{-1}$, and using

fractionated samples with polymer concentrations down to 0.005 wt% the cloud points are not effected by concentration. The molecular weight of NSN (Table 2-1) falls between the molecular weights studied in these experiments and therefore the low concentration of NSN (0.05 – 0.1 wt%) used in these turbidity studies could result in an cloud point higher than the gel point value of the phase transition temperature.

The high cloud points from turbidity measurements could also be explained with respect to the mechanism involved during the phase transition. The compacting of the PNIPAM coil prior to globule formation and aggregation are events that cannot be distinguished from each other by turbidity measurements. As a result of the low concentrations and molecular weight of the polymer used for the turbidity measurements, the cloud point may appear higher than the LCST as only the globule aggregation stage may produce enough turbidity in the solution to change the absorbance at 500 nm.

While the turbidity measurements were performed on 0.1 and 0.05 wt%, the polymer solutions for rheological experiments were significantly higher, 5 and 10 wt%, and this difference in concentration could also explain the difference in results. Most light scattering and fluorescence studies on single chain behaviour at the phase transition temperature to determine the mechanism of PNIPAM collapse, used polymers with a low polydispersity <1.05 index and high molecular weight $M_w > 10^6$, in order to produce meaningful results, and reduce any intermolecular interactions^{190–192,264}. The situation may be quite different for concentrated solutions. Although the polymer chains will collapse and aggregate, inter-chain entanglements may occur below the LCST, resulting in experimental values lower than the LCST. Rheology time sweeps showed that $G' = G''$ at 8.1 °C for 10 wt% NSN and 9.3 °C for 5 wt% NSN. However the effect of temperature on both G' and G'' changed for a 2nd (23.5 -24 °C) and 3rd (33.5 -34 °C) transition, that is not seen in turbidity studies. The values for the 2nd transition are consistent with turbidity measurements, assuming the cloud points occur at a temperature 2-3 °C higher than expected due to low concentration. The temperature of the 2nd transition is also associated with a minimum value in the loss tangent, where the polymer is behaving most elastically and gel like. The decrease in the $G' - G''$ gel point temperature with increasing concentration is also indicative that high concentrations of

NSN may result in increased entanglements and viscosity in the polymer solution and therefore a lower gel point than the actual LCST value.

Based on these results, it is likely the true LCST occurs around 25 °C for NSN, where the 2nd rheology transition occurs and a few degrees lower than the cloud point. The turbidity measurements use dilute solutions and therefore may only show the turbidity once full polymer collapse and aggregation has occurred. Whilst the concentrated solutions used for rheology measurements show gel like behaviour at lower temperatures due to chain entanglements.

Another important point in the LCST characterisation is the solvent NSN was dissolved in. Turbidity measurements were carried out in both water and DMEM, whilst the rheological measurements were only performed in DMEM. DMEM used for the rheological studies contains MgSO₄ among other inorganic salts to support cell growth *in-vitro*, and may be contributing to the change in the phase transition temperature of PNIPAM as seen by rheology. Although the variation in the cloud point values was less than 1 °C between water and DMEM (Table 2-3), the effect may be greater in the more concentrated solutions used for rheology. This could be justified by investigating the gel point of NSN in pure water at the same concentrations. Furthermore a value of 25 °C for the LCST is typical of PNIPAM copolymerised with a hydrophobic monomer. Considering the decrease in the LCST upon copolymerisation with styrene from previously published results, and the effect of hydrophilic monomers increasing the LCST the combination of styrene in the PNIPAM backbone and NVP grafts may cancel each other. The fact the LCST is lower than 32 °C indicates the styrene has a bigger effect than NVP, which would be expected as the NVP within the polymer is separated from the collapsible PNIPAM chain, and the two chains can behave relatively independent of each other.

Zhao et al. synthesised NVP-g-NIPAM and linear NVP-co-NIPAM polymers containing 20 wt% NIPAM and 80 wt% NVP. The graft copolymer has a LCST of 35.5 °C, whilst the linear polymer did not exhibit a phase transition. The high hydrophilic content of NVP directly bonded to NIPAM prevents the chain collapse. In the graft

polymer the hydrophilic NVP backbone only increases the LCST by a few degrees, even though the proportion of NVP in the polymer is 4 times greater than NIPAM, as the distribution of the two monomers are separated from each other. This provides further evidence that the presence of hydrophilic or hydrophobic monomers do not greatly affect the LCST unless they exist in the same part of the polymer as PNIPAM, otherwise the PNIPAM can still collapse into globules.

Solutions of NSN exhibit a degree of hysteresis when cooled down, as shown by turbidity. During heating, the solutions begin to go turbid around 26 °C, however when the solutions are cooled back down the turbidity begins to decrease around the LCST but the dramatic drop occurs in the region of 23 – 20 °C. This could be a result of intra-chain interactions within NSN, although the globule aggregates may have separated above 23 °C, the chains are still crumpled coils. Wu et al. have shown that the crumpled coils formed in the first stage of the phase transition are stable for at least 44 hours, and therefore the balance between the hydrophobic effects of aggregations dominates over and hydrogen bonding between water until lower temperatures. Wu has also shown intra-chain hydrogen bonding in crumpled coils is maintained until lower temperatures than the LCST²⁶⁴. Other groups have also observed hysteresis between the heating and cooling turbidity, but to a larger extent, where the hysteresis was 11 °C.²⁵⁷ The temperature difference was a lot smaller in my results, as the full extent of intra-chain collapse may not have been observed in turbidity, and below a certain size the polymer chains would not have been observed. Alternatively the presence of NVP grafts could contribute to less stable crumpled coils compared with linear PNIPAM, due to less intra-chain hydrogen bonding.

2.5.3 Conclusions on the LCST of NSN

From the above results it is obvious that behaviour of NSN at the temperature when the phase transition occurs is complex, and values can vary between experimental conditions and samples. There are a wealth of theories that offer explanations based on the data, however to fully understand the behaviour further work needs to be carried out on NSN. Accurate determination of the LCST requires an integrated use of techniques.

DSC measurements, as well as NSN concentrations, to confirm the LCST of 24°C is accurate. Static and dynamic light scattering experiments on dilute solutions of NSN would allow determination of the mechanism involved in the phase transition. Whilst fluorescence probes within the backbone and the NVP grafts could show how the different chains in the polymer behave at the LCST. Rheology studies using NSN gels right down to the minimum gelation concentration would also be useful in exploring whether the high concentrations are causing the low temperature G' and G'' crossover. A phase transition temperature of 24 °C is suitable for a tissue engineering scaffold as the polymer will gelate at physiological temperature. The small degree of hysteresis in the cooling of the polymer is also advantageous, as it will allow the scaffolds to be manipulated during *in-vitro* experiments without collapse.

2.5.4 NSN-collagen hybrid gel properties with blend

The potential of the NSN-collagen hybrid gels as tuneable tissue engineering scaffolds, requires the properties of the gels to be easily altered by varying the composition. Syneresis measurements, mechanical testing and SEM imaging clearly show the composition does affect the properties of the resulting gels. Below 2.5 wt% NSN solutions are unable to form self-supporting gels, and are therefore unsuitable as cell scaffolds. By blending lower NSN concentrations with collagen, gels could be formed. Therefore blending the two materials is advantageous as a self-supporting gel can still be formed, that contains a low NSN concentration, as some cell scaffold applications may not be favourable to a high synthetic content, but still require its presence for its mechanical strength.

The extent of syneresis in the gels is a result of the mechanism of gel formation. PNIPAM based hydrogels form by the aggregation of polymer globules held together by physical forces, including Van de Waals and hydrophobic effects. In the process of aggregation, water is expelled from the solutions and therefore the gel does not maintain the volume of the initial solution. Collagen gels however, are formed by the polymerisation of collagen molecules into fibrils and maintain their initial size in the absence of any cells. Yoshioka et al. synthesised bio-synthetic copolymers of NIPAM

and gelatine (43:57% respectively) that were not prone to syneresis when crosslinked. But when solutions of 2.2 wt% gelatine and 2.8 wt% PNIPAM were just mixed together, the opposite occurred²⁶⁵. Depending upon the blend, our hybrids of collagen and NSN display reduced syneresis compared with NSN alone, or no syneresis at all. However without crosslinking, gelatine is water soluble, and does not form gels in the same manner collagen solutions do, therefore Yoshioka's results are not altogether surprising. Equilibrium of the NSN gels was not a fast process, the syneresis of NSN₅ gels continued for a period of 36 hours. Wu et al. demonstrated by measurements of the hydrodynamic radii of linear PNIPAM, that globule aggregation is slow at the LCST. Although globules formed quickly, shown by an initial decrease in R_h , the aggregation continued for at least the 3.4 hour period studied. Similarly Zhang et al. showed PNIPAM microgels are prone to syneresis during a 25 hour period^{266,267}.

Blending NSN₅ with 0.3 wt% collagen decreased the syneresis of the gel, where the effect increased with decreasing NSN concentration, and was almost entirely inhibited in Col-NSN_{0.25} gels. At low concentrations NSN cannot form gels, as the concentration of NSN globules is not high enough to sufficiently aggregate together. With a decrease in aggregation of the polymer globules, you would also expect a decrease in syneresis as the media is not being excluded from a continuous polymer gel phase. Furthermore when the concentrations of collagen and NSN are similar, the collagen fibrils within the gel may dominate the gelation process preventing the polymer globules from aggregating or even collapsing. The syneresis behaviour of Col-NSN_{2.5} and Col-NSN_{1.25} compared with NSN suggests the presence of collagen may prevent the polymer chains from collapsing to the same extent as within NSN₅. This behaviour was observed in other bio-synthetic gels, where the presence of biological polymers also reduced syneresis. PNIPAM grafted HA hydrogels by Mortinsen et al. were less prone to syneresis when the PNIPAM grafts were smaller compared with larger grafts. They proposed less syneresis occurred in the hydrogels with small grafts, as 'transient gels' formed with minimal entanglements between PNIPAM chains. With larger grafts the hydrogels had more stability from a high number of entanglements²⁴³.

The effect of collagen during the phase transition of NSN can also be seen in rheological studies. During time sweeps of the hybrid gels at 37 °C, both G' and G'' initially increase quickly in magnitude after the onset of gelation but then decrease. Where the decrease occurs quicker and more sharply in the hybrids with a lower NSN concentration. Whilst the shear measurements were performed the aggregating NSN and collagen separate from some of the water in the sample. Once the gel is no longer one continuous phase the measurements recorded by the rheometre are no longer representative of just the hybrid gel. In the hybrid gels with a lower concentration of NSN, the aggregation of the globules may occur faster as there are less entanglements with neighbouring chains, therefore a faster drop in the moduli of the gels. When the NSN concentration was similar to collagen, the hybrid gels behaved more like collagen, again suggesting that collagen gel can dominate over the NSN globule behaviour. The shear moduli of Col-NSN_{0.5} and Col-NSN_{0.25} did not decrease like the other hybrid blends, and the initial solution volume was maintained. Furthermore the moduli continued to steadily increase for the length of the run as the collagen exhibited strain-stiffening behaviour^{268,269}. Therefore if hybrid gels are made from higher concentrations of collagen, which match the NSN concentration, it may be possible to produce syneresis free gels with even larger shear moduli.

Although the phase separation prevents accurate determination of the elastic properties of the gels, the overall effect of the blend on the mechanical properties can still be observed. In most bio-synthetic gels, the mechanical strength increases with inclusion of a synthetic polymer, and continues to increase with the proportion of the synthetic component^{235,249,250,270}, but the hybrid gels are weaker than gels made purely from the synthetic polymer. Our results support these findings; there is a very obvious trend in the peak moduli values of the hybrid gels at the beginning of each run, when gelation first occurs. The stiffest gels contain the highest concentration of NSN, whilst hybrid gels of collagen and NSN have lower moduli than NSN only gels, but are stiffer than collagen only gels. At higher concentrations of NSN, there are more globules aggregating together, leading to a stiffer gel. From syneresis measurements, it is clear that the NSN globules would have continued to aggregate after the 30 minute measurement period, and the resulting gel would have contained a denser polymer

phase and therefore likely to have shear moduli at equilibrium even higher than the peak moduli values. This conclusion could be confirmed by performing shear, compression and tensile testing of the hybrid gels once they have fully formed and equilibrated. In contrast to these results are the mechanical properties of bio-synthetic IPN's, which tend to be higher than the equivalent synthetic polymer network^{238,239}, however these gels are pre-formed before use and therefore not injectable. Any cells encapsulated during crosslinking would not remain viable due to the harsh chemical environment. The bio-synthetic collagen NSN gel is held together by physical crosslinks, crosslinking the collagen with glutaraldehyde could improve mechanical properties to greater than PNIPAM alone but this would limit the use of the gel.

SEM microscopy offered further information on how the different hybrid gels formed dependent on NSN concentration. At the higher concentrations, the collagen fibrillar network was more open and porous compared with collagen alone, as the NSN aggregation is probably the dominant process in gelation, where the aggregation may interfere with the fibril formation of collagen. The collagen fibrils appear thickened, which is likely a result of NSN globules aggregating with them. In agreement with the syneresis experiments and rheology data, when the concentration of collagen and NSN are similar, the gel properties were dominated by collagen, and therefore the structure of the gel was similar to collagen only gels. Col-NSN_{0.5} and Col-NSN_{0.25} gels were composed of thinner fibrils and had less clumping of aggregates on the fibres, as shown by the SEM micrographs and fibre diameter measurements.

These results imply the collagen fibrils and NSN globules in the hybrid gel are able to interact with one another. Collagen gels are hydrophilic, whilst the styrene monomers and isopropyl group of PNIPAM are hydrophobic and therefore unlikely to interact. However any exposed amides of the NIPAM monomer and the NVP graft chains are hydrophilic and can hydrogen bond with the collagen. This must be occurring to some degree, as by eye the gels appear homogenous in texture and SEM images do not appear to have two separate phases. Similarly, in bio-synthetic scaffolds made from polymerisation of PNIPAM in the presence of a collagen sponge, PNIPAM seemed coat and aggregate on the collagen fibrils. When the PNIPAM concentration was increased

the collagen network was less visible and the scaffold structure was dominated by PNIPAM.²⁵⁵ Fibronectin has also been shown to coat PNIPAM coated surfaces above the LCST²⁷¹.

Taking together the results from SEM, syneresis and rheology it appears the gel formation mechanisms and resulting properties of NSN and collagen hybrid gels are dominated by the concentration of NSN, but the aggregation of NSN globules can be hindered by the presence of collagen fibrils (Figure 2-15). Gelation of NSN occurs through chain collapse and aggregation, with significant reductions in volume. With low concentrations of NSN, the collagen network hinders aggregation and there is no change in gel volume. At higher concentrations of NSN, a collagen fibril network forms within the hydrogel, but the degree of syneresis increases with increasing NSN content. When the NSN concentration is below 1.25 wt% it appears the fibrillar collagen network that forms in the hybrids is similar to a collagen only gel, and the fibrillation mechanism of gel formation dominates over NSN aggregation. Whilst increasing the concentration of NSN has a big effect on the mechanical properties of the gels.

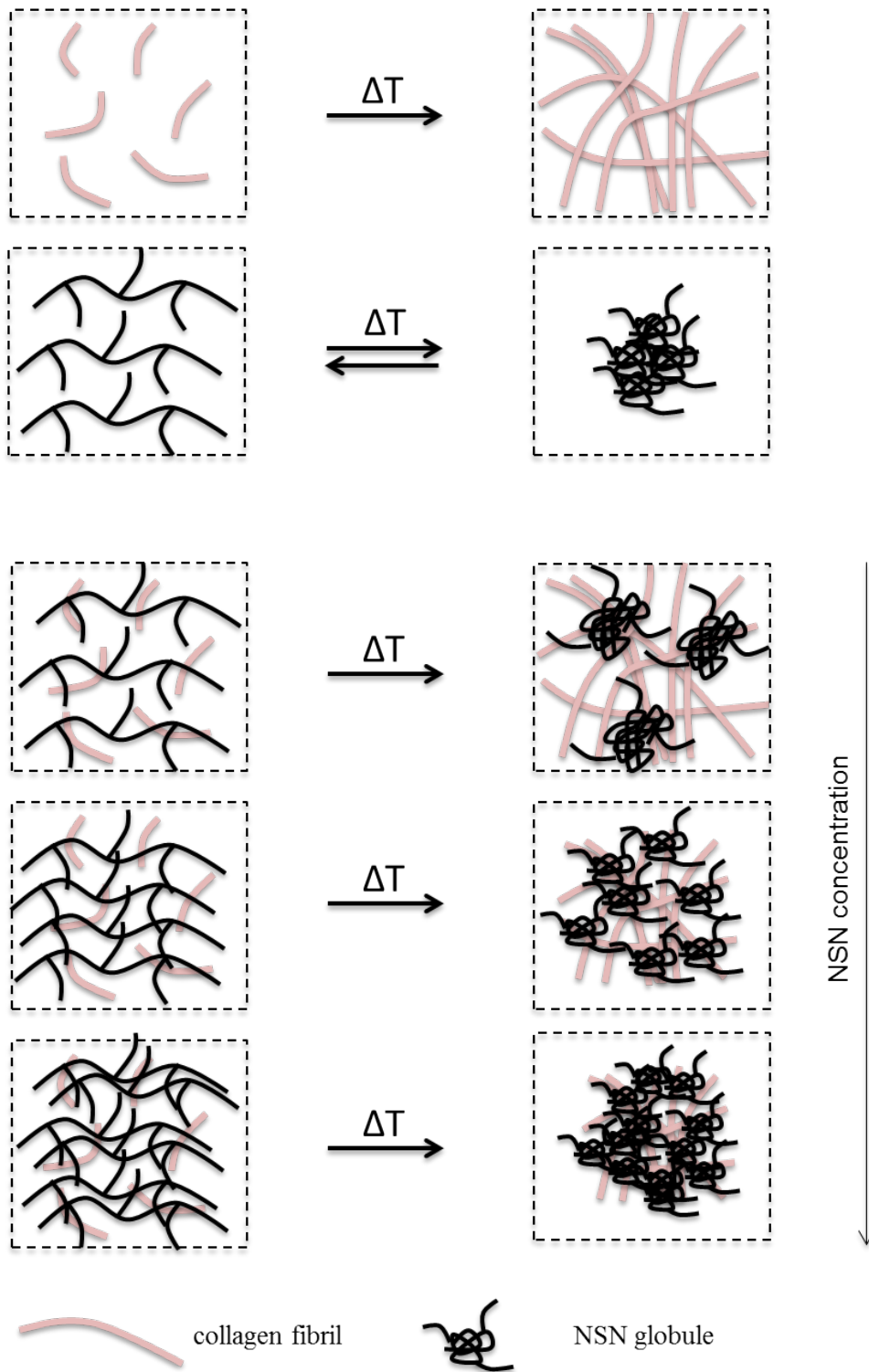


Figure 2-15 Mechanisms of gel formation in different hydrogel blends. Dotted lines represent initial solution volume.

2.6 Conclusion

Hybrid gels of NSN and collagen have the potential to be used for a range of applications. At low NSN concentrations, below 1.25 wt%, the gels have low mechanical properties, but the syneresis is reduced and a range of porosities are observed. These gels are also more likely to be more cell adhesive as more of the collagen fibrils are exposed. These materials could be useful for soft tissue applications. Whilst the higher NSN concentration gels are tough, and potentially less cell adhesive and have potential as scaffolds for harder tissues such as bone and cartilage. Although other groups have demonstrated bio-synthetic gels which have variable mechanical properties based on the ratio of synthetic to natural polymer, these require chemical synthesis to amend the composition.

The following chapter explores the use of these hybrid gels with low (col-NSN_{0.5}) and high concentrations of NSN (col-NSN₅) for two different tissue engineering challenges, to demonstrate the versatility of this hybrid system as a tissue scaffold for multiple applications.

Chapter 3 Tissue Engineering Applications of collagen I – NSN gels

3.1 Introduction

Tissue engineering of bone, skin and cartilage has already been well studied with commercial products and treatments available or undergoing clinical trials¹⁵⁹. Although tissue engineering as a means to produce organs is also being explored for the kidney²⁷², liver²⁷³ and pancreas, successes are often limited to the use of decellularised tissues²⁷⁴, or the transplant of donor tissue to make neo-organs, where the latter technique is commonly used to replace the bladder with sections from the bowel. The small number of tissue engineered products in use is largely due to the complex structure of organs and the need for a vascular supply for tissue survival, however research is well underway with solutions using 3D printing to create patterned tissues and microfluidics to introduce primitive vascular networks^{275,276}. Many basic organ models have been developed for use as *in-vitro* research models to further our understanding of biological mechanisms of development and disease and as alternatives for toxicity screens^{277,278}.

Tissue engineered approaches have recently been used by a small number of research groups to develop artificial human lymph nodes (aLN) to study LN organogenesis and organ function during immune responses^{279,280}. Although the initial events in embryonic development of the LN are well studied, the later events in the maturation of the dense stromal network and development of the compartmentalised structure are less well understood. Knock out mice models have been used to examine the role of signalling pathways and cytokines in organogenesis, but these often result in an absence of lymph nodes (LN) and secondary lymphoid tissues. An alternative approach to understand the maturation of the LN, is to develop *in-vitro* organ models and then examine the role of gene deficiency using knock out cell lines. ALN models could reduce the number of mice used in research. Furthermore an *in-vitro* model could be used to examine the formation of ectopic lymphoid tissue that occurs in many autoimmune diseases. For this tissue engineering challenge, hybrid gels with low NSN content will be used as scaffolds for developing an aLN.

In addition as cartilage repair has been a major goal in tissue engineering, the tougher hybrid blends that contain higher concentrations of NSN will also be investigated here, as potential injectable scaffolds for cartilage engineering, to demonstrate the versatility of the hybrid gels. The high mechanical properties of the high NSN gels lend themselves to this application, as the articulating surfaces in the hip and knee are under high mechanical strains.

3.1.1 Lymph node function and structure

In the peripheral tissue, immature dendritic cells, macrophages and neutrophils, survey for pathogens. Upon encounter with foreign material they become activated and mature into antigen presenting cells (APCs), migrating via the afferent lymphatics to the regional LNs, where they interact with B and T lymphocytes to initiate the adaptive immune response^{281,282}. Due to the specificity of lymphocytes for a particular antigen, the probability of this interaction within the body is low; therefore the LN has a highly specialised structure to efficiently aid in the antigen presentation (Figure 3-1). From the afferent lymphatics, lymph passes into the sub-capsular sinuses that surround the lobules of the organ, and deeper in the centre of LN through transverse and medullary sinuses. Naive lymphocytes enter the LN through high endothelial vessels (HEV), specialised blood vessels, unique to lymphoid organs. Non-haematopoietic, stromal cells provide architecture and structural support within the LN, compartmentalising the lobules into B-cell follicles around the periphery of the organ and T-cell zones within the cortex. Fibroblastic reticular cells (FRCs) and follicular dendritic cells (FDCs) are two well-studied sub-sets, which define the follicles and the cortex respectively. Within the follicle, FDCs form an interconnected network, and within the cortex FRCs assemble around ECM fibrils creating conduit channels²⁸³⁻²⁸⁵. Initially the role of the stromal cells in the organ were largely ignored, the cells were believed to simply provide a structural framework within the LN.

However this is not the case, the stromal networks provide a substratum for lymphocyte migration and directionality and produce gradients of soluble factors to guide the migration²⁸⁶. Chemokines CCL19 and CCL21, produced by FRCs guide the migration

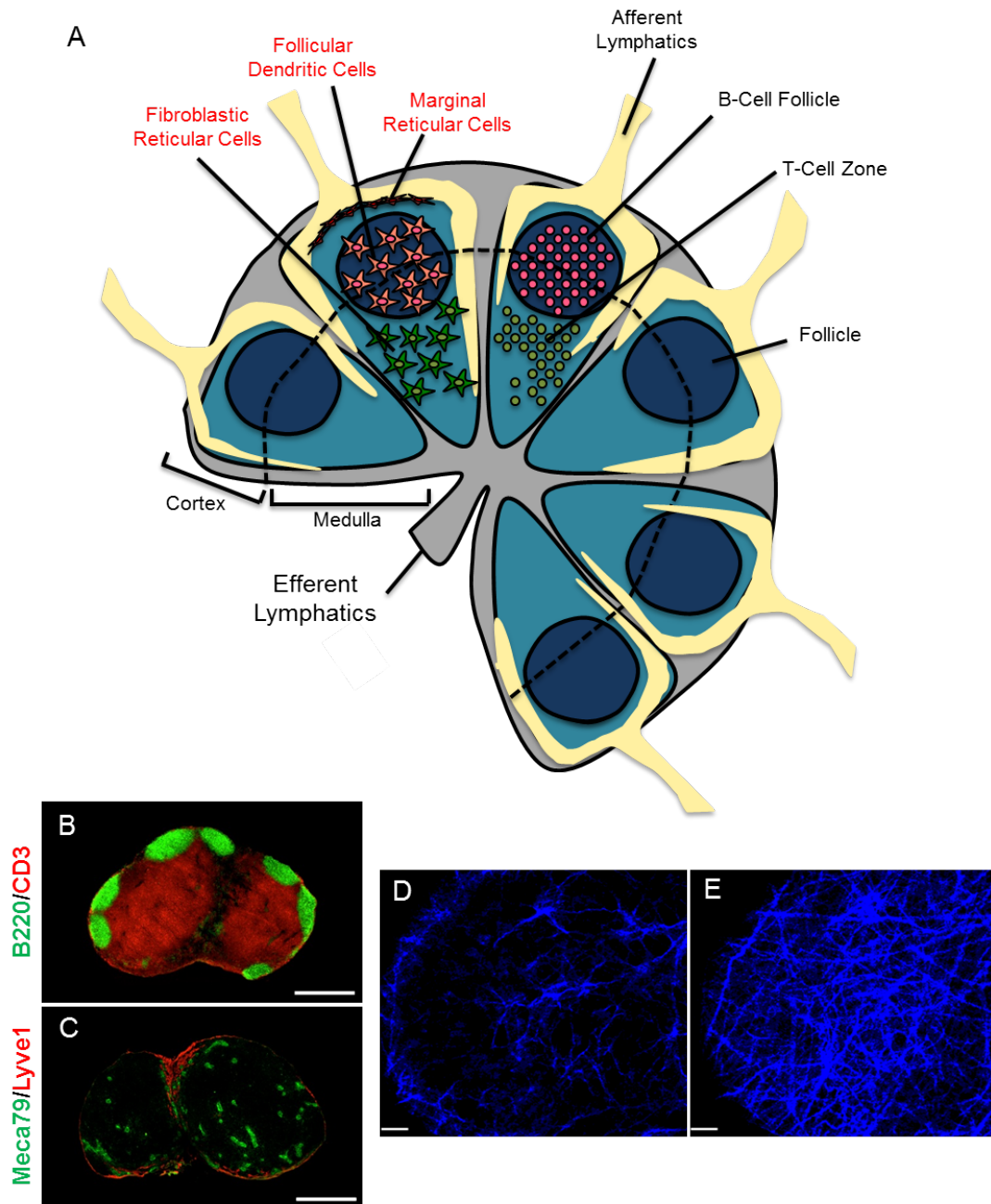


Figure 3-1 Schematic of lymph node structure.

The lymph node is divided up into distinct lobules (A), which are compartmentalised into B-cell follicles (B220 staining, green) (B) in the cortex and T-cell zones (CD3 staining, red) (C) within the medulla, by the underlying stromal networks. The lymphatic networks (Lyve1 staining, red) transport lymph into the organ, whilst naïve lymphocytes enter via the high endothelial venules (Meca79 staining, green) (C). Networks of fibroblastic reticular cells are situated in the medulla supporting T-cell function and migration whilst follicular dendritic cells are located in the follicles. Around the periphery of the lobules, is a third stromal subset, the marginal reticular cells. The lymph node contains a network of collagen fibres (second harmonic generation, blue) (D) and is encased within a collagen capsule (E). Histology images courtesy of Anne Thuery and Amy Sawtell.

of CCR7 expressing T-cells with APCs within the T-cell zone, whilst FDCs release CXCL13 to mediate the migration of CXCR5 B-cells into, and within the follicles^{287–289}. The survival and proliferation of naïve B and T cells are also regulated by FRCs and FDCs, which produce IL-7²⁸⁹ and BAFF²⁹⁰. As well as stimulating migration through chemotaxis, lymphocytes directly adhere and migrate along the stromal cell network. FRCs surrounding the HEVs have been demonstrated to control the entry of naïve lymphocytes into the LN and provide a substratum for both T and B-cell migration within the paracortex, through direct cell-cell adhesion²⁹¹ mediated by FRC expression of VCAM-1 and ICAM-1^{292,293}. At the follicle boundaries FRCs may also prevent naïve T-cell access. Similarly FDCs also express ICAM-1 and VCAM-1, and direct B-cell migration within the follicles²⁹¹.

Additionally to supporting lymphocyte survival the stromal networks contribute to antigen presentation. FDCs are involved in antigen presentation to naïve B-cells^{294,295}, whilst FRCs can induce T-cell tolerance through presentation of peripheral tissue antigens²⁹⁶. The FRC conduit system of the LN^{283–285}, carries low molecular weight molecules into the central cortex²⁹⁷, where dendritic cells associated with the conduits, extend thin processes into the channels and probe for soluble antigens within the lymph²⁹⁸. The LN contains relatively little ECM, most is enclosed within the FRC conduits^{282,297}. Collagen I and III fibrils and collagen VI are enclosed as reticular fibres, covered with basement membrane proteins and FRCs¹⁰⁴. The entire LN is enclosed in a collagen I and elastin capsule, from which several collagen III trabeculae extend into the organ.

3.1.2 Development of lymphoid organs

Through experiments using knock-out mice, deficient in key genes involved in secondary lymphoid tissue organogenesis, mechanisms involved in the development of the LN have been identified. Interactions between haematopoietic lymphoid tissue inducer cells (LTi), and stromal lymphoid tissue organiser cells (LTo) are fundamental for development^{299,300}. LTi cells are derived from the fetal liver, whilst LTo are believed to be mesenchymal in origin as they express high levels of adhesion molecules, ICAM-

1, VCAM-1 and MadCAM-1 and receptors PDGFR- α and - β ³⁰¹. The FDC networks of the LN are also derived from mesenchyme, as they express Mfge8 and PDGFR β , and in the absence of PDGFR β ⁺, Peyer's patches (PP), another secondary lymphoid tissue, do not contain FDC networks³⁰². The developmental origins of FRCs are currently unknown, like FDCs it is expected they are derived from surrounding mesenchymal tissue. Research in mice has shown that LNs develop around embryonic day 10.5, via budding of endothelial cells from larger veins. Connective tissue then enters the sacs forming the earliest structure reminiscent of the organ. Initially retinoic acid from nearby developing nerve fibres is believed to stimulate the expression of CXCL13 on mesenchymal cells, recruiting pre- LTi to the site of the developing LN²⁹⁹. Signalling between LTis and mesenchymal cells through LT $\alpha_1\beta_2$ and its receptor LT β R on the mesenchymal cells, results in maturation of the mesenchymal cells to LTo cells and a continual loop of adhesion molecule and chemokine expression by the LTo. This consequently leads to further recruitment of LTi cells and increased LT $\alpha_1\beta_2$ signalling^{299,303}. Chemokines CXCL13, CCL19 and CCL21 and adhesion molecules ICAM-1, VCAM-1 and MadCAM-1 aid in the recruitment and retention of infiltrating haematopoietic cells and the LN anlagen increases in size. This process is similar in all secondary lymphoid organs^{299,303}.

3.1.3 Maturation of FDC and FRC stromal networks

As well as being involved in the development of secondary lymphoid organs, LT and another inflammatory cytokine, tumour necrosis factor (TNF) signalling are also important in the maturation and maintenance of the resulting stromal architecture. The initial mesenchymal cells present at the site of the developing LN express intermediate levels of ICAM-1 and VCAM-1. Without further LT signalling and the presence of LTi cells, the mesenchymal cells are unable to mature into ICAM-1^{high}/VCAM-1^{high} cells³⁰⁴. In LT β or LT α knock out mice, where most LNs are absent, mesenteric LN can still be found in some animals, but the structures of the resulting LT β deficient LNs lack FDC networks³⁰⁵. Disruption of signalling through TNFR1, also results in LNs lacking FDCs^{305,306}. In contrast to PPs, where FDC network maturation is dependent upon B-

cell sources of LT and TNF, Expression of TNF from both B and T cells complement each other in the development of FDC networks in the LN^{307–309}.

Isolation of FRCs from LNs has been useful in determining the development of FRC based reticular networks. When cultured *in-vitro*, isolated murine FRCs co-cultured with the non-adherent cell fraction of the LN, can assemble into connected networks, with increasing expression of the FRC marker ER-TR7³¹⁰. Similarly to FDC development, the FRC network formation is stimulated through TNF and LT signalling, where combined stimulation of TNF α and anti-LT β R produced the most extensive *in-vitro* FRC network³¹⁰. In contrast to experiments by Fletcher et al. who demonstrated LN FRC networks formed in the absence of B and T-cells³¹¹, the *in-vitro* FRC network formation could also be stimulated by co-culture with T-cells. However in the absence of B and T-cells during *in-vivo* FRC development, LT and TNF signalling from LTis and other cells can stimulate network formation. Ngo et al. also reported normal FRC development in the absence of B-cells³¹², and Coles et al. demonstrated natural killer cells are able promote stromal network formation in the absence of lymphocytes³¹³. Taken together this indicates that although B and T-cells are a source of LT and TNF in murine LN development, unlike FDC development, their expression from a specific cell type is not necessary to form FRC networks.

3.1.4 Current developments in modelling LN

Modelling the LN has currently been explored by two approaches, which both use collagen based scaffolds seeded with murine stromal cell lines. Currently there have been no developments using human stromal cells. Suematsu et al. developed aLNs containing FRC stromal networks, distinct B and T cell zones and HEV like blood vessels by seeding the thymus derived stromal cell line TEL-2 into collagen sponges²⁷⁹. However these were not true *in-vitro* models, the collagen sponges were implanted *in-vivo*, where stromal networks formed and lymphocytes migrated into the tissues. This does however highlight that a stroma – collagen system has potential to develop into lymphoid-like tissue given the right cues. A second aLN has been designed by seeding immortalised murine FRCs into a polyurethane - collagen scaffold. Within the 3D

scaffold the FRCs organised into a network, and expressed CCL21. Upon exposure to small fluid flows the network formation and CCL21 production increased²⁸⁰. Although these examples show progress is being made in producing models of the LN, only one is an *in-vitro* model that reduces the use of mice. Furthermore both models use immortalised cell lines, which may not fully recapitulate the behaviour of LN stromal networks.

3.1.5 Articular Cartilage

Articular cartilage, or hyaline cartilage is a smooth anisotropic connective tissue, found on the surface of articulating bones, which acts as a shock absorber and to reduce friction and wear whilst transferring loads over joints during movement. Lesions can form in cartilage following trauma, often caused by sporting injuries or through diseases of the joint. Without treatment the lesions can increase in size and progress towards osteoarthritis (OA). Osteoarthritis is most commonly found in joints that undergo high levels of articulation in everyday life, including but not limited to, the knee, hip, hands, feet and the back. It is the common joint disorder in the USA, effecting 10% of men and 13% of women over the age of sixty in 2010³¹⁴, with the incidence expected to increase as the population lives longer. When the protective cartilage layer of the joint is damaged, surrounding healthy cartilage can be worn away, the underlying bone becomes exposed and thickens and the surrounding tissues adapt to compensate for the instability caused. The joint becomes swollen, painful and inflamed. When the disease is severe, the inflammation and swelling can prevent motility in the joint and often the only route of treatment is through highly invasive total joint replacement (TJR). Treatment of cartilage lesions at an early stage could help to prevent the disease progression, and improve the quality of life for a patient.

3.1.6 Structure and composition of articular cartilage

Articular cartilage is an avascular tissue, with a low cell density, mainly composed of collagen II and proteoglycans (Figure 3-2). The structure of the ECM and cellular composition varies from the superficial zone at the cartilage surface, to the deep calcified regions at the bone surface, to aid the tissue function (Figure 3-3). In contrast

to most connective tissues cartilage contains collagen II, another fibril forming collagen with a similar structure to collagen I. Owing to its fibrillar nature, collagen II is strong in tension, where the exact arrangement of the collagen II fibres within cartilage, confers the function of the tissue.

The fibrils are thin, roughly 20 nm in diameter, and run parallel with the surface of the tissue within the superficial zone, therefore this region of the tissue has the highest tensile strength, which is necessary at the articulating surface^{315,316}. In the middle zone collagen fibrils are wider in diameter and orientated in multiple directions to resist loading. Whilst in the deep zone, fibrils are at their widest, between 70 – 120 nm in diameter, to strengthen the integration into the bone³¹⁷. In contrast to collagen I, collagen II has a higher content of hydroxyl lysine residues to aid in electrostatic interactions with the highly negatively charged proteoglycans also present in cartilage³¹⁸. The collagen fibrils in cartilage are approximately 80-90% collagen II, but also contain collagen IX and XI³¹⁹⁻³²¹, which are believed to limit the size of fibrils during their assembly³²¹. Proteoglycans are also present within cartilage, these are mechanically weak compared with collagen II; where their function within cartilage is to maintain a high water content. Aggrecan is a large 225-250 kDa proteoglycan, specific to cartilage. It contains GAG side chains, specifically chondroitin and keratan sulphate, bound to a HA core. The GAG side chains are organised into a bottle-brush arrangement around HA, caused by the repulsion of adjacent negative charges from carboxyl and phosphate functionality^{322,323}. Each GAG side chain typically contains 100 negatively charged groups, creating a large osmotic swelling pressure, and maintaining water within the tissue³²⁴.

Compared with other connective tissues, cartilage has a very small population of cells. Chondrocytes are found singly or within aggregates or columns surrounded by a pericellular matrix (PCM), unique from the bulk ECM of cartilage, which may provide a protective environment for the cells, when the tissue is subjected to mechanical strains³²⁵. The PCM is predominately formed of collagen VI, and also contains decorin, aggrecan, HA and collagens type II and IX³²⁶. Like the ECM, the morphology and distribution of chondrocytes varies with tissue depth. In the superficial region, the cells

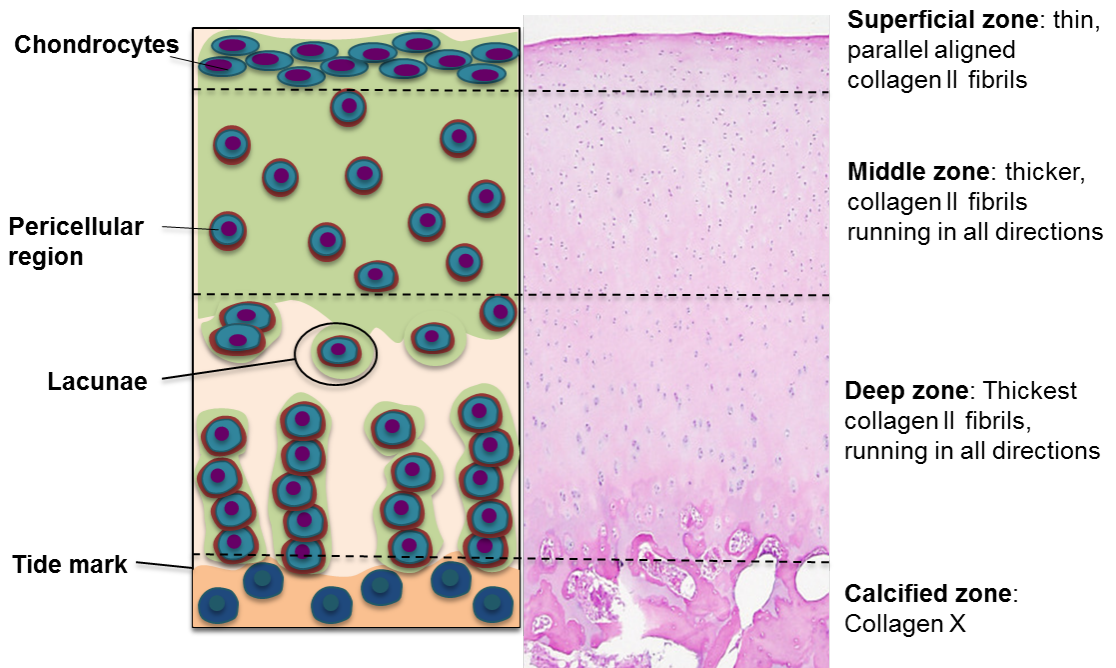


Figure 3-2 Distribution of chondrocytes and collagen within articular cartilage. Within the superficial zone at the articulating surface, chondrocytes are flattened and surrounded by thin, highly aligned collagen II fibrils. In the middle and deep zones, collagen II fibrils run in all directions to provide high compressive strength and aid the integration into the bone in the calcified region, which contains hypertrophic chondrocytes. Adapted from^{320,327}

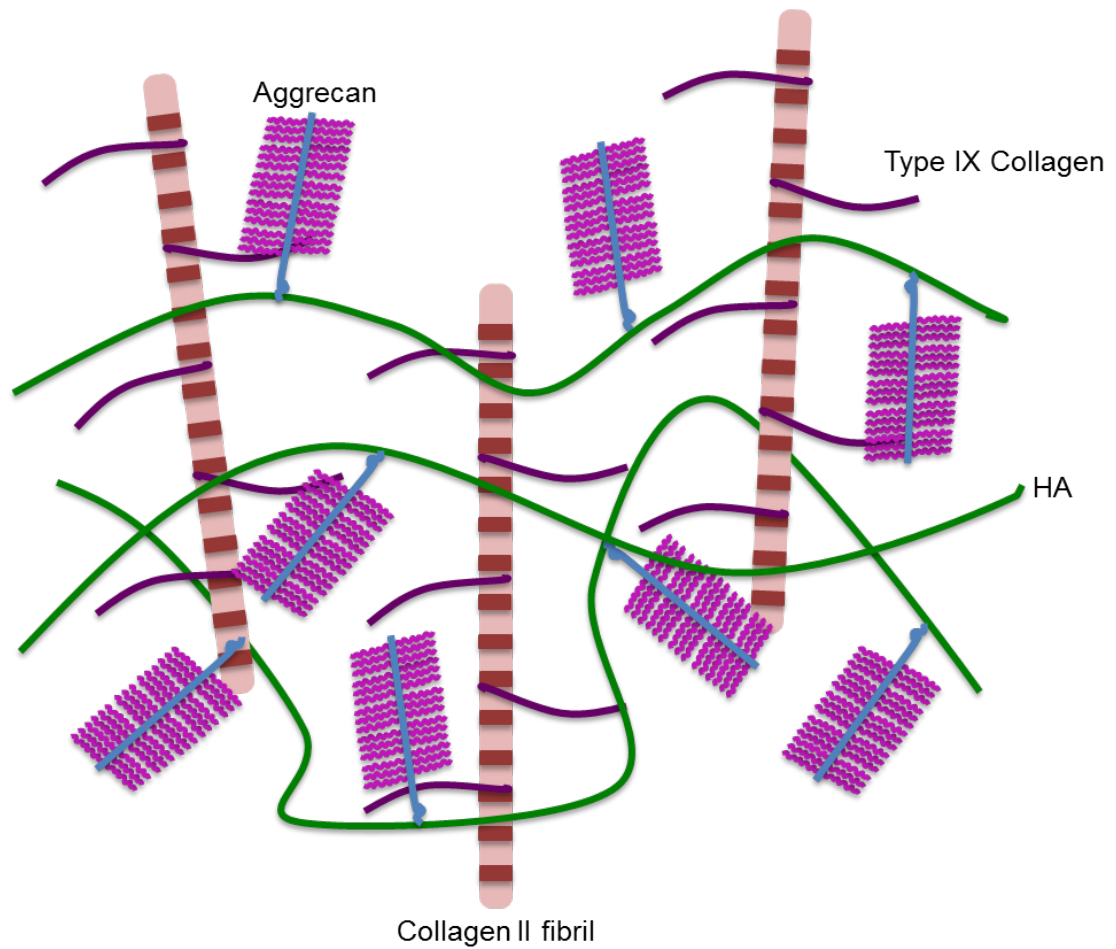


Figure 3-3 Extracellular matrix of articular cartilage. Predominately composed of collagen II fibrils, where the fibril diameter size is controlled by collagen IX and collagen XI (not shown) within the fibrils. Large aggregates of the cartilage specific GAG, Aggrecan, which is bound to hyaluronic acid maintain high volumes of water within the tissue. Adapted from³²⁰

are flattened and disc like, in the middle zone chondrocytes adopt a rounder morphology, and in the deep region, where cartilage integrates into the underlying bone, the chondrocytes are terminally differentiate and become hypertrophic, producing a collagen X rich matrix. Additionally they produce high levels of osteonectin, a matrix protein associated with calcification in bone formation³²⁸.

3.1.7 Cartilage repair strategies

Only small defects in cartilage, which extend down into the subchondral bone are able to undergo spontaneous healing. When the underlying bone is fractured a blood clot forms and is accompanied by the release of growth factors and migration of MSCs into the clot, which produce new ECM. However the newly formed cartilage is generally scar tissue, with characteristics of hyaline cartilage, that is much weaker than articular cartilage³²⁹. Current treatments for cartilage damage either focus upon providing pain relief through administration of non-steroidal anti-inflammatory drugs, COX2 inhibitors or debridement of the area to remove the damaged cartilage and surgical techniques to repair the damaged area. Micro-fracture into the underlying bone can promote MSC migration into the damaged area to restore the cartilage, but like the spontaneous repair seen in deep defects the cartilage formed is often weaker and does not provide long-term repair. Autologous chondrocyte implantation (ACI) is also used to repair cartilage lesions and can be used for large and full thickness defects^{23,330}. A small biopsy of healthy cartilage is taken from a non-weight bearing surface and the cells are expanded in culture. The expanded cells are then implanted into the defect and held in place with a sutured membrane, which is either synthetic (chondroguide) or harvested from healthy tibia periosteum from the individual. However the success of this technique to produce high quality hyaline cartilage is disputed, where the technique might be improved by combining chondrocytes or MSCs with a chondro-inductive cell scaffold.

However given all the advances in cartilage repair therapies, over 70000 total knee replacements (TKR) are still carried out in England and Wales each year and the number is rising³³¹. The distal end of the femur and proximal end of the tibia are cut and the articulating surface is replaced with metal and ultra high molecular poly-ethylene

(UHMWPE). The surgical procedure is very invasive, with high post-operative pain and long re-habitation periods. TKRs are expensive and can often require revision surgery³³². The wear of the synthetic components is also linked to immune responses and loosening of the implanted components within the bone⁷. A new cartilage repair therapy would ideally aim to regenerative cartilage at the early stages of the disease to a similar strength as native hyaline cartilage and reduce the need for TKRs. Reducing the pain and discomfort to the patient as well as the direct and indirect economic costs.

3.1.8 Tissue engineering cartilage

In embryonic development, *in-vivo* culturing of MSCs in diffusion chambers, *in-vivo* cartilage repair from underlying bone and *in-vitro* chondrogenesis in cell pellets, cartilage development occurs by the condensation of MSCs into a dense structure and their differentiation into chondrocytes, characterised by the production of a cartilaginous matrix predominately containing collagen II and aggrecan^{26,44,48,329}. In each situation, chondrogenic precursors maintain a rounded morphology making few cell-ECM and many cell – cell interactions. The compact arrangement of cells also results in a decrease in oxygen concentration. *In-vitro* differentiation experiments have demonstrated the importance of these factors upon chondrogenesis. When cultured in 2D monolayers, isolated chondrocytes spread and attach, losing their *in-vivo* spherical morphology and they downregulate chondrocyte specific markers¹⁵³. The *in-vivo* phenotype can however be recovered when the cell are encapsulated within non-adhesive agarose gels that prevent cell spreading¹²². MSCs also favour chondrogenic differentiation when maintained in a rounded morphology as cell pellets or suspended in agarose gels, highlighting that although cell-cell contacts may play a role in the differentiation, given the appropriate biochemical cues and cell shape isolated MSCs can also undergo chondrogenesis³³³. *In-vitro* MSCs require the addition of TGF- β 3 alongside condensation to differentiate towards cartilage tissue⁴⁸. With TGF- β 3 treatment, cell shape also effects the differential capacity of MSCs. MSCs allowed to spread out on large fibronectin coated surfaces produce early markers of myogenic differentiation, whilst MSCs cultured on small fibronectin islands, with little substrate attachment, remaining rounded, express chondrogenic markers³³⁴. Furthermore

disruption of the actin cytoskeleton of MSCs and chondrocytes leads to cells with a more rounded morphology in both 2D and 3D and an increase in GAG deposition and SOX9 expression³³⁵.

The chondrogenic potential of MSCs in 3D also varies with the properties of the scaffold that is used. ADSCs encapsulated in alginate gels exhibit a rounded morphology, while within gelatine they can spread and proliferate. In gelatine, agarose and alginate, ADSCs are able to synthesise a cartilaginous matrix, but the matrix formed in gelatine is fibrocartilage like, whereas the matrix that ADSCs produce in alginate and agarose gels that did not allow cell attachment, more closely resembled native cartilage³³⁶. Hypoxia also plays a role in chondrogenesis. Within dense pellets of cells, the oxygen gradient is reduced and therefore this effect will also contribute to the differentiation of the cells. Compared with normoxia (20% oxygen), MSCs cultured in hypoxic conditions (1% oxygen) increase expression of collagen II, aggrecan and SOX9 and produce a richer GAG matrix^{129,130}.

From the above it is clear that like MSC differentiation towards other cell types, chondrogenesis involves a complex interplay of physical and biochemical factors. Although condensation of precursors is essential *in-vivo* and *in-vitro* in cell pellets, it is not clear whether the direct cell- cell interactions or simply just the shape the cell adapts are crucial for the differentiation. As hypoxia also contributes, the condensation may also just serve to reduce the oxygen gradient. Therefore potential biomaterial based cartilage repair strategies could explore the chondrogenesis of isolated MSCs forced into rounded morphologies. The scaffold would need to contain minimal sites for cell adhesion and have good mechanical properties to withstand the high compressive and tensile forces in the articulating joint, hence a synthetic material could be favourable. Furthermore synthetic materials can be designed with controllable degradation rates. The quality of tissue engineered cartilage may be improved where the scaffold used degrades slowly, altering the ECM produced by MSCs or chondrocytes during remodelling.

3.2 Aims and synopsis

Presented within this chapter are two possible applications of MSCs for tissue engineering and the potential of the collagen – NSN hybrid gels as MSC supporting tissue scaffolds.

To model the entire LN is a major challenge and it is clear that the organogenesis of the LN is a complicated process. Therefore to reduce the complexity of the organ, haematopoietic cells are removed from this model. The model will focus upon the development of lymphoid stromal cell networks by differentiating MSCs with the soluble cues stromal cells receive from LTis during development. An *in-vitro* stromal cell type has been previously developed from ADSCs in 2D (unpublished data, B Glaysher). To move this into 3D, ADSCs will be encapsulated within the hybrid gels with inflammatory cytokines to develop a model of lymphoid mesenchyme. Low NSN content hydrogels will be used for this application, to achieve cell adhesion and spreading, whilst mimicking the mechanical properties of the organ. The reversibility of the lymphoid mesenchyme phenotype will also be examined, by performing MSC differentiation assays following cytokine induction.

In contrast to the LN model, BM-MSCs will be used to investigate the potential of the hybrid gels for cartilage repair. BM-MSCs are an appropriate choice, as they may have improved chondrogenic potential compared with other MSC sources. Furthermore as they will be situated in close proximity to the damaged cartilage, they may be migrate into the gel and contribute to the tissue remodelling. High NSN content gels will be used for this application as they have higher bulk mechanical strength which will be essential for supporting the developing tissue under the forces of the knee joint.

The aims of this chapter are:

1. Characterisation of a lymphoid mesenchyme cell line derived from ADSCs, assessing the cell phenotype and reversibility

2. Translate a 2D model of lymphoid mesenchyme into 3D using low NSN content hybrid gels and spheroid models
3. Investigate the chondrogenic capacity of BM-MSCs within high NSN content hybrid gels.

3.3 Methods

3.3.1 Cell Culture

ADSCs. Human ADSCs were purchased from Invitrogen (Stem Pro Human ADSCs). The cells had been sourced from lipoaspirate tissue and had been previously expanded for one passage prior to cryopreservation and shipping. ADSCs were expanded in culture in MesenPRO RS Medium (Invitrogen) for one passage and then cultured in basal media (DMEM supplemented with 10% FBS, 2mM L-glutamine and 1% p/s) for at least one passage prior to experimental use. Cells were passaged when they reached 80-90% confluency, first washed in 1x PBS and incubated with TrypLE Express (Invitrogen) to detach cells, and re-seeded at 5000/cm². All experiments were carried out with cells between passage 3-5. Flow cytometry analysis performed by Invitrogen confirmed these cells were positive for CD29, CD44, CD73, CD90, CD105 and CD166 and negative for CD14, CD31, CD45 and Lin1.

BM-MSCs. Human BM-MSCs were isolated from the tibia plateau of the knee, obtained from arthroplasty procedures under ethics guidelines. The bone was broken up roughly into 2 cm² pieces and cultured bone marrow side down in a 10 cm² petri dish, covered with basal media (DMEM supplemented with 15% batch-tested FBS, 2mM L-glutamine and 1% p/s). Cells were left to evade from the bone marrow for 7 days, after which the medium and bones were removed and 10 ml of fresh media was added. BM-MSCs preferentially adhered to the treated TCP whilst contaminating red blood cells and lymphocytes were removed through washing and passaging. Cells were passaged (1:3) when 80-90% confluent and tested for mycoplasma. Cells from each donor were identified as kneeXXX, where XXX is a unique number given to each donor knee. All experiments were carried out with cells between passage 3-5. Basal media for all further cell culture consisted of DMEM supplemented with 10% batch-tested FBS, 2mM L-glutamine and 1% p/s

3.3.2 Mycoplasma testing

Cells for testing were seeded at a density of 5000/cm² into a 24 well plate in basal media and left to adhere. Once the cells were spread the cell culture medium was removed and the cells were gently rinsed in 1x PBS. Adherent cells were fixed and permeabilised in methanol (200 µl/well) for 5 minutes and then rinsed three times in 1x PBS. The cells were incubated in DAPI (200 µl/well) for 5 minutes in the dark and then rinsed three times in 1x PBS. DAPI stained cells were viewed under UV illumination to assess for mycoplasma infection. Infected cells were discarded.

3.3.3 Induction of lymphoid mesenchyme phenotype in ADSCs

Basal media was supplemented with recombinant human interleukin-4 (IL-4) (50 ng/ml, Peprotech), recombinant murine tumour necrosis factor α (TNF- α) (10 ng/ml) and anti-human lymphotoxin- β receptor (anti-huLT β R) (100 ng/ml, Biogen IDEC, Inc) for at least 2 days. Supplemented media was changed every 2-3 days.

3.3.4 Flow cytometry

Cell were detached as above, washed twice in FACS buffer (1x PBS containing 1% bovine serum albumin (BSA) and 5 mM ethylenediaminetetracetic acid (EDTA, Invitrogen) and then re-suspended 5– 20 x10⁴ cells/well in a 96 well V-bottomed plate (Fisher). 100 µl of FACS buffer containing primary antibodies (see Table 3-1) was added to each well, and the cells were incubated for 30 minutes at 4 °C. A further 100 µl of FACS buffer was added to each well and the plate centrifuged for 5 minutes at 450 rpm. The plate was quickly flicked to remove the FACS buffer and the cells were washed a further two times in 200 µl FACS buffer. Secondary or conjugated antibodies were diluted in 100 µl of FACS buffer and incubated with cells for 30 minutes at 4 °C in the dark (Table 3-2). The cells were washed as before and suspended in 300 µl of FACS buffer in micro test tubes (Biorad) on ice and kept in the dark prior to analysis. Samples were analysed using a Cyan, flow cytometre, using unstained cells as controls, collecting at least 1 x10⁵ events where possible. Data was analysed using Summit (Beckman Coulter) and FlowJo (Tree Star).

Antigen	Conjugate	Clone	Supplier	Dilution
Hu ICAM-1	PE	HA58	Ebioscience	1/200
Hu VCAM-1	biotin	1G11B1	Abcam	1/200
Hu Podoplanin	purified	D2-40	Covance	1/200
Hu CD11b	FITC	ICRF44	Ebioscience	1/200
Hu CD14	FITC	M5E2	BD Bioscience	1/200
Hu CD29	purified	HUTS-21	BD bioscience	1/200
Hu CD31	FITC	WM-59	Ebioscience	1/200
Hu CD34	647	4H11	Ebioscience	1/200
Hu CD44	FITC	IM7	Ebioscience	1/200
Hu CD45	PB	H130	Ebioscience	1/200
Hu CD73	purified	AD2	BD Bioscience	1/200
Hu CD90	PE-Cy5	ebio5E10	Ebioscience	1/200
Hu CD105	purified	8N6	Ebioscience	1/200
Hu CD106	purified	STA	Ebioscience	1/200

Table 3-1 Primary Antibodies

Specificity	Conjugate	Supplier	Dilution
Ms IgG (H+L)	488	Invitrogen	1/500
Ms IgG (H+L)	594	Invitrogen	1/500
Streptavidin	647	Invitrogen	1/500

Table 3-2 Secondary Antibodies

3.3.5 Adipogenic differentiation

Cells for differentiation were seeded confluent in 96-well plates (20000/cm²) in basal cell culture media and left to attach overnight. The following day the media was replaced with either adipogenic media (basal cell culture media supplemented with 1μM dexamethasone (Sigma Aldrich), 500μM 3-isobutyl-1-methylxanthine (IBMX, Sigma Aldrich), 1μg/ml insulin (Sigma Aldrich) and 100μM indomethacin (Sigma Aldrich)) or basal cell culture media for non-adipogenic controls. Media was replaced every 2-3 days.

3.3.6 Osteogenic differentiation

Cells for differentiation were seeded confluent in 96-well plates (for pNPP and pico green assays) and 48-well plates (for staining) (20000/cm²) in basal cell culture media and left to attach overnight. The following day the media was replaced with either osteogenic media (basal cell culture media supplemented with 50μg/ml L-ascorbic acid-2-phosphate (Sigma Aldrich), 5mM β-glycerophosphate (Sigma Aldrich) and 10nM dexamethasone) or basal cell culture media for non-osteogenic controls. Media was replaced every 2-3 days.

3.3.7 Chondrogenic differentiation

MSCs obtained from knees were centrifuged at 450 rpm for 5 minutes in universal tubes or 15ml Falcon tubes with basal media, to form pellets (240000 cells/pellet). The following day the media was replaced with either chondrogenic media (DMEM supplemented with 1% p/s, 2mM L-glut, 1% ITS⁺ liquid media supplement (Sigma Aldrich), 50μg/ml L-ascorbic acid-2-phosphate, 100nM dexamethasone, 40μg/ml L-proline (Sigma Aldrich), and 10 ng/ml transforming growth factor-β3 (TGF-β3, Peprotech)) or basal chondrogenic media (DMEM supplemented with 1% p/s, 2mM L-glut, 1% ITS⁺, 50μg/ml L-ascorbic acid-2-phosphate, 100nM dexamethasone and 40μg/ml L-proline) for non-chondrogenic controls. Media was replaced every 2-3 days.

3.3.8 Oil Red O staining

Media was removed from cells, which were then washed once in 1x PBS and fixed in 4% PFA for 10 minutes for staining on days 1, 7,14 and 21 of adipogenic differentiation. Fixed cells were then washed once in dH₂O and incubated for 5 minutes in 60% isopropanol (IPA). The cells were then stained in oil red O (0.3 % oil red O w/v in 60 ml 99% IPA and 40 ml dH₂O, filtered before use, Sigma Aldrich) for 10 minutes and washed three times in dH₂O. The cells were kept moist and imaged immediately to prevent lipids from bursting. The stain was eluted from the cells by incubating with 50 μ l of 99% IPA for 10 minutes and measuring the absorbance at 490 nm on a plate reader (Dynex Technologies MRX II).

3.3.9 Alizarin Red staining

Cells were washed once in 1x PBS and fixed in 4% PFA for 20 minutes for staining on days 1, 7,14 and 21 of osteogenic differentiation. Fixed cells were washed three times in PBS and stained in 40 mM alizarin red (in dH₂O, pH 4.2, filtered before use, Sigma Aldrich) for 20 minutes. The cells were then washed in PBS three times and in tap water to remove non-specific staining. The plates were then air dried prior to imaging.

3.3.10 Alkaline Phosphatase staining

Cells were washed twice in PBS and incubated at room temperature for 2 minutes with alkaline phosphatase (ALP) reagent. (0.2 mg/ml naphthol AS-MX (Sigma Aldrich) dissolved in 1% N,N-dimethylformamide (DMF) and diluted in 0.1 M Tris(base) (pH 9.2, Sigma Aldrich) containing 1 mg/ml Fast Red TR (Santa Cruz Biotechnology) sterile filtered before use). The ALP reagent was removed, and the cells then fixed in 4% PFA for 5 minutes. Fixed cells were washed in PBS and dH₂O and incubated in 1% silver nitrate solution on a light box for 30 minutes. Cells were washed three times in dH₂O and incubated in 2.5% sodium thiosulphate (pH 9.2, Sigma Aldrich) for 5 minutes. Prior to imaging the cells were washed twice in dH₂O and stored in 20% glycerol (Sigma Aldrich).

3.3.11 pNPP and pico green assays

Cells were washed in 0.2M carbonate buffer (2:1 v/v solution of 0.2M sodium carbonate (Sigma Aldrich) to 0.2M sodium bicarbonate (Sigma Aldrich), pH 10.2) and lysed with 150 μ l triton lysis buffer (0.1% Triton-X (Fisher) in 0.2M carbonate buffer) accompanied by 3 freeze/thaw cycles (-80°C/21°C). Upon the last thaw the contents of the wells were pipetted up and down to fully lyse the cells and 50 μ l of the lysate was transferred to either a 96-well plate for the para-Nitrophenylphosphate (pNPP) assay and to a black 96-well plate for the pico green assay.

pNPP standards (0.5, 0.3, 0.2, 0.1, 0.05, 0.025, 0.0125 and 0 μ M/ml in 0.2M carbonate buffer) were prepared by diluting pNPP stock solution (10mM, Sigma Aldrich). pNPP stock substrate (1 mg/ml pNPP (Sigma Aldrich) in 9ml 0.2 M carbonate buffer and 1ml 100 mM magnesium chloride (Sigma Aldrich)) was diluted 1:2 v/v with dH₂O and 50 μ l was added to each sample well. Samples were incubated at 37 °C for up to 1 hour. The absorbance of each sample and standards was measured at 405 nm on a plate reader.

Pico green standards (8, 4, 2, 1,0.5, 0.25 and 0 μ g/ml in triton lysis buffer) were prepared from salmon sperm DNA stock (100 μ g/ml in triton lysis buffer). 50 μ l of pico green reagent (1:50 dilution of pico green (Invitrogen) in TE buffer (10mM tris (Invitrogen) and 1mM EDTA, pH 7.5)) was added to the standards and samples and the plates were incubated at room temperature in the dark for 5 minutes. The fluorescence was read on a plate reader (BMG Polarstar Optima for absorbance, fluorescence and luminescence) at 485 nm excitation and 538 nm emission.

3.3.12 Culturing MSCs within hybrid gels

Hybrid gels were prepared as previously described in section 2.3.12. MSCs were suspended within the gel on ice, prior to gelation. The cell suspension was pipetted with pre-chilled tips into either PEI coated metal rings, adhered to glass bottomed Petri dishes or into 96 well v-bottomed plates. 30 μ l of gel-cell suspension was used for both molds. ADSCs were used in the aLN experiments and BM-MSCs were used for cartilage engineering.

3.3.13 ADSC Spheroids

2% methylcellulose was prepared by autoclaving 6 g methylcellulose (4000 centipoises, Sigma Aldrich) in a Schott bottle, which was subsequently dissolved in 150 ml of pre-warmed DMEM (60 °C) at room temperature. A further 100 ml of DMEM was added to solution, which was stirred for a further 2-3 hours until clear. The methylcellulose stock was centrifuged at 3600g for 2 hours to remove any insoluble particulate. The clear supernatant was stored at 4 °C until required. Spheroids of 6×10^5 cells were formed by suspending ADSCs at 4×10^5 /ml in 0.25 % methyl cellulose solution (diluted in basal media, from the 2% stock). 150 µl aliquots of the cell suspension were transferred into a non-adherent 96 well U-bottomed plate (Fisher). Overnight the cells aggregated into spheroids.

3.3.14 ADSC viability in low NIPAM content gels

Cells cultured within the hybrid gels were labelled using LIVE/DEAD viability/cytotoxicity kit (Molecular probes). Each gel was covered in 2ml of live/dead staining solution (4µM Ethidium homodimer 1 and 2µM Calcein AM in sterile PBS) and incubated at 37 °C for 30 mins. 200ul of fresh staining solution was then added to each gel and the labelled cells were visualised by confocal microscopy. A dead cell control was created by treating a gel in 70% methanol prior to staining with the live/dead reagent.

To release cells from collagen gels, the gels were carefully transferred to 1.5 ml eppendorfs using forceps and ground using a disposable pestle followed by incubation on a shaker at 37 °C in 0.4 mg/ml liberase RT (Roche) until the collagen had been digested (3 - 10 minutes). In hybrid gels, the liberase digestion was combined with cooling on ice and pipetting to break up the polymer. The isolated cells were centrifuged at 450 rpm for 5 minutes and washed twice in PBS, then resuspended in basal media in 6-well plates.

3.3.15 Imaging

Cryosectioning. Hydrogels, spheroids and chondrogenic pellets for sectioning were first washed in 1x PBS, embedded in Optimal cutting temperature compound (OCT, TissueTek) and subsequently flash frozen in liquid nitrogen. Samples were stored at -20 °C prior to sectioning. 10 µm sections were cut using a cryostat (Bright Instruments, OCT5000) at -20 °C and collected on poly-L-Lysine slides (Thermoscientific).

Immunofluorescent staining of sections. Slides were left to defrost for a few minutes prior to fixing. All washing steps were in 1x PBS for 5 minutes, repeated 3 times. Sections were then fixed in 4% PFA for 10 minutes at room temperature then washed in 1x PBS. For intracellular staining, the sections were incubated with 0.1% Triton-X (in PBS) for 10 minutes and washed in PBS. Sections were blocked with blocking buffer (0.1% BSA in PBS with 10% serum (species secondary antibody raised in)) for 30 minutes and then stained with primary or conjugated antibodies, diluted in blocking buffer overnight at 4 °C. Sections were then washed in PBS and incubated with secondary antibodies and DAPI diluted in blocking buffer (if required) for 1 hour at room temperature in the dark. Secondary antibody was washed from the sections with PBS. The sections were mounted with 5 µl of prolong gold (Life Technologies), No.1.5 cover slips (Fisherbrand) and sealed with nail polish.

For collagen II staining, antigen retrieval was performed prior to blocking. The sections were incubated with Proteinase K solution at 37 °C for 20 min, followed by a 10 minute incubation at room temperature. The sections were then washed as previously described.

Proteinase K stock 20x : 16 mg proteinase K (5-15U/mg, Sigma Aldrich) in 10 ml TE buffer and 10 ml glycerol. TE buffer: 50 mM TrisBase, 1 mM EDTA, 0.5% Triton-X.

Immunofluorescent staining of whole collagen gels. All wash steps were in 1x PBS to immerse the gel on a rocker, where the PBS was replaced every 10 minutes 3 times. Gels were fixed by removing culture media and incubating with 4% PFA at room temperature for 30 minutes, the gels were then washed in PBS. The cells were permeabilised with 0.1% Triton-X, where the Triton was replaced 4 times over an hour

and the gels were subsequently washed in PBS. Gels were then blocked and stained using the protocol for sections, with the secondary antibody incubations increased to 2 hours. Following staining the gels were immersed in 2ml of 1x PBS to prevent drying.

Slides and gels were imaged using a LSM710 invert confocal microscope (Zeiss).

Hematoxylin and Eosin staining. Prior to cryosectioning whole gels were fixed in PFA as in the above method and then incubated in 15% sucrose solution for 3 hours and 30% sucrose overnight. Gels were then sectioned as before. Slides were mounted in a staining rack and sequentially stained.

1. Harris hematoxylin for 3-5 minutes
2. Rinse in running water for 5 minutes
3. Dip in 0.5% eosin 12 times (1.5g eosin in 95% ethanol)
4. Dip in water until stain no longer streaks
5. 10 dips in 50% ethanol
6. 10 dips in 70% ethanol
7. Submerge in 95% ethanol of 30 seconds
8. Submerge in 100% ethanol for 1 minute

Sections were then mounted with DPX mountant.

3.3.16 cDNA synthesis and qPCR

RNA extraction. RNA was extracted using the RNeasy Mini kit (Qiagen). For cells grown in a 2D monolayer 350 μ l of RLT lysis buffer was added directly to cells.

Spheroids were transferred using cut pipette tips to 1.5 ml eppendorfs and washed once in PBS. 150 μ l of RLT lysis buffer was added to the tube and the spheroids disaggregated using a hand held motorised pestle. A further 200 μ l of RLT lysis buffer was then added to the tube. For cell-laden hydrogels, cells were isolated as described in section 3.3.14. The isolated cells were centrifuged at 450 rpm for 5 minutes and washed twice in PBS. 350 μ l of RLT lysis buffer was added to the cells.

For all culture methods the lysate was then pipetted up and down and transferred to a QIAshredder column (Qiagen) to homogenise. 350 µl of 70% ethanol was added to the homogenised lysate and mixed well by pipetting. The ethanol/lysate solution was transferred to a RNeasy spin column and centrifuged to load the RNA on the column. The column was washed in RW1 and RPE buffers and eluted using 30 µl of RNase free H₂O. RNA concentration was measured using a nanodrop (Thermo Scientific). RNA was stored at – 80 °C until required.

cDNA synthesis. Extracted RNA was used for cDNA synthesis using an EZ-First Strand cDNA synthesis kit (Geneflow). Each RNA sample was mixed with 1 µl 10x Oligo(dT) primer and DEPC treated water to a total volume of 10 µl and heated at 70 °C for 10 minutes to anneal primers. 2 µl Dithiothreitol (DTT) and 8 µl 2.5x RT reaction mix was added to each RNA sample and the solution mixed well. The samples were incubated on a thermal cycler (Labcycler, SensoQuest) for 60 minutes at 42 °C to synthesise the cDNA and for 15 minutes at 70 °C to stop the reaction. The newly synthesised cDNA was diluted to 100 µl and stored at -20 °C prior to polymerase chain reactions (PCR). cDNA was stored at -20 °C until required.

Primer Design. Primers were previously designed using NCBI primer blast software (National centre for biotechnology, <http://www.ncbi.nlm.nih.gov/>). They were designed to span exon-exon boundaries and give products between 200-300 bp in size.

Gene	Primer Sequence
Hu GAPDH	<i> fwd</i> TGCACCACCAACTGCTTAGC
	<i> rev</i> GGCATGGACTGTGGTCATGAG
Hu ICAM-1	<i> fwd</i> ATGGGCAGTCAACAGCTA
	<i> rev</i> GCAGCGTAGGGTAAGGTT
Hu VCAM-1	<i> fwd</i> GTCTCCAATCTGAGCAGCAA
	<i> rev</i> TGGGAAAAACAGAAAAGAGGTG
Hu IL-4 R	<i> fwd</i> TGAGTGGAGCCCCAGCACCAA
	<i> rev</i> ACAGGCAGACGGCCAGGATGA

Table 3-3 Primer sequences

qPCR. Real time PCR was performed on an ABI17300 prism system (Applied Biosystems) using a 96 well format. A master mix for each primer pair was made Table 3-3), and each well contained 4 μ l cDNA (or nuclease free H₂O for controls), 12.5 μ l sybr green PCR master mix (Applied Biosystems), 6.5 μ l nuclease free water and 1 μ l each of forward and reverse primer (Sigma Aldrich). For each gene of interest 3 technical replicates were carried out. The plate was centrifuged for 2 minutes at 3600 rpm prior to reaction. The qPCR thermal cycling programme consisted of 50 °C for 2 minutes followed by 95 °C for 10 minutes, and 40 cycles of 95 °C for 15 seconds, 60 °C for 1 minute and 72 °C for 30 seconds, and then 72 °C for 5 minutes. The plate was then

held at 4 °C until removed from the cycler. The data was analysed using ABI17000 software and normalised against GAPDH for changes in the cycle threshold.

3.3.17 MTT viability assay

Cells were seeded at the desired density within 30 µl hydrogels. 3-(4,5-dimethylthiazol-2-yl)-2,5-diphenyltetrazolium bromide (MTT, Sigma Aldrich) was dissolved in 1x PBS (5mg/ml) and sterile filtered. Spent medium was removed from cell-laden hydrogels and replaced with 100 µl of fresh basal medium and 25 µl of MTT solution. Samples were incubated for 4 hours at 37 °C. MTT containing medium was then removed from each well and replaced with 100 µl of cell lysis solution (0.1M HCl in 2-propanol) and the cells/cell-laden hydrogels were incubated at 4 °C until the scaffolds became translucent and did not contain any remaining purple formazan product. 50 µl of lysis solution from each well was transferred to a fresh 96-well plate and the absorbance of each was measured at 570 nm using an ELISA plate reader. Alternatively after 4 hours of incubation with MTT, the cell-laden hydrogels were flash frozen in liquid N₂ in OCT, sectioned and immediately imaged to assess the distribution of formazan throughout the hydrogels.

3.3.18 Alcian blue staining

Sections were fixed as previously described in section 3.3.15, and briefly washed twice in dH₂O. The sections were then incubated in 1% alcian blue stain (8GX alcian blue in dH₂O, Sigma Aldrich) for 30 minutes. Excess stain was removed by brief washes in dH₂O, and the slides were mounted with 20% glycerol.

3.3.19 Statistics

Significance was calculated using Kruskal-Wallis non-parametric analysis and Dunn's post-test comparison of all pairs of samples. P values were calculated using GraphPad Prism software where, $p > 0.05$ = not significant, $0.01 - 0.05$ = significant *, $0.001 - 0.01$ = very significant ** and $p < 0.001$ = extremely significant ***.

3.4 Results: In-vitro modelling of lymphoid mesenchyme

3.4.1 Cytokine treatment induces a lymphoid mesenchyme phenotype in 2D ADSCs

The supporting backbone of the LN is a series of stromal networks that are derived from the mesenchyme. To engineer the stromal networks of the LN I used a previously developed a protocol using inflammatory cytokines to induce a lymphoid phenotype in 2D ADSCs (unpublished results, B Glaysher). Treatment of ADSCs with the cytokines IL-4, TNF- α and an agonistic antibody specific for the lymphotoxin β receptor, resulted in the upregulation of markers of lymphoid stroma, specifically adhesion molecules ICAM-1, VCAM-1 and podoplanin (Figure 3-4). Anti- LT β R was used in place of LT $\alpha_1\beta_2$ to provide signalling through LT β R, as it improved induction of the lymphoid mesenchyme phenotype (unpublished data). In ADSCs without the cytokine treatment 34% of ADSC express ICAM-1, while less than 1% express VCAM-1 (Figure 3-4B), compared with 97% of post-treated ADSCs expressing ICAM-1, and 84% expressing both ICAM-1 and VCAM-1 (Figure 3-4C). Podoplanin expression on the ADSCs varied among the population, but a large shift is observed in the MFI of the untreated ADSCs, which increases from 6.78 up to 32.05 when the ADSCs received cytokine induction (Figure 3-4D). Treated only with IL-4, ADSCs upregulated VCAM-1, while the combination of TNF- α and anti-LT β R upregulated both ICAM-1 and VCAM-1 expression, where over 99% of cells expressed ICAM-1, highlighting the combined treatment of all three factors is necessary for lymphoid mesenchyme induction (Figure 3-4E).

3.4.2 Lymphoid mesenchyme induction reduces the differential capacity of 2D ADSCs

ADSCs are able to differentiate into fat, bone and cartilage tissue when cultured in basal media supplemented with soluble factors. Following the cytokine induction of 2D ADSCs into lymphoid mesenchyme, the tri-lineage differential capacity of the cells may be reduced, therefore the effect of the cytokine treatment on ADSC adipogenesis and osteogenesis was examined. ADSCs were cultured for 21 days in adipogenic (AM), osteogenic (OM) or basal media (BM) supplemented with the lymphoid inducing

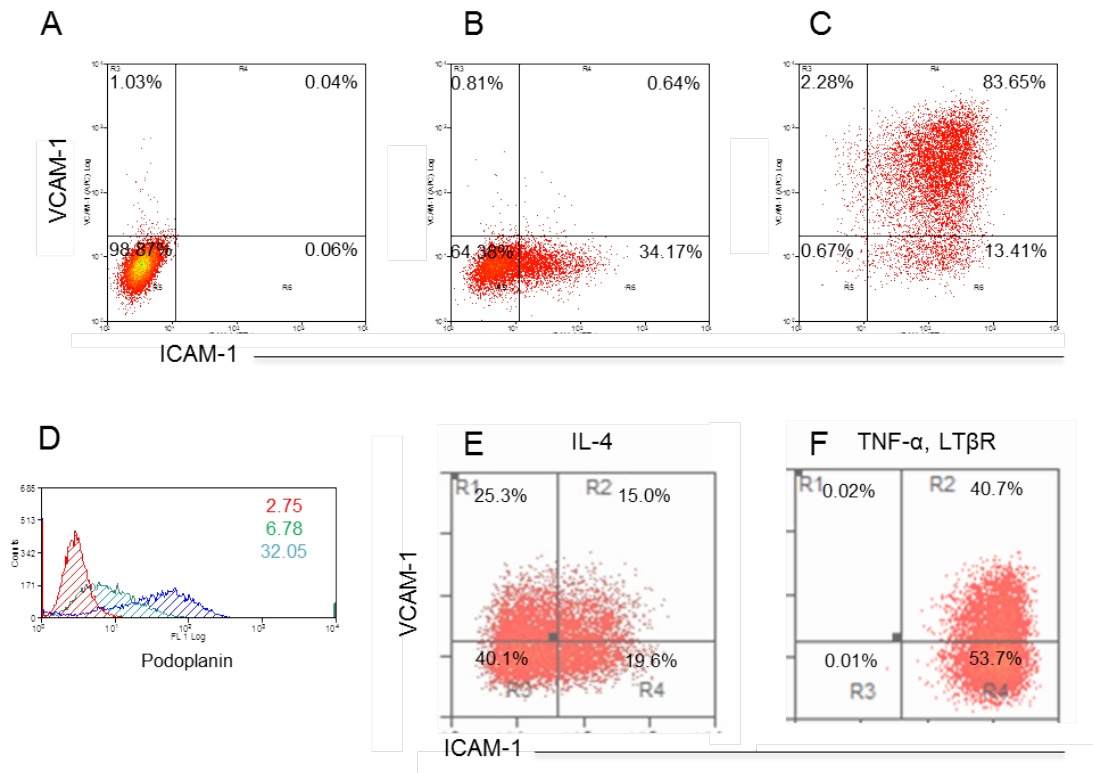


Figure 3-4: 2D ADSCs can be induced into a lymphoid mesenchyme phenotype upon induction with cytokines, as characterised by marker expression. ICAM-1 and VCAM-1 expression on unstained ADSCs (A), ADSCs without cytokine induction express intermediate levels of lymphoid mesenchyme marker ICAM-1, whilst VCAM-1 expression is negligible (B), When treated with IL-4, TNF- α and anti-LT β R, ADSCs express high levels of both ICAM-1 and VCAM-1, indicating induction into a lymphoid mesenchyme phenotype. (C). Additionally with the cytokine treatment podoplanin expression also increases on ADSCs (D). Numbers indicate MFI of unstained ADSCs (red), untreated ADSCs (green) and cytokine treated ADSCs (blue). When treated with either IL-4 (E) or TNF- α and anti-LT β R (F) the induction of the phenotype shown by ICAM-1 and VCAM-1 expression is reduced, indicating all 3 factors are required for efficient induction.

cytokines. ADSCs without cytokine treatment were able to differentiate into adipocytes, shown by Oil Red O (ORO) staining of lipids forming in the cells (Figure 3-5A). There was no spontaneous differentiation of untreated or cytokine treated ADSCs cultured in BM. Adipogenesis was inhibited in ADSCs treated with cytokines. The effect was quantified by measuring the ORO stain eluted from the lipids with iso-propyl alcohol. In the presence of cytokines, adipogenesis was significantly reduced after 14 days of differentiation, compared with adipogenic controls, the ORO concentration was roughly equal to, or lower than ADSCs cultured in basal media (Figure 3-5). Alkaline phosphatase (ALP), an enzyme produced by osteo-progenitors, was measured to quantify osteogenesis of the ADSCs. In the presence of ALP, pNPP is hydrolysed to pNP, a coloured substrate that can be quantified spectrophotometrically. By measuring the DNA content with pico green, the pNP concentration is then normalised against the cell number. Control ADSCs in OM, underwent osteogenesis as expected, with significantly high levels of ALP activity, and cell proliferation compared with control ADSCs in BM (Figure 3-6). ADSCs in BM supplemented with cytokines, had no significant difference in pNP concentration or cell number compared with control ADSCs in BM. In osteogenic conditions, ADSCs treated with cytokines displayed low ALP activity over the entire 21 day period, which was comparable to basal conditions. However, in OM the cytokine treated ADSCs did undergo an increase in cell number comparable to control ADSCs in OM. When normalised to DNA content, ALP was significantly reduced in cytokine treated ADSCs compared with controls.

As ADSCs have previously been shown to have reduced adipogenic capacity when supplemented with TNF- α and anti-LT β R³³⁷, the effect of IL-4 alone on adipogenesis and osteogenesis was also examined. Supplemented only with IL-4, ADSCs were able to differentiate towards an adipogenic lineage comparable to untreated ADSCs. Both treated and untreated ADSCs followed a similar differentiation process, with small lipids forming within a few cells after 7 days of treatment, then an increase in lipid density at day 14 and again at day 21 (Figure 3-7A). By day 21 the entire cell population of treated and untreated ADSCs positively stained for ORO. Mature adipocytes are also observed in both cultures at day 21, characterised by the presence of cells with a single large lipid rather than multiple smaller ones. Elution of ORO stain

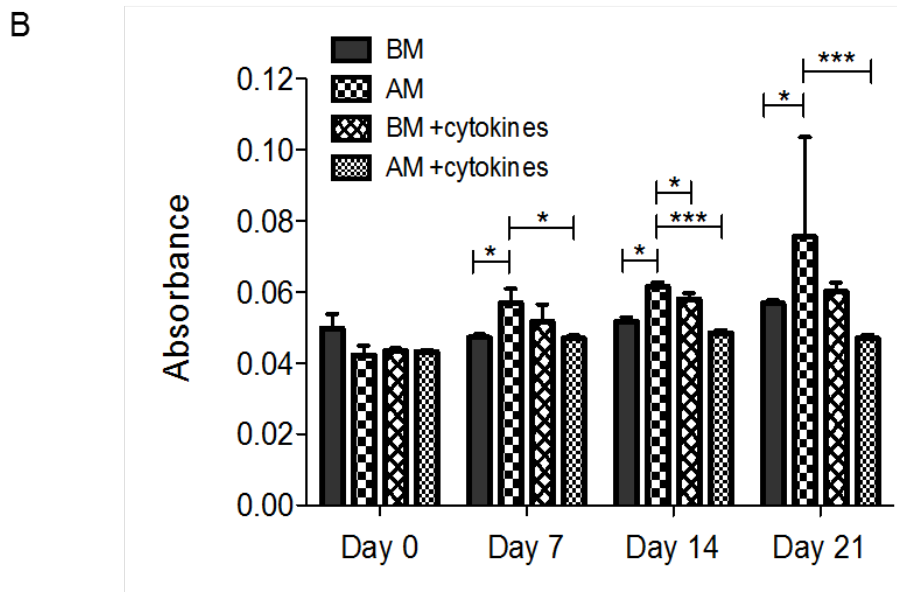
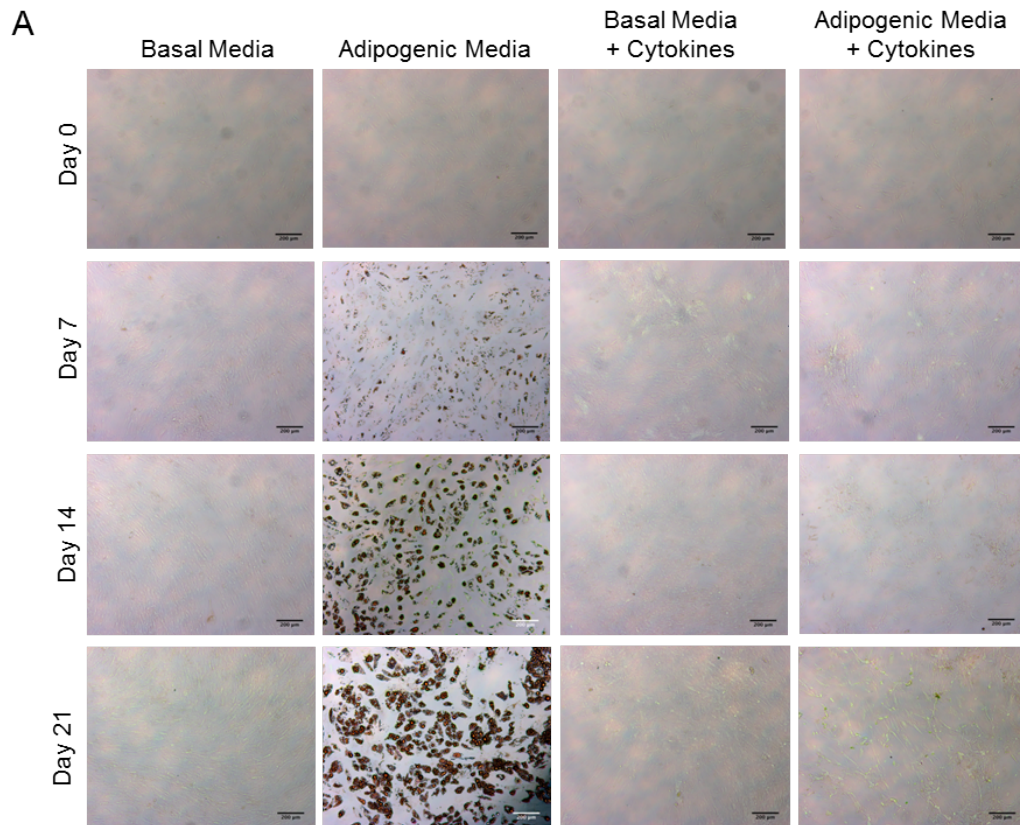


Figure 3-5 Lymphoid mesenchyme induction inhibits 2D ADSC adipogenesis. ADSCs cultured within basal media (BM) or adipogenic media (AM) with or without cytokine induction over 21 days. ADSCs treated with cytokines were unable to differentiate towards adipocytes, shown by an absence of Oil Red O staining of lipids (scale bars are 200 μ m) (A). Total Oil Red O stain was eluted from adipogenic cultures with IPA for quantification (n=6) (B).

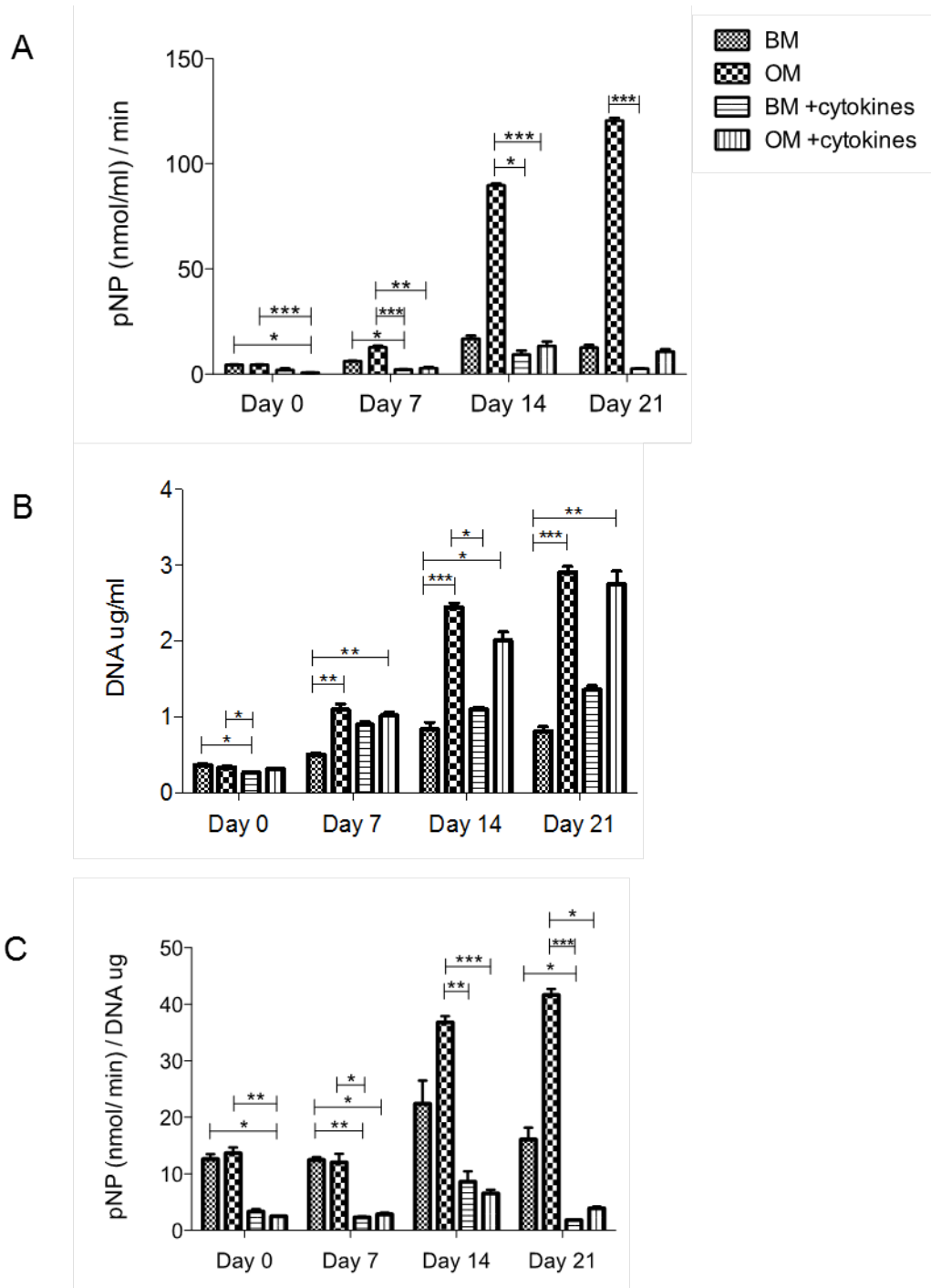


Figure 3-6: Lymphoid mesenchyme induction inhibits 2D ADSC osteogenesis. ADSCs cultured within basal media (BM) or osteogenic media (OM) with or without cytokine induction over 21 days. ADSCs treated with cytokines also had reduced osteogenic potential as shown by alkaline phosphatase expression, however proliferation was unaffected. Quantified by pNPP hydrolysis to pNP by alkaline phosphatase (A), Pico green DNA quantification (B) and pNP normalised to DNA content (C). Results are mean \pm SEM (n=6)

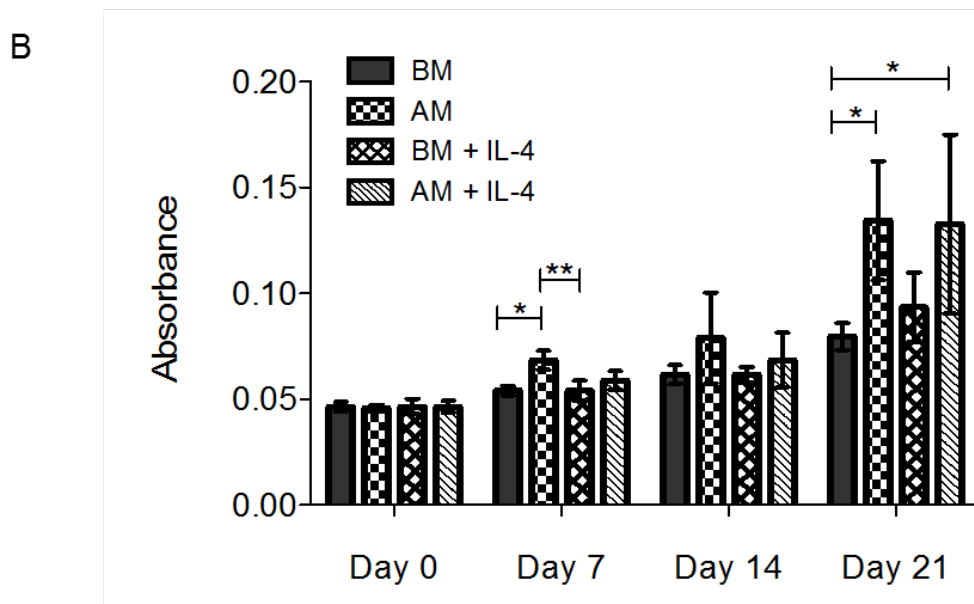
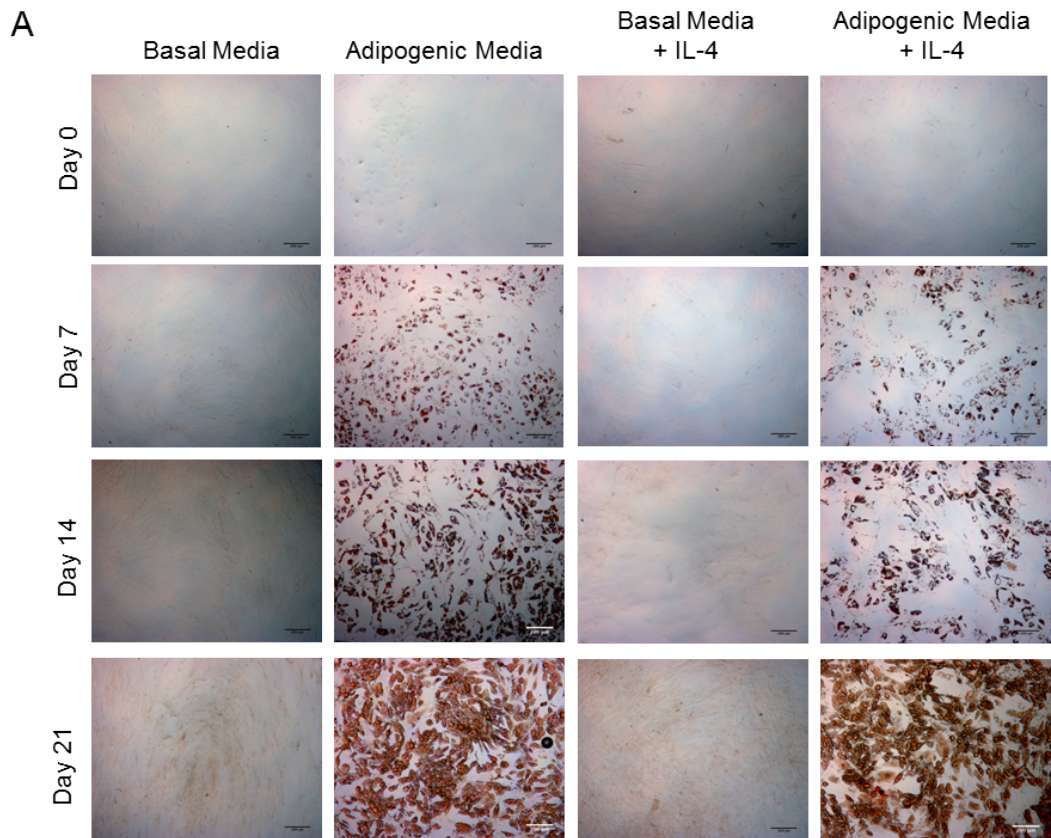


Figure 3-7: IL-4 lymphoid mesenchyme induction of 2D ADSCs does not affect adipogenesis ADSCs cultured within basal media (BM) or adipogenic media (AM) with or without IL-4 treatment over 21 days. The adipogenic capacity of ADSCs treated with IL-4 was unaffected by IL-4 as shown by Oil Red O staining. (scale bars are 200 μ m) (A). Total Oil Red O stain was eluted from adipogenic cultures with IPA for quantification (n=6) (B).

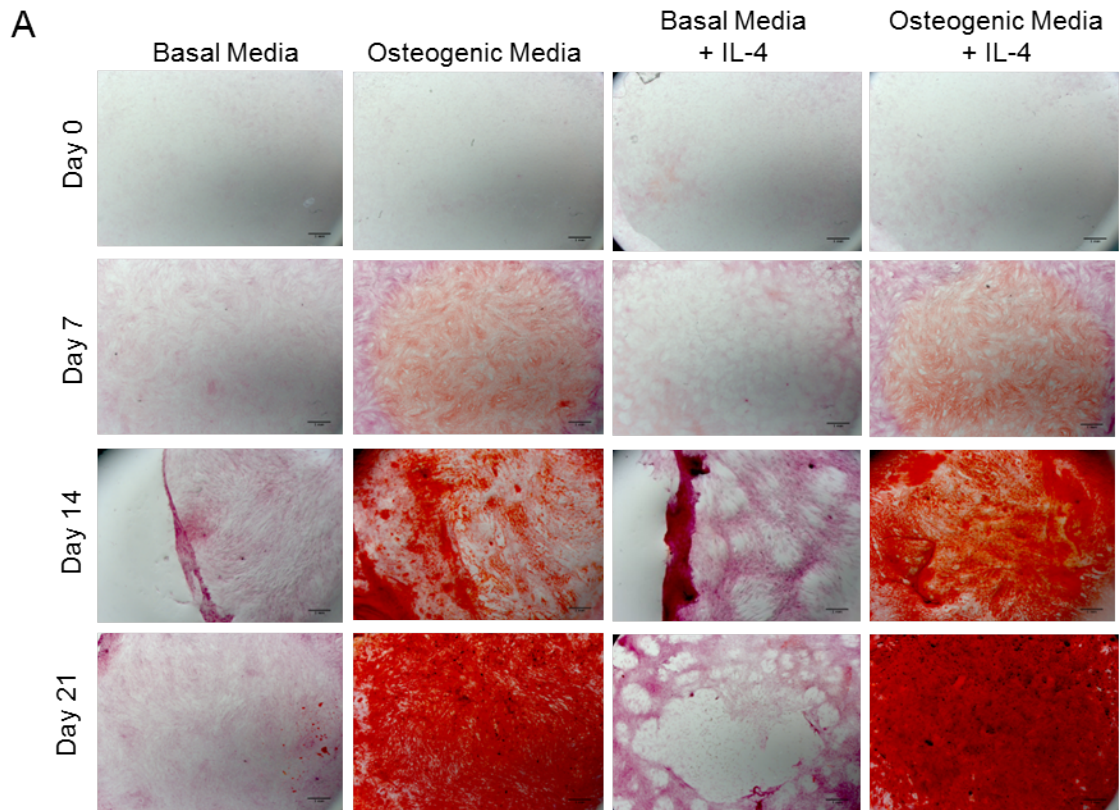


Figure 3-8: IL-4 lymphoid mesenchyme induction of 2D ADSCs does not affect mineralisation ADSCs cultured within basal media or osteogenic media with or without IL-4 treatment over 21 days. The osteogenic capacity of the ADSCs was unaffected by IL-4 treatment, as shown by Alizarin red staining of mineralization (scale bars are 200 μ m).

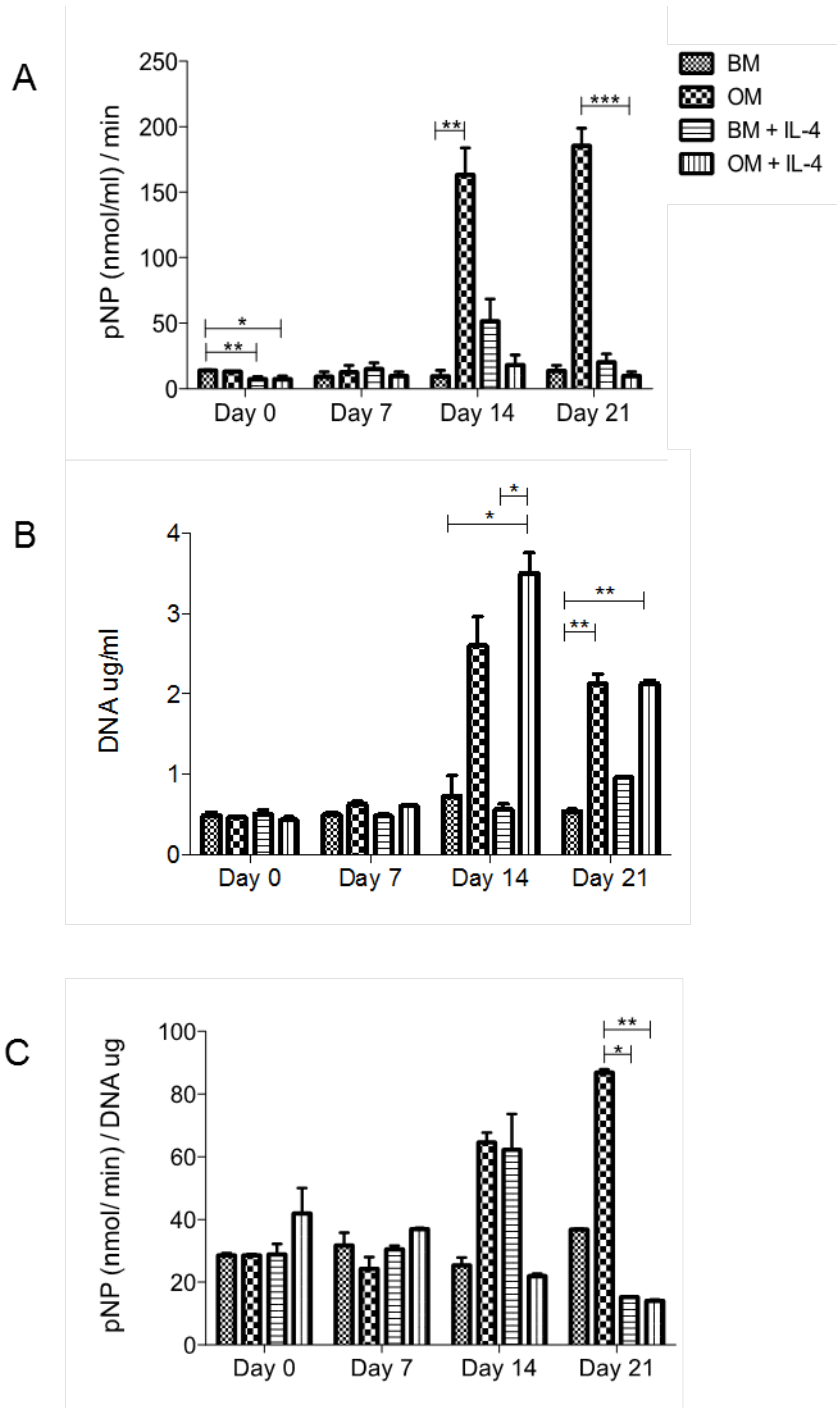


Figure 3-9: IL-4 lymphoid mesenchyme induction of 2D ADSCs affects ALP activity but not cell proliferation
 ADSCs cultured within basal media (BM) or osteogenic media (OM) with or without IL-4 treatment over 21 days. ADSCs treated with IL-4 had reduced alkaline phosphatase expression, but proliferation was unaffected. Quantified by pNPP hydrolysis to pNP by alkaline phosphatase (A), Pico green DNA quantification (B) and pNP normalised to DNA content (C). Results are mean \pm SEM (n=6).

showed no significant difference between adipogenesis of the treated and untreated ADSCs at any time point (Figure 3-7B).

Similarly to full cytokine treatment, 2D ADSCs in OM, supplemented with IL-4, had basal levels of ALP expression over the 21 day differentiation period, but displayed a similar rate of proliferation as untreated ADSCs in OM. DNA content increased up to day 14 and began to fall at day 21 in the osteogenic conditions (Figure 3-9). To further explore the effect of the IL-4 treatment on differentiation, calcium deposition in the ECM of the osteogenically differentiating ADSCs was examined by staining with Alizarin red. In OM, ADSCs without treatment produced a calcium rich matrix following 14 days of differentiation, which further intensifies by day 21 (Figure 3-8). ADSCs in BM have low levels of staining, which is similar between days 7 – 21. As a result of the high cell density used in the experiment, the confluent monolayer of ADSCs in BM detached and contracted at the later time points. Alizarin red staining of IL-4 treated ADSCs in OM is similar to untreated ADSCs in OM at each time point, where the staining also intensified with time in culture.

3.4.3 The lymphoid mesenchyme phenotype is reversible

To examine the reversibility and longevity of the cytokine treatment on 2D ADSC lymphoid mesenchyme induction, the cells were pre-treated with IL-4, TNF- α and anti-LT β R, or IL-4, TNF- α and anti-LT β R and then supplemented with AM or OM with or without continued treatment for 14 days (Figure 3-10A). ADSCs cultured in AM or OM where the cytokine treatment was removed at the beginning of the 14 days of differentiation, were able to differentiate comparably to untreated controls (Figure 3-10, Figure 3-11). ADSCs which continued to receive cytokine treatment during differentiation, differentiated into lipid filled cells, when only treated with IL-4 similarly to the previous experiment, whilst adipogenesis was inhibited in TNF- α and anti-LT β R, and IL-4, TNF- α and anti-LT β R treated ADSCs (Figure 3-10B). In the osteogenic samples, alizarin red staining was replaced with alkaline phosphatase and von Kossa staining, to examine both ALP activity and mineralisation simultaneously.

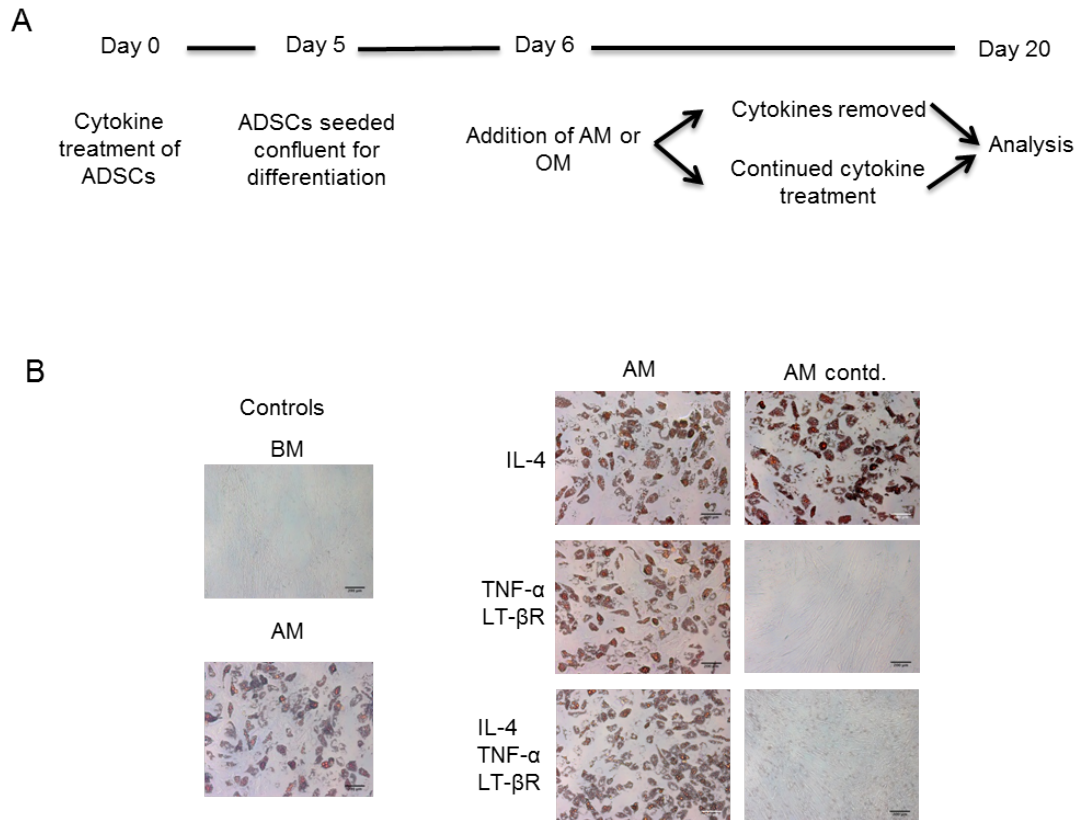


Figure 3-10: Priming of 2D ADSCs with lymphoid mesenchyme inducing cytokines does not affect adipogenesis.

Experimental scheme of ADSCs differentiation following pretreatment with cytokines (A). ADSCs were initially primed for 5 days with or without cytokine treatment, and subsequently seeded confluent for differentiation. Cytokine treatment was stopped prior to differentiation or continued throughout. The lymphoid mesenchyme phenotype is reversible as shown by adipogenically differentiating ADSCs, following removal of cytokines. Oil Red O staining of ADSCs after 14 days differentiation (scale bars are 200 μ m) (B).

Following 14 days of differentiation in OM, ALP activity, as measured by pNP, was not significantly different between ADSCs where cytokine treatment was discontinued prior to differentiation and untreated ADSCs (Figure 3-11A). Cells that received continued cytokine treatment during osteogenic differentiation had reduced ALP activity, although this was not significant after 14 days. Surprisingly, when treatment was continued with the combined treatment of all three factors, ALP activity was comparable to control ADSCs in OM. Positive alkaline phosphatase staining was observed in all ADSC conditions in OM, when cytokine treatment was removed at the start of differentiation (Figure 3-11B). In the continued presence of cytokines, staining decreased in the presence of IL-4 or TNF- α /anti-LT β R, but was absent when all three were used. In comparison with the previous osteogenic results and the ALP staining in this experiment, where ALP decreases when all three cytokines are used, the increase seen in ALP activity by pNP when treatment was continued in this experiment may be an anomaly and requires a repeat experiment to confirm. A small number of von Kossa stained mineralised nodules were however present in all osteogenic conditions, including the continued treatment of ADSCs with IL-4, TNF- α and anti-LT β R. In OM, cell proliferation was similar between control ADSCs and ADSCs without continued cytokine treatment. ADSCs that received continued cytokine treatment were less proliferative than control ADSCs and ADSCs with continued treatment, but the difference was not significant and proliferation remained higher than ADSCs in BM.

To further examine the induced lymphoid mesenchyme phenotype of ADSCs following cytokine treatment and differentiation, flow cytometry analysis of the stromal markers ICAM-1 and VCAM-1 was performed on ADSCs with and without continued treatment. Compared with ADSCs maintained in BM, adipogenically differentiated ADSCs appeared as two populations when gated on side scatter (SS) and forward scatter (FS) (Figure 3-12A). Both populations contained cells of a similar size, but a second population of ADSCs with a larger SS was present in the adipogenically differentiated cells. These populations are referred to as SS^{mid} and SS^{high}, making up 79 and 21% of the gated cells respectively. When the cytokine treatment is removed a similar profile is seen in the cell population, indicating the cells are differentiating, however in the continued presence of TNF- α /anti-LT β R or all 3 factors during

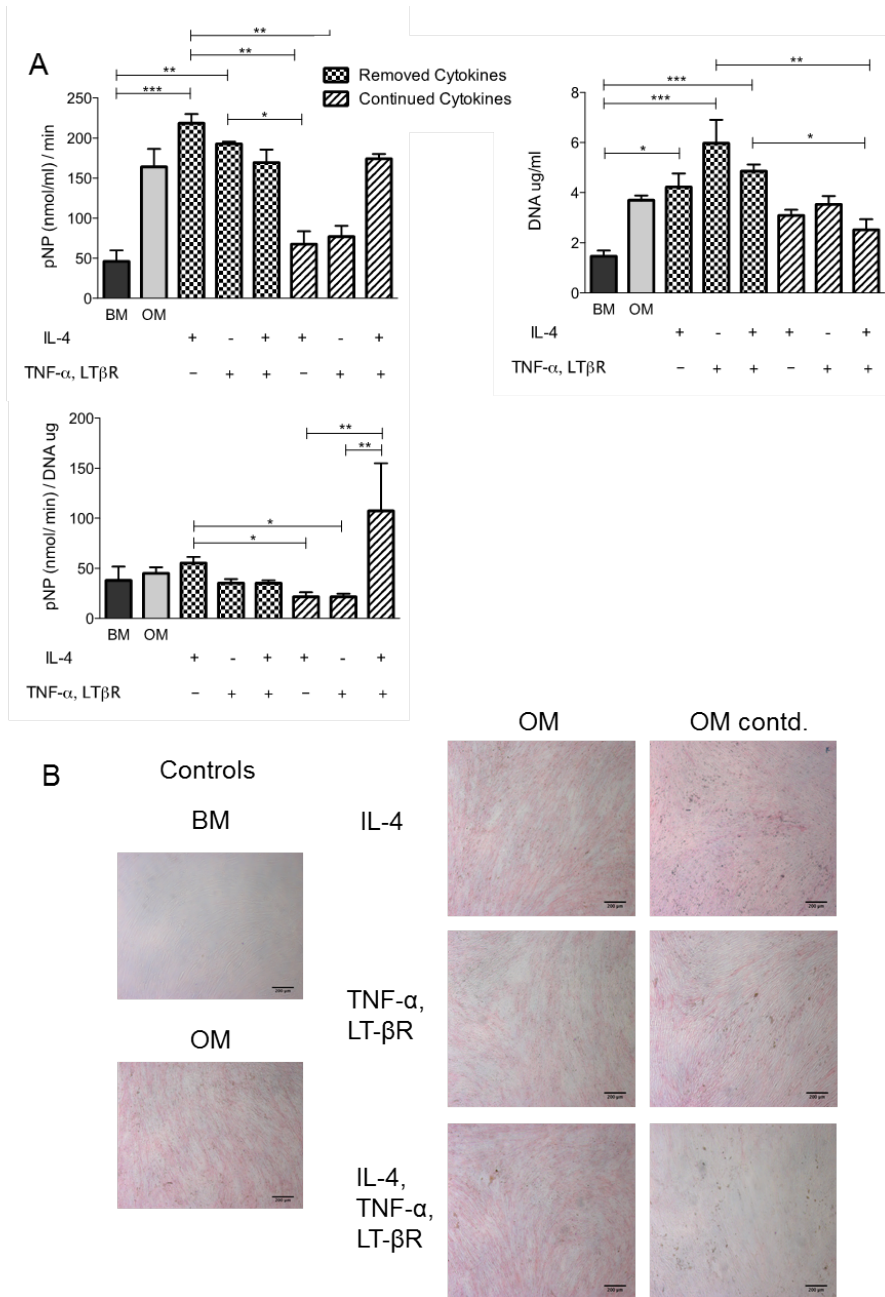
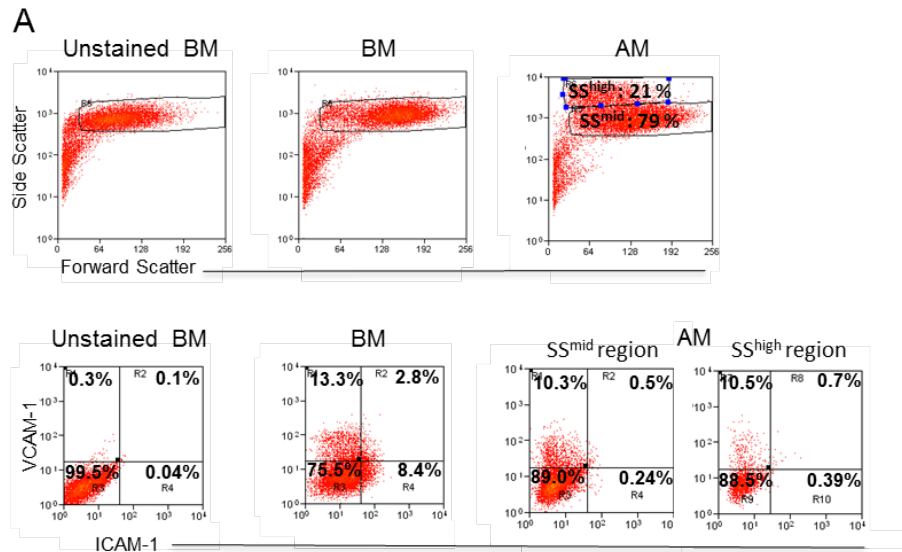


Figure 3-11 Priming of 2D ADSCs with lymphoid mesenchyme inducing cytokines does not affect osteogenesis.

ADSCs were initially primed for 5 days with or without cytokine treatment, and subsequently seeded confluent for differentiation. Cytokine treatment was stopped prior to differentiation or continued throughout. The lymphoid mesenchyme phenotype is reversible as shown by osteogenically differentiating ADSCs, following removal of cytokines. Alkaline phosphatase expression of ADSCs following 14 days differentiation (A), pNP production by alkaline phosphatase, Pico green DNA quantification and pNP normalised to DNA content. Results are mean \pm SEM (n=6). Reversal of the phenotype also confirmed through alkaline phosphatase and Von Kossa stain of control ADSCs and ADSCs in OM with and without continued treatment (scale bars are 200 μ m) (B).



B

			% of cells/ population	ICAM-1 ⁺	VCAM-1 ⁺	ICAM-1 ⁺ / VCAM-1 ⁺
Cytokines removed	IL-4	SS ^{mid}	76.5	0.1	19.2	0.35
		SS ^{high}	23.5	0.34	19.94	1.19
	TNF- α , LT- β R	SS ^{mid}	74.5	0.96	14.20	0.23
		SS ^{high}	25.5	0.31	30.98	0.37
Cytokines continued	IL-4	SS ^{mid}	86.1	1.92	12.66	1.05
		SS ^{high}	13.9	2.47	15.71	3.23
	TNF- α , LT- β R	SS ^{mid}	66.7	0.29	41.42	0.17
		SS ^{high}	33.3	0.23	26.92	0.26
IL-4, TNF- α , LT- β R	SS ^{mid}	90.7	58.31	4.39	4.67	
	SS ^{high}	9.3	83.01	0.82	14.83	
IL-4, TNF- α , LT- β R	SS ^{mid}	90.1	14.57	13.49	66.49	
	SS ^{high}	9.9	14.24	0.70	84.25	

Figure 3-12 Expression of lymphoid mesenchyme markers ICAM-1 and VCAM-1 decreases in adipogenic 2D ADSCs

Expression of stromal markers ICAM-1 and VCAM-1 in control ADSCs (A) A second SS^{high} population of cells was present in cells differentiated in adipogenic media (AM). Following adipogenic differentiation (in the absence of cytokines) ICAM-1 and VCAM-1 expression was lower in AM compared with ADSCs cultured in basal media (BM). Analysis of ICAM-1 and VCAM-1 expression in adipogenically differentiating cells with or without continued cytokine induction following 5 days of priming (B). Following the removal of cytokines SS^{mid} and SS^{high} populations of ADSCs were present with low ICAM-1 and VCAM-1 expression indicating reversal of the lymphoid phenotype. Where cytokine treatment continued, the SS^{high} population was low, and ADSCs expressed ICAM-1 and VCAM-1 as expected based on the cytokine induction mix used.

adipogenesis, the SS^{high} population decreased to 9 %. In un-supplemented BM, ADSCs express low levels of ICAM-1 (8.36%) and VCAM-1 (13.3%), which fall to 0.24% and 10.29% respectively in AM and show little variation between SS^{mid} and SS^{high} populations (Figure 3-12B). ADSCs in AM with removed cytokines also have negligible ICAM-1 expression. VCAM-1 expression is higher than the control ADSCs, and is higher in the SS^{high} population. In the continued presence of cytokines, the proportion of double positive ICAM-1⁺ VCAM-1⁺ expressing cells approaches that of treated cells in BM. Supplemented only with IL-4, ADSCs express low levels of ICAM-1, and intermediate levels of VCAM-1, where the VCAM-1 expression is lower in the more adipogenic SS^{high} cells. In the presence of TNF- α /anti-LT β R there is an increase in double positive cells, and a large increase in ICAM-1 expressing cells in both SS populations. Again the combined effect of IL-4, TNF- α and anti-LT β R is highlighted, as the ADSCs supplemented with all three factors have the highest proportion of double positive cells at 66.49% for SS^{mid} and 84.25% and for SS^{high}.

3.4.4 Development of 3D models of lymphoid stroma

To move the lymphoid stromal model into 3D, ADSCs were encapsulated within collagen or hybrid gels. Collagen containing a suspension of ADSCs, prior to its gelation, forms gels with a uniform distribution of cells, and takes the shape of the parent solution. Over 24 hours ADSCs within the gel spread out and attach to the collagen matrix, forming a 3D network of cells (Figure 3-13A). The rings used as moulds were coated with a combination of polyethylene imine and glutaraldehyde prior to adding the collagen solution; to promote crosslinking of the gel to the mould and to reduce any cell mediated contraction. Following 5 days of culture the ADSC containing gels were fixed and stained with phalloidin, to identify the actin cytoskeleton and morphology of the cells and DAPI. Gels were imaged used a confocal microscope, where different planes throughout the gel could be visualised. Collagen gels seeded with a high density of ADSCs (5×10^6 cells/ml) were noticeably pulled apart by the cells (Figure 3-13B). An optimal seeding density of 2×10^6 cells/ml was chosen for creating stromal models, as cellular networks formed at this density, and there was minimal cell contraction. The top surface of the gels consistently contained a higher density of cells

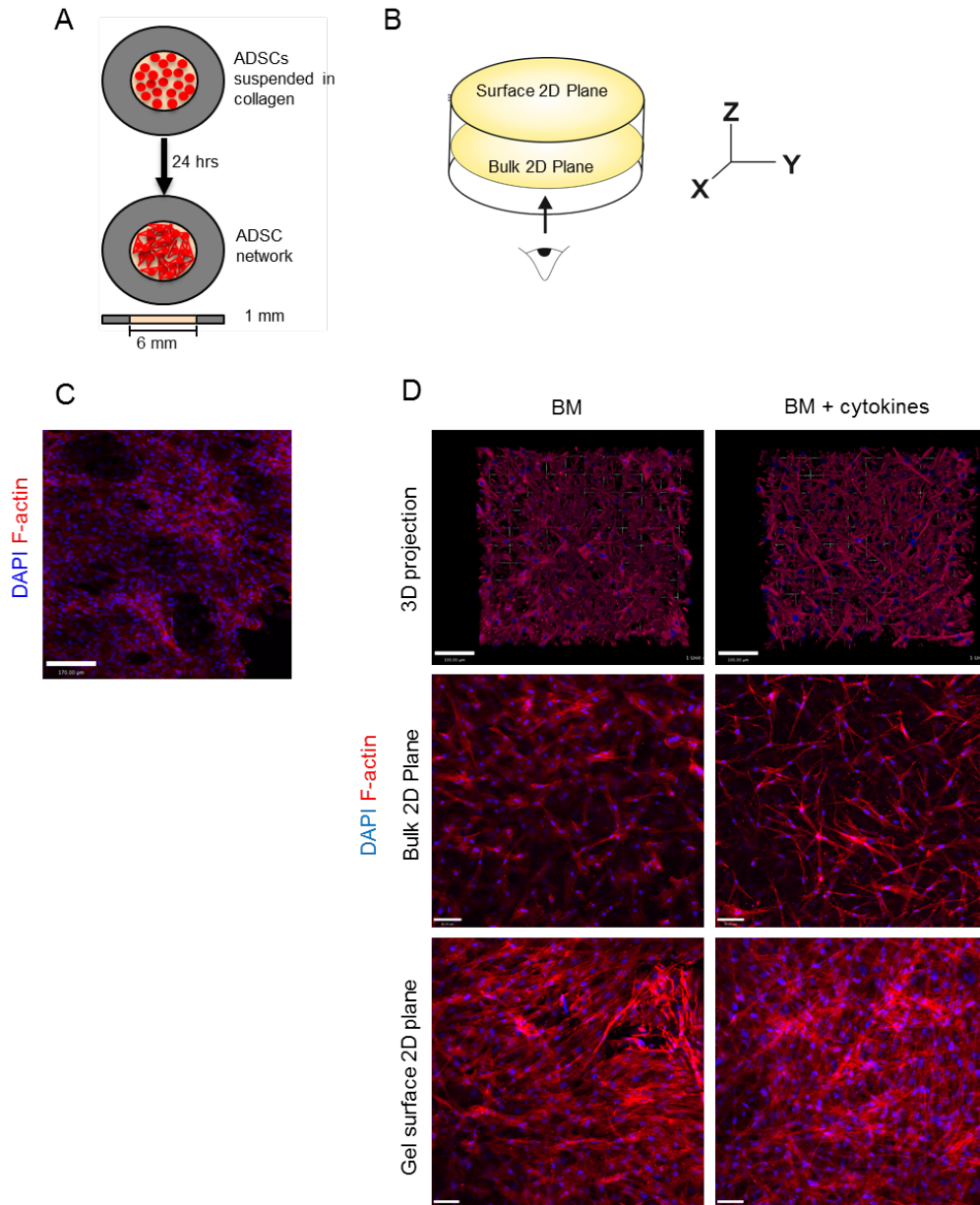


Figure 3-13 Development of 3D ADSC stromal networks in collagen gels.

ADSCs were suspended in liquid collagen and moulded into PEI-glutaraldehyde coated washers. Overnight the cells spread out and attach to the gel forming networks (A). Immunofluorescent imaging was obtained using a confocal microscope, where images were taken at different depths throughout the gel (B). 2D plane showing collagen contraction by high densities of ADSCs (C) scale bars are 170 μm . ADSC networks (2 mil cell/ ml) in collagen gels with and without cytokines treatments (D). 3D projections are overlays of combined Z-plane images. Representative images of 2D Z-planes at the gel surface and within the bulk of the gel. 3D projections, scale 100 μm and 2D planes, scale bars are 80 μm .

compared with the distribution of cells in the centre (Figure 3-13C), which is probably the result of increased cell proliferation at the gel/media interface where there is increased nutrient and oxygen concentration in comparison to the bulk of the gels. To induce the stromal phenotype in 3D, the collagen gels containing ADSCs were covered in BM or BM supplemented with IL-4, TNF-alpha and anti-LT β R and cultured for 5 days. Each gel was briefly washed in PBS prior to and after fixing. Over a 30 min wash, the gels turned from pink to white as the media was exchanged with PBS, indicating the gels are media permeable. In both treated and untreated conditions the ADSCs spread out within the gels to form networks. The morphology of the ADSCs varied in 3D, where untreated cells were wider and had fibroblastic and cuboidal morphologies, containing organised actin stress fibres running perpendicularly with the widest part of the cell, while the treated cells were very thin and elongated compared with untreated cells. They contained several processes at their extremities, and also had aligned actin fibres within the extensions. In both the treated and untreated samples, the ADSCs seemed to have a finer and elongated morphology in the surfaces of the gels.

At the seeding density of 2×10^6 cells/ml, over 5 days of culture, the collagen gels were still prone to contraction. Therefore the collagen - NSN gels with mechanical properties at the lower end of the spectrum were examined as an alternative to collagen. Four different blends were examined, which each contained 0.3 wt% collagen while the NSN concentration varied between 0.25 – 1.25 wt %. The addition of NSN to the collagen gels resulted in an increase in opacity, however at these lower concentrations at least 100 μ m depth of the gels could be imaged by confocal microscopy. To initially demonstrate the potential of the hybrid gels as cell scaffolds, their biocompatibility was examined by looking at cell viability. In all four blends of the hybrid gels, ADSCs were able to spread out within the gels and form networks. Live-dead staining showed few dead cells, and viable cells with fibroblastic-like morphologies in all gels after 5 days of culture (Figure 3-14). Following 5 days culture in 3D, the ADSCs could also be released from the gels and cultured back in 2D on TCP (Figure 3-15). The cells were released using a combination of liberase enzyme digestion at 37 °C, to break up the collagen fibrils and cooling and disruption of the gels by pipetting to break up the aggregated hydrogel particles. A larger number of cells were released from the collagen

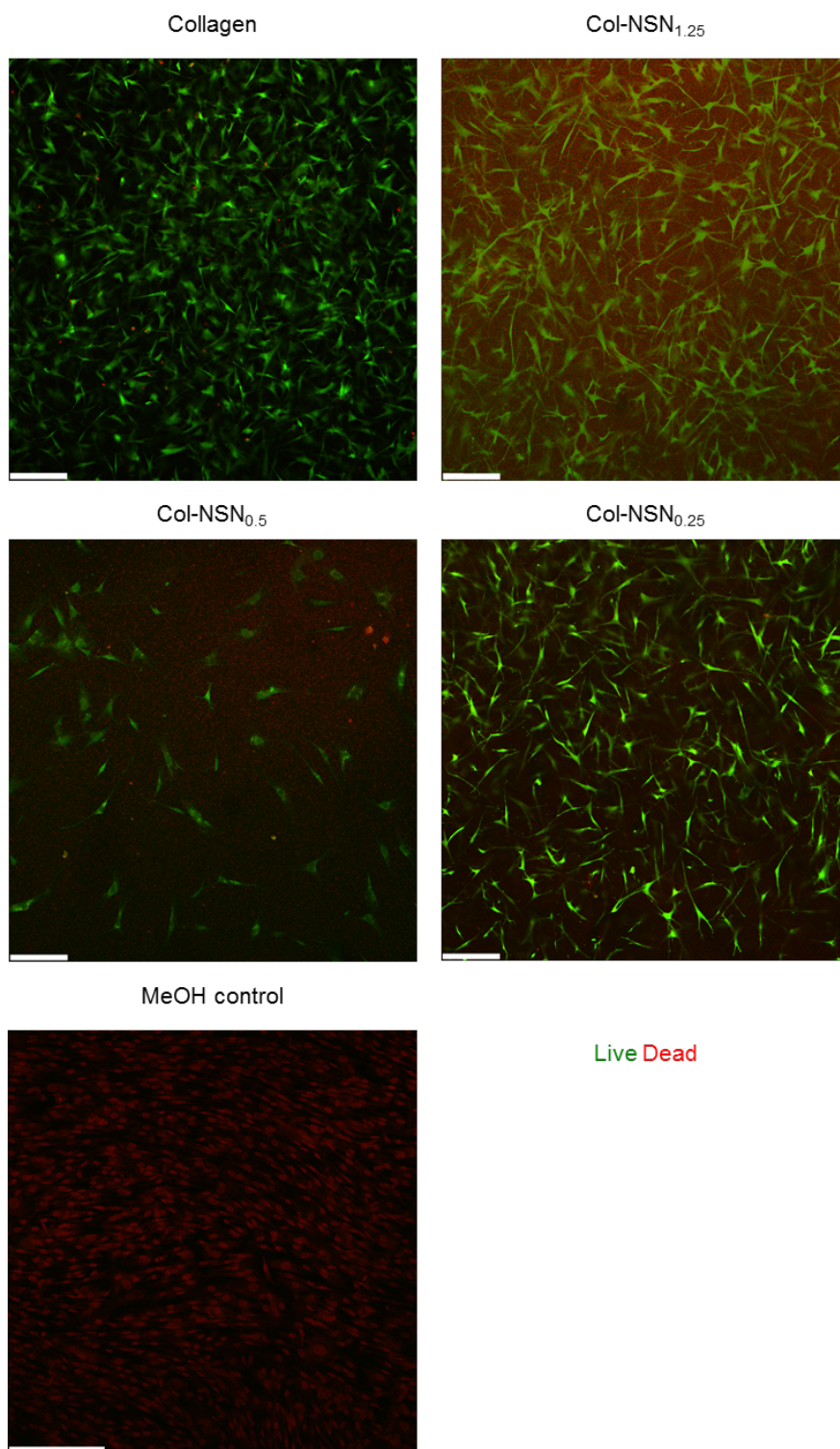


Figure 3-14 ADSCs encapsulated within col-NSN hydrogels are viable. Live-dead staining of ADSCs in collagen and col-NSN gels. Representative 2D images taken in the bulk of the gels. Calcein-am live cells (green) and ethidium homodimer-1 dead cell (red). Cells were treated with MeOH as a negative control.

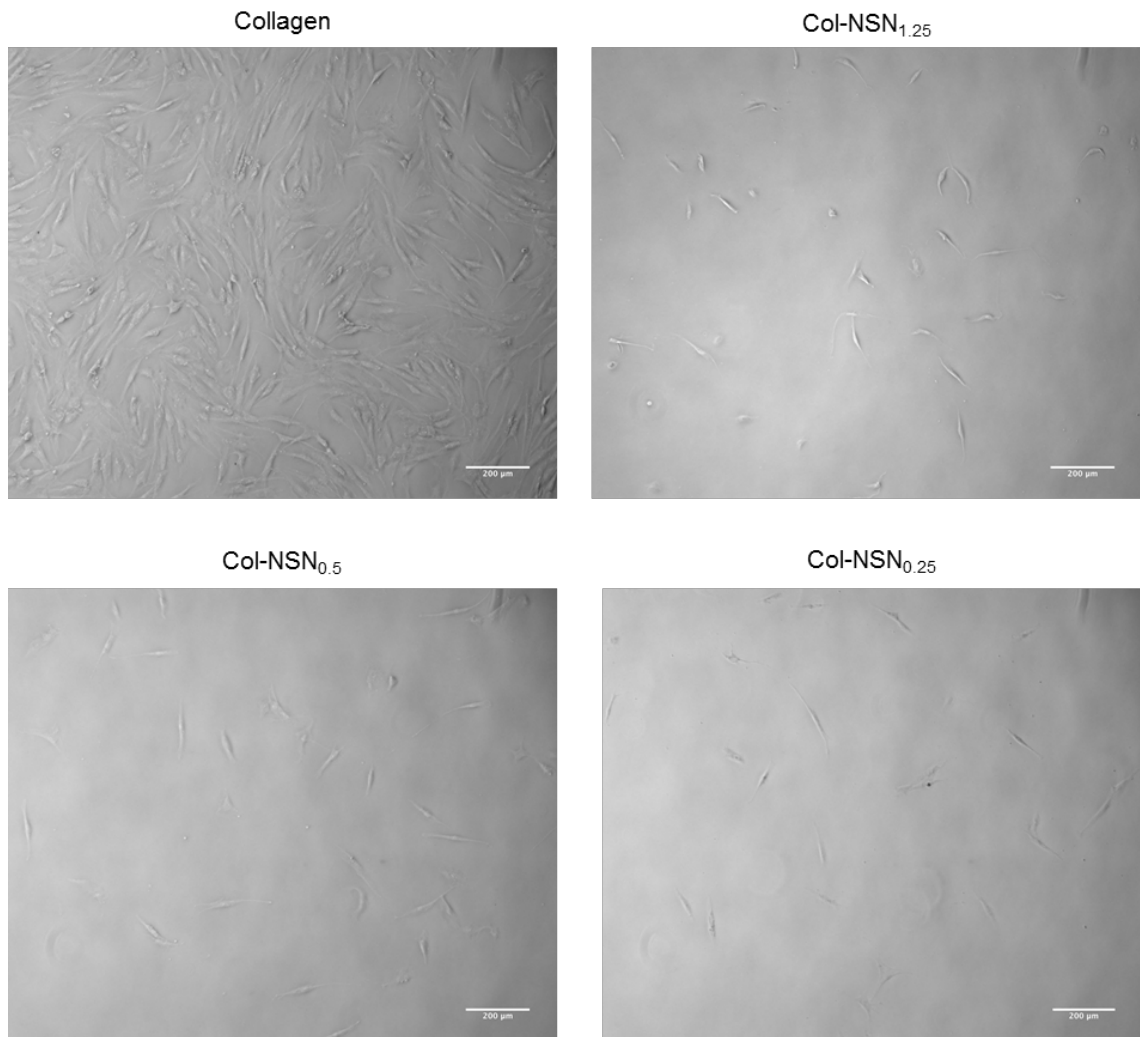


Figure 3-15: ADSCs cultured within the hybrid gels can be released and re-plated as 2D monolayers. Hybrid gels digested enzymatically with liberase and cooled on ice to release cells. Scale bars are 200 µm.

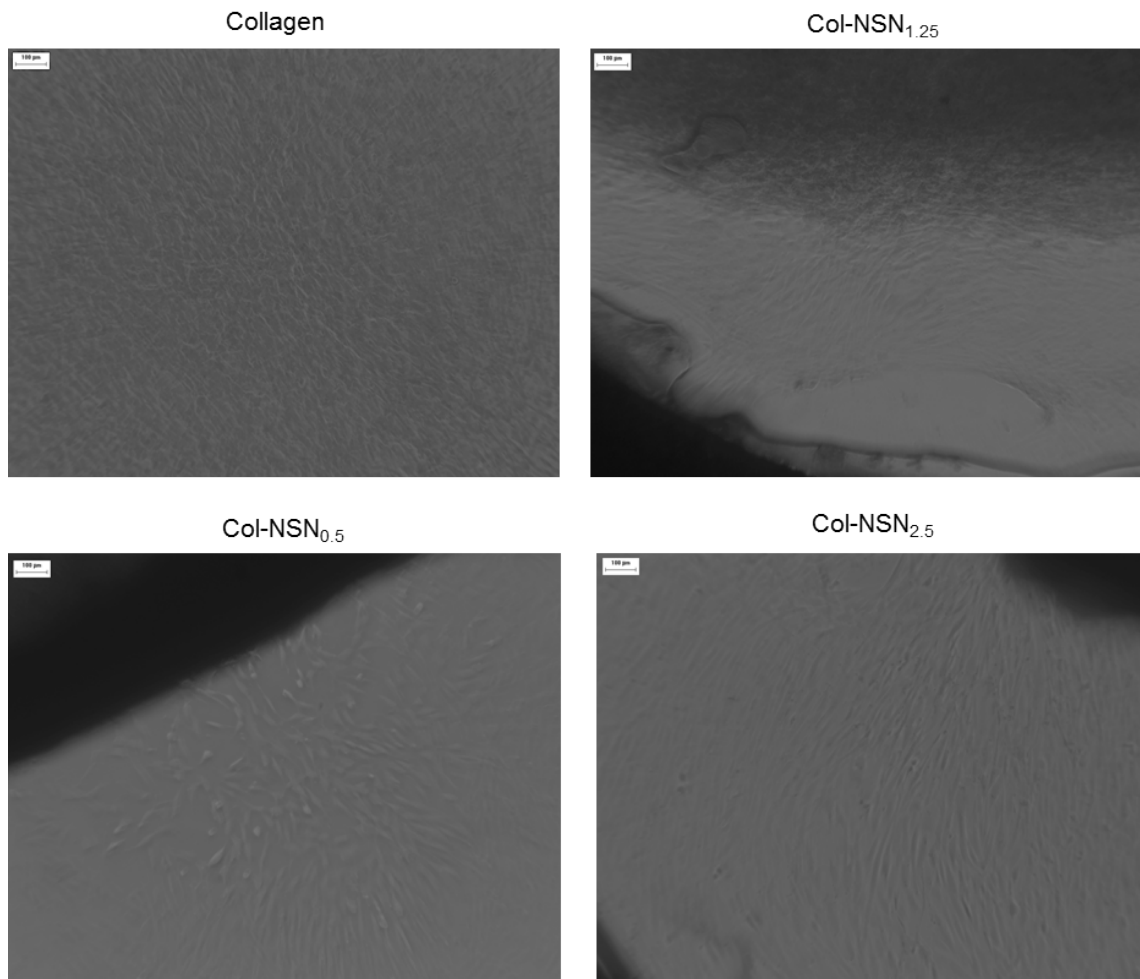


Figure 3-16: Hybrid gels do not release cytotoxic products into cell culture media. ADSC outgrowth from collagen and hybrid gels into TCP regions surrounding the gels . Scale bars are 100 µm.

only gels, as the hybrids could not be fully disaggregated. However cells could be removed from the hybrids and adhere and grow in 2D culture in the same manner. After overnight culture of the cells released from the hybrids in 2D, there were no obvious dead cells floating within the media, indicating the lower number of cells was due to problems in cell release rather than cell death caused by the hybrid scaffold. ADSCs can also be seen growing out of the hybrid gels onto the surrounding TCP from the hybrid gels, indicating the hydrogels are not releasing anything cytotoxic into the media (Figure 3-16). To visualise the ADSC network within the hybrid gels in more detail, the gels were fixed in PFA, subjected to sucrose gradient and cryo-sectioned. ADSCs within collagen gels had spread out and had fibroblastic morphologies, appearing to align with collagen fibrils to form a dense tissue (Figure 3-17). In col-NSN_{1.25}, the ADSC density appeared reduced compared with collagen and the cells were fine and spread with an array of morphologies from fibroblastic to stellate. While in col-NSN_{0.5} the cells populated the gel, almost as well as collagen and had similar fine and delicate morphologies, with several processes extended from the main cell body, similarly to the cytokine induced ADSCs in collagen.

To assess whether ADSCs were able to migrate within the gels, and the effect of the NSN content on cell migration, different blends of gels were cast on top of a transwell membrane. GFP expressing HT1080 cells were then seeded onto the surface of the gels. HT1080s are a human cell line, derived from fibrosarcoma, they were used as they are a robust and proliferative cell type and therefore their migratory capacity would be more profound compared with the ADSCs. The media within the bottom of the well contained 20% FBS as a chemo-attractant whilst the media within the transwell did not contain any serum. The gels were left for 7 days and then imaged throughout using two-photon imaging to examine how well the cells could migrate into each blend. Images of the cells in random z-planes of each the gel were then measured using velocity software to determine the average cell depth in each gel (Figure 3-18A). Images from the surface of each gel show that as the concentration of NSN within each gel increases, the cell distribution is less uniform across the gel surface. This difference could be due to cell proliferation. In the collagen gels and hybrids with low NSN concentration, the cells may be more proliferative due to the increased adhesion to the scaffold and 2D like

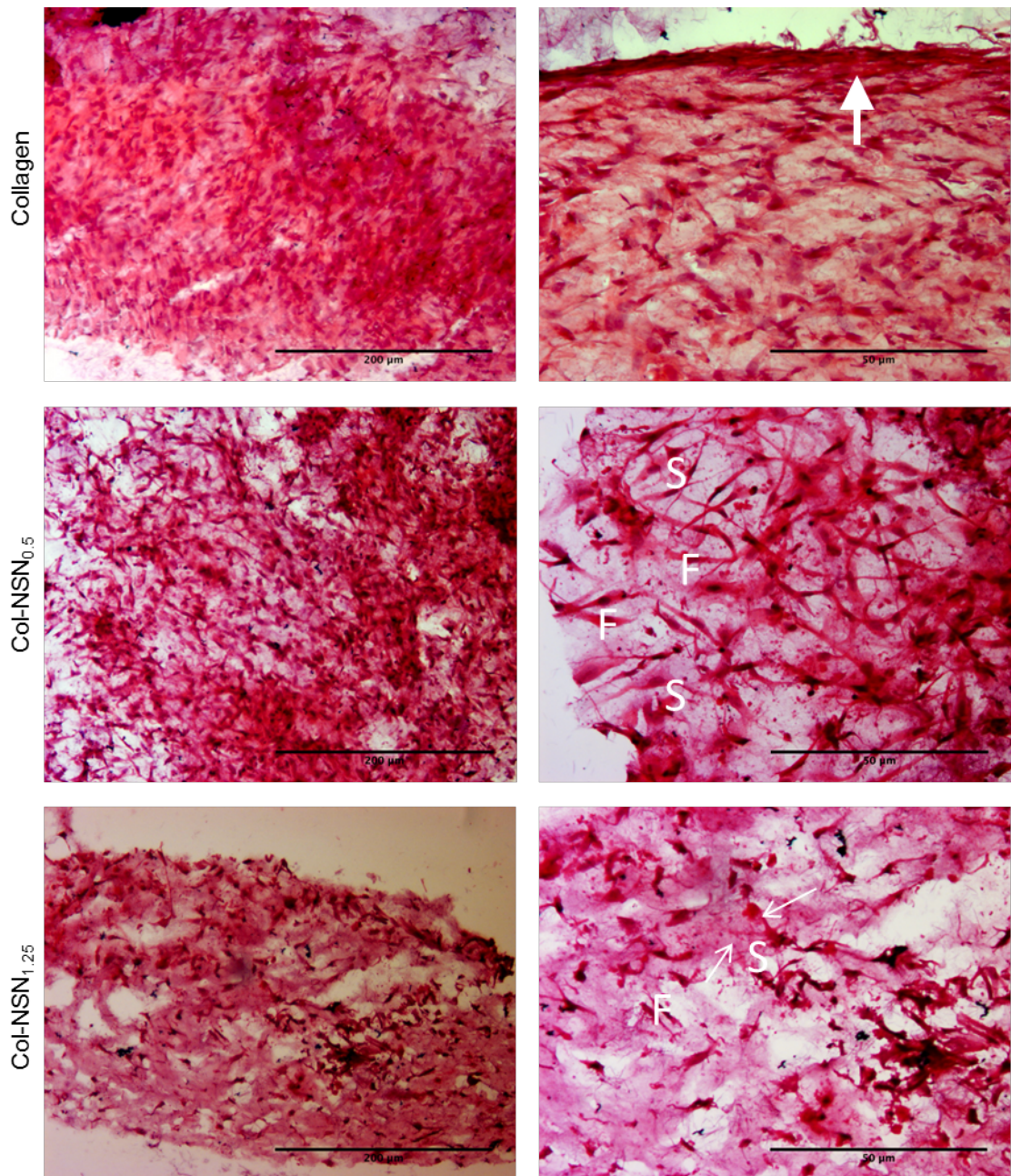


Figure 3-17 ADSC networks and cell morphologies in hybrid gels are affected by gel composition. Hematoxylin and eosin stained sections of ADSCs encapsulated within collagen, col-NSN_{1.25} and col-NSN_{0.5} hybrid gels. In collagen gels ADSCs form a dense layer at the surface of the gel (thick arrow). Within col-NSN_{0.5} the cells adopt a range of morphologies due to the accessible collagen fibrils for adhesion. Both stellate, with multiple processes (marked s) and fibrblastic (marker f). This is also observed in the col-NSN_{1.25} gels. Thin arrows indicate the presence of thin, elongated processes from the cells. Top row scale 200 μm , bottom row 50 μm .

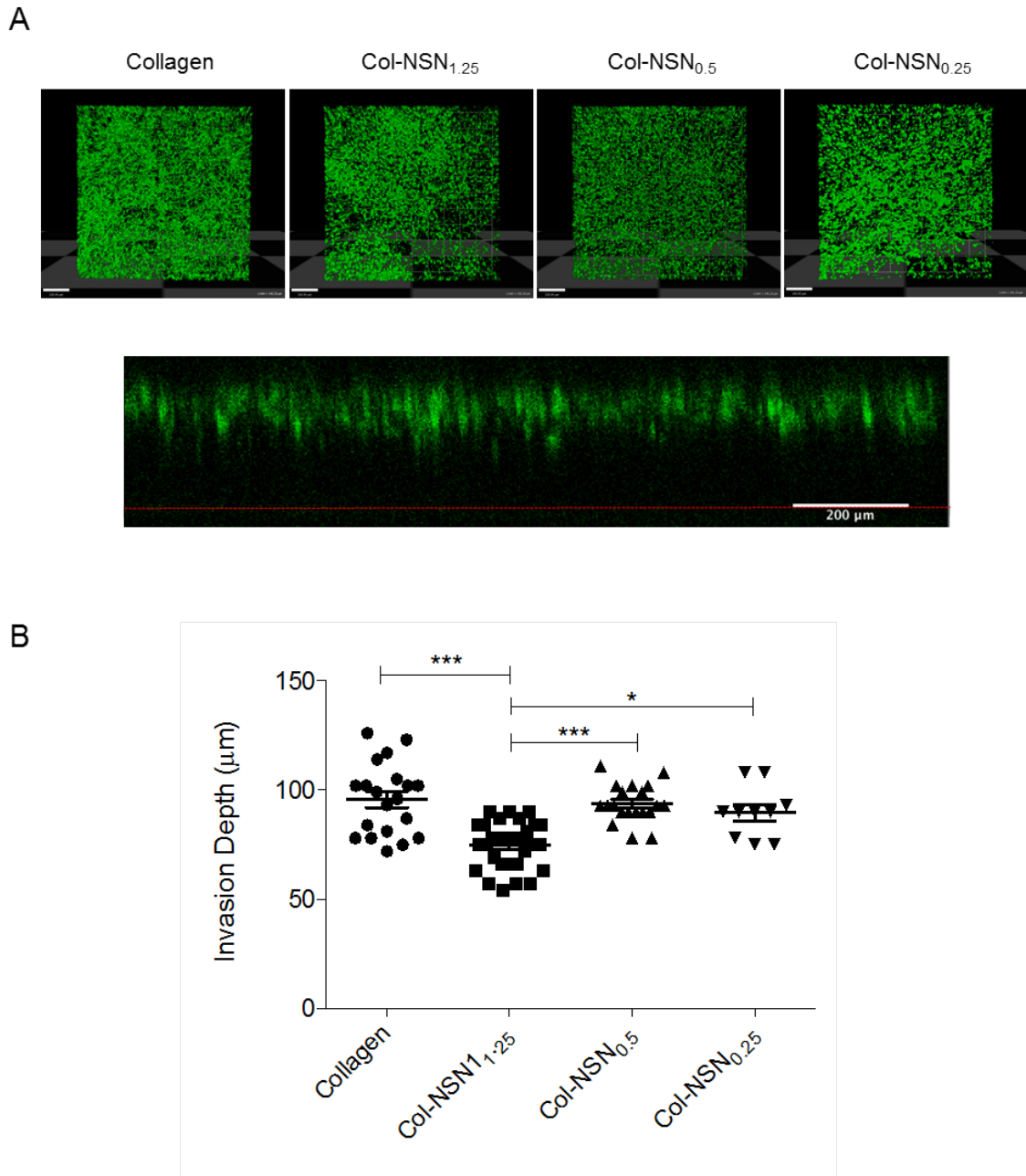


Figure 3-18 HT1080s invasion into collagen and hybrid gels is affected by hydrogel composition. HT1080s are able to migrate within all hybrid gels comparably to collagen, however the depth of invasion is reduced in col-NSN_{1.25} gels. Combined Z-plane images of GFP HT1080s on the surface and within collagen and hybrid gels. HT1080s were seeded within gels on top of transwell membranes, the bottom well contained 20% FBS as a chemoattractant (A) scale bars are 100 μm. Side view of HT1080s invading into gels, red line indicates the transwell membrane. Measured invasion depths of ADSCs in different gels (B). Results are mean ± SEM (n=3 gels, where at least 10 depth profiles were measured).

adhesions compared with the higher NSN gels. The depth profiles of the cells into each gels, was similar for the collagen gels, col-NSN_{0.5} and col-NSN_{0.25}, which again is probably a factor of increased cell attachment to collagen when there is less NSN present (Figure 3-18B). The migratory capacity of the cells in col-NSN_{1.25} was significantly lower than the collagen control. Together these results show ADSC networks can be formed in 3D in collagen and collagen – NSN blends, where the presence of NSN within the scaffold alters cellular morphology and migratory capacity as its concentration increases. This may be the result of a reduction of exposed cell adhesion ligands on the collagen fibrils, as they become coated with NSN globules, as well as the NSN globules forcing the collagen fibrils into a more open network and increasing the spacing between cell adhesive ligands.

3.4.5 Effect of 3D environment upon lymphoid mesenchyme phenotype

As 3D engineered tissues are more representative of natural tissues than 2D cell culture, the effect of the cytokine induction of ADSCs into lymphoid mesenchyme may vary between ADSCs maintained in 2D and 3D. As well as using the hybrid gels as a scaffold to develop 3D models of lymphoid mesenchyme, cell spheroids were also explored as an alternative 3D model of lymphoid mesenchyme. Using both models allowed for comparison of a dense scaffold free 3D environment with the open ADSC networks formed in the hybrid gels. 3D ADSC were formed from 60,000 ADSCs suspended in methyl cellulose in non-adherent U-bottomed plates. Over 24 hours the cells formed a single multi-cell aggregate at the bottom of the well (Figure 3-19B). Over 2-3 days the aggregates compacted and became more spheroidal, with tightly packed cells. At the time of spheroid formation the methyl cellulose BM was either supplemented with cytokines to induce differentiation of the cells into lymphoid mesenchyme or left untreated.

After 5 days of culture the spheroids were washed in PBS and disaggregated using a motorised pestle and RNA was extracted to examine the change in ICAM-1 and VCAM-1 expression upon lymphoid mesenchyme induction in 3D. ADSCs treated with

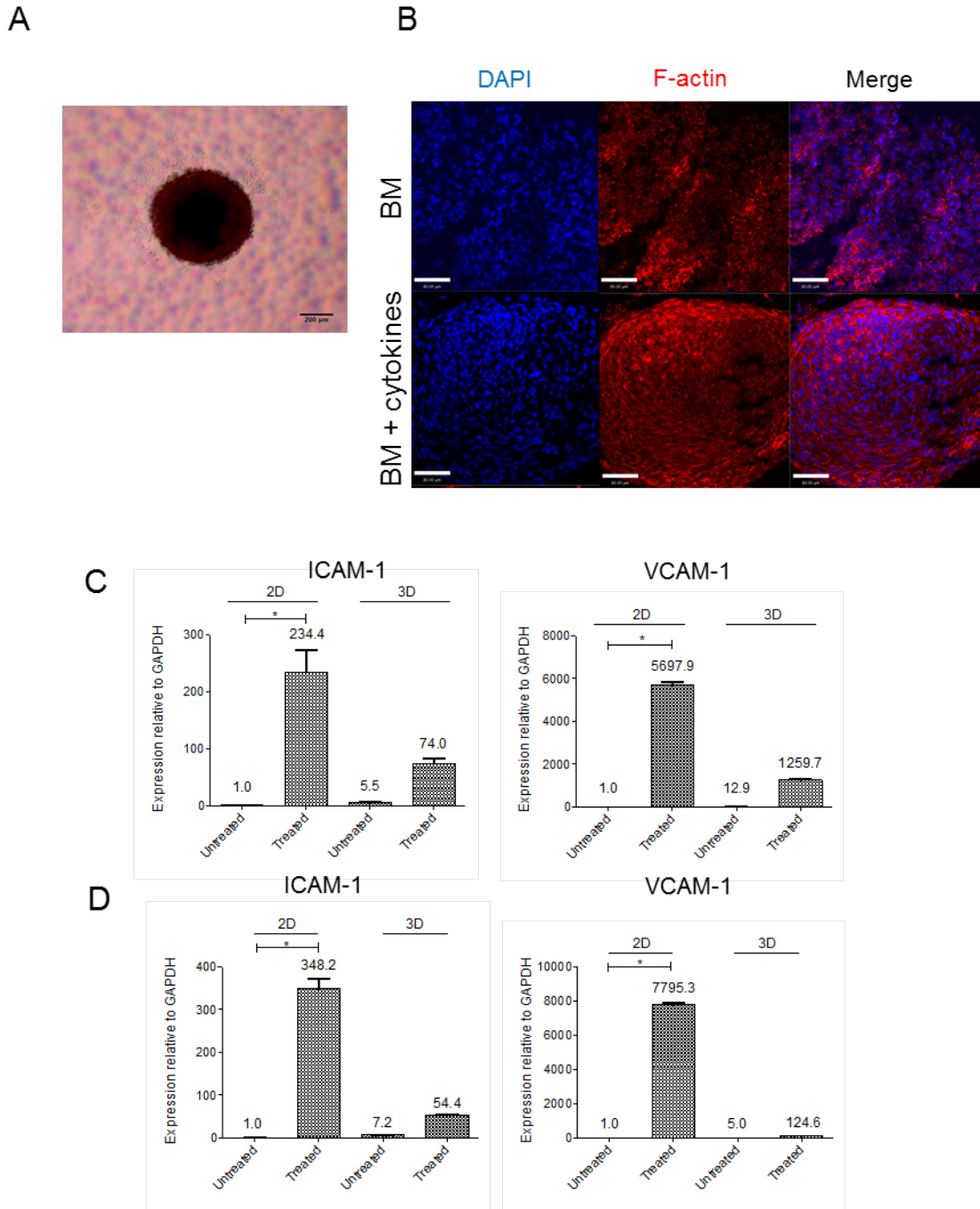


Figure 3-19 Analysis of spheroids as 3D models of lymphoid stroma. Example MSC spheroid formed in methyl cellulose media (Image courtesy of Julia Marshall) (A). ADSC morphology and distribution in 60,000 cell spheroids, scale bars are 80 μ m (B). qPCR analysis of ICAM-1 and VCAM-1 expression following cytokine induction in 2D monolayers compared with spheroids, results show mean \pm SEM, n=3. Where ADSCs were treated with cytokines at the time of spheroid formation (C) or primed in 2D for 5 days prior to spheroid formation (D).

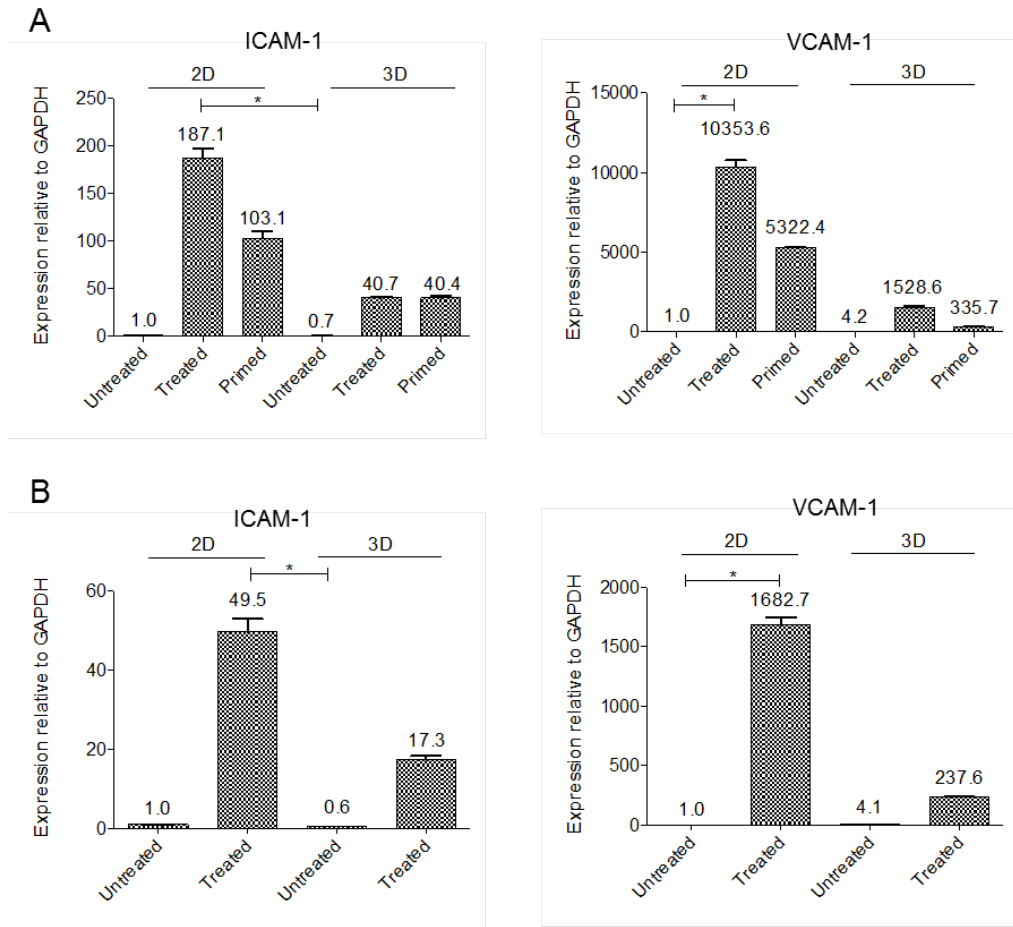


Figure 3-20 Lymphoid mesenchyme induction in 3D is lower than 2D
 Following cytokine induction, ICAM-1 and VCAM-1 expression is lower than 2D monolayer controls. The same result is observed when ADSCs are primed in 2D prior to spheroid formation. qPCR analysis of ICAM-1 and VCAM-1 expression in ADSC spheroids (A) and ADSCs encapsulated in col-NSN_{0.5} (B). Results show mean \pm SEM, n=3.

	2D							3D			
	ICAM-1+	VCAM-1+	ICAM-1 ⁺ VCAM-1+	ICAM-1 qPCR	VCAM-1 PCR	Adipo	Osteo	Spheroids		Gels	
								ICAM-1 qPCR	VCAM-1 qPCR	ICAM-1 qPCR	VCAM-1 qPCR
Untreated	++	neg	neg	-	-	+	+	+	+	+	+
IL-4	++	++	++	n/a	n/a	+	-	n/a	n/a	n/a	n/a
TNF- α anti-LT β R	+++	neg	++	n/a	n/a	n/a	n/a	n/a	n/a	n/a	n/a
IL-4, TNF- α , anti-LT β R	+	+	+++	+++	+++	-	-	+	+++	+	+++

Table 3-4: Summary of cytokine induced lymphoid mesenchyme experiments

For FACS results, + 1-10%, ++ 10-50%, +++ 50%+. Differentiation results indicate positive Oil Red O stain for adipogenic assays and ALP activity as determined by pNPP assay. For qPCR data + up to 100 fold increase in expression, ++ up to 100 fold increase in expression and +++ <100 fold increase in expression.

the lymphoid inducing cytokines in 2D monolayers and within 3D spheroids upregulated stromal markers ICAM-1 and VCAM-1 (Figure 3-19C). In both 2D and 3D culture, VCAM-1 was more strongly upregulated than ICAM-1, in agreement with the previous 2D FACS results (Figure 3-4).

Interestingly, the expression levels of ICAM-1 and VCAM-1 in the untreated 3D spheroids were higher than in 2D untreated cells, however the overall cytokine induced increase in ICAM-1 and VCAM-1 expression was much lower in 3D compared with 2D. As the cells were treated with cytokines at the same time as forming the cell spheroids, the induction efficiency may have been reduced.

Therefore ADSCs were also primed with the cytokines in 2D prior to generation of 3D spheroids to assess whether the tightly packed conformation of the cells in the spheroids was affecting the induction of the lymphoid mesenchyme phenotype as defined by ICAM-1 and VCAM-1 expression (Figure 3-19D). Even with five days of priming in 2D first, the upregulation of ICAM-1 and VCAM-1 expression in ADSCs in 3D spheroids was still lower than in 2D monolayers. To directly compare the effects of the of priming, ADSCs were cultured in 2D with or without cytokines, prior to spheroid formation for 5 days, treatment was then continued in 3D spheroids for 5 days. Surprisingly ADSCs that were primed in 2D expressed lower levels of ICAM-1 and VCAM-1 than ADSCs without 2D pre-treatment. Again VCAM-1 was more strongly upregulated than ICAM-1, and the overall increase in adhesion molecules was lower in 3D compared with 2D (Figure 3-20A).

Alongside the spheroid study, ADSCs from the same batch were encapsulated in Col-NSN_{0.5} gels and the cytokine induction study was performed in parallel. Col-NSN_{0.5} blends were chosen for this experiment, as ADSCs within this blend had good viability, and were able to spread and migrate within the gels similarly to collagen controls. Col-NSN_{0.5} gels had bulk mechanical properties similar to the LN and also prevented NSN and cell mediated contraction. After 5 days the gels were treated with liberase and cooling cycles to release as many cells as possible for RNA extraction. In order to

extract high levels of uncontaminated RNA, the cells were washed several times in PBS and the digestion times optimised.

In the col-NSN_{0.5} gels, cytokine treatment of the ADSCs was similar to the spheroid model, with induction in 2D resulting in a higher upregulation of ICAM-1 and VCAM-1 compared with the 3D cell networks in the hydrogel (Figure 3-20B). In summary the induction of the lymphoid mesenchyme, as quantified by ICAM-1 and VCAM-1 expression, was reduced in 3D compared with 2D, in both highly compact cell only models and open networks within col-NSN_{0.5} hybrid gels. Table 3-4 summaries the lymphoid mesenchyme induction experiments in the 2D and 3D systems.

3.5 Results: Cartilage engineering using high NSN content gels

3.5.1 Isolation and characterisation of BM-MSCs for cartilage therapies

To examine the potential of hybrid gels with high concentrations of NSN for cartilage engineering, they were used in combination with BM-MSCs. BM-MSCs were used rather than ADSCs as they are found in subchondral bone underlying damaged cartilage and therefore are one of the likely cell types which may migrate into the hybrid gel scaffold *in-vivo*. BM-MSCs were isolated from the bone marrow of tibia plateau of the knee. Bones were broken up into small pieces (1-2cm²) and cultured for a week, allowing BM-MSCs to evade. BM-MSCs were purified by plastic adherence, where contaminating red blood cells and lymphocytes were removed in washing and passaging. BM-MSCs were characterised by analysis of MSC markers by flow cytometry and their capacity to differentiate towards bone, fat and cartilage. BM-MSCs were isolated from 3 donors and representative cell surface marker profiles and differentiation assays are summarised in Figure 3-21A. BM-MSCs from all donors expressed cell surface markers CD73, CD90, CD105, CD29 and CD44. CD106 (VCAM-1) expression varied between donors, and was generally expressed at low levels. All donors had negligible expression of CD11b, CD14, CD31 and CD45 markers of macrophage, neutrophils, endothelial cells and leucocytes respectively, indicating any contaminating cells derived from the bone marrow had not been isolated or were lost in culture and passaging of the cells (Figure 3-21A).

Isolated BM-MSCs were able to differentiate towards fat under adipogenic conditions. ORO stained lipids appeared after 7 days of differentiation, and continued to increase to day 14, however the staining was not present across all cells, and the number and size of lipids varied between cells (Figure 3-21B). Elution of the stain could not be quantified due to low levels of staining. Osteogenic differentiation of the BM-MSCs was more successful. After 14 days of culture in OM the differentiated osteoblasts had produced a calcium rich ECM and had significantly higher levels of ALP activity compared with undifferentiated BM-MSCs (Figure 3-21C). ALP activity was accompanied by increased proliferation between days 14 to 21 (Figure 3-21D). Normalised with DNA content, ALP activity increased and peaked at day 14 before falling at between days 14 – 21, characteristic of early stage osteogenic differentiation.

For chondrogenesis BM-MSCs were centrifuged into high-density pellets to produce the cell condensation required differentiation. The pellets were cultured in basal chondrogenic media (BM) consisting of DMEM, supplemented with ITS⁺, dexamethasone and L-proline or chondrogenic media (CM), which additionally contained TGF- β 3. At each time point the pellets were flash frozen and cryo-sectioned to examine the ECM production by the differentiating BM-MSCs. Alcian blue and collagen II staining, showed the cells synthesised a dense chondrogenic matrix at the periphery of the pellets, which surrounded rounded BM-MSCs. Deposition of a GAG rich matrix, shown by Alcian Blue staining, occurred and steadily increased from 7 days of chondrogenesis (Figure 3-22), while low levels of collagen II matrix were present from day 7, but limited to the exterior of the cell pellet (Figure 3-23).

3.5.2 NSN-collagen hybrid gels for cartilage repair

To examine the potential of high NSN content hybrid gels for cartilage repair an *in-vitro* assay was performed by suspending 8×10^6 cells/ml of BM-MSCs within col-NSN₅. Col-NSN₅ was used for these experiments as it had the highest mechanical properties of any of the gels examined, and most likely to withstand the forces in the knee. The suspension was prepared on ice and pipetted into v-bottomed plates as a representative mould for a small cartilage defect.

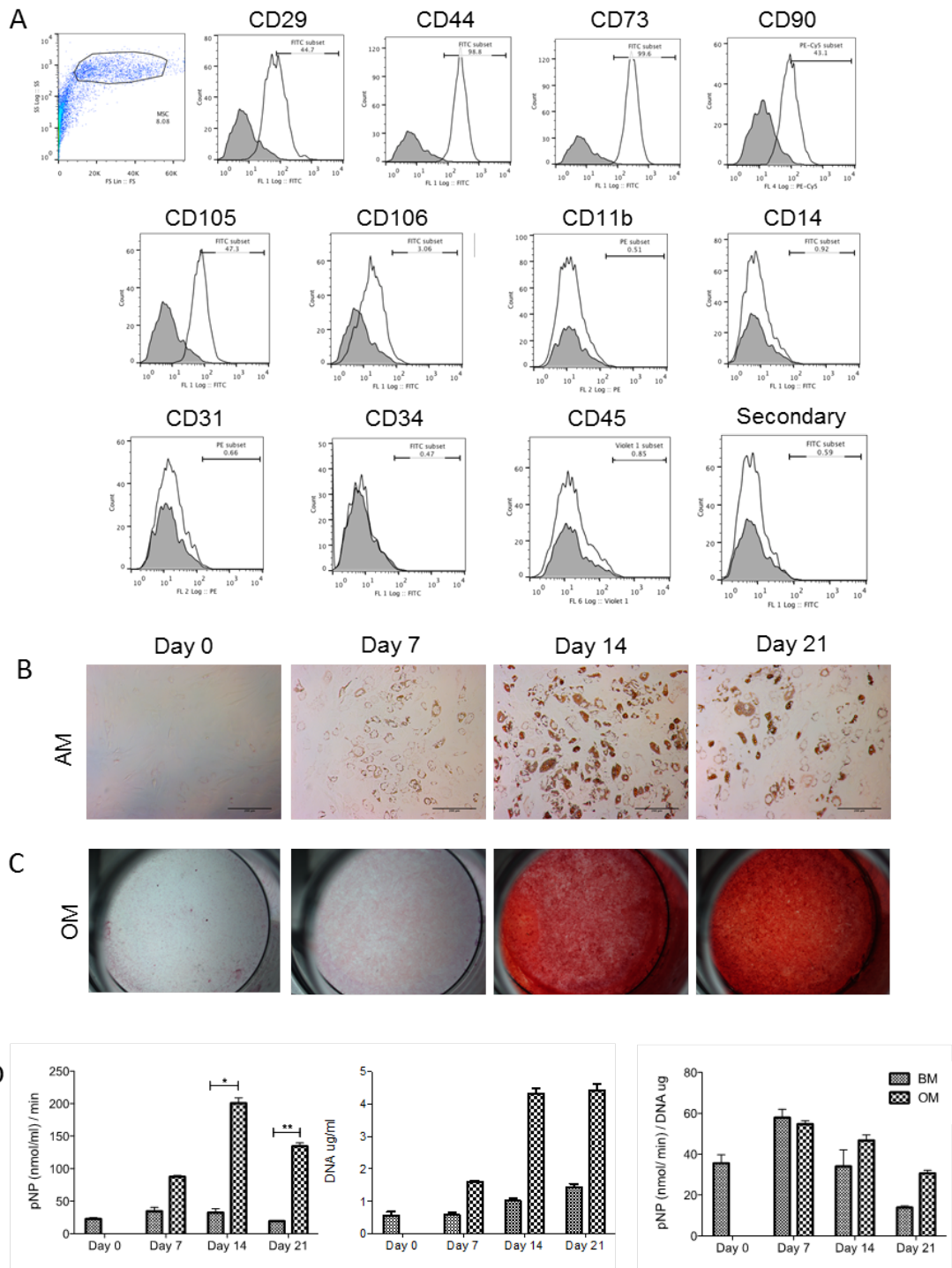


Figure 3-21 Characterisation of cell surface markers and differential capacity of BM-MSCs. FACS analysis of common MSC cell surface markers, where negative controls are unstained cells (A). Oil Red O staining of adipogenic differentiation of BM-MSCs over 21 days, scale bars are 200 μm (B). Alizarin red staining of osteogenic differentiation of BM-MSCs over 21 days (C). ALP activity in osteogenically differentiated BM-MSCs, pNP normalised to DNA content (D).

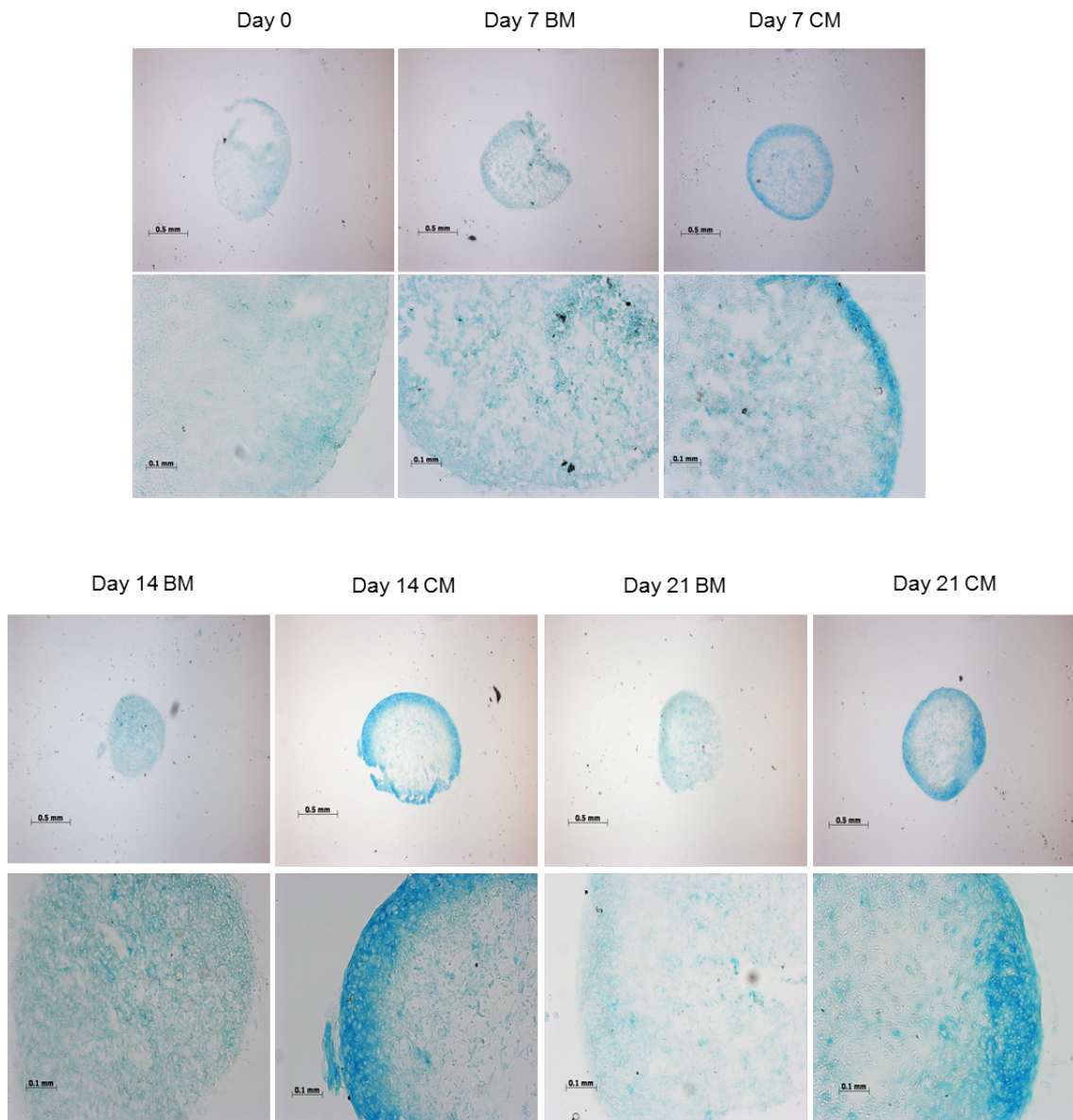


Figure 3-22 GAG expression in BM-MSCs cell pellets following chondrogenic differentiation . Cryo-sections of BM-MSCs pellets following 21 days culture in basal media (BM) or differentiation in chondrogenic media (CM). The GAG rich cartilage matrix is stained in the sections with Alcian Blue, top row scale 500 μm, bottom row 100 μm. At Day 0 low levels of GAG staining is observed. BM-MSCs in CM produce a dense GAG rich matrix at the periphery of the pellets, where cells are contained in the lacunae like voids within the matrix.

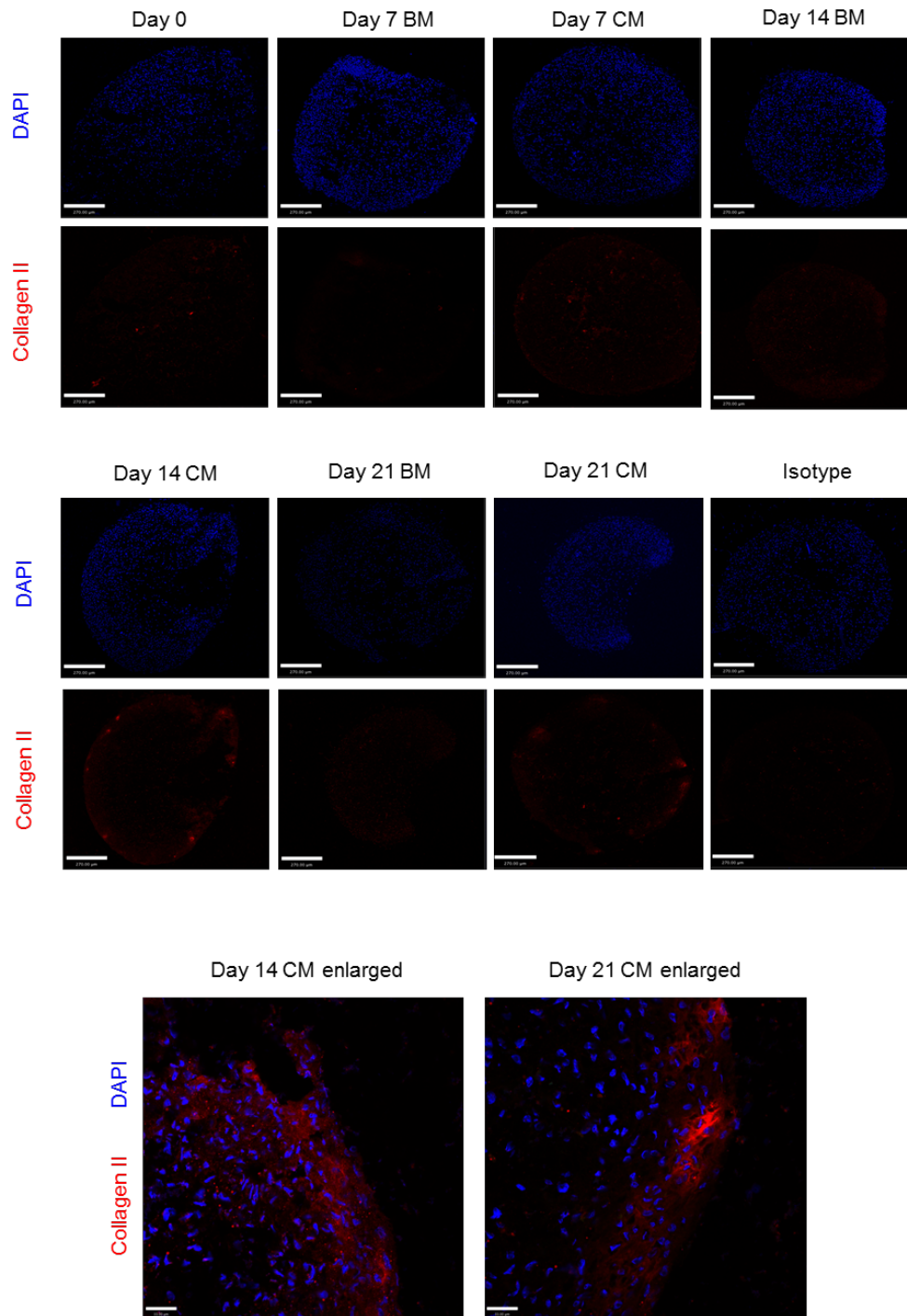


Figure 3-23: Collagen II expression in BM-MSCs cell pellets following chondrogenic differentiation.

Cryo-sections of BM-MSCs pellets following 21 days culture in basal media (BM) or differentiation in chondrogenic media (CM). Immunofluorescent staining of collagen II matrix in BM-MSC sections. Collagen II expression is absent in pellets cultured in BM and early time points of CM. Similarly to GAG expression, at the later time points, day 14 and 21 a collagen II rich matrix is found at the periphery of pellets differentiated in CM. Scale bars are 270 μm and 33 μm in enlarged sections.

As the gels are significantly denser than col-NSN_{1.25} – col-NSN_{0.25}, and the hydrogel will contain the cells for a prolonged period of time during *in-vitro* chondrogenesis assays or cartilage repair *in-vivo*, the viability of BM-MSCs was examined over 3 weeks, rather than 5 days. Live-dead staining could not be used, as the gels were very opaque, and cell membranes may be damaged during sectioning, and may create false negative results (Figure 3-24A). Therefore the gels were incubated with MTT to identify metabolically active cells within the gels. MTT is reduced to formazan by NAD(P)H-dependent cellular oxidoreductase enzymes produced by metabolically active cells. Elution of formazan did not produce reliable results therefore gels were immediately sectioned and imaged, to examine the distribution of formazan and therefore metabolically active cells throughout the gels (Figure 3-24B). One day after gelation, metabolically active cells were found throughout the gel, with the highest staining seen on the outermost section, where cells were at the gel-media interface. A similar distribution of MTT staining was apparent at day 7, however this decreased with time in culture. By day 14 high densities of viable cells were present at the gel surface, while within the gel staining was clustered in specific areas. This was also observed by day 21. MTT staining was not visible in blank gels without cells.

When cultured in chondrogenic conditions with col-NSN5 for 3 weeks, the BM-MSCs began to synthesise a GAG matrix throughout the gel (Figure 3-25). The alcian blue staining was not as strong as within the BM-MSC pellets, but intensified in CM at day 14 and day 21. By day 21, a rich GAG matrix was present as the periphery of the gel, similar to the pellet culture. Collagen II staining was not observed during the 3 week period (Figure 3-26). Immuno-fluorescent staining of the high synthetic sections proved very difficult due to their opacity and fragility during staining.

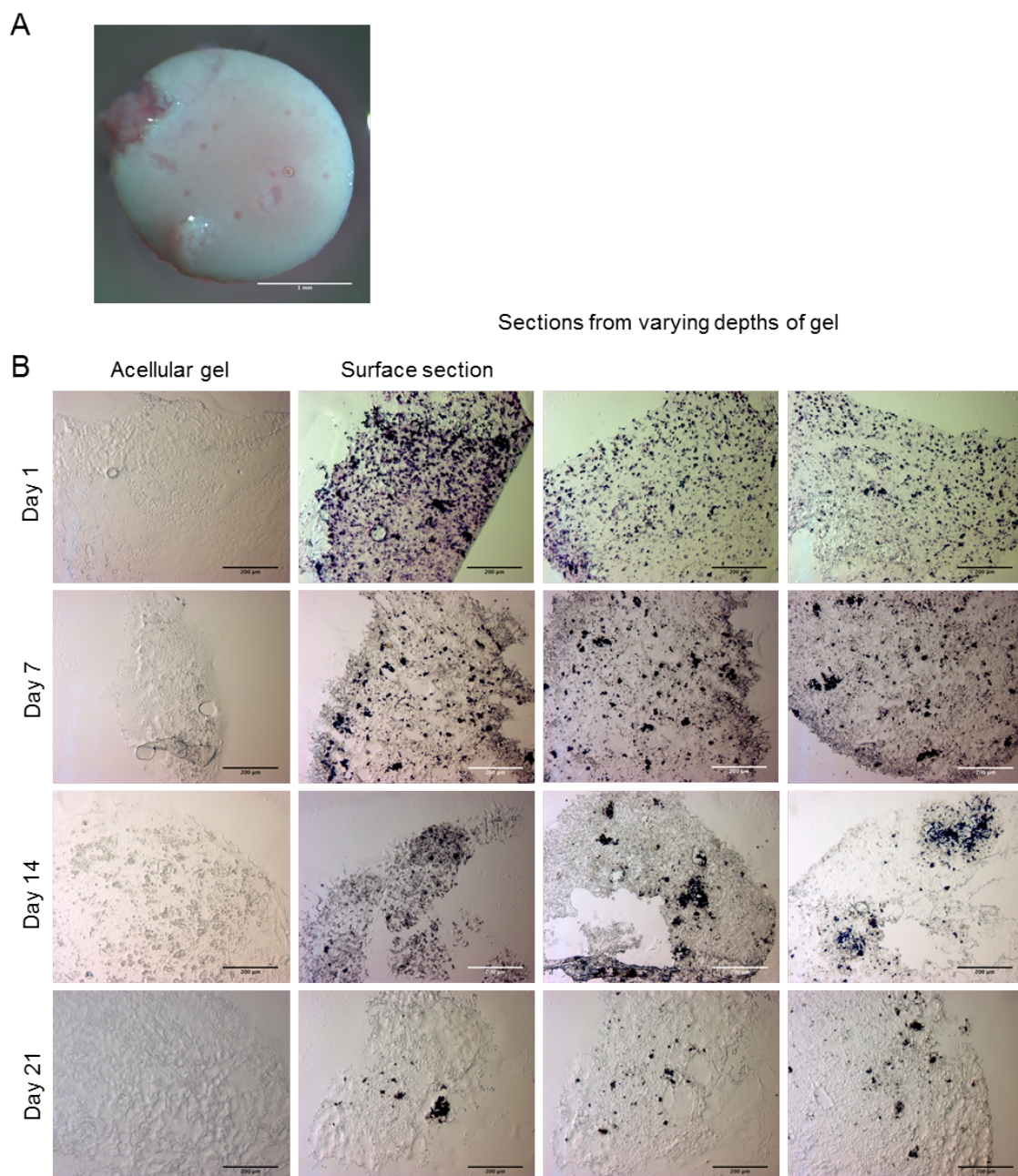


Figure 3-24 Viability of BM-MSCs with col-NSN₅ hydrogels. Representative image of a whole col-NSN₅ hydrogel (A). Col-NSN₅ gels containing BM-MSCs were incubated with MTT for 4 hours and then sectioned to examine formazan distribution, indicating metabolically active cells (B). The assay was performed on gels cultured in BM at regular time points up to 21 days. Acellular gels were included as controls for endogenous formazan reduction. Scale bars are 200 μ m.

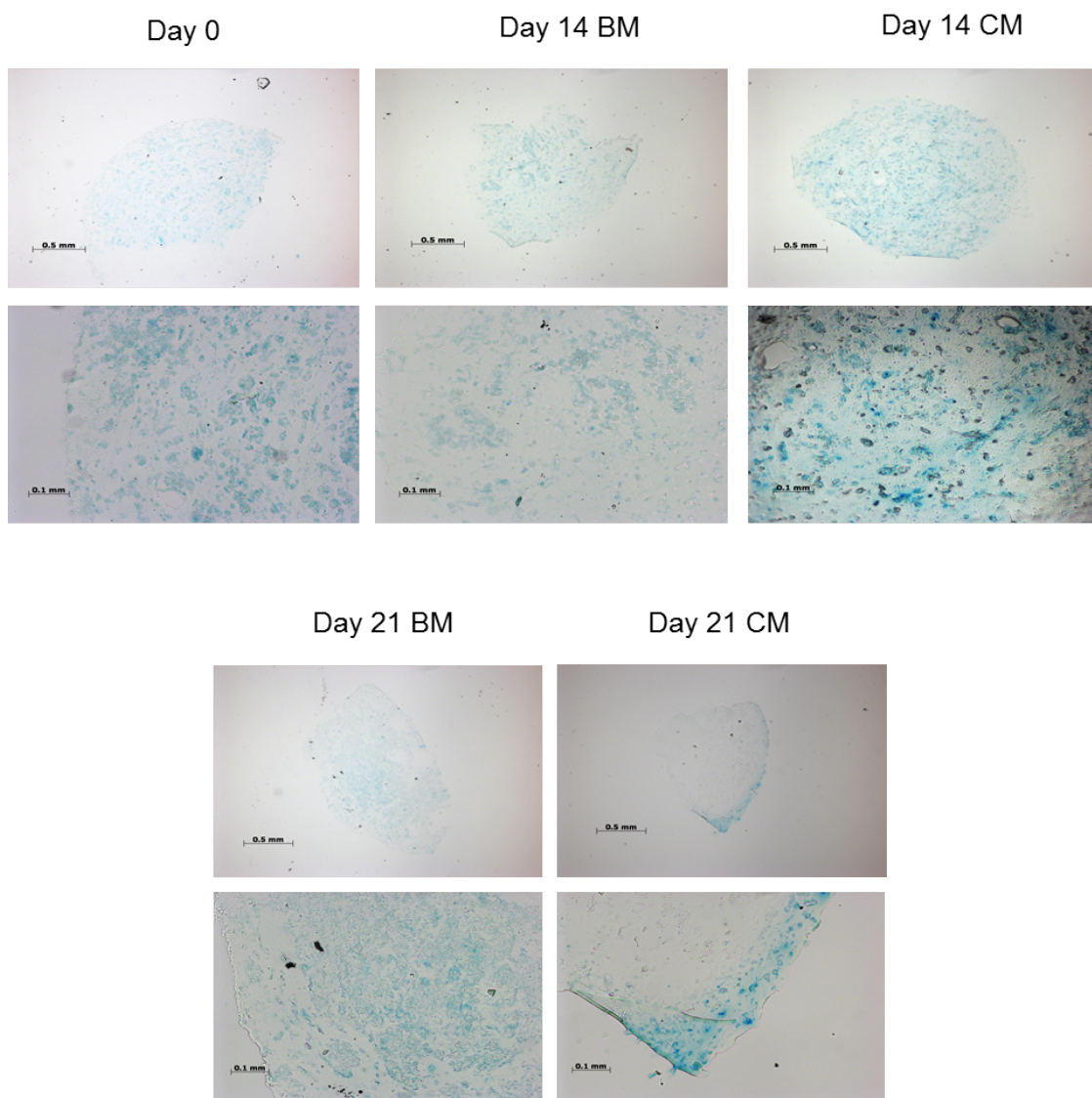


Figure 3-25 GAG expression in BM-MSCs containing col-NSN₅ hydrogels following chondrogenic differentiation .

Cryo-sections of col-NSN₅ hydrogels containing BM-MSCs 21 days culture in basal media (BM) or differentiation in chondrogenic media (CM). The GAG rich cartilage matrix is stained in the sections with Alcian Blue, top row scale 500 μm, bottom row 100 μm. Prior to differentiation (day 0) the hydrogels contain low levels of GAG matrix. A deeper blue GAG stain is observed in the hydrogels maintained in CM.

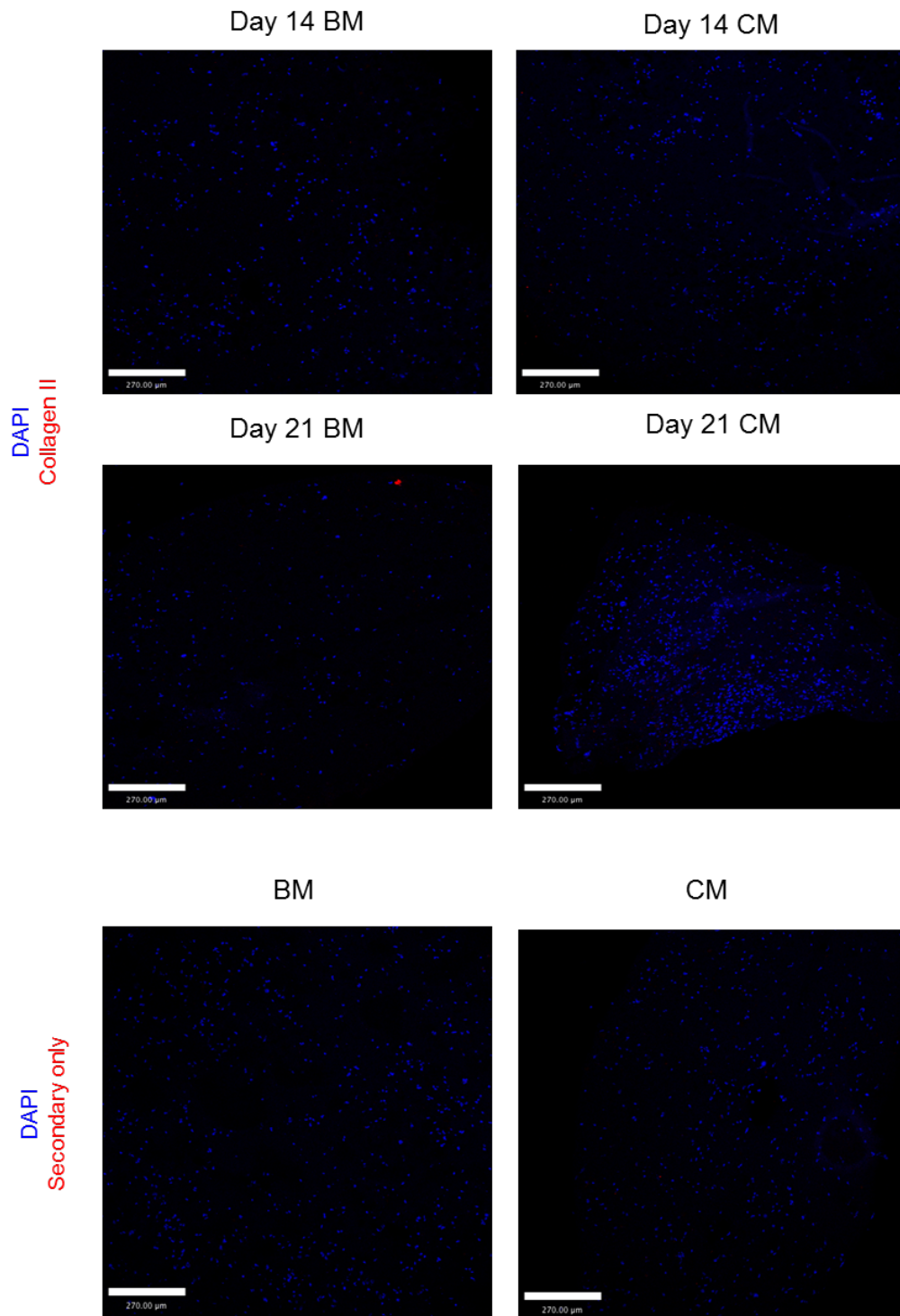


Figure 3-26: Collagen II expression in BM-MSCs containing col-NSN₅ hydrogels following chondrogenic differentiation.

Cryo-sections of col-NSN₅ hydrogels containing BM-MSCs 21 days culture in basal media (BM) or differentiation in chondrogenic media (CM). Collagen II matrix is stained in the sections with Alcian Blue, top row scale 500 μm, bottom row 100 μm. Prior to differentiation (day 0) the hydrogels contain low levels of GAG matrix. A deeper blue GAG stain is observed in the hydrogels maintained in CM.

3.6 Discussion

When modelling/engineering tissues and organs it is important to consider the cell type being used. Primary cells can lose their phenotype during *in-vitro* expansion, while transformed cells may have altered gene expression, resulting in changes in cell proliferation and they could be potentially malignant. MSCs are however an attractive cell type, due to their multipotency, and their role *in-vivo* in tissue repair and homeostasis. MSCs are viable in varying blends of the collagen and NSN hydrogels, which have NSN concentrations from 0.5 – 5 wt %. This chapter examines the potential of collagen -NSN for two very different MSC tissue engineering applications.

3.6.1 Adipose derived stem cells for modelling lymphoid mesenchyme

ADSCs are an appropriate choice for modelling the stromal networks of the LN, as the stroma has previously been shown to be mesenchymal in origin and the anlagen of the LN develops close to adipose tissue^{299,337}. Furthermore a population of adipocyte progenitor cells has been recently found in the developing inguinal LNs of mice, which closely associate with surrounding adipose tissue³³⁷. As ADSCs are easily isolated from routine lipoaspirates, they also offer a plentiful supply of cells for modelling a human LN. The ADSCs were treated with TNF- α and an antibody against LT β R, to mimic the action of LT binding, as these factors are involved in the development and maturation of the stromal networks within lymphoid tissues^{305–312}. In screens of other factors, which may influence induction of the stromal phenotype of ADSCs, IL-4 in combination with TNF- α and anti-LT β R was found to further the expression of lymphoid markers in ADSCs (unpublished results). Therefore the combination of the three factors was used to induce ADSCs into lymphoid stroma in 2D. Similarly it has been shown in *in-vitro* assays of FRC network formation, treatment with both TNF- α and anti-LT β R were more effective than either alone, in stimulating cells to produce a ER-TR7 rich FRC network³¹⁰.

3.6.2 Induction of a reversible lymphoid mesenchyme phenotype in 2D ADSCs

Prior to extending the model into 3D, the degree of cytokine induction on ADSCs into a stromal mesenchymal phenotype was examined. This focused on how committed the ADSCs were following the cytokine treatment and whether the induction was reversible through examining the adipogenic and osteogenic potential of the treated ADSCs. In the presence of the lymphoid mesenchyme inducing cytokines, the adipogenic and osteogenic differentiation capacity of ADSCs was reduced. Adipogenesis of the ADSCs could be inhibited by the combination of TNF- α and anti-LT β R as well as all three factors. It has been previously shown that TNF- α inhibits adipogenic differentiation³³⁸, therefore this result is not surprising. In studies by Benezech et al. the adipocyte precursors found in the developing LNs, which are thought to differentiate into the lymphoid stroma, also had blocked adipogenesis when treated with TNF- α , LT β R or the combination of both³³⁷. In their study only adipogenesis was examined. In osteogenesis assays, cytokine treatment with IL-4 only, TNF- α and anti-LT β R or the combination of all three factors were all able to reduce ALP activity to basal levels, however cell proliferation and deposition of a calcium matrix still occurred.

Osteogenic differentiation of MSCs precedes initially through cell proliferation and collagen I expression, followed by differentiation to committed osteo-progenitors, marked by down regulation of collagen I, and an increase in ALP activity. Lastly ALP expression is downregulated and osteonectin (ON), osteocalcin (OC) and osteopontin (OP) are upregulated as the MSCs differentiate into mature osteoblasts accompanied with matrix maturation^{339,340}. The reduction in ALP activity of the ADSCs in OM, suggests the cytokine treatment either commits the ADSCs to a phenotype unable to undergo the later stages of osteogenic differentiation or the presence of the cytokines inhibits the signalling pathways involved in the switch from proliferation to terminal differentiation. Although alizarin red staining shows the formation of a calcium matrix, this may not be indicative of a mature osteogenic ECM and terminal differentiation, furthermore von Kossa staining of mineralised nodules is low in the cytokine treated cells. As there is a reduction in ALP activity the ADSCs are unlikely to be differentiating towards committed osteo-progenitors, and matrix maturation would not

be expected. To make further conclusions on the extent of osteogenic differentiation following cytokine induction of ADSCs, analysis of late stage osteogenesis markers ON, OC and OP should be investigated. TNF- α has also been previously implicated as a negative regulator of osteogenesis. Low physiological concentrations (0.01 ng/ml) may be required for osteogenesis to occur, but at concentrations greater than 0.1 ng/ml, TNF- α has been associated with reduction in ALP activity, osteocalcin expression and mineralisation³⁴¹⁻³⁴³, which agrees with the results presented in this chapter. The effect of TNF- α on osteogenesis has been shown to occur through the NF- κ B signalling pathway, and therefore LT signalling may also inhibit osteogenesis by a similar mechanism. The effect of IL-4 on osteogenesis has also been studied to a lesser extent, where it has been reported that IL-4 can induce osteoporosis in mice and inhibit ALP activity *in-vitro* in osteoblasts^{344,345}.

To examine whether the differentiation was inhibited by the presence of the cytokines, or due to the differentiation of the ADSCs into a more committed lymphoid mesenchyme cell type, ADSCs were primed with cytokine treatment and then differentiated. When the cytokine treatment was removed, and differentiation medium was added to the cells, ADSCs in all groups were able to differentiate towards both osteogenic and adipogenic lineages over 14 days. Only in the continued presence of cytokines, was differentiation inhibited. With the addition of 5 days of 'priming' prior to differentiation, the results mimicked the differentiation seen without cell priming. Again the combination of the three factors blocked adipogenesis and osteogenesis, while the presence of IL-4 alone was not sufficient. Taken together these results suggest the cytokine induced lymphoid mesenchyme phenotype is reversible, or the cytokine treatment is only sufficient to promote ADSCs differentiation into an early stromal phenotype.

In addition to examining the differentiation potential of ADSCs with cytokine treatment, flow cytometry analysis of ICAM-1 and VCAM-1 was performed on adipogenically differentiated ADSCs with 5 days of cytokine priming prior to differentiation. ICAM-1 expression on control ADSCs in basal media was much lower compared with previous cytokine treatment protocols, which may be the result of the

prolonged culture period of 3 weeks in these experiments. This finding could be confirmed by measuring ICAM-1 expression of ADSCs in BM following three weeks of continued cytokine treatment. The differing SS in the ADSC population following adipogenesis with cytokine treatment, may be due to lipid formation within the cells during adipogenesis, resulting in increased granularity in the cells. In a recent study comparing methods of adipocyte characterisation, two SS scatter populations were also observed in MSCs undergoing adipogenesis. The SS high population stained strongly for Nile red and had higher expression of the adipogenic marker FABP4 compared with the SS low population³⁴⁶. The absence of the SS^{high} population in ADSCs in BM media is also indicative that the more granular cells are lipid filled adipocytes. Similarly, ADSCs without continued cytokine treatment that underwent adipogenesis, as confirmed by ORO staining, also contained two SS populations, where the proportion of cells within each population was similar to the control ADSCs in AM. From ORO stains it appears most of the cell population are adipogenic, therefore the SS^{high} population may only represent a proportion of the adipogenically differentiated ADSCs, which contain very large lipids. Furthermore the presence of large lipids within the differentiated ADSCs could cause the cells to become buoyant and lost in the staining procedures.

There was a small reduction in the SS^{high} population of ADSCs previously treated with all three factors, which was accompanied by a small increase in ICAM-1 expression, and ICAM-1/VCAM-1 double positive cells suggesting the cytokine treatment may have some lasting effects on the ADSCs differential capacity. VCAM-1 expression is also higher in the ADSCs without continued cytokine treatment, which may also be a lasting effect of the cytokine treatment. Where cytokine treatment was continued, the SS^{high} population was similar to the ADSC control with only IL-4 treatment, and decreased to less than 10% in the presence of TNF- α and anti-LT β R or all three factors, accompanying the absence of lipid filled cells. Taking into account the low basal expression of ICAM-1 following three weeks of cell culture, the ICAM-1 and VCAM-1 expression under the different cytokine treatments mirrored the expression seen in ADSCs following five days of cytokine treatment, with the highest number of double positive cells in the ADSCs treated with all three factors.

Together these results suggest the lymphoid mesenchyme phenotype achieved through cytokine treatment is reversible. This finding is important as it demonstrates the *in-vitro* 2D model of lymphoid stroma developed here, is consistent with the *in-vivo* properties of lymphoid tissue stromal networks. As well as being essential for the organogenesis of lymphoid tissue, LT and TNF- α signalling are also necessary to maintain the compartmentalised structure of secondary lymphoid tissues^{307,309,347}. This includes the networks of marginal reticular cells, which may be directly derived from early mesenchymal cells found in the developing LN, which require constitutive LT β R signalling for their maintenance³⁴⁸. Furthermore the formation of ectopic lymphoid tissue in autoimmune diseases also requires continued expression of LT for formation and maintenance³⁴⁹. Expression of LT signalling in non-lymphoid tissue can induce the formation of tissue structures³⁵⁰, which resemble the structure and function of secondary lymphoid organs, including lymphoid stromal networks, B and T-cell regions, germinal centres and lymphatic and vascular networks³⁵¹. Inhibition of LT signalling using LT β R fusion proteins can be used to prevent ectopic lymphoid tissue formation, as previously demonstrated in transplants of allogenic cardiac grafts in mice³⁵². Furthermore stromal cells isolated from tonsils also have plasticity, although they can be induced to express ICAM-1 and VCAM-1 following LT and TNF- α treatment, they also express classical MSC markers CD73, CD90 and CD105 and display tri-lineage differentiation capacity³⁵³.

Unlike other routes of MSC differentiation, lymphoid mesenchyme is a transient phenotype, which appears to require constitutive expression of LT β R and TNF- α to be maintained. To further this, it would be important to study the tri-lineage differential capacity of different stromal sub-sets isolated from adult lymphoid tissues. As well as TNF- α and anti-LT β R treatment for induction, ADSCs may also require additional soluble and physical cues to retain the phenotype. *In-vivo* lymphoid stromal cells have been shown to mature through two stages from ICAM-1^{int}, VCAM-1^{int} cells to ICAM-1^{high}, VCAM-1^{high}, which requires the interaction of the stromal cells with LT_i cells as well as signalling through LT β R³⁰⁴. Therefore although the cytokine treatment can induce an early stromal phenotype, without co-culture and signalling from LT_i cells full differentiation may not occur.

3.6.3 3D stromal networks can be formed within hybrid gels

To progress the LN model into 3D, ADSCs were either encapsulated within collagen or hybrid gels or formed into dense cell spheroids. The different models enabled comparison of a cell only model with cells contained in ECM based scaffolds. Altering the microenvironment of the ADSCs to 3D alters the cell morphology, adhesions with neighbouring cells and the ECM, the mechanical forces cells are exposed to as exerted by adjacent cells and the ECM and changes the distribution of oxygen, nutrients and cytokines the cells are exposed to. These biomechanical factors can all influence cellular behaviour as discussed within the introduction. 3D engineered tissues could be created using spheroids, collagen and hybrid gels. Whether treated or untreated with cytokines ADSCs formed 3D networks within collagen gels, however the morphology of the cells differed. Without treatment the ADSCs resembled their 2D morphology, spread and fibroblastic, while the treated cells were finer and thinner with long extended processes, similar in morphology to FDCs³⁵⁴ and *in-vitro* 3D cultured FRCs³¹¹.

As collagen gels can be prone to contraction, and are weaker than their col-NSN counterparts, col-NSN_{0.5} was chosen for maintaining ADSCs in 3D. Similarly to collagen only gels, ADSCs were also able spread out and adhere within the NSN containing gels, forming networks of cells throughout the scaffold. Although immunofluorescent imaging could not be used to assess the cell distribution in the hybrid gels, spread ADSCs could be viewed within the gels by bright field microscopy and in H+E stained sections. Within the hybrid gels the morphology of the cells varied with NSN concentration. Within col-NSN_{1.25} the ADSCs were spread, but had irregular morphologies, some smaller and more spherical, while others showed more spreading. The shape of some of the ADSCs suggests apoptosis was occurring. However ADSCs in the col-NSN_{0.5} gels were finer and elongated, with multiple processes and resembled the morphology of the cytokine treated cells in collagen only gels. Live-dead stains, also showed ADSCs in gels with the highest NSN concentration (col-NSN_{1.25}) had altered morphology compared with cells in collagen. These apparent differences in cellular morphology between the blends is potentially due to the increased porosity within the gels with increased NSN concentration, and the aggregation of NSN onto the collagen

fibrils within the gel. From these observations of cellular morphology, SEM analysis of gel composition, and previous reports on RGD ligand density and spacing^{151,334,355,356}, the following is proposed with respect to cell attachment and shape within the different hydrogel blends. When the concentration of NSN is low there are a small number of collapsed polymer globules interacting with the collagen fibrils and therefore a sufficient number of collagen fibrils exposed to facilitate cell attachment. Therefore cells exhibit a fibroblastic morphology, becoming more elongated with increasing NSN concentration, as spacing between adhesive ligands increases, while at the highest concentrations, the adhesive regions are limited and separated by distances too large for cells to make multiple attachments, causing cells to adopt a rounded morphology with few scaffold adhesions, and potentially undergo apoptosis. Beyond this optimal NSN concentration for cell attachment, the hybrid gels are therefore more suitable for applications where cells favour a rounded morphology and limited adhesions, therefore col-NSN₅, which was assumed to have few exposed collagen fibrils was used in the chondrogenesis assays described later.

The effect of NSN concentration on cell adhesion is also observed in the cell invasion assays in the hybrid gels. For migration cells require a substratum to adhere to in order to produce the force required for movement³⁵⁷, in gels with a higher concentration of NSN, the reduced number of adhesion ligands compared with collagen only gels, may contribute to reduced cellular migration. The porosity of the gels increased with NSN concentration. To permit migration the scaffold pores need to be large enough to allow cells to squeeze through, but not so big that there are minimal contacts between cells and the ECM, preventing adhesion and migration³⁵⁸. With increased NSN concentration, there is likely to be a reduction in protease degradable sites that are accessible on the collagen fibrils, which could contribute towards a reduction in cell migration, as the matrix cannot be as easily remodelled by cell proteases, compared with collagen only gels. The stiffness of the hybrid gel may also influence migration, as the ability of cells to squeeze through pores in the gel may be reduced in stiffer materials³⁵⁷.

3.6.4 Lymphoid mesenchyme induction in 3D

Surprisingly in the 3D models of lymphoid stroma, the extent of cytokine induction as measured by increases in ICAM-1 and VCAM-1 expression, was lower. As the 3D models are more representative of the *in-vivo* cellular microenvironment, it could be expected that the 3D models would further increase the stromal mesenchyme differentiation compared with ADSCs in 2D monolayers. Alternatively the 2D model may induce artificially high expression of ICAM-1 and VCAM-1, compared with 3D models and *in-vivo*, due to the absence of diffusion gradients. In 3D, cells have an altered morphology compared with 2D with increased contacts with neighbouring cells and the ECM in multiple directions. These factors could all contribute to the variation in lymphoid mesenchyme induction. Without cytokine induction, VCAM-1 expression increased 4 to 10 fold in ADSC spheroids and hybrid gels, suggesting the change from 2D to 3D alone has a small effect of the phenotype. ICAM-1 expression did show cytokine independent upregulation in 3D, but this varied between donors.

The discrepancy between 2D and 3D following cytokine treatment may be result of cytokine diffusion. In 2D monolayers the induction may be higher than 3D as the entire cell population are directly exposed to the cytokines, whilst in 3D the cytokine availability is reduced due to diffusion gradients created by the presence of neighbouring cells and ECM, potentially limiting cytokine diffusion to the periphery of the spheroid. Limited diffusion has been previously observed in osteosarcoma spheroids, where chemotherapy drug penetration was limited to the periphery of the spheroids³⁵⁹. However even with priming of the ADSCs in 2D prior to cytokine induction, ICAM-1 and VCAM-1 expression was lower in the 3D environment, suggesting the ADSCs in the centre of the spheroid lost the lymphoid mesenchyme phenotype in the absence of continued cytokine cues, or the 3D environment promotes downregulation of the phenotype. A more detailed analysis of the lymphoid mesenchyme in spheroids could be achieved by examining the distribution of ICAM-1 and VCAM-1 expressing cells within the spheroids. In similar spheroids cultures, spheroid size has been shown to effect cell responses to TNF- α . MSC treated with TNF- α had the highest expression of TNF- α stimulated gene/protein 6 (TSG-6), in spheroids

containing 25,000 cells. The expression decreased in larger spheroids and was accompanied by increases in apoptotic and necrotic cells, suggesting both cytokine and oxygen diffusion decreased as spheroid size increased³⁶⁰. In endothelial cell spheroids treated with TNF- α , ICAM-1 and VCAM-1 expression was also limited to the periphery of the spheroids, where in monolayer culture all cells expressed both adhesion molecules³⁶¹. Mathematical modelling of ESC spheroids supports these results. Oxygen and cytokine gradients are observed in spheroids with radii greater than 100 μm , where their concentration decreases from the periphery to the centre of the spheroids¹²⁸. The cytokine treated ADSC spheroids described in thesis had radii of $289 \pm 2.7 \mu\text{m}$ after formation, which fell to $214 \pm 3.1 \mu\text{m}$ after five days of culture, and therefore are likely to experience similar cytokine diffusion gradients. Inducing the phenotype into smaller spheroids, where diffusion gradients are minimised will determine whether diffusion was a key factor in the differences observed in lymphoid mesenchyme induction in 2D and 3D environments.

The use of hybrid gels as a 3D microenvironment for lymphoid mesenchyme modelling should have improved diffusion of cytokines compared with spheroids, as the collagen NSN hydrogels have porosity as shown by SEM micrographs, and the ADSCs are less tightly compacted. During media changes and fixing, DMEM exchanged quickly out of the gels, visualised by a colour change in the entire gel. Furthermore for a LN model where lymphocytes may later be introduced, porous areas within the gel will be required to permit their influx and create follicle regions. The differences in cytokine induced ICAM-1 and VCAM-1 expression between ADSCs in spheroids and hybrid gels, compared with 2D monolayer treatment were not dissimilar.

The collagen fibrils within the hybrid gels may have the capacity to bind the cytokines. Collagen I has previously been shown to bind TNF- α , and this could produce gradients and reservoirs of the cytokines within the gels, reducing the diffusion of cytokines throughout the gel³⁶². Although the cytokines may not directly bind with the collagen fibrils of the hybrid gel, the cytokines could interact with fibrils and NSN globules through electrostatic interactions. Many collagen and PNIPAM hydrogel systems have been shown to provide sustained cytokine and drug release *in-vitro* and *in-vivo*,

although the exact mechanisms involved in the binding are unknown³⁶³. This effect in the hybrid gels could be confirmed by adding fluorescent sample drug and cytokine compounds of variable molecular weight on top of the hybrid gels in a Transwell® system, followed by periodic analysis of the compound distribution within the gels and the supernatant below the gels to investigate the extent of diffusion.

Although there are differences between both 3D systems, both models create environments that will influence cellular behaviour differently than 2D. As discussed within the introduction, topography and the mechanical stiffness of the scaffold, cell shape and pore size effect cell fate. Both 3D models introduce cell-cell and cell-ECM contacts, provide substrates for cell adhesion which are softer than TCP, are likely to generate cytokine gradients and reduce the extent of cell spreading compared with 2D. The 3D systems provide microenvironments for ADSCs, which are more comparable to each other than to 2D monolayer culture, and therefore the results of cytokine induction of the phenotype in the two different 3D models are likely to be similar to each and vary from 2D results. There have not been any previous studies examining spheroids with cell encapsulation in collagen based gels and their differences in behaviour. To separate whether the change in cytokine induction was due to diffusion or changes in cell shape and adhesion, which does vary between the two 3D models, is difficult to examine, as modifications to the 3D microenvironment of the ADSCs tend to affect all of these variables. Encapsulating ADSCs within very thin cell sheets and smaller spheroids could be one method to examine the effects of diffusion, while patterned surfaces with variable adhesive ligands could provide more insight into the effects of cell shape on the induction.

These results demonstrate the suitability of the hybrid gels as cell scaffolds for modelling the lymphoid mesenchyme and stroma. Within the developing LN anlagen and the mature organ, there will be variable gradients of soluble $LT\alpha$ and $TNF-\alpha$ as well as $LT\alpha_1\beta_3$ expressing LTi cells and lymphocytes³⁴⁸, it is unlikely the entire organ contains a similar distribution of the cytokines. Although the exact mechanisms of lymphoid stroma maturation to FDCs and FRCs are unknown, signalling through $LT\beta R$ plays a role and the variation in cytokine concentrations and lymphocyte subsets in

different regions of the LN are likely to contribute. As previously mentioned, treatment in 2D may cause an overexpression of lymphoid markers that is not related to the phenotype seen in 3D, and produce a population of lymphoid mesenchymal cells that are more homogenous than the stroma of the LN.

It will be interesting to explore how permanent the lymphoid mesenchyme phenotype is following stromal induction in 3D, and whether the 3D microenvironment promotes differentiation of the ADSCs to a more committed phenotype. This could be investigated by performing differentiation assays of the ADSCs in 3D with the cytokine treatment and by examining the differential capacity of the ADSCs previously cultured in 3D with cytokine induction and then differentiated in 2D. Analysis of homeostatic chemokines produced by the stromal networks of the LN, such as CXCL13, CCL19 and CCL21, and their distribution throughout the engineered lymphoid tissues will provide a greater understanding of how representative the model is.

3.6.5 Isolation of bone marrow derived MSCs for cartilage repair

Primary MSCs were successfully isolated from the knee bone marrow of three patients undergoing TKRs, cells from each donor were plastic adherent and displayed fibroblastic like morphologies in 2D culture. All donors were positive for MSC cell surface markers. Expression of CD106 in all donors was low, which is characteristic of MSCs that have aged *in-vitro*⁷⁰. The adipogenic and osteogenic differential capacity of the BM-MSCs as shown by ORO staining of fat lipids and alizarin red staining of calcium deposition, was less prominent than seen in ADSCs. The BM-MSCs used in the differentiation assays were sourced from patients aged 69-81 with OA where there had been damage to the articular cartilage and underlying bone, whilst the Invitrogen brought ADSCs may have been sourced from healthy tissues and younger patients and therefore have improved differential capacity. Furthermore several studies have suggested ADSCs may contain more adipogenic progenitors than BM-MSCs and this improves their adipogenic differentiation⁶⁸. Cultured in 3D pellets with TGF- β , the BM-MSCs produced a chondrogenic like ECM, which intensified over 21 days. Alcian blue stained proteoglycans were present from day 7 at the periphery of the pellets, and

the depth of the proteoglycan staining, into the centre of the pellets, increased up to day 21. Collagen II rich ECM was also present at the periphery of the pellets after 7 days of culture. Within the ECM, were unstained regions where the BM-MSCs had adopted a rounded chondrogenic like morphology. Although these results show BM-MSCs isolated from patients with OA have reduced differential capacity compared with ADSCs, they could be expanded *in-vitro* in high enough numbers for chondrogenesis and were able to produce a chondrogenic matrix. Furthermore these experiments were performed *in-vitro*, as BM-MSCs have the ability to differentiate into cartilage *in-vivo*⁷⁷ without additional soluble factors, their differential capacity may be improved *in-vivo*.

3.6.6 Potential of High NSN content hydrogels for cartilage repair

As the extent of matrix remodelling of high NSN content by BM-MSCs is unknown, there are two potential strategies for using the hybrid gels for cartilage repair. BM-MSCs could be directly encapsulated within the gel, where they will be able to remodel the collagen network, and potentially the NSN aggregates, replacing the gel with a newly formed cartilage matrix. Alternatively, acellular hybrid gels could be implanted, and BM-MSCs could be promoted to migrate into the gel from the surrounding tissue, remodelling the collagen fibrils at the gel-cartilage boundary, to aid with integration of the gel into the cartilage. In the second strategy, a cartilage matrix may not be produced throughout the implanted gel, but the stiff NSN gel could instead replace the role of the cartilage. Initially the encapsulation of BM-MSCs within the hybrid gels was investigated, as ultimately replacing damaged cartilage with newly regenerated cartilage matrix would be more beneficial than replacement with a synthetic material, which could be prone to mechanical degradation over time.

The potential of the hybrid gels as injectable scaffolds for cartilage repair, was investigated by encapsulating a high density of BM-MSCs into col-NSN₅ and culturing in chondrogenic media for 21 days. Viability of the BM-MSCs over 21 days was examined using MTT. In metabolically active cells, MTT is reduced into formazan and coloured substrate, and therefore used as a determinant of cell viability. As the cell laden gels were dense and had diameters over 2 mm in the widest areas, the gels were

sectioned throughout to examine the formazan distribution. One potential caveat of this study is the ability of the MTT reagent to diffuse into the centre of the gel. However in the sections from the gels, after one day of culture a similar formazan distribution was seen in all sections throughout the gels, except for the outermost section. At the later time points, there was no discrepancy in formazan distribution in the outermost sections. Therefore the increase seen at the periphery of the gels at day 1 is likely due to increased cellular metabolism of the cells before they were adapted to 3D culture and because they were located at the gel-liquid interface, with similar levels of oxygen and nutrients as 2D culture, rather than MTT diffusion. At the later time points the distribution of formazan is similar throughout, indicating the increased metabolism at the surface at day 1, is likely due to slower changes in cellular behaviour during adaptation to 3D. Similarly to the unknown diffusion in the lower NSN content gels, diffusion with col-NSN₅ could also be examined using a range of fluorescently labelled compounds of variable molecular weights. The distribution of formazan within the gels, demonstrated metabolically active cells were present at each time point investigated, where the staining decreased with time in culture. It has already been shown the hybrid gels do not release anything cytotoxic, therefore any cell death that is occurring must be the result of reduced oxygen and nutrient diffusion into the gel or reduction in cell attachment and spreading. Where there is a reduction in formazan at day 14 and day 21, it is not limited to the periphery of the gels, which would be indicative of a decrease in cell metabolism and viability as a result of reduced oxygen concentration in the centre of the gels. Instead the formazan is distributed randomly throughout the gel sections, therefore suggesting the BM-MSCs are not undergoing apoptosis due to decreased oxygen gradients. Although the MTT assay gives an indication of viability of the encapsulated cells over the 21 day period, further experiments are required. To confirm whether the decrease in formazan production was a result of reduced metabolism or cell death, this could be correlated with Ki67 staining to examine cell proliferation, and TUNEL and caspase-3 staining to identify whether cells were undergoing apoptosis and necrosis.

BM-MSCs encapsulated within the col-NSN₅ gels synthesised a GAG matrix, but no collagen II staining was observed within the gels after 21 days of culture. The same

cells were able to synthesise GAGs and collagen II in cell pellets, therefore the reduction in matrix production could be correlated with decreased cell metabolism or viability. To confirm this similar viability assays would also need to be performed in the BM-MSCs cell pellets also undergoing chondrogenesis. The hybrid gels were also larger than the pellets, almost 2 mm in diameter. Although hypoxia can induce chondrogenic differentiation, when the oxygen content is too low, the differential effect may be lost³⁶⁴. It was assumed that cell shape alone might be sufficient to induce chondrogenesis when combined with TGF- β 3 supplemented media, where the col-NSN₅ gels would reduce cell spreading and give cells a rounded morphology. However the absence of direct cell-cell contact and very limited cell attachment could also be responsible for the decrease in matrix production. Although there was an absence in noticeable matrix production, investigation of the early chondrogenic markers may demonstrate the BM-MSCs within the gels are differentiating towards chondrocytes. Q-PCR analysis of SOX-9, collagen I expression and N-cadherin would provide further information of the differential capacity of the cells.

To improve the potential of the hybrid gels for cartilage repair, matrix deposition and cell viability needs to be improved. Incorporation of increased collagen content into the hybrids with a high NSN concentration was previously proposed as a method to reduce syneresis within the gels, this might also increase matrix deposition by improving cell metabolism and viability by cell attachment. Furthermore the hybrid gels contain collagen I, which should be quickly remodelled during chondrogenesis, but is not found in native cartilage. Incorporation of collagen II into the hybrid gels may improve BM-MSCs chondrogenesis, as shown in other *in-vitro* comparison studies of chondrogenic differentiation of MSCs in collagen I and collagen II gels^{365,366}. Lastly, although the high NSN content gels approach the mechanical properties of mature native cartilage, during endochondral ossification the developing cartilage is softer than the mature tissue. Using hybrid gels with a lower NSN concentration that have mechanical properties more reminiscent of developing cartilage may be more effective in directing MSC differentiation and chondrogenesis.

3.7 Conclusion

The results in this chapter examine two applications of MSCs used in combination with collagen-NSN hybrid gels for tissue engineering as a means for generating models for experimentation or for tissue repair. In summary ADSCs and BM-MSCs have both been shown to be viable within the hybrid gels, and their behaviour is affected by the NSN concentration within the gels. These results demonstrate the versatility of the hybrid gels, initially varying the composition of the blends focused upon altering the mechanical properties to mimic different tissues, but this chapter has demonstrated that the variation in hybrid gel composition also alters cell attachment and migration as NSN content reduces exposed collagen fibrils for cell adhesion. The reversibility of the 2D model of ADSC derived lymphoid mesenchyme was examined, where the results demonstrated ADSCs lose the phenotype in the absence of continued cytokine treatment, mimicking the results seen in *in-vivo* experiments of lymphoid tissue. The lymphoid mesenchyme model was successfully transferred into 3D using the hybrid gels, where the extent of ICAM-1 and VCAM-1 induction decreased in 3D compared with 2D, due to the presence of cytokine gradients in 3D. The behaviour of the ADSCs in the hybrid gels was mirrored in ADSCs spheroids, thus indicating encapsulating of ADSCs within the hybrid gels is an appropriate method for maintaining cells in 3D. Lastly high NSN content gels were explored as injectable scaffolds for cartilage repair. The results obtained are preliminary, but demonstrate BM-MSCs can remain metabolically active for at least 21 days in the gels and that a primitive GAG ECM is formed under chondrogenic conditions. The further potential of the hybrid gels as tissue engineering scaffolds will be discussed in chapter 4.

Chapter 4 General Discussion

Tissue engineering requires the development of specific scaffolds to support cells within 3D by providing a surface for adherence, a template for new tissue growth and a mechanical environment that can withstand the forces at a given site in the body. The influence of the microenvironment in which a cell is situated was discussed in chapter 1, where the mechanical properties, the surface features, and the porosity of the scaffold were all demonstrated to direct cell fate. Furthermore the combination of these factors dictates the overall shape and spreading of the cell and its behaviour. Synthetic hydrogels have been attractive candidates for cell scaffolds, as their ability to maintain high volumes of water makes them good mimics of the ECM, and they can be tailored synthetically to alter the mechanical properties and degradability of the scaffold.

However one drawback of many synthetic hydrogels is their poor biocompatibility, as cells are unable to adhere to and remodel the gels. PNIPAM based hydrogels are commonly used in tissue engineering as they are thermoresponsive, and therefore can be used to encapsulate and release cells, and can be injected to fill a particular shape prior to gelation. However, PNIPAM hydrogels are generally non-cell adhesive and not degradable^{218,267}. The solution to the poor biocompatibility, investigated in this thesis, is the development of a bio-synthetic hydrogel which combines a thermoresponsive PNIPAM based synthetic hydrogel that has good mechanical strength, with collagen to permit cell attachment and a degree of tissue remodelling within the scaffold.

Generally scaffolds for tissue engineering are created with a specific application in mind, and cannot be easily tailored once fabricated, to amend their physical properties. The PNIPAM – biological hybrids that have been produced by other research groups can only be tuned by increasing or decreasing the concentration of a polymer dissolved in aqueous solution, which effects the mechanical properties of the resulting hydrogel, and tends to have a lesser effect on biocompatibility^{235,250}. However the collagen- NSN blends described in this thesis, are tuned by simply mixing solutions of NSN and collagen at the time of gelation. Therefore I explored how varying the blend of collagen

and NSN in the hydrogels firstly affected the structure, and physical properties of the hydrogels, as described in chapter 2, and secondly how different blends could therefore be used for different tissue engineering applications, as described in chapter 3.

1.10 Synthesis and properties of collagen-NSN hydrogels

NSN was synthesised by a 3- step procedure, initially creating and functionalising NVP macromonomers, followed by *in-situ* synthesis of the NIPAM – styrene backbone and incorporation of the NVP macromonomers. The resulting polymer, had a LCST of 25 °C, and could therefore be combined with collagen solutions and cell suspensions, to produce a bio-synthetic gel, containing a uniform distribution of cells, which could gelate at 37°C. As expected, the properties of the resulting hydrogels were dominated by the concentration of the two components, as seen in other bio-synthetic hydrogels produced, where the mechanical properties decrease when the proportion of biological hydrogel is increased^{250,367}. At concentrations below the minimum gelation concentration of NSN, the hydrogels had properties similar to collagen only gels, with the lowest mechanical properties, a fibrillar network of fibres and an absence or very low degree of syneresis, upon gel formation. Within these hydrogels, ADSCs and HT1080 cells were able to spread out and attach, where the cell morphologies were influenced by the NSN content. The properties of the hydrogels with higher concentrations of NSN (2.5 wt% upwards) were dominated by the synthetic component, having increased mechanical properties under the application of shear stress. However as the concentration of NSN exceeded collagen, syneresis increased, where the size of equilibrated NSN₅ hydrogels were only 30 % of their original volume. Although the morphology of cells in these gels was not examined, it was assumed the high NSN content resulted in cells with rounded morphologies.

The incorporation of collagen into the NSN hydrogels was able to improve their potential as cell scaffolds. The scaffolds were cell adhesive and reduced NSN associated syneresis, while the presence of NSN improved the mechanical strength of collagen. These results highlight the use of the hybrid gels may involve compromising a particular property such as biocompatibility versus mechanical strength, in favour of

another, when used as cell scaffolds. Given the complexity and variation in tissues and organs within the human body, creating a scaffold suitable to mimic all of them is likely to be impossible. However these results demonstrate the tunability of the collagen-NSN scaffolds and their potential in engineering various tissues, which has not previously been achieved for a bio-synthetic PNIPAM based hydrogel. The blends containing low concentrations of NSN, will be useful for the tissue engineering of soft biological tissues, where the effect of cell morphology in 3D and extent of cell adhesion to a collagen based scaffold could be examined, by varying the concentration of NSN within the gel to reduce cell adhesion, whilst maintaining constant collagen concentration. To date most studies on cell morphology and attachment are performed in 2D^{123,151,356}. The collagen-NSN hydrogel system provides a system for investigating these effects in 3D. The introduction of NSN, also introduces a non-degradable component into collagen based gels, and variation in its concentration is also likely to impact the extent of tissue remodelling within the scaffold. Furthermore, the thermoresponsive nature of NSN will permit cell release and analysis following experimentation. The inclusion of low concentrations of NSN into collagen gels, improved the mechanical properties compared with collagen only gels, therefore the hybrids may also have potential as collagen based gels for microfluidic engineering, where previously high concentrations of collagen were necessary which reduced the ability of cell migration and remodelling within the gel¹⁷¹.

The tougher hydrogels, which contain higher concentrations of NSN, have mechanical properties approaching the values experimentally determined for muscle and cartilage. Although these gels may be less cell adhesive, due to the low collagen concentration, they may be applicable for tissue engineering of these tougher tissues by mimicking the mechanics, which are important for tissue function. To demonstrate the applications of the collagen-NSN hydrogels, different blends were examined for use as cell scaffolds for MSCs, specifically for developing 3D models of lymphoid stroma, and as injectable therapies for cartilage repair. The low NSN containing hydrogels were able to support viable ADSCs, and preliminary results suggest BM-MSCs were metabolically active in high NSN containing gels over 21 days.

1.11 Development of an aLN using ADSCs and collagen-NSN hydrogels

To model the stromal networks of the LN, ADSCs were induced into a lymphoid mesenchyme phenotype by treating the cells with IL-4, TNF- α and LT β R. This was shown to be an appropriate model, with induced ADSCs expressing lymphoid markers ICAM-1, VCAM-1 and podoplanin. The *in-vitro* phenotype of the cytokine treated ADSCs was transient, unlike the more committed differentiation of MSCs into fat and bone, as removal of the cytokines permitted classical MSC differentiation, whilst continued treatment inhibited adipogenic and osteogenic differentiation. These results are in agreement with the *in-vivo* stromal networks of the lymph node and other secondary lymphoid tissues, which require constitutive expression of LT and TNF- α in varying degrees in order to develop and maintain stromal networks^{307,309}. Therefore the ADSC model builds upon previous research, which demonstrates lymphoid stromal networks are mesenchymal in origin and likely to be derived from surrounding adipose tissue^{304,337}. The model does however require further experimentation to examine its validity as an aLN. Beyond cell surface marker expression and the differential capacity of the induced ADSCs, the behaviour of the induced lymphoid mesenchymal cells in co-culture with lymphocytes and following activation with antigen, to mimic an immune response, should be investigated to demonstrate the functionality of the *in-vitro* model.

A range of the low NSN content hydrogels were used as scaffolds for translating the 2D lymphoid mesenchyme model into 3D. The LN contains networks of reticular ECM fibres composed of collagen I, and mechanical tests have demonstrated the LN is a soft organ, with elastic moduli in the region of the low NSN gels¹³⁴. ADSCs were viable and formed networks within the gels, presumably through integrin binding to exposed collagen fibres. As the NSN aggregates onto the collagen fibres, the cell attachment and spreading were reduced with increasing NSN concentration. Therefore an optimal blend of col-NSN_{0.5} was chosen to mimic the morphology of FRCs and FDCs within the lymph node. This blend was also more open and porous compared with collagen only gels and therefore should permit the migration of lymphocytes and capillaries into the

scaffolds in further development of the model. Alongside the hydrogels, spheroids were examined as an alternative 3D model for the LN, to produce a dense network of cells.

Both methods produced 3D networks of ADSCs, which had similar levels of ICAM-1 and VCAM-1 expression following cytokine induction, however their expression was significantly lower than in 2D. As previously discussed, diffusion within the models is likely to occur and the extent of this needs to be identified to differentiate between whether the reduced expression was caused by diffusion of the cytokines throughout the 3D models, or whether the 3D model is more representative and accurate, and the lack of cytokine gradients and cell shape of ADSCs in monolayers caused the discrepancies. These differences in lymphoid mesenchyme induction in 2D and 3D models could be used to examine how and why different lymphoid stromal subsets form and mature within the LN as a function of gradients of cytokines. Using the variable blends of col-NSN, I was able to fabricate 3D networks of the ADSCs, where the cell morphology and adhesions could be perturbed through NSN concentration, and therefore potentially direct the cellular behaviour. Although the lymphoid mesenchyme induction in spheroids and col-NSN gels produced similar results, the hybrid gels will be most suitable in progressing the aLN model into 3D. The presence of ECM components in the hybrid gels provides a starting template for the lymphoid mesenchyme cells to organise and potentially develop conduit like structures around the collagen fibrils. Current aLN models that have been developed rely on the body as a bioreactor to induce the compartmentalisation and remodelling into lymphoid like tissue. Although this produces models, which resemble the LN, they still require the use of mice, and therefore are not reducing the numbers of animal used in research, one of the key aims in developing tissue models. Furthermore the previously developed models use transformed murine cell lines. This thesis describes the first 3D human aLN model using primary cells.

1.12 Potential of collagen-NSN hydrogels for injectable cartilage regeneration

To examine the potential of the hybrids for cartilage repair, *in-vitro* chondrogenesis assays were performed in the tougher col-NSN₅ gels. Within cartilage, chondrocytes are isolated in lacunae, making few cell –cell adhesions, mainly interacting with the ECM. BM-MSCs were seeded within the liquid gels to create a similar uniform distribution of cells, and due to the high NSN concentrations, which were likely to prevent cell adhesion to collagen, the cells appeared rounded, in small pockets within the gel. BM-MSCs were metabolically active within the gels over 21 days, and began to synthesise a cartilaginous GAG matrix. As discussed within chapter 3, the application of the high NSN hybrid gels for cartilage repair could be approached from two directions, either delivering the gel without cells, which would remain within the cartilage defect and replace the damaged cartilage, or using the hybrid gels seeded with BM-MSCs as a template for cartilage repair, where the collagen network could be remodelled and the NSN replaced over time by new ECM and degradation by the mechanics of the joint. The exact blend of the hybrid gel would be likely to dictate how the material functioned. In col-NSN₅, only small amounts of cartilage like ECM were formed compared with BM-MSC cell pellets, therefore this blends would be more appropriate to replace the damaged cartilage. To improve the chondrogenic capacity of the cells, higher concentrations of collagen could be added to the gel, this would improve cell attachment and also cell viability. However the mechanical properties of the gel would then be compromised. Again this highlights the importance of using the most appropriate scaffold for its application and the potential of tunable hydrogel scaffolds.

1.13 Effect of hydrogel composition on gelation mechanism and resulting properties

The following model is proposed in the relation to the collagen – NSN hybrid gels and cellular behaviour, building upon the model proposed in chapter 2 (Figure 4-1). Collagen gels take the shape and volume of the parent solution, with cells adhering to the fibrils after several hours of culture. The introduction of NSN into the collagen gels impairs cell adhesion, and thus affects cell shape and migration, by reducing the area of

exposed fibrils and integrin binding sequences. In gels with high NSN concentrations, the effect is intensified, and the gelation is also accompanied with syneresis. Cells within the high NSN hybrids are rounded, and may also have forces imposed onto them by the aggregation of NSN during gelation. The model is also extended into the future development of the gels, which aim to maintain the mechanical properties achieved through the presence of NSN, whilst aiming to alleviate syneresis and improve cell adhesion by increasing the collagen concentration within the hybrid gels from 0.3 wt% up to 1 – 2 wt%. Using higher concentrations of collagen, it is proposed that the increased number and the presence of thicker collagen fibrils which are forming within the gel will be able to reduce the extent of NSN aggregation thus reducing the shrinking of the gels, and increasing the sites of cell adhesion. Furthermore, collagen gelation is not temperature dependent in the same manner as PNIPAM, although the gelation rate increases at higher temperatures, fibril formation and gelation can occur at any temperature, therefore these gels could be formed via a two step mechanism to also alter the materials properties. Initially collagen would be allowed to gel below the LCST of NSN, and subsequently the temperature could then be raised above the LCST to allow NSN aggregation to occur, which may be hindered by the pre-formed collagen network and therefore may reduce the degree of syneresis associated with NSN gelation.

1.14 Future Work

Presented within this thesis are preliminary results for two 3D models utilising the collagen-NSN hybrid gels as scaffolds. To further this research further characterisation of the hybrid gels will be beneficial. This includes visual analysis of the gelation point by an invert test, further analysis of the phase transition to determine the true LCST using DSC, AFM analysis of the collagen-NSN blends to examine how efficiently the materials blend and further compression mechanical testing.

The suitability of ADSCs and col-NSN_{0.5} as a model for an aLN was demonstrated in chapter 3. To further this, the model needs to incorporate a co-culture of with lymphocytes and requires further validation against *in-vivo* levels of ICAM-1 and VCAM-1 expression within the lymph nodes. Since submitting this thesis, further work

has been performed on the hybrid gels for cartilage repair. To improve cell attachment the collagen content within the gels has been increased to 0.5 and 0.75 wt%. Histological examination of these blends containing BM-MSCs, following 21 days in chondrogenic conditions shows production of a significantly improved collagen II and GAG rich matrix compared with the col-NSN₅ blends. The extent of chondrogenesis in several of these new blends will be quantified through qPCR analysis of the chondrogenic transcription factor SOX9 and matrix molecules aggrecan, collagen I, collagen II, collagen X and lubricin. Where the ratio of collagen I to II will provide an indication of the maturity of the matrix and collagen X will identify hypertrophy.

1.15 Conclusion

Within this thesis I have developed a unique bio-synthetic hydrogel scaffold, that can be used for multiple applications by varying the ratio of NSN to collagen. The gelation process is controlled by temperature, and therefore does not require harsh conditions that may compromise cell viability. The thermoresponsive nature of the gels also lends them to applications, which require injectable scaffolds. Following synthesis of the NSN and isolation of collagen, solutions can be produced from each component and the hydrogels are straightforward to produce by simply mixing and incubating at room temperature. Therefore this hydrogel system also has good commercial potential, as the two components could be purchased as a cell scaffold system where the end user can easily create a scaffold to meet their desired application. The system could also be marketed for testing the effect of natural versus synthetic scaffolds, scaffold elasticity and cell adhesion parameters on cell fate and behaviour.

This thesis examined the variation in NSN on hydrogel properties and cellular behaviour and only demonstrates two applications of the resulting gels. This system could be furthered by producing an entire range of col-NSN hybrid gels, where collagen concentration is also varied, and determining the physical properties of each to blend to produce a catalogue of scaffolds.

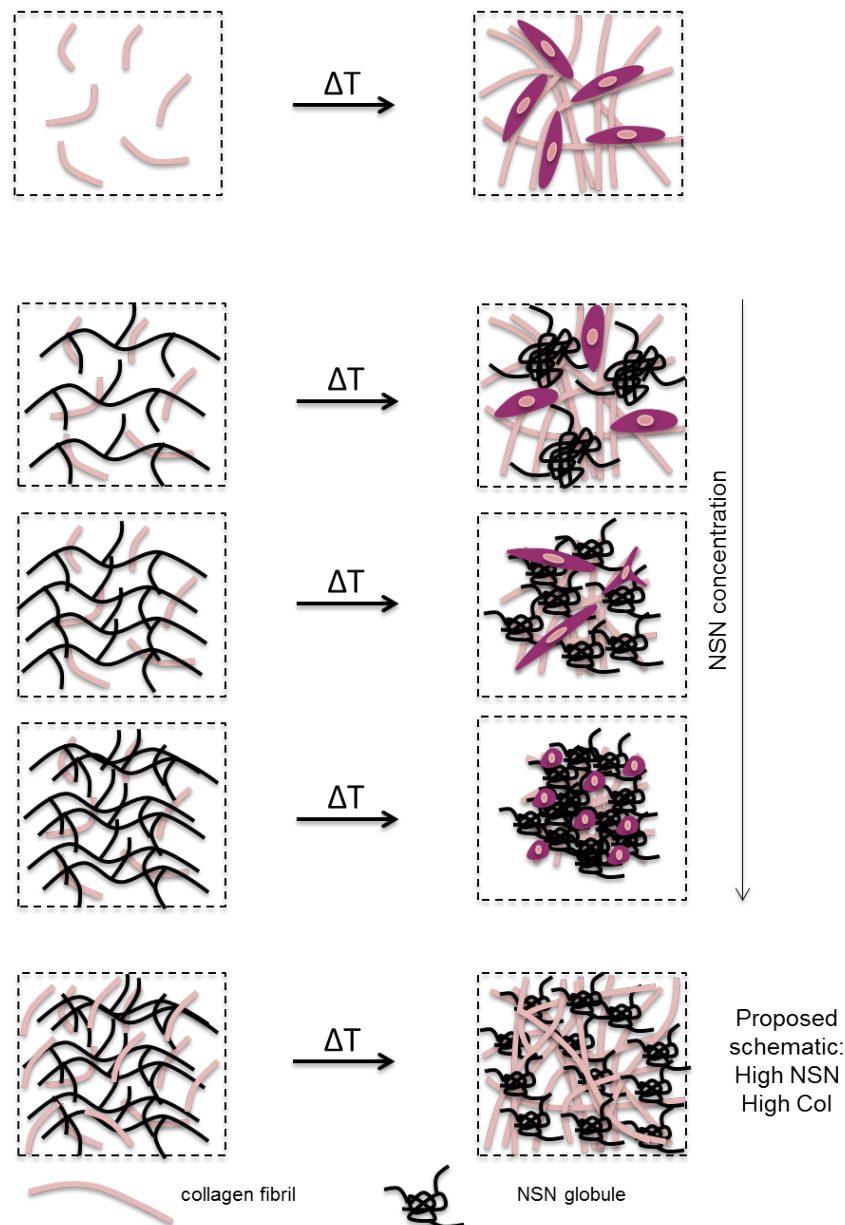


Figure 4-1 Proposed mechanism of col-NSN gelation and cellular adhesion

Collagen gels form from collagen monomers into aligned fibrils maintaining the volume of the parent solution. In contrast, NSN forms hydrogels by aggregation and the gels are prone to syneresis. At low concentrations of NSN, similar to collagen, no syneresis is observed and cells adhere similarly to collagen gels. As the NSN concentration increases the gels become more prone to syneresis, and cell morphology is altered as a result of unexposed collagen fibrils. At high NSN concentrations, the combination of high syneresis and unexposed collagen fibrils leads to rounded cells, with few adhesions. Therefore it is proposed hybrid gels made from collagen concentrations which equal the NSN concentration will have reduced syneresis and improved cell adhesion whilst maintaining the high mechanical properties. Dotted lines indicate volume of parent solution and syneresis, ΔT indicates a change in temperature.

Abbreviations

¹H-NMR – hydrogen nuclear magnetic resonance
2D – 2 dimensional
3D – 3 dimensional
AAc – acrylic acid
ACI - autologous chondrocyte implantation
ADSC – adipose derived stromal cell
AIBN – azobisisobutyronitrile
aLN- artificial lymph node
ALP- alkaline phosphatase
AM – adipogenic media
APC- antigen presenting cell
BCM- basal chondrogenic media
BM – basal media
BM-MSC – bone marrow mesenchymal stromal cell
BMP-2 – bone morphogenetic protein 2
BMSC – bone marrow stromal cell
BSA - bovine serum albumin
CD – cluster of differentiation
CFU-F- colony forming unit fibroblast
CM – chondrogenic media
DAPI – 4',6-diamidino-2-phenylindole
DCM – dichloromethane
DEX - dexamethasone
DLS – dynamic light scattering
DMA – dynamic mechanical analysis
DMEM – Dulbecco's Modified Eagle's Medium
DMF – dimethylformamide
DSC- differential scanning calorimetry
ECM – extracellular matrix
EDTA – ethylene diaminetetra acetic acid

ESC – embryonic stem cell
FBS – fetal bovine serum
FDC- follicular dendritic cell
FRC- fibroblastic reticular cell
FS – forward scatter
g - graft
G'-storage modulus
G''- loss modulus
GPC- gel permeation chromatography
HEV-high endothelial venule
HSC – haematopoietic stem cell
ICAM-1 – intercellular adhesion molecule - 1
IL-4 – interleukin 4
IL-4R – interleukin 4 receptor
IMBX - 1-methyl-3-isobutylxanthine
IPE – 2-isopropoxyethanol
IPN - interpenetrating network
GAG – glycosaminoglycan
GPC – gel permeation chromatography
HA – hyaluronan
HUVEC – human umbilical vein endothelial cell
LCST – lower critical solution temperature
LT – lymphotoxin
LTβR – lymphotoxin β receptor
LTi - lymphoid tissue inducer cell
LTo - lymphoid tissue organiser cell
LN- lymph node
MALDI-ToF - matrix assisted laser desorption time-of-flight spectroscopy
 M_n – number average molecular weight
MSC – mesenchymal stem/stromal cell
MTT – 3-(4,5-dimethylthiazol-2-yl)-2,5-diphenyltetrazolium bromide
MVEC - micro-vascular endothelial cell

M_w – weight average molecular weight
NASI- N-acryloxysuccinimide
NIPAM – N-isopropylacrylamide
NVP – N-vinylpyrrolidone
NSN – poly(NIPAM-*co*-styrene-*graft*-NVP)
OA – osteoarthritis
OM – osteogenic media
ONVP – oligo N-vinylpyrrolidone
ONVP-OH – hydroxyl functionalised oligo N-vinylpyrrolidone
ONVP-VB – vinyl benzene functionalised oligo N-vinylpyrrolidone
ORO – Oil Red O
Pa - Pascal
PBS – phosphate buffered saline
PCM - pericellular matrix
PDEMAC- poly(dimethylacetamide)
PDI – polydispersity index
PEG – poly(ethylene glycol)
PEI – poly(ethylene imine)
PHEMA- poly(2-hydroxyethyl methacrylate)
PMVE – poly(methyl vinyl ether)
pNP- para-Nitrophenol
pNPP- para-Nitrophenylphosphate
PNIPAM- poly(N-isopropylacrylamide)
PP- Peyers patch
p/s – penicillin/ streptomycin
PVP – poly(vinylpyrrolidone)
PVCAP- poly(vinylcaprolactam)
RGD- arginine-glycine-aspartic acid
SEC – size exclusion chromatography
SEM – scanning electron microscopy
sIPN – semi interpenetrating network
SLS- static light scattering

SMC – smooth muscle cell

SS - side scatter

TCP – tissue culture plastic

TGF- β – transforming growth factor β

TJR – total joint replacement

TNF- α – tumour necrosis factor α

UC-MSC – umbilical cord blood mesenchymal stem cell

VCAM-1 – vascular cell adhesion molecule -1

VBC – 4-vinylbenzyl chloride

wt% - weight percent

References

1. Langer, R. & Vacanti, J. P. Tissue Engineering. *Science* (80-.). **260**, 920–926 (1993).
2. Nations, U. *World Population Ageing 2013*. xii (2013).
3. Transplant, N. B. and. *Transplant Activity in the UK. Activity Report 2010/11*. (2011).
4. Health, N. I. of. Medline Plus: Organ Rejection. at <<http://www.nlm.nih.gov/medlineplus/ency/article/000815.htm>>
5. Porter, M. *et al. National Joint Registry Annual Report 2012*. **50**, (2012).
6. Fisher, John, McEwen, H. *et al. Wear, Debris, and Biologic Activity of Cross-linked Polyethylene in the Knee: Benefits and Potential Concerns*. *Clin. Orthop. Relat. Res.* **428**, 114–119 (2004).
7. Abu-Amer, Y., Darwech, I. & Clohisy, J. C. Aseptic loosening of total joint replacements: mechanisms underlying osteolysis and potential therapies. *Arthritis Res. Ther.* **9 Suppl 1**, S6 (2007).
8. Mollon, B., Kandel, R., Chahal, J. & Theodoropoulos, J. The clinical status of cartilage tissue regeneration in humans. *Osteoarthritis Cartilage* **21**, 1824–33 (2013).
9. Matoka, D. J. & Cheng, E. Y. Tissue Engineering in Urology. *Can. Urol. Assoc. J.* **3**, 403–408 (2009).
10. Cairns, B. A., DeSerres, S., Peterson, H. D. & Meyer, A. A. Skin replacements. The biotechnological quest for optimal wound closure. *Arch. Surg.* **128**, 1246–1252 (1993).
11. Eisenbud, D., Huang, N., Luke, S. & Silberkland, M. Skin Substitutes and Wound Healing: Current Status and Challenges. *Wounds* **16**, (2004).
12. R E, B. & J, R. Transplantation studies on sheets of pure epidermal epithelium and on epidermal cell suspensions. *Br. J. Plast. Surg.* **5**, 25–36 (1952).
13. Rheinwald, J. G. & Green, H. Serial Cultivation of Strains of Human Epidermal Keratinocytes: the Formation of Keratinizing Colonies froellsm Single C. *Cell* **6**, 331–334 (1975).
14. Rheinwald, J. G. & Green, H. Formation of a Keratinizing Epithelium in Culture by a Cloned Cell Line Derived from a Teratoma. *Cell* **6**, 317–330 (1975).
15. Green, H., Kehinde, O. & Thomas, J. Growth of cultured human epidermal cells into multiple epithelia suitable for grafting. *Proc. Natl. Acad. Sci.* **76**, 5665–5668 (1979).

16. MacNeil, S. Progress and opportunities for tissue-engineered skin. *Nature* **445**, 874–80 (2007).
17. Integra: Soft Tissue Solutions. at <<http://www.integralife.com>>
18. Berthiaume, F., Maguire, T. & Yarmush, M. Tissue Engineering and Regenerative Medicine: History, Progress, and Challenges. *Annu. Rev. Chem. Biomol. Eng.* **2**, 403–430 (2011).
19. Apligraf. (2014). at <http://www.apligraf.com/patient/what_is_apligraf/what_is_apligraf.html>
20. Falanga, V. & Sabolinski, M. Original articles A bilayered living skin construct (APLIGRAF ®) accelerates complete closure of hard-to-heal venous ulcers. 201–207 (1999).
21. Tsai, R., Li, L. & Chen, J. Reconstruction of damaged corneas by transplantation of autologous limbal epithelial cells. *N. Engl. J. Med.* **343**, 86–93 (2000).
22. Brookes, J. P., Fields, K. L. & Raff, M. C. Studies on cultures rat Schwann cells. I. Establishment of purified populations from cultures of peripheral nerve. *Brain Res.* 105–118 (1979).
23. Brittberg, M. *et al.* Treatment of Deep Cartilage Defects in the Knee with Autologous Chondrocyte Transplantation. *N. Engl. J. Med.* **331**, 889–895 (1994).
24. Atala, A., Bauer, S. B., Soker, S., Yoo, J. J. & Retik, A. B. Tissue-engineered autologous bladders for patients needing cystoplasty. *Lancet* **367**, 1241–6 (2006).
25. Geoffrey, D. *et al.* Population Expansion, Clonal Growth, and Specific Differentiation Patterns in Primary Cultures of Hepatocytes Induced by HGF/SF, EGF and TGF α in a Chemically Defined (HGM) Medium. *J. Cell Biol.* **132**, 1133–1149 (1996).
26. Pittenger, M. F. *et al.* Multilineage potential of adult human mesenchymal stem cells. *Science* **284**, 143–7 (1999).
27. Lacroix, P. Recent investigations on the growth of bone. *Nature* **156**, 576 (1945).
28. Urist, M. R. Bone : Formation by Autoinduction. *Science (80-)*. **150**, 893–899 (1965).
29. Sampath, T. K. & Reddi, A. H. Dissociative extraction and reconstitution of extracellular matrix components involved in local bone differentiation. *Proc. Natl. Acad. Sci.* **78**, 7599–7603 (1981).
30. Langer, R. & Folkman, J. Polymers for the sustained release of proteins and other macromolecules. *Nature* **263**, 797–799 (1976).

31. Vacanti, J. P. *et al.* Selective cell transplantation using bioabsorbable artificial polymers as matrices. *J. Pediatr. Surg.* **23**, 3–9 (1988).
32. Cao, Y., Vacanti, J. P., Paige, K. T., Upton, J. & Vacanti, C. A. Transplantation of Chondrocytes Utilizing a Polymer-Cell Construct to Produce Tissue-Engineered Cartilage in the Shape of a Human Ear. *Plast. Reconstr. Surg.* **100**, 297–302 (1997).
33. Macchiarini, P. *et al.* Clinical transplantation of a tissue-engineered airway. *Lancet* **372**, 2023–30 (2008).
34. Gonfiotti, A. *et al.* The first tissue engineered airway transplantation: 5-year follow up results. *Lancet* **383**, 238–244 (2014).
35. Alonso, L. & Fuchs, E. Stem cells of the skin epithelium. *Proc. Natl. Acad. Sci. U. S. A.* **100 Suppl**, 11830–5 (2003).
36. Toma, J. G. *et al.* Isolation of multipotent adult stem cells from the dermis of mammalian skin. *Nat. Cell Biol.* **3**, 778–84 (2001).
37. Blanpain, C. & Fuchs, E. Epidermal homeostasis: a balancing act of stem cells in the skin. *Nat. Rev. Mol. Cell Biol.* **10**, 207–17 (2009).
38. Leedham, S. J., Brittan, M., McDonald, S. a C. & Wright, N. a. Intestinal stem cells. *J. Cell. Mol. Med.* **9**, 11–24 (2005).
39. Doetsch, F., Caillé, I., Lim, D. a, García-Verdugo, J. M. & Alvarez-Buylla, a. Subventricular zone astrocytes are neural stem cells in the adult mammalian brain. *Cell* **97**, 703–16 (1999).
40. Johansson, C. B. *et al.* Identification of a neural stem cell in the adult mammalian central nervous system. *Cell* **96**, 25–34 (1999).
41. Gage, F. H. & Temple, S. Neural stem cells: generating and regenerating the brain. *Neuron* **80**, 588–601 (2013).
42. Genever, P. Biomedical Tissue Research Groups.
43. Ashton, B. A., Eaglesom, C. C. & Owen, M. E. Distribution of Fibroblastic Colony-Forming Cells in Rabbit Bone Marrow and Assay of their Osteogenic Potential by an in vivo Diffusion Chamber Method In Vivo Culture in Diffusion Chambers. *Calcif. Tissue Int.* **36**, 83–86 (1984).
44. Caplan, A. L. Mesenchymal Stem Cells. *J. Orthop. Res.* **9**, 641–50 (1991).
45. Owen, M. E., Cavé, J. & Joyner, C. J. Clonal analysis in vitro of osteogenic differentiation of marrow CFU-F. *J. Cell Sci.* **87**, 731–8 (1987).

46. Ashhurst, D. E., Ashton, B. A. & Owen, M. E. The collagens and glycosaminoglycans of the extracellular matrices secreted by bone marrow stromal cells cultured in vivo in diffusion chambers. *J. Orthop. Res.* **8**, 741–9 (1990).
47. Mackay, A. M. *et al.* Chondrogenic differentiation of cultured human mesenchymal stem cells from marrow. *Tissue Eng.* **4**, 415–28 (1998).
48. Johnstone, B., Hering, T. M., Caplan, A. L., Goldberg, V. M. & Yoo, J. U. In vitro chondrogenesis of bone marrow-derived mesenchymal progenitor cells. *Exp. Cell Res.* **238**, 265–72 (1998).
49. Gartner, S. & Kaplan, H. S. Long-term culture of human bone marrow cells. *Proc. Natl. Acad. Sci. U. S. A.* **77**, 4756–9 (1980).
50. Lim, B. *et al.* Characterization of reticulofibroblastoid colonies (CFU-RF) derived from bone marrow and long-term marrow culture monolayers. *J. Cell. Physiol.* **127**, 45–54 (1986).
51. Wakitani, S., Saito, T. & Caplan, A. I. Myogenic cell derived from rat bone marrow mesenchymal stem cells exposed to 5-azacytidine. *Muscle and Nerve* **18**, 1417–1426 (1995).
52. Dezawa, M. *et al.* Bone marrow stromal cells generate muscle cells and repair muscle degeneration. *Science* **309**, 314–7 (2005).
53. Caplan, A. L. & Bruder, S. P. Mesenchymal stem cells: building blocks for molecular medicine in the 21st century. *Trends Mol. Med.* **7**, 259–64 (2001).
54. Le Blanc, K., Tammik, C., Rosendahl, K., Zetterberg, E. & Ringdén, O. HLA expression and immunologic properties of differentiated and undifferentiated mesenchymal stem cells. *Exp. Hematol.* **31**, 890–6 (2003).
55. Le Blanc, K. *et al.* Treatment of severe acute graft-versus-host disease with third party haploidentical mesenchymal stem cells. *Lancet* **363**, 1439–41 (2004).
56. Zuk, P. a *et al.* Multilineage cells from human adipose tissue: implications for cell-based therapies. *Tissue Eng.* **7**, 211–28 (2001).
57. Zuk, P. A. *et al.* Human Adipose Tissue Is a Source of Multipotent Stem Cells □. **13**, 4279–4295 (2002).
58. Gimble, J. & Guilak, F. Adipose-derived adult stem cells: isolation, characterization, and differentiation potential. *Cytotherapy* **5**, 362–9 (2003).
59. Lee, O. K. *et al.* Isolation of multipotent mesenchymal stem cells from umbilical cord blood. *Blood* **103**, 1669–75 (2004).

60. Romanov, Y. A., Svintsitskaya, V. A. & Smirnov, V. N. Searching for Alternative Sources of Postnatal Human Mesenchymal Stem Cells: Candidate MSC-Like Cells from Umbilical Cord. *Stem Cells* **21**, 105–110 (2003).
61. Bieback, K., Kern, S., Klüter, H. & Eichler, H. Critical parameters for the isolation of mesenchymal stem cells from umbilical cord blood. *Stem Cells* **22**, 625–34 (2004).
62. De Bari, C. *et al.* Mesenchymal multipotency of adult human periosteal cells demonstrated by single-cell lineage analysis. *Arthritis Rheum.* **54**, 1209–21 (2006).
63. Young, H. E. *et al.* Human reserve pluripotent mesenchymal stem cells are present in the connective tissues of skeletal muscle and dermis derived from fetal, adult, and geriatric donors. *Anat. Rec.* **264**, 51–62 (2001).
64. Wagner, W. *et al.* Comparative characteristics of mesenchymal stem cells from human bone marrow, adipose tissue, and umbilical cord blood. *Exp. Hematol.* **33**, 1402–16 (2005).
65. Kern, S., Eichler, H., Stoeve, J., Klüter, H. & Bieback, K. Comparative analysis of mesenchymal stem cells from bone marrow, umbilical cord blood, or adipose tissue. *Stem Cells* **24**, 1294–301 (2006).
66. Gronthos, S. *et al.* Surface protein characterization of human adipose tissue-derived stromal cells. *J. Cell. Physiol.* **189**, 54–63 (2001).
67. Winter, A. *et al.* Cartilage-like gene expression in differentiated human stem cell spheroids: a comparison of bone marrow-derived and adipose tissue-derived stromal cells. *Arthritis Rheum.* **48**, 418–29 (2003).
68. Noël, D. *et al.* Cell specific differences between human adipose-derived and mesenchymal-stromal cells despite similar differentiation potentials. *Exp. Cell Res.* **314**, 1575–84 (2008).
69. Dominici, M. *et al.* Minimal criteria for defining multipotent mesenchymal stromal cells. The International Society for Cellular Therapy position statement. *Cytotherapy* **8**, 315–7 (2006).
70. Boxall, S. A. & Jones, E. Markers for characterization of bone marrow multipotential stromal cells. *Stem Cells Int.* **2012**, 1–12 (2012).
71. Wagner, W. *et al.* Replicative senescence of mesenchymal stem cells: a continuous and organized process. *PLoS One* **3**, e2213 (2008).
72. Liu, F. *et al.* Changes in the expression of CD106, osteogenic genes, and transcription factors involved in the osteogenic differentiation of human bone marrow mesenchymal stem cells. *J. Bone Miner. Metab.* **26**, 312–20 (2008).

73. Simmons, P. J. & Torok-Storb, B. Identification of stromal cell precursors in human bone marrow by a novel monoclonal antibody, STRO-1. *Blood* **78**, 55–62 (1991).
74. Gronthos, S. Molecular and cellular characterisation of highly purified stromal stem cells derived from human bone marrow. *J. Cell Sci.* **116**, 1827–1835 (2003).
75. Friedenstein, a J., Piatetzky-Shapiro, I. I. & Petrakova, K. V. Osteogenesis in transplants of bone marrow cells. *J. Embryol. Exp. Morphol.* **16**, 381–90 (1966).
76. Friedenstein, A. J. Precursor cells of mechanocytes. *Int. Rev. Cytol. a Surv. cell biology* **47**, 327–355 (1976).
77. Ashton, B. A. *et al.* Formation of bone and cartilage by marrow stromal cells in diffusion chambers in vivo. *Clin. Orthop. Relat. Res.* 294–307 (1980).
78. Bab, I., Ashton, B. a., Syftestad, G. T. & Owen, M. E. Assessment of anin vivo diffusion chamber method as a quantitative assay for osteogenesis. *Calcif. Tissue Int.* **36**, 77–82 (1984).
79. Owen, M. Marrow stromal stem cells. *J. Cell Sci. Suppl.* **10**, 63–76 (1988).
80. Mardon, H. J., Bee, J., Klaus van dar, M. & Owen, M. E. Development of osteogenic tissue in diffusion chambers from early precursor cells in bone marrow of adult rats. *Cell Tissue Res.* **250**, 157–165 (1987).
81. Caplan, A. L. & Koutroupas, S. The control of muscle and cartilage development in the chick limb: the role of differential vascularization. *J. Embryol. Exp. Morphol.* **29**, 571–83 (1973).
82. Caplan, A. I., Zwilling, E. & Kaplan, N. O. 3-Acetylpyridine:Effects in vitro Related to Teratogenic Activity in Chicken Embryos. *Science (80-.)*. **160**, 1009–1010 (1968).
83. Friedenstein, A. J. & Chailakjhan, R. K. The development of fibroblast colonies in monolayer cultures of guinea-pig bone marrow and spleen cells. *Cell Tissue Kinet.* **3**, 393–403 (1970).
84. Friedenstein, A. J., Chailakjhan, R. K. & Gerasimov, U. V. Bone marrow osteogenic stem cells: in vitro cultivation and transplantation in diffusion chambers. *Cell Tissue Kinet.* **20**, 263–272 (1987).
85. Dexter, T. M., Allen, T. D. & Lajtha, L. G. Conditions controlling the proliferation of haemopoietic stem cells in vitro. *J. Cell. Physiol.* **91**, 335–44 (1977).
86. Piersma, A. *et al.* Characterization of fibroblastic stromal cells from murine bone marrow. *Exp. Hematol.* **13**, 237–243 (1985).

87. Howlett, C. R. *et al.* Mineralization in in vitro cultures of rabbit marrow stromal cells. *Clin. Orthop. Relat. Res.* **213**, 251–263 (1986).
88. Beresford, J. N., Bennett, J. H., Devlin, C., Leboy, P. S. & Owen, M. E. Evidence for an inverse relationship between the differentiation of adipocytic and osteogenic cells in rat marrow stromal cell cultures. *J. Cell Sci.* **102 (Pt 2)**, 341–51 (1992).
89. Rickard, D. J., Sullivan, T. A., Shenker, B. J., Leboy, P. S. & Kazhdan, I. Induction of rapid osteoblast differentiation in rat bone marrow stromal cell cultures by Dexamethasone and BMP-2. *Dev. Biol.* **161**, 218–228 (1994).
90. Ashton, B. a *et al.* Characterization of cells with high alkaline phosphatase activity derived from human bone and marrow: preliminary assessment of their osteogenicity. *Bone* **6**, 313–9 (1985).
91. Haynesworth, S. E., Goshima, J., Goldberg, V. M. & Caplan, a I. Characterization of cells with osteogenic potential from human marrow. *Bone* **13**, 81–8 (1992).
92. Bennett, J. H., Joyner, C. J., Triffitt, J. T. & Owen, M. E. Adipocytic cells cultured from marrow have osteogenic potential. *J. Cell Sci.* **99 (Pt 1)**, 131–9 (1991).
93. Caplan, A. L. Effects of then nicotinamide-sensitive tertogen 3-acetylpyridine on chick limb cells in culture. *Exp. Cell Res.* **62**, 341–355 (1970).
94. Kopen, G. C., Prockop, D. J. & Phinney, D. G. Marrow stromal cells migrate throughout forebrain and cerebellum , and they differentiate into astrocytes after. *Proc. Natl. Acad. Sci.* **96**, 10711–10716 (1999).
95. Woodbury, D., Schwarz, E. J., Prockop, D. J. & Black, I. B. Adult rat and human bone marrow stromal cells differentiate into neurons. *J. Neurosci. Res.* **61**, 364–370 (2000).
96. Neuhuber, B. *et al.* Reevaluation of in vitro differentiation protocols for bone marrow stromal cells: Disruption of actin cytoskeleton induces rapid morphological changes and mimics neuronal phenotype. *J. Neurosci. Res.* **77**, 192–204 (2004).
97. Lu, P., Blesch, A. & Tuszynski, M. H. Induction of bone marrow stromal cells to neurons: Differentiation, transdifferentiation, or artifact? *J. Neurosci. Res.* **77**, 174–191 (2004).
98. Tondreau, T. *et al.* Bone marrow – derived mesenchymal stem cells already express specific neural proteins before any differentiation. *Differentiation* **72**, 319–326 (2004).
99. Toma, C., Pittenger, M. F., Cahill, K. S., Byrne, B. J. & Kessler, P. D. Human Mesenchymal Stem Cells Differentiate to a Cardiomyocyte Phenotype in the Adult Murine Heart. *Circulation* **105**, 93–98 (2002).

100. Pijnappels, D. a *et al.* Forced alignment of mesenchymal stem cells undergoing cardiomyogenic differentiation affects functional integration with cardiomyocyte cultures. *Circ. Res.* **103**, 167–76 (2008).
101. Rose, R. a, Keating, A. & Backx, P. H. Do mesenchymal stromal cells transdifferentiate into functional cardiomyocytes? *Circ. Res.* **103**, e120 (2008).
102. Rose, R. a *et al.* Bone marrow-derived mesenchymal stromal cells express cardiac-specific markers, retain the stromal phenotype, and do not become functional cardiomyocytes in vitro. *Stem Cells* **26**, 2884–92 (2008).
103. Siegel, G. *et al.* Bone marrow-derived human mesenchymal stem cells express cardiomyogenic proteins but do not exhibit functional cardiomyogenic differentiation potential. *Stem Cells Dev.* **21**, 2457–70 (2012).
104. Kramer, R. H., Rosen, S. D. & McDonald, K. A. Basement-membrane components associated with the extracellular matrix of the lymph node. *Cell Tissue Res.* **252**, 367–375 (1988).
105. Pöschl, E. *et al.* Collagen IV is essential for basement membrane stability but dispensable for initiation of its assembly during early development. *Development* **131**, 1619–28 (2004).
106. Kuhn, K. *Structure and function of Collagen types.* 2 (Academic Press, 1987).
107. Kielty, C. M., Sherratt, M. J. & Shuttleworth, C. A. Elastic fibres. *J. Cell Sci.* **115**, 2817–28 (2002).
108. Engel, J. *et al.* Shapes , Domain Organizations and Flexibility of Laminin and Fibronectin , Two Multifunctional Proteins of the Extracellular Matrix. *J. Mol. Biol.* **150**, 97–120 (1981).
109. Pankov, R. Fibronectin at a glance. *J. Cell Sci.* **115**, 3861–3863 (2002).
110. Campbell, K. P. Three muscular dystrophies: loss of cytoskeleton-extracellular matrix linkage. *Cell* **80**, 675–9 (1995).
111. Gilmore, a P. Anoikis. *Cell Death Differ.* **12 Suppl 2**, 1473–7 (2005).
112. Hynes, R. O. Integrins: versatility, modulation, and signaling in cell adhesion. *Cell* **69**, 11–25 (1992).
113. Ruoslahti, E. RGD and other recognition sequences for integrins. *Annu. Rev. Cell Dev. Biol.* **12**, 697–715 (1996).

114. Perlin, L., MacNeil, S. & Rimmer, S. Cell adhesive hydrogels synthesised by copolymerisation of arg-protected Gly-Arg-Gly-Asp-Ser methacrylate monomers and enzymatic deprotection. *Chem. Commun.* 5951–5953 (2008).
115. Knight, C. G. *et al.* The collagen-binding A-domains of Integrins $\alpha 1\beta 1$ and $\alpha 2\beta 1$ recognize the same specific amino acid sequence, GFOGER, in native (triple-helical) collagens. *J. Biol. Chem.* **1**, 35–40 (2000).
116. Burridge, K. & Chrzanowska-Wodnicka, M. Focal adhesions, contractility, and signaling. *Annu. Rev. Cell Dev. Biol.* **12**, 463–518 (1996).
117. Massia, S. P. & Hubbell, J. a. An RGD spacing of 440 nm is sufficient for integrin alpha V beta 3-mediated fibroblast spreading and 140 nm for focal contact and stress fiber formation. *J. Cell Biol.* **114**, 1089–1100 (1991).
118. Chen, C. S. Geometric Control of Cell Life and Death. *Science (80-.)*. **276**, 1425–1428 (1997).
119. Kim, S.-H., Turnbull, J. & Guimond, S. Extracellular matrix and cell signalling: the dynamic cooperation of integrin, proteoglycan and growth factor receptor. *J. Endocrinol.* **209**, 139–51 (2011).
120. Parsons, J. T. Focal adhesion kinase: the first ten years. *J. Cell Sci.* **116**, 1409–1416 (2003).
121. Hakkinen, K., Harunaga, J., Doyle, A. & KM., Y. Direct comparisons of the morphology, migration, cell adhesions, and actin cytoskeleton of fibroblasts in four different three-dimensional extracellular matrices. *Tissue Eng. Part A* **17**, 713–24 (2011).
122. Benya, P. D. & Shaffer, J. D. Dedifferentiated chondrocytes reexpress the differentiated collagen phenotype when cultured in agarose gels. *Cell* **30**, 215–24 (1982).
123. McBeath, R., Pirone, D. M., Nelson, C. M., Bhadriraju, K. & Chen, C. S. Cell shape, cytoskeletal tension, and RhoA regulate stem cell lineage commitment. *Dev. Cell* **6**, 483–95 (2004).
124. Ingber, D. E. The mechanochemical basis of cell and tissue regulation. *Mech. Chem. Biosyst.* **1**, 53–68 (2004).
125. Takai, Y., Sasaki, T. & Matozaki, T. Small GTP-Binding Proteins. *Physiol. Rev.* **81**, 154–188 (2001).
126. Shin, Y. *et al.* In vitro 3D collective sprouting angiogenesis under orchestrated ANG-1 and VEGF gradients. *Lab Chip* **11**, 2175–81 (2011).

127. Auerbach, R., Lewis, R., Shinnars, B., Kubai, L. & Akhtar, N. Angiogenesis assays: A critical overview. *Clin. Chem.* **49**, 32–40 (2003).
128. Van Winkle, A. P., Gates, I. D. & Kallos, M. S. Mass transfer limitations in embryoid bodies during human embryonic stem cell differentiation. *Cells. Tissues. Organs* **196**, 34–47 (2012).
129. Khan, W. S., Adesida, A. B. & Hardingham, T. E. Hypoxic conditions increase hypoxia-inducible transcription factor 2alpha and enhance chondrogenesis in stem cells from the infrapatellar fat pad of osteoarthritis patients. *Arthritis Res. Ther.* **9**, R55 (2007).
130. Robins, J. C. *et al.* Hypoxia induces chondrocyte-specific gene expression in mesenchymal cells in association with transcriptional activation of Sox9. *Bone* **37**, 313–22 (2005).
131. Pelham, R. J. & Wang, Y.-L. Cell locomotion and focal adhesions are regulated by substrate flexibility. *Proc. Natl. Acad. Sci.* **94**, 13661–13665 (1997).
132. Yeung, T. *et al.* Effects of substrate stiffness on cell morphology, cytoskeletal structure, and adhesion. *Cell Motil. Cytoskeleton* **60**, 24–34 (2005).
133. Halliday, N. L. & Tomasek, J. J. Mechanical properties of the extracellular matrix influence fibronectin fibril assembly in vitro. *Experimental cell Res.* **217**, 109–117 (1995).
134. Levental, I., Georges, P. C. & Janmey, P. a. Soft biological materials and their impact on cell function. *Soft Matter* **3**, 299 (2007).
135. Engler, A. J., Sen, S., Sweeney, H. L. & Discher, D. E. Matrix elasticity directs stem cell lineage specification. *Cell* **126**, 677–89 (2006).
136. Lo, C. M., Wang, H. B., Dembo, M. & Wang, Y. L. Cell movement is guided by the rigidity of the substrate. *Biophys. J.* **79**, 144–52 (2000).
137. Wang, H. B., Dembo, M. & Wang, Y. L. Substrate flexibility regulates growth and apoptosis of normal but not transformed cells. *Am. J. Physiol. Cell Physiol.* **279**, C1345–50 (2000).
138. Jain, R. K., Au, P., Tam, J., Duda, D. G. & Fukumura, D. Engineering vascularized tissue. *Nat. Biotechnol.* **23**, 821–3 (2005).
139. Murphy, C. M. & O'Brien, F. J. Understanding the effect of mean pore size on cell activity in collagen-glycosaminoglycan scaffolds. *Cell Adh. Migr.* **4**, 377–381 (2010).
140. Reilly, G. C. & Engler, A. J. Intrinsic extracellular matrix properties regulate stem cell differentiation. *J. Biomech.* **43**, 55–62 (2010).

141. Stevens, M. M. & George, J. H. Exploring and engineering the cell surface interface. *Science* **310**, 1135–8 (2005).
142. Lien, S.-M., Ko, L.-Y. & Huang, T.-J. Effect of pore size on ECM secretion and cell growth in gelatin scaffold for articular cartilage tissue engineering. *Acta Biomater.* **5**, 670–9 (2009).
143. Zeltinger, J., Sherwood, J. K., Graham, D. A., Müller, R. & Griffith, L. G. Effect of pore size and void fraction on cellular adhesion, proliferation and matrix deposition. *Tissue Eng.* **7**, 557–572 (2001).
144. O'Brien, F. J., Harley, B. a, Yannas, I. V & Gibson, L. J. The effect of pore size on cell adhesion in collagen-GAG scaffolds. *Biomaterials* **26**, 433–41 (2005).
145. Murphy, C. M., Haugh, M. G. & O'Brien, F. J. The effect of mean pore size on cell attachment, proliferation and migration in collagen-glycosaminoglycan scaffolds for bone tissue engineering. *Biomaterials* **31**, 461–6 (2010).
146. Nehrer, S. *et al.* Matrix collagen type and pore size influence behaviour of seeded canine chondrocytes. *Biomaterials* **18**, 769–76 (1997).
147. Hofmann, S. *et al.* Control of in vitro tissue-engineered bone-like structures using human mesenchymal stem cells and porous silk scaffolds. *Biomaterials* **28**, 1152–62 (2007).
148. Tsuruga, E., Takita, H., Itoh, H., Wakisaka, Y. & Kuboki, Y. Pore size of porous hydroxyapatite as the cell-substratum controls BMP-induced osteogenesis. *J. Biochem.* **121**, 317–324 (1997).
149. Kuboki, Y., Jin, Q., Kikuchi, M., Mamood, J. & Takita, H. Geometry of Artificial ECM: Sizes of Pores Controlling Phenotype Expression in BMP-Induced Osteogenesis and Chondrogenesis. *Connect. Tissue Res.* **43**, 529–534 (2002).
150. Park, J. S. *et al.* The effect of matrix stiffness on the differentiation of mesenchymal stem cells in response to TGF- β . *Biomaterials* **32**, 3921–30 (2011).
151. McBride, S. H. & Knothe Tate, M. L. Modulation of stem cell shape and fate A: the role of density and seeding protocol on nucleus shape and gene expression. *Tissue Eng. Part A* **14**, 1561–72 (2008).
152. Ruiz, S. A. & Chen, C. S. Emergence of patterned stem cell differentiation within multicellular structures. *Stem Cells* **26**, 2921–7 (2008).
153. Holtzer, H., Abbott, J., Lash, J. & Holtzer, S. The Loss of Phenotypic Traits by Differentiated Cells In Vitro I. Dedifferentiation of Cartilage Cells. *Proc. Natl. Acad. Sci.* **46**, 1533–1542 (1960).

154. Choi, Y. S. *et al.* The alignment and fusion assembly of adipose-derived stem cells on mechanically patterned matrices. *Biomaterials* **33**, 6943–51 (2012).
155. McMurray, R. J. *et al.* Nanoscale surfaces for the long-term maintenance of mesenchymal stem cell phenotype and multipotency. *Nat. Mater.* **10**, 637–44 (2011).
156. Oh, S. *et al.* Stem cell fate dictated solely by altered nanotube dimension. *Proc. Natl. Acad. Sci. U. S. A.* **106**, 2130–5 (2009).
157. Dalby, M. J., McCloy, D., Robertson, M., Wilkinson, C. D. W. & Oreffo, R. O. C. Osteoprogenitor response to defined topographies with nanoscale depths. *Biomaterials* **27**, 1306–15 (2006).
158. Brammer, K. S., Oh, S., Frandsen, C. J., Varghese, S. & Jin, S. Nanotube surface triggers increased chondrocyte extracellular matrix production. *Mater. Sci. Eng. C* **30**, 518–525 (2010).
159. Ratner, B. D., Hoffman, A. S., Schoen, F. J. & Lemons, J. *Biomaterials science: an introduction to materials in medicine*. 1130–1133 (Elsevier, 2013).
160. Hench, L. & Paschall, H. Direct Chemical Bond of Bioactive Glass-Ceramic Materials to Bone and Muscle. *J. Biomed. Mater. Res.* **42**, 25–42 (1973).
161. Hench, L. & Best, S. *Biomaterials Science: An introduction to materials in medicine*. 128–151 (2013).
162. Haycock, J. W. *3D Cell Culture: Methods and Proctocols*. 1–16 (2011).
163. Cook, A. D. *et al.* Characterization and development of RGD-peptide-modified poly(lactic acid-co-lysine) as an interactive, resorbable biomaterial. *J. Biomed. Mater. Res.* **35**, 513–523 (1997).
164. IUPAC. IUPAC Gold Book - Hydrogel. at <<http://goldbook.iupac.org/HT07519.html>>
165. Lee, K. Y. & Mooney, D. J. Hydrogels for Tissue Engineering. *Chem. Rev.* **101**, 1869–1879 (2001).
166. Drury, J. L. & Mooney, D. J. Hydrogels for tissue engineering: scaffold design variables and applications. *Biomaterials* **24**, 4337–4351 (2003).
167. Lutolf, M. P. & Hubbell, J. A. Synthetic biomaterials as instructive extracellular microenvironments for morphogenesis in tissue engineering. *Nat. Biotechnol.* **23**, 47–55 (2005).
168. Chandrakasan, G., Torchia, D. a & Piez, K. a. Preparation of intact monomeric collagen from rat tail tendon and skin and the structure of the nonhelical ends in solution. *J. Biol. Chem.* **251**, 6062–7 (1976).

169. Habermehl, J. *et al.* Preparation of ready-to-use, stockable and reconstituted collagen. *Macromol. Biosci.* **5**, 821–8 (2005).
170. Beghé, F. *et al.* Lyophilized non-denatured type-I collagen (Condress) extracted from bovine Achilles' tendon and suitable for clinical use. *Int. J. Tissue React.* **14**, s11–19 (1992).
171. Cross, V. L. *et al.* Dense type I collagen matrices that support cellular remodeling and microfabrication for studies of tumor angiogenesis and vasculogenesis in vitro. *Biomaterials* **31**, 8596–8607 (2010).
172. Yang, Y., Motte, S. & Kaufman, L. J. Pore size variable type I collagen gels and their interaction with glioma cells. *Biomaterials* **31**, 5678–88 (2010).
173. Raub, C. B. *et al.* Noninvasive assessment of collagen gel microstructure and mechanics using multiphoton microscopy. *Biophys. J.* **92**, 2212–22 (2007).
174. Te Nijenhuis, K. in *Adv. Polym. Sci. thermoreversible networks* 160–193 (1997).
175. Chen, W. Y. J. & Abatangelo, G. Functions of hyaluronan in wound repair. *Wound repair Regen.* **7**, 79–89 (1999).
176. Baier Leach, J., Bivens, K. a, Patrick, C. W. & Schmidt, C. E. Photocrosslinked hyaluronic acid hydrogels: natural, biodegradable tissue engineering scaffolds. *Biotechnol. Bioeng.* **82**, 578–89 (2003).
177. Burdick, J. a & Prestwich, G. D. Hyaluronic acid hydrogels for biomedical applications. *Adv. Mater.* **23**, H41–56 (2011).
178. Berger, J., Reist, M., Mayer, J. ., Felt, O. & Gurny, R. Structure and interactions in chitosan hydrogels formed by complexation or aggregation for biomedical applications. *Eur. J. Pharm. Biopharm.* **57**, 35–52 (2004).
179. Rowley, J. A., Madlambayan, G. & Mooney, D. J. Alginate hydrogels as synthetic extracellular matrix materials. *Biomaterials* **20**, 45–53 (1999).
180. Smidsrød, O. & Skjåk-Braek, G. Alginate as immobilization matrix for cells. *Trends Biotechnol.* **8**, 71–8 (1990).
181. Wichterle, O. & Lim, D. Hydrophilic gels for biological use. *Nature* **185**, 117–118 (1960).
182. Ringsdorf, H., Venzmer, J. & Winnik, F. M. Fluorescence Studies of Hydrophobically Modified poly(N-isopropylacrylamides). *Macromolecules* **24**, 1678–1686 (1991).

183. Maeda, Y., Nakamura, T. & Ikeda, I. Hydration and Phase Behavior of Poly(N - vinylcaprolactam) and Poly (N -vinylpyrrolidone) in Water. *Macromolecules* **35**, 217–222 (2002).
184. Maeda, Y. IR Spectroscopic Study on the Hydration and the Phase Transition of Poly(vinyl methyl ether) in Water. *Langmuir* **17**, 1737–1742 (2001).
185. Lutz, J.-F., Akdemir, O. & Hoth, A. Point by point comparison of two thermosensitive polymers exhibiting a similar LCST: is the age of poly(NIPAM) over? *J. Am. Chem. Soc.* **128**, 13046–7 (2006).
186. Chee, C. K., Rimmer, S. & Swanson, L. Time-resolved fluorescence anisotropy studies of the temperature-induced intramolecular conformation transition of poly(N-isopropylacrylamide) in dilute aqueous solutions. *Polymer (Guildf)*. **38**, 483–486 (1997).
187. Winnik, F. M. Fluorescence studies of aqueous solutions of poly(N-isopropylacrylamide) below and above their LCST. *Macromolecules* **23**, 233–242 (1990).
188. Chee, C. K., Rimmer, S., Soutar, I. & Swanson, L. Fluorescence investigations of the thermally induced conformational transition of poly(N -isopropylacrylamide). *Polymer (Guildf)*. **42**, 5079–5087 (2001).
189. Chee, C. K., Rimmer, S., Rutkaite, R., Soutar, I. & Swanson, L. Time-resolved fluorescence anisotropy measurements in the study of poly(N-isopropyl acrylamide)-based systems. *J. Photochem. Photobiol. A Chem.* **180**, 1–8 (2006).
190. Wu, C. & Zhou, S. Laser light scattering study of the phase transition of poly(N-isopropylacrylamide) in water. 1. single chain. *Macromolecules* **28**, 8381–8387 (1995).
191. Winnik, F. M. Phase transition of aqueous poly-(N-isopropylacrylamide) solutions: a study by non-radiative energy transfer. *Polymer (Guildf)*. **31**, 2125–2134 (1990).
192. Wu, C. & Wang, X. Globule-to-Coil Transition of a Single Homopolymer Chain in Solution. *Phys. Rev. Lett.* **80**, 4092–4094 (1998).
193. Kubota, K., Fujishige, S. & Ando, I. Single-chain transition of poly(N-isopropylacrylamide) in water. *J. Phys. Chem.* **94**, 5154–5158 (1990).
194. Wang, X., Qiu, X. & Wu, C. Comparison of the coil-to-globule and the globule-to-coil transitions of a single poly(N -isopropylacrylamide) homopolymer chain in water. *Macromolecules* **31**, 2972–2976 (1998).
195. Schild, H. G. Poly(N-isopropylacrylamide) - experiment, theory and application. *Prog. Polym. Sci.* **17**, 163–249 (1992).

196. Priest, J. H., Murray, S. L., Nelson, J. & Hoffman, A. S. Lower critical solution temperatures of aqueous copolymers of N-isopropylacrylamide and other N-substituted acrylamides. *ACS Symp. Ser.* **350**, 255–264 (1987).
197. Chee, C. K., Rimmer, S., Shaw, D. A., Soutar, I. & Swanson, L. Manipulating the thermoresponsive behavior of poly(N-isopropylacrylamide). 1. On the conformational behavior of a series of N-Isopropylacrylamide - styrene statistical copolymers. *Macromolecules* **34**, 7544–7549 (2001).
198. Wintgens, V. & Amiel, C. Physical gelation of amphiphilic poly(N-isopropylacrylamide): influence of the hydrophobic groups. *Macromol. Chem. Phys.* **209**, 1553–1563 (2008).
199. Shen, Z. *et al.* Synthesis and phase behavior of aqueous poly(N-isopropylacrylamide-co-acrylamide), poly(N-isopropylacrylamide-co-N,N-dimethylacrylamide) and poly(N-isopropylacrylamide-co-2-hydroxyethyl methacrylate). *Colloid Polym. Sci.* **284**, 1001–1007 (2006).
200. Zhang, G. & Wu, C. Effect of comonomer distribution on the coil-to-globule transition of a single AB copolymer chain in dilute solution. *Macromolecules* **35**, 2723–2727 (2002).
201. Kohori, F. *et al.* Preparation and characterization of thermally responsive block copolymer micelles comprising poly(N-isopropylacrylamide-b-DL-lactide). *J. Control. Release* **55**, 87–98 (1998).
202. Yoshioka, H., Mikami, M., Mori, Y. & Tsuchida, E. Preparation of poly(N-isopropylacrylamide)-B-poly(ethylene glycol) and calorimetric analysis of Its aqueous solution. *J. Macromol. Sci. Part A Pure Appl. Chem.* 109–112 (1994).
203. Chee, C.-K. *et al.* Manipulating the thermoresponsive behaviour of poly(N-isopropylacrylamide) 3. On the conformational behaviour of N-isopropylacrylamide graft copolymers. *Soft Matter* **5**, 3701 (2009).
204. Chee, C.-K., Rimmer, S., Soutar, I. & Swanson, L. Synthesis and conformational behaviour of luminescently labelled poly[styrene-graft-(N-isopropyl acrylamide)] copolymers. *Polym. Int.* **55**, 740–748 (2006).
205. Chen, G. & Hoffman, A. S. Temperature-induced phase transition behaviors of random vs. graft copolymers of N-isopropylacrylamide and acrylic acid. *Macromol. Rapid Commun.* 175–182 (1995).
206. Zhang, Y., Furyk, S., Bergbreiter, D. E. & Cremer, P. S. Specific ion effects on the water solubility of macromolecules: PNIPAM and the Hofmeister series. *J. Am. Chem. Soc.* **127**, 14505–10 (2005).

207. Schild, H. G. & Tirrell, D. A. Microcalorimetric detection of lower critical solution temperatures in aqueous polymer solutions. *J. Physical Chem.* **94**, 4352–4356 (1990).
208. Wei, H., Zhang, X.-Z., Zhou, Y., Cheng, S.-X. & Zhuo, R.-X. Self-assembled thermoresponsive micelles of poly(N-isopropylacrylamide-b-methyl methacrylate). *Biomaterials* **27**, 2028–34 (2006).
209. Chung, J. E. *et al.* Thermo-responsive drug delivery from polymeric micelles constructed using block copolymers of poly(N-isopropylacrylamide) and poly(butylmethacrylate). *J. Control. Release* **62**, 115–27 (1999).
210. Okano, T., Yamada, N., Okuhara, M. & Sakai, H. Mechanism of cell detachment from hydrophobic polymer surfaces. **16**, 297–303 (1995).
211. Akiyama, Y., Kikuchi, A., Yamato, M. & Okano, T. Ultrathin poly(N-isopropylacrylamide) grafted layer on polystyrene surfaces for cell adhesion/detachment control. *Langmuir* **20**, 5506–11 (2004).
212. Yamato, M., Konno, C., Utsumi, M., Kikuchi, A. & Okano, T. Thermally responsive polymer-grafted surfaces facilitate patterned cell seeding and co-culture. *Biomaterials* **23**, 561–7 (2002).
213. Tsuda, Y. *et al.* The use of patterned dual thermoresponsive surfaces for the collective recovery as co-cultured cell sheets. *Biomaterials* **26**, 1885–93 (2005).
214. Tsuda, Y., Kikuchi, A., Yamato, M., Chen, G. & Okano, T. Heterotypic cell interactions on a dually patterned surface. *Biochem. Biophys. Res. Commun.* **348**, 937–44 (2006).
215. Tsuda, Y. *et al.* Cellular control of tissue architectures using a three-dimensional tissue fabrication technique. *Biomaterials* **28**, 4939–4946 (2007).
216. Miyahara, Y. *et al.* Monolayered mesenchymal stem cells repair scarred myocardium after myocardial infarction. *Nat. Med.* **12**, 459–65 (2006).
217. Klouda, L. & Mikos, A. G. Thermoresponsive hydrogels in biomedical applications. *Eur. J. Pharm. Biopharm.* **68**, 34–45 (2008).
218. Klouda, L. *et al.* Thermoresponsive, in situ cross-linkable hydrogels based on N-isopropylacrylamide: fabrication, characterization and mesenchymal stem cell encapsulation. *Acta Biomater.* **7**, 1460–7 (2011).
219. Hacker, M. C., Klouda, L., Ma, B. B., Kretlow, J. D. & Mikos, A. G. Synthesis and Characterization of Injectable, Thermally and Chemically Gelable, Amphiphilic Poly(N-isopropylacrylamide)-Based Macromers. *Biomacromolecules* **9**, 1558–1570 (2008).

220. Uludag, H., Norrie, B., Kousinioris, N. & Gao, T. Engineering temperature-sensitive poly(N-isopropylacrylamide) polymers as carriers of therapeutic proteins. *Biotechnol. Bioeng.* **73**, 510–21 (2001).
221. Gao, T., Kousinioris, N. A., Wozney, J., Winn, S. & Uludag, H. Synthetic Thermoreversible Polymers Are Compatible with Osteoinductive Activity of Recombinant Human Bone Morphogenetic Protein 2. *Tissue Eng.* **8**, 429–440 (2002).
222. Smith, E., Yang, J., McGann, L., Sebald, W. & Uludag, H. RGD-grafted thermoreversible polymers to facilitate attachment of BMP-2 responsive C2C12 cells. *Biomaterials* **26**, 7329–38 (2005).
223. Kim, S. & Healy, K. E. Synthesis and characterization of injectable poly(N-isopropylacrylamide-co-acrylic acid) hydrogels with proteolytically degradable cross-links. *Biomacromolecules* **4**, 1214–23 (2003).
224. IUPAC. IUPAC Gold Book - IPN. at <<http://goldbook.iupac.org/I03117.html>>
225. IUPAC. IUPAC Gold Book - sIPN.
226. Kim, S., Chung, E. H., Gilbert, M. & Healy, K. E. Synthetic MMP-13 degradable ECMs based on poly(N-isopropylacrylamide-co-acrylic acid) semi-interpenetrating polymer networks. I. Degradation and cell migration. *J. Biomed. Mater. Res. A* **75**, 73–88 (2005).
227. Chung, E. H. *et al.* Biomimetic artificial ECMs stimulate bone regeneration. *J. Biomed. Mater. Res. Part A* **79A**, 815–826 (2006).
228. Li, Y. J., Chung, E. H., Rodriguez, R. T., Firpo, M. T. & Healy, K. E. Hydrogels as artificial matrices for human embryonic stem cell self-renewal. *J. Biomed. Mater. Res. Part A* **79A**, 1–5 (2006).
229. Wall, S., Yeh, C., Tu, R., Mann, M. & Healy, K. Biomimetic matrices for myocardial stabilization and stem cell transplantation. *J. Biomed. tissue Res. part A* **95**, 1055–1066 (2010).
230. An, Y. H., Webb, D., Gutowska, A., Mironov, V. A. & Friedman, R. J. Regaining Chondrocyte Phenotype in Thermosensitive Gel Culture. *Anat. Rec.* **263**, 336–341 (2001).
231. Au, A. *et al.* Thermally reversible polymer gel for chondrocyte culture. *J. Biomed. Mater. Res. A* **67**, 1310–9 (2003).
232. Na, K. *et al.* Delivery of dexamethasone, ascorbate, and growth factor (TGF beta-3) in thermo-reversible hydrogel constructs embedded with rabbit chondrocytes. *Biomaterials* **27**, 5951–7 (2006).

233. Vernengo, J., Fussell, G. W., Smith, N. G. & Lowman, A. M. Evaluation of Novel Injectable Hydrogels for Nucleus Pulposus Replacement. 64–69 (2007). doi:10.1002/jbmb
234. Comolli, N., Neuhuber, B., Fischer, I. & Lowman, A. In vitro analysis of PNIPAAm-PEG, a novel, injectable scaffold for spinal cord repair. *Acta Biomater.* **5**, 1046–55 (2009).
235. Almany, L. & Seliktar, D. Biosynthetic hydrogel scaffolds made from fibrinogen and polyethylene glycol for 3D cell cultures. *Biomaterials* **26**, 2467–77 (2005).
236. Dikovsky, D., Bianco-Peled, H. & Seliktar, D. The effect of structural alterations of PEG-fibrinogen hydrogel scaffolds on 3-D cellular morphology and cellular migration. *Biomaterials* **27**, 1496–506 (2006).
237. Lopes, C. M. A. & Felisberti, M. I. Mechanical behaviour and biocompatibility of poly(1-vinyl-2-pyrrolidinone)-gelatin IPN hydrogels. *Biomaterials* **24**, 1279–1284 (2003).
238. Kaur, H. & Chatteji, P. R. Interpenetrating hydrogel networks. 2. Swelling and mechanical properties of gelatin-polyacrylamide interpenetrating networks. *Macromolecules* 4868–4871 (1990).
239. Santin, M. *et al.* Synthesis and characterization of a new interpenetrated poly(hydroxyethylmethacrylate)- gelatin composite polymer. *Biomaterials* **17**, 1459–1467 (1996).
240. Ohya, S., Nakayama, Y. & Matsuda, T. Thermoresponsive artificial extracellular matrix for tissue engineering: hyaluronic acid bioconjugated with poly(N-isopropylacrylamide) grafts. *Biomacromolecules* **2**, 856–63 (2001).
241. Ohya, S., Sonoda, H., Nakayama, Y. & Matsuda, T. The potential of poly(N-isopropylacrylamide) (PNIPAM)-grafted hyaluronan and PNIPAM-grafted gelatin in the control of post-surgical tissue adhesions. *Biomaterials* **26**, 655–9 (2005).
242. Tan, H. *et al.* Thermosensitive injectable hyaluronic acid hydrogel for adipose tissue engineering. *Biomaterials* **30**, 6844–53 (2009).
243. Mortisen, D., Peroglio, M., Alini, M. & Eglin, D. Tailoring thermoreversible hyaluronan hydrogels by “click” chemistry and RAFT polymerization for cell and drug therapy. *Biomacromolecules* **11**, 1261–72 (2010).
244. Peroglio, M., Eglin, D., Benneker, L. M., Alini, M. & Grad, S. Thermoreversible hyaluronan-based hydrogel supports in vitro and ex vivo disc-like differentiation of human mesenchymal stem cells. *Spine J.* **13**, 1627–39 (2013).

245. Choi, S. *et al.* Combination of ascorbate and growth factor (TGF b -3) in thermo-reversible hydrogel constructs embedded with rabbit chondrocytes for neocartilage formation. *J. Biomed. Mater. Res. Part A* **83A**, 897–905 (2007).
246. Na, K. *et al.* Synergistic effect of TGFbeta-3 on chondrogenic differentiation of rabbit chondrocytes in thermo-reversible hydrogel constructs blended with hyaluronic acid by in vivo test. *J. Biotechnol.* **128**, 412–22 (2007).
247. Na, K. *et al.* Combination material delivery of dexamethasone and growth factor in hydrogel blended with hyaluronic acid constructs for neocartilage formation. *J. Biomed. Mater. Res. part a* **83A**, 779–786 (2007).
248. Ohya, S., Nakayama, Y. & Matsuda, T. In vivo evaluation of poly(N-isopropylacrylamide) (PNIPAM)-grafted gelatin as an in situ-formable scaffold. *J. Artif. Organs* **7**, 181–186 (2004).
249. Ohya, S. & Matsuda, T. Poly (N-isopropylacrylamide) (PNIPAM)-grafted gelatin as thermoresponsive three-dimensional artificial extracellular matrix: molecular and formulation parameters vs. cell proliferation potential. *J. Biomater. Sci. Polym. Ed.* **16**, 809–827 (2005).
250. Ohya, S., Kidoaki, S. & Matsuda, T. Poly(N-isopropylacrylamide) (PNIPAM)-grafted gelatin hydrogel surfaces: interrelationship between microscopic structure and mechanical property of surface regions and cell adhesiveness. *Biomaterials* **26**, 3105–11 (2005).
251. Matsuda, T., Saito, Y. & Shoda, K. Cell sorting technique based on thermoresponsive differential cell adhesiveness. *Biomacromolecules* **8**, 2345–2349 (2007).
252. Ibusuki, S., Fujii, Y., Iwamoto, Y. & Matsuda, T. Tissue-engineered cartilage using an injectable and in situ gelable thermoresponsive gelatin: fabrication and in vitro performance. *Tissue Eng.* **9**, 371–84 (2003).
253. Chen, J.-P. & Cheng, T.-H. Preparation and evaluation of thermo-reversible copolymer hydrogels containing chitosan and hyaluronic acid as injectable cell carriers. *Polymer (Guildf)*. **50**, 107–116 (2009).
254. Kim, J. H., Lee, S. B., Kim, S. J. & Lee, Y. M. Rapid temperature/pH response of porous alginate-g-poly(N-isopropylacrylamide) hydrogels. *Polymer (Guildf)*. **43**, 7549–7558 (2002).
255. Nistor, M.-T., Chiriac, A. P., Vasile, C., Verestiuc, L. & Nita, L. E. Synthesis of hydrogels based on poly(NIPAM) inserted into collagen sponge. *Colloids Surf. B. Biointerfaces* **87**, 382–90 (2011).
256. Liu, Z. & Rimmer, S. Studies on the free radical polymerization of N-vinylpyrrolidinone in 3-methylbutan-2-one. 1200–1207 (2002).

257. Lapworth, J. W., Hatton, P. V., Goodchild, R. L. & Rimmer, S. Thermally reversible colloidal gels for three-dimensional chondrocyte culture. *J. R. Soc. Interface* **9**, 362–375 (2011).
258. Winter, H. H. & Chambon, F. Analysis of linear viscoelasticity of a crosslinking polymer at the gel point. *J. Rheol. (N. Y. N. Y.)* **30**, 367 (1986).
259. Ranucci, E. *et al.* Synthesis and molecular weight characterization of end- f unctioalized N-vinyl-2-pyrrolidone oligomers. **774**, 763–774 (1995).
260. Ranucci, E., Macchi, L., Annunziata, R., Ferruti, P. & Chiellini, F. End-functionalised 1-vinyl-2-pyrrolidinone oligomers bearing lactate functions at one end. 706–713 (2004). doi:10.1002/mabi.200400061
261. Ranucci, E., Ferruti, P., Annunziata, R., Gerges, I. & Spinelli, G. NMR spectroscopy and MALDI-TOF MS characterisation of end-functionalised PVP oligomers prepared with different esters as chain transfer agents. *Macromol. Biosci.* **6**, 216–27 (2006).
262. Boutris, C., Chatzi, E. G. & Kiparissides, C. Characterization of the LCST behaviour of aqueous poly(N-isopropylacrylamide) solutions by thermal and cloud point techniques. *Polymer (Guildf)*. **38**, 2567–2570 (1997).
263. Fujishige, S., Kubota, K. & Ando, I. Phase transition of aqueous solutions of poly(N-isopropylacrylamide) and poly(N-isopropylmethacrylamide). *J. Phys. Chem.* **93**, 3311–3313 (1989).
264. Cheng, H., Shen, L. & Wu, C. LLS and FTIR studies on the hysteresis in association and dissociation of poly(N- isopropylacrylamide) chains in water. *Macromolecules* **39**, 2325–2329 (2006).
265. Yoshioka, H., Mori, Y., Tsukikawa, S. & Kubota, S. Thermoreversible gelation on cooling and on heating of an aqueous gelatin-poly(N-isopropylacrylamide) conjugate. *Polym. Adv. Technol.* **9**, 155–158 (1998).
266. Gan, T. T., Guan, Y. & Zhang, Y. J. Thermogelable PNIPAM microgel dispersion as 3D cell scaffold: effect of syneresis. *J. Mater. Chem.* **20**, 5937–5944 (2010).
267. Cheng, D., Wu, Y., Guan, Y. & Zhang, Y. Tuning properties of injectable hydrogel scaffold by PEG blending. *Polymer (Guildf)*. **53**, 5124–5131 (2012).
268. Storm, C., Pastore, J., MacKintosh, F., Lubensky, T. & Janmey, P. Nonlinear elasticity in biological gels. *Lett. to Nat.* **435**, 191–194 (2005).
269. Motte, S. & Kaufman, L. J. Strain stiffening in collagen I networks. *Biopolymers* **99**, 35–46 (2013).

270. Tan, H., Chu, C. R., Payne, K. a & Marra, K. G. Injectable in situ forming biodegradable chitosan-hyaluronic acid based hydrogels for cartilage tissue engineering. *Biomaterials* **30**, 2499–506 (2009).
271. Kushida, A. *et al.* Decrease in culture temperature releases monolayer endothelial cell sheets together with deposited fibronectin matrix from temperature-responsive culture surfaces. *J. Biomed. Mater. Res.* **45**, 355–362 (1999).
272. Uzarski, J. S., Xia, Y., Belmonte, J. C. I. & Wertheim, J. a. New strategies in kidney regeneration and tissue engineering. *Curr. Opin. Nephrol. Hypertens.* **23**, 399–405 (2014).
273. Palakkan, A. a, Hay, D. C., Anil Kumar, P. R., Kumary, T. V & Ross, J. a. Liver tissue engineering and cell sources: issues and challenges. *Liver Int.* **33**, 666–76 (2013).
274. Bolland, F. *et al.* Development and characterisation of a full-thickness acellular porcine bladder matrix for tissue engineering. *Biomaterials* **28**, 1061–70 (2007).
275. Khademhosseini, A. & Langer, R. Microengineered hydrogels for tissue engineering. *Biomaterials* **28**, 5087–92 (2007).
276. Lovett, M., Lee, K., Edwards, A. & Kaplan, D. L. Vascularization Strategies for Tissue Engineering. *Tissue Eng. Part B-Reviews* **15**, 353–370 (2009).
277. Elliott, N. T. & Yuan, F. A. N. A Review of Three-Dimensional In Vitro Tissue Models for Drug Discovery and Transport Studies. *J. Pharm. Sci.* **100**, 2–8 (2011).
278. Griffith, L. G. & Swartz, M. a. Capturing complex 3D tissue physiology in vitro. *Nat. Rev. Mol. Cell Biol.* **7**, 211–24 (2006).
279. Suematsu, S. & Watanabe, T. Generation of a synthetic lymphoid tissue-like organoid in mice. *Nat. Biotechnol.* **22**, 1539–45 (2004).
280. Tomei, A. a, Siegert, S., Britschgi, M. R., Luther, S. a & Swartz, M. a. Fluid flow regulates stromal cell organization and CCL21 expression in a tissue-engineered lymph node microenvironment. *J. Immunol.* **183**, 4273–83 (2009).
281. Mueller, S. N. & Germain, R. N. Stromal cell contributions to the homeostasis and functionality of the immune system. *Nat. Rev. Immunol.* **9**, 618–29 (2009).
282. Willard-Mack, C. L. Normal structure, function, and histology of lymph nodes. *Toxicol. Pathol.* **34**, 409–24 (2006).
283. Clark, S. L. The reticulum of lymph nodes in mice studied with the electron microscope. *Am. J. Anat.* **110**, 217–57 (1962).

284. Gretz, J. E., Kaldjian, E. P., Anderson, a O. & Shaw, S. Sophisticated strategies for information encounter in the lymph node: the reticular network as a conduit of soluble information and a highway for cell traffic. *J. Immunol.* **157**, 495–499 (1996).
285. Gretz, J. E., Anderson, a O. & Shaw, S. Cords, channels, corridors and conduits: critical architectural elements facilitating cell interactions in the lymph node cortex. *Immunol. Rev.* **156**, 11–24 (1997).
286. Buettner, M., Pabst, R. & Bode, U. Stromal cell heterogeneity in lymphoid organs. *Trends Immunol.* **31**, 80–6 (2010).
287. Legler, D. F. *et al.* B cell-attracting chemokine 1, a human CXC chemokine expressed in lymphoid tissues, selectively attracts B lymphocytes via BLR1/CXCR5. *J. Exp. Med.* **187**, 655–60 (1998).
288. Cyster, J. G. *et al.* Follicular stromal cells and lymphocyte homing to follicles. *Immunol. Rev.* **176**, 181–93 (2000).
289. Link, A. *et al.* Fibroblastic reticular cells in lymph nodes regulate the homeostasis of naive T cells. *Nat. Immunol.* **8**, 1255–65 (2007).
290. Schiemann, B. *et al.* An essential role for BAFF in the normal development of B cells through a BCMA-independent pathway. *Science* **293**, 2111–4 (2001).
291. Bajénoff, M. *et al.* Stromal cell networks regulate lymphocyte entry, migration, and territoriality in lymph nodes. *Immunity* **25**, 989–1001 (2006).
292. Cupedo, T. *et al.* Presumptive lymph node organizers are differentially represented in developing mesenteric and peripheral nodes. *J. Immunol.* **173**, 2968–75 (2004).
293. Turley, S. J., Fletcher, A. L. & Elpek, K. G. The stromal and haematopoietic antigen-presenting cells that reside in secondary lymphoid organs. *Nat. Rev. Immunol.* **10**, 813–25 (2010).
294. Tew, J. G. *et al.* Follicular dendritic cells and presentation of antigen and costimulatory signals to B cells. *Immunol. Rev.* **156**, 39–52 (1997).
295. Banchereau, J. & Steinman, R. M. Dendritic cells and the control of immunity. *Nature* **392**, 245–52 (1998).
296. Fletcher, A. L. *et al.* Lymph node fibroblastic reticular cells directly present peripheral tissue antigen under steady-state and inflammatory conditions. *J. Exp. Med.* **207**, 689–97 (2010).
297. Gretz, J. E., Norbury, C. C., Anderson, a O., Proudfoot, a E. & Shaw, S. Lymph-borne chemokines and other low molecular weight molecules reach high endothelial venules

- via specialized conduits while a functional barrier limits access to the lymphocyte microenvironments in lymph node cortex. *J. Exp. Med.* **192**, 1425–40 (2000).
298. Sixt, M. *et al.* The conduit system transports soluble antigens from the afferent lymph to resident dendritic cells in the T cell area of the lymph node. *Immunity* **22**, 19–29 (2005).
299. Van de Pavert, S. A. & Mebius, R. E. New insights into the development of lymphoid tissues. *Nat. Rev. Immunol.* **10**, 664–74 (2010).
300. Roozendaal, R. & Mebius, R. E. Stromal cell-immune cell interactions. *Annu. Rev. Immunol.* **29**, 23–43 (2011).
301. Honda, K. *et al.* Molecular Basis for Hematopoietic/Mesenchymal Interaction during Initiation of Peyer’s Patch Organogenesis. *J. Exp. Med.* **193**, 621–630 (2001).
302. Krautler, N. J. *et al.* Follicular Dendritic Cells Emerge from Ubiquitous Perivascular Precursors. *Cell* **150**, 194–206 (2012).
303. Mebius, R. E. Organogenesis of lymphoid tissues. *Nat. Rev. Immunol.* **3**, 292–303 (2003).
304. Bénézech, C. *et al.* Ontogeny of stromal organizer cells during lymph node development. *J. Immunol.* **184**, 4521–30 (2010).
305. Fu, Y. X., Huang, G., Matsumoto, M., Molina, H. & Chaplin, D. D. Independent signals regulate development of primary and secondary follicle structure in spleen and mesenteric lymph node. *Proc. Natl. Acad. Sci. U. S. A.* **94**, 5739–43 (1997).
306. Ettinger, R. *et al.* Effects of tumor necrosis factor and lymphotoxin on peripheral lymphoid tissue development. *Int. Immunol.* **10**, 727–41 (1998).
307. Tumanov, A. V *et al.* Cellular source and molecular form of TNF specify its distinct functions in organization of secondary lymphoid organs. *Blood* **116**, 3456–64 (2010).
308. Tumanov, A. *et al.* Distinct role of surface lymphotoxin expressed by B cells in the organization of secondary lymphoid tissues. *Immunity* **17**, 239–50 (2002).
309. Tumanov, A. V., Kuprash, D. V. & Nedospasov, S. a. The role of lymphotoxin in development and maintenance of secondary lymphoid tissues. *Cytokine Growth Factor Rev.* **14**, 275–288 (2003).
310. Katakai, T., Hara, T., Sugai, M., Gonda, H. & Shimizu, A. Lymph node fibroblastic reticular cells construct the stromal reticulum via contact with lymphocytes. *J. Exp. Med.* **200**, 783–95 (2004).

311. Fletcher, A. L. *et al.* Reproducible Isolation of Lymph Node Stromal Cells Reveals Site-Dependent Differences in Fibroblastic Reticular Cells. *Front. Immunol.* **2**, 1–15 (2011).
312. Ngo, V. N., Cornall, R. J. & Cyster, J. G. Splenic T zone development is B cell dependent. *J. Exp. Med.* **194**, 1649–60 (2001).
313. Coles, M. C. *et al.* Role of T and NK cells and IL7/IL7r interactions during neonatal maturation of lymph nodes. *Proc. Natl. Acad. Sci. U. S. A.* **103**, 13457–62 (2006).
314. Zhang, Y. & Jordan, J. M. Epidemiology of osteoarthritis. *Clin. Geriatr. Med.* **26**, 355–369 (2010).
315. Eyre, D. Collagen of articular cartilage. *Arthritis Res.* **4**, 30–5 (2001).
316. Akizuki, S. *et al.* Tensile properties of human knee joint cartilage: I. Influence of ionic conditions, weight bearing, and fibrillation on the tensile modulus. *J. Orthop. Res.* **4**, 379–92 (1986).
317. Bruckner, P. & van der Rest, M. Structure and function of cartilage collagens. *Microsc. Res. Tech.* **28**, 378–84 (1994).
318. Gelse, K. Collagens—structure, function, and biosynthesis. *Adv. Drug Deliv. Rev.* **55**, 1531–1546 (2003).
319. Mandler, M., Eich-Bender, S. G., Vaughan, L., Winterhalter, K. H. & Bruckner, P. Cartilage contains mixed fibrils of collagen types II, IX, and XI. *J. Cell Biol.* **108**, 191–7 (1989).
320. Poole, A. R. *et al.* Composition and Structure of Articular Cartilage. *Clin. Orthop. Relat. Res.* **391**, S26–S33 (2001).
321. Blaschke, U. K. Collagen XI Nucleates Self-assembly and Limits Lateral Growth of Cartilage Fibrils. *J. Biol. Chem.* **275**, 10370–10378 (2000).
322. Heinegard, D. & Oldeberg, A. Structure and biology of cartilage and bone matrix noncollagenous macromolecules. *FASEB J.* 2402–2051 (1989). doi:10.1007/SpringerReference_33640
323. Hardingham, T. & Fosang, A. Proteoglycans: many forms and many functions. *FASEB J.* **6**, 861–870 (1992).
324. Kiani, C. H., Chen, L. I., Wu, Y. A. O. J. I., Yee, A. L. J. & Yang, B. U. B. Structure and function of aggrecan. **12**, 19–32 (2002).

325. Poole, C. A., Flint, M. H. & Beaumont, B. W. Chondrons in cartilage: ultrastructural analysis of the pericellular microenvironment in adult human articular cartilages. *J. Orthop. Res.* **5**, 509–22 (1987).
326. Poole, C. A. Articular cartilage chondrons: form, function and failure. *J. Anat.* **191** (Pt 1, 1–13 (1997).
327. Slomianka, L. School of Anatomy and Human Biology - The univeristy of Western Australia: Cartilage Histology. at <<http://www.lab.anhb.uwa.edu.au/mb140/CorePages/Cartilage/Cartil.htm>>
328. Pacifici, M. *et al.* Hypertrophic chondrocytes. The terminal stage of differentiation in the chondrogenic cell lineage? *Ann. N. Y. Acad. Sci.* **599**, 45–57 (1990).
329. Hunziker, E. B. Articular cartilage repair: basic science and clinical progress. A review of the current status and prospects. *Osteoarthritis Cartilage* **10**, 432–63 (2002).
330. Peterson, L. *et al.* Two- to 9-year outcome after autologous chondrocyte transplantation of the knee. *Clin. Orthop. Relat. Res.* 212–34 (2000).
331. NHS Choices: Knee Replacement. (2012). at <<http://www.nhs.uk/conditions/knee-replacement/Pages/Kneereplacementexplained.aspx>>
332. Kurtz, S., Ong, K., Lau, E., Mowat, F. & Halpern, M. Projections of Primary and Revision Hip and Knee Arthroplasty in the United States from 2005 to 2030. *J. Bone Jt. Surg.* **89**, 780–785 (2007).
333. Mauck, R. L., Yuan, X. & Tuan, R. S. Chondrogenic differentiation and functional maturation of bovine mesenchymal stem cells in long-term agarose culture. *Osteoarthritis Cartilage* **14**, 179–89 (2006).
334. Gao, L., McBeath, R. & Chen, C. S. Stem cell shape regulates a chondrogenic versus myogenic fate through Rac1 and N-cadherin. *Stem Cells* **28**, 564–72 (2010).
335. Woods, A., Wang, G. & Beier, F. RhoA/ROCK signaling regulates Sox9 expression and actin organization during chondrogenesis. *J. Biol. Chem.* **280**, 11626–34 (2005).
336. Awad, H. A., Wickham, M. Q., Leddy, H. a, Gimble, J. M. & Guilak, F. Chondrogenic differentiation of adipose-derived adult stem cells in agarose, alginate, and gelatin scaffolds. *Biomaterials* **25**, 3211–22 (2004).
337. Bénézech, C. *et al.* Lymphotoxin- β Receptor Signaling through NF- κ B2-RelB Pathway Reprograms Adipocyte Precursors as Lymph Node Stromal Cells. *Immunity* **37**, 721–34 (2012).

338. Cawthorn, W. P., Heyd, F., Hegyi, K. & Sethi, J. K. Tumour necrosis factor-alpha inhibits adipogenesis via a beta-catenin/TCF4(TCF7L2)-dependent pathway. *Cell Death Differ.* **14**, 1361–73 (2007).
339. Lian, J. B. & Stein, G. S. Development of the osteoblast phenotype: molecular mechanisms mediating osteoblast growth and differentiation. *Iowa Orthop. J.* **15**, 118–40 (1995).
340. Frith, J. Transcriptional Control of Mesenchymal Stem Cell Differentiation. 216–227 (2008). doi:10.1159/000127448s
341. Tomomatsu, N. *et al.* LPS-Induced inhibition of Osteogenesis is TNF-alpha dependant in a murine tooth extraction model. *J. Bone Miner. Res.* **24**, 1770–1781 (2009).
342. Kotake, S. & Nanke, Y. Effect of TNF α on osteoblastogenesis from mesenchymal stem cells. *Biochim. Biophys. Acta* **1840**, 1209–13 (2014).
343. Huang, H. *et al.* Dose-specific effects of tumor necrosis factor alpha on osteogenic differentiation of mesenchymal stem cells. *Cell Prolif.* **44**, 420–7 (2011).
344. Lacey, D. L., Erdmann, J. M., Suzuki, H. & Ohara, J. MC3T3 osteoblastic cells express receptors for and respond to interleukin-4. *J. Bone Miner. Res.* S1–307 (1991).
345. Lewis, D. B. *et al.* Osteoporosis induced in mice by overproduction of interleukin 4. *Proc. Natl. Acad. Sci. U. S. A.* **90**, 11618–22 (1993).
346. Aldridge, A. *et al.* Assay validation for the assessment of adipogenesis of multipotential stromal cells--a direct comparison of four different methods. *Cytotherapy* **15**, 89–101 (2013).
347. Spahn, T. W., Eugster, H., Fontana, A. & Domschke, W. Role of Lymphotoxin in Experimental Models of Infectious Diseases: Potential Benefits and Risks of a Therapeutic Inhibition of the Lymphotoxin-beta Receptor Pathway. *Infect. Immun.* **73**, 7077–7088 (2005).
348. Katakai, T. *et al.* Organizer-Like Reticular Stromal Cell Layer Common to Adult Secondary Lymphoid Organs. *J. Immunol.* **181**, 6189–6200 (2008).
349. Browning, J. L. Inhibition of the lymphotoxin pathway as a therapy for autoimmune disease. *Immunol. Rev.* **223**, 202–20 (2008).
350. Kratz, A., Campos-Neto, A., Hanson, M. S. & Ruddle, N. H. Chronic inflammation caused by lymphotoxin is lymphoid neogenesis. *J. Exp. Med.* **183**, 1461–72 (1996).
351. Drayton, D. L., Liao, S., Mounzer, R. H. & Ruddle, N. H. Lymphoid organ development: from ontogeny to neogenesis. *Nat. Immunol.* **7**, 344–53 (2006).

352. Motallebzadeh, R. *et al.* Blocking lymphotoxin signaling abrogates the development of ectopic lymphoid tissue within cardiac allografts and inhibits effector antibody responses. *FASEB J.* **26**, 51–62 (2012).
353. Amé-Thomas, P. *et al.* Human mesenchymal stem cells isolated from bone marrow and lymphoid organs support tumor B-cell growth: role of stromal cells in follicular lymphoma pathogenesis. *Blood* **109**, 693–702 (2007).
354. Szakal, A. K., Gieringer, R. L., Kosco, H. & Tew, J. G. Isolated follicular dendritic cells: cytochemical antigen localisation, nomarski, SEM, and TEM morphology. *J. Immunol.* **134**, 1349–1359 (1985).
355. Maheshwari, G., Brown, G., Lauffenburger, D. A., Wells, A. & Griffith, L. G. Cell adhesion and motility depend on nanoscale RGD clustering. *J. Cell Sci.* **113** (Pt 1, 1677–86 (2000).
356. Chen, C. S., Alonso, J. L., Ostuni, E., Whitesides, G. M. & Ingber, D. E. Cell shape provides global control of focal adhesion assembly. *Biochem. Biophys. Res. Commun.* **307**, 355–361 (2003).
357. Zaman, M. *et al.* Migration of tumor cells in 3D matrices is governed by matrix stiffness along with cell-matrix adhesion and proteolysis. *Proc. Natl. Acad. Sci.* **103**, 10889–10894 (2006).
358. Kuntz, R. M. & Saltzman, W. M. Neutrophil motility in extracellular matrix gels: mesh size and adhesion affect speed of migration. *Biophys. J.* **72**, 1472–80 (1997).
359. West, G. W., Weichselbaum, R. & Little, J. B. Limited Penetration of Methotrexate into Human Osteosarcoma Spheroids as a Proposed Model for Solid Tumor Resistance to Adjuvant Chemotherapy Limited Penetration of Methotrexate into Human Osteosarcoma Spheroids as a Proposed Model for Solid Tumor Resista. *Cancer Res.* **40**, 3665–3668 (1980).
360. Bartosh, T. J. *et al.* Aggregation of human mesenchymal stromal cells (MSCs) into 3D spheroids enhances their anti-inflammatory properties. *Proc. Natl. Acad. Sci.* **107**, 13724–13729 (2010).
361. Korff, T. & Augustin, H. G. Integration of endothelial cells in multicellular spheroids prevents apoptosis and induces differentiation. *J. Cell Biol.* **143**, 1341–52 (1998).
362. Alon, R. *et al.* TNF-alpha binds to the N-terminal domain of fibronectin and augments the beta1-integrin-mediated adhesion of CD4+ T lymphocytes to the glycoprotein. *J. Immunol.* **152**, 1304–1313 (1994).
363. Premaraj, S. *et al.* Sustained delivery of bioactive cytokine using a dense collagen gel vehicle collagen gel delivery of bioactive cytokine. *Arch. Oral Biol.* **51**, 325–33 (2006).

364. Pilgaard, L. *et al.* Effect of oxygen concentration, culture format and donor variability on in vitro chondrogenesis of human adipose tissue-derived stem cells. *Regen. Med.* **4**, 539–548 (2009).
365. Lu, Z., Doulabi, B. Z., Huang, C., Bank, R. a & Helder, M. N. Collagen type II enhances chondrogenesis in adipose tissue-derived stem cells by affecting cell shape. *Tissue Eng. Part A* **16**, 81–90 (2010).
366. Bosnakovski, D. *et al.* Chondrogenic Differentiation of Bovine Bone Marrow Mesenchymal Stem Cells (MSCs) in Different Hydrogels: Influence of Collagen Type II Extracellular Matrix on MSC Chondrogenesis. *Biotechnol. Bioeng.* **93**, 1152–1162 (2006).
367. Gonen-Wadmany, M., Goldshmid, R. & Seliktar, D. Biological and mechanical implications of PEGylating proteins into hydrogel biomaterials. *Biomaterials* **32**, 6025–33 (2011).